

SPACE-TIME SEISMICITY AND DEVELOPMENT OF A GEOGRAPHICAL  
INFORMATION SYSTEM DATABASE WITH INTERACTIVE  
GRAPHICS FOR THE YELLOWSTONE REGION

by

Jamie Mark Farrell

A thesis submitted to the faculty of  
The University of Utah  
in partial fulfillment of the requirements for the degree of

Master of Science

in

Geophysics

Department of Geology and Geophysics

The University of Utah

August 2007

Copyright © Jamie Mark Farrell 2007

All Rights Reserved

THE UNIVERSITY OF UTAH GRADUATE SCHOOL

**SUPERVISORY COMMITTEE APPROVAL**

of a thesis submitted by

This thesis has been read by each member of the following supervisory committee and by majority vote has been found to be satisfactory.

---

---

Chair:

---

---

---

---

THE UNIVERSITY OF UTAH GRADUATE SCHOOL

**FINAL READING APPROVAL**

To the Graduate Council of the University of Utah:

I have read the thesis of \_\_\_\_\_ in its final form and have found that (1) its format, citations, and bibliographic style are consistent and acceptable; (2) its illustrative materials including figures, tables, and charts are in place; and (3) the final manuscript is satisfactory to the supervisory committee and is ready for submission to The Graduate School.

---

Date

---

Chair: Supervisory Committee

Approved for the Major Department

---

Chair/Dean

Approved for the Graduate Council

---

David S. Chapman  
Dean of The Graduate School

## ABSTRACT

The Yellowstone National Park, Wyoming, region is one of the most seismically active areas of the U.S., experiencing the M7.5 Hebgen Lake earthquake, the largest historic earthquake in the U.S. interior, as well as more than 26,000 well recorded earthquakes from 1973 to 2003. This activity offers the opportunity to study the time and spatial occurrence of earthquakes and its dominance of earthquake swarms and how they relate to tectonic and volcanic processes. A study of the time and spatial nature of the swarms by analyses of the time rate of occurrence defined by the  $b$ -value is the main objective of this thesis. The earthquake size distribution follows, in most instances, a power law. The  $b$ -value is the slope of this power law and is commonly used to describe the relative occurrence of large and small earthquakes. To accurately map  $b$ -values, the entire earthquake catalog had to be filtered to identify statistically dependent time related events defined as swarms from independent single shocks. An algorithm was employed that identified earthquake swarms based on interevent times and distances. A total of 57 Yellowstone swarms were identified from 1984 – 2003 using the above algorithm,. The swarms vary in duration from 1 to 46 days with the number of events varying from 30 to 722. All swarm events as well as the 597 events triggered by the 2002 Denali Fault earthquake were then removed from the catalog. A magnitude of completeness of  $M_C=1.5$  was calculated for the remaining catalog and all events with  $M_C<1.5$  were

removed as well. The  $b$ -value distribution for the Yellowstone National Park region was determined using an algorithm developed in ZMAP with the deswarmed catalog.

Results show that the spatial distribution of  $b$ -values in Yellowstone reveal areas of relatively high and low  $b$ -values mixed in with areas of normal crustal values ( $b \approx 1.0$ ). High  $b$ -values (up to  $1.54 \pm 0.06$ ) for areas beneath and north of the Mallard Lake resurgent dome are interpreted to be due to variations in stresses that are likely related to the migration of magmatic and hydrothermal fluids below the surface. An area of high  $b$ -values (up to  $1.34 \pm 0.13$ ) near the Hebgen Lake fault zone just west of the Yellowstone caldera could be evidence of magmatic fluids flowing out of the volcanic system or could be indicative of a relatively low stress regime resulting from the 1959 Hebgen Lake earthquake. An area of low  $b$ -values (as low as  $0.63 \pm 0.09$ ) south of the caldera indicates that there is a lack of smaller earthquakes relative to larger events and is evidence that the stress in the crust is relatively high. This could be due to the loading of the East Mt. Sheridan fault and the Teton fault by the Yellowstone volcanic system.

The Yellowstone GIS database developed for this study is an extension of an earlier database and was planned as a central web site for geological, geophysical and geographical information of the Yellowstone region. Over the past 40 years, extensive geologic and geophysical data have been acquired on the active volcano-tectono processes of this system such as heatflow, seismic velocity models from active and passive seismic experiments, geodetic measurements, fault-stress interaction, earthquake processes, etc. Also, these data will expand rapidly as EarthScope continues to come online. The database website, (<http://www.yellowstonegis.utah.edu>) provides online, near-realtime information for the visitor, researcher, general public, students, and

emergency managers maintaining our long term outreach and educational goals. To assist with the visualization of some three- and four-dimensional datasets, such as earthquakes, seismic velocity models, geodetic measurements, geodynamic models, etc., various visualization tools have been employed to provide 3D data representation. These datasets were imported into the Fledermaus software allowing the user to view a 3D representation of the Yellowstone volcanic system. Since this region is constantly changing the datasets are updated continuously providing true time- and 3D spatial information. The data will become part of the Geosciences Network (GEON) which is developing cyberinfrastructure for integrative research to enable transformative advances in geoscience research and education (<http://www.geongrid.org>). Using the GEON portal (<http://portal.geongrid.org>) one can view, download and even manipulate certain datasets.

## TABLE OF CONTENTS

ABSTRACT .....	iv
LIST OF FIGURES .....	ix
LIST OF TABLES .....	xiv
ACKNOWLEDGEMENTS .....	xv
Chapters	
1. INTRODUCTION .....	1
1.1. Yellowstone Seismicity .....	1
1.2. Objectives .....	3
2. YELLOWSTONE VOLCANO-MAGMATIC SETTING .....	5
2.1. Regional Geology .....	5
2.2. Volcanic History .....	9
2.3. Geophysical Characteristics .....	9
3. SEISMICITY AND DEFORMATION OF THE YELLOWSTONE REGION .....	15
3.1. Yellowstone Earthquakes .....	15
3.2. Remotely Triggered Earthquakes in Yellowstone .....	17
3.3. Focal Depth Variations Across the Yellowstone Caldera .....	18
3.4. Focal Mechanisms and Stress Orientations .....	19
3.5. Crustal and Mantle Tomography .....	22
3.6. Geodetic Data (GPS, InSAR, and Leveling) .....	23
4. CALCULATION OF EARTHQUAKE RECURRENCE RATES .....	26
4.1. Earthquake Data .....	26
4.2. Identification of Earthquake Swarms .....	27
4.3. Calculating $b$ -values .....	32
4.4. How is the $b$ -value Interpreted? .....	34

5.	RESULTS .....	37
	5.1. Earthquake Swarm Analyses .....	37
	5.2. Magnitude of Completeness .....	44
	5.3. <i>b</i> -value Maps.....	49
6.	THE YELLOWSTONE GEON-GIS DATABASE.....	61
	6.1. Objectives .....	61
	6.2. GEON .....	62
	6.3. Geographical Information Systems.....	64
	6.4. Data Hierarchy .....	64
	6.5. Examples of Data.....	65
	6.6. Data Visualization.....	69
	6.7. Website .....	72
7.	DISCUSSION.....	74
	7.1. Earthquake Swarm Identification .....	74
	7.2. <i>b</i> -value Distribution .....	75
8.	CONCLUSIONS.....	83
Appendices		
A.	TABLE OF YELLOWSTONE EARTHQUAKE SWARMS .....	86
B.	TEMPORAL DISTRIBUTIONS OF EARTHQUAKES IN YELLOWSTONE SWARMS .....	92
C.	PLOTS OF INDIVIDUAL EARTHQUAKE SWARM EPICENTERS.....	140
D.	LIST OF CURRENT AND PLANNED DATA IN THE YELLOWSTONE GIS DATABASE .....	156
	REFERENCES .....	160

## LIST OF FIGURES

### Figure

1.1.	Earthquakes in Yellowstone from 1973 – 1981 and 1981 – 2003.....	2
2.1.	General geologic map of the Yellowstone Plateau.....	6
2.2.	Map of the Yellowstone-Snake River Plain-Newberry system.....	8
2.3.	A Topographic map of the Yellowstone volcanic field.....	10
2.4.	Complete Bouguer gravity anomaly map of Yellowstone National Park.....	11
2.5.	Index map of Yellowstone showing hydrothermal features.....	13
3.1.	Focal depth distribution for A and B quality earthquakes, 1973-2003.....	20
3.2.	Seismic, geodetic, and geologic stress indicators across Yellowstone.....	21
3.3.	Plot of Yellowstone Plateau seismicity, deformation, and moment release.....	24
4.1.	Seismicity map showing the locations of A, B, and C quality events from 1984 – 2003.....	28
4.2.	Generalized plots of number of earthquakes vs. time for the three types of earthquake sequences.....	29
5.1.	Swarm locations identified using the 10 minimum definition of a swarm.....	39
5.2.	Swarm locations identified using the 30 minimum definition of a swarm.....	41
5.3.	Swarm locations identified using the 50 minimum definition of a swarm.....	42
5.4.	Cumulative number of earthquakes vs. time for the different catalogs used to calculate <i>b</i> -values.....	45
5.5.	Yellowstone seismic network for 1984 – 1994 and 1995 – 2003.....	46

5.6.	Magnitude of completeness calculations for the 30 minimum deswarmed catalog.....	48
5.7.	Earthquakes used to calculate $b$ -values for the various deswarmed and non-deswarmed catalogs.....	50
5.8.	$b$ -value maps for the various catalogs shown in Figure 5.7.....	51
5.9.	Utsu test results comparing the various $b$ -value maps.....	52
5.10.	Utsu test and frequency-magnitude distribution comparison for the 30 minimum $b$ -value map vs. the 50 minimum $b$ -value map.....	54
5.11.	Spatial $b$ -value distribution for the 30 minimum deswarmed catalog.....	55
5.12.	Errors in the $b$ -value calculation.....	57
5.13.	$b$ -values with depth.....	58
5.14.	$b$ -values through time.....	60
6.1.	Epicenters and hypocenters for the A & B quality earthquakes from 1973 – 1981 and 1984 - 2003.....	67
6.2.	Partial melt and CO <sub>2</sub> gas bodies imaged by local earthquake tomography .....	68
6.3.	Data visualization of Yellowstone’s magma chamber and earthquake swarms.....	70
6.4.	Data visualization of panoramic photos and GPS benchmarks.....	71
6.5.	The Yellowstone-Teton Epicenter.....	73
7.1	High $b$ -value areas indicative of the presence of magmatic fluids.....	78
B.1.	Number of earthquakes vs. time for swarm numbers 1 – 6.....	93
B.2.	Number of earthquakes vs. time for swarm numbers 7 – 12.....	94
B.3.	Number of earthquakes vs. time for swarm numbers 13 – 18.....	95
B.4.	Number of earthquakes vs. time for swarm numbers 19 – 24.....	96
B.5.	Number of earthquakes vs. time for swarm numbers 25 – 30.....	97

B.6.	Number of earthquakes vs. time for swarm numbers 31 – 36.....	98
B.7.	Number of earthquakes vs. time for swarm numbers 37 – 42.....	99
B.8.	Number of earthquakes vs. time for swarm numbers 43 – 48.....	100
B.9.	Number of earthquakes vs. time for swarm numbers 49 – 54.....	101
B.10.	Number of earthquakes vs. time for swarm numbers 55 – 60.....	102
B.11.	Number of earthquakes vs. time for swarm numbers 61 – 66.....	103
B.12.	Number of earthquakes vs. time for swarm numbers 67 – 72.....	104
B.13.	Number of earthquakes vs. time for swarm numbers 73 – 78.....	105
B.14.	Number of earthquakes vs. time for swarm numbers 79 – 84.....	106
B.15.	Number of earthquakes vs. time for swarm numbers 85 – 90.....	107
B.16.	Number of earthquakes vs. time for swarm numbers 91 – 96.....	108
B.17.	Number of earthquakes vs. time for swarm numbers 97 – 102.....	109
B.18.	Number of earthquakes vs. time for swarm numbers 103 – 108.....	110
B.19.	Number of earthquakes vs. time for swarm numbers 109 – 114.....	111
B.20.	Number of earthquakes vs. time for swarm numbers 115 – 120.....	112
B.21.	Number of earthquakes vs. time for swarm numbers 121 – 126.....	113
B.22.	Number of earthquakes vs. time for swarm numbers 127 – 132.....	114
B.23.	Number of earthquakes vs. time for swarm numbers 133 – 138.....	115
B.24.	Number of earthquakes vs. time for swarm numbers 139 – 144.....	116
B.25.	Number of earthquakes vs. time for swarm numbers 145 – 150.....	117
B.26.	Number of earthquakes vs. time for swarm numbers 151 – 156.....	118
B.27.	Number of earthquakes vs. time for swarm numbers 157 – 162.....	119
B.28.	Number of earthquakes vs. time for swarm numbers 163 – 168.....	120

B.29.	Number of earthquakes vs. time for swarm numbers 169 – 174.....	121
B.30.	Number of earthquakes vs. time for swarm numbers 175 – 180.....	122
B.31.	Number of earthquakes vs. time for swarm numbers 181 – 186.....	123
B.32.	Number of earthquakes vs. time for swarm numbers 187 – 192.....	124
B.33.	Number of earthquakes vs. time for swarm numbers 193 – 198.....	125
B.34.	Number of earthquakes vs. time for swarm numbers 199 – 204.....	126
B.35.	Magnitude vs. time for swarm numbers 1 – 16.....	127
B.36.	Magnitude vs. time for swarm numbers 17 - 32.....	128
B.37.	Magnitude vs. time for swarm numbers 33 - 48.....	129
B.38.	Magnitude vs. time for swarm numbers 49 - 64.....	130
B.39.	Magnitude vs. time for swarm numbers 65 - 80.....	131
B.40.	Magnitude vs. time for swarm numbers 81 - 96.....	132
B.41.	Magnitude vs. time for swarm numbers 97 - 112.....	133
B.42.	Magnitude vs. time for swarm numbers 113 - 128.....	134
B.43.	Magnitude vs. time for swarm numbers 129 - 144.....	135
B.44.	Magnitude vs. time for swarm numbers 145 - 160.....	136
B.45.	Magnitude vs. time for swarm numbers 161 - 176.....	137
B.46.	Magnitude vs. time for swarm numbers 177 - 192.....	138
B.47.	Magnitude vs. time for swarm numbers 193 – 204.....	139
C.1.	Swarm epicenter maps for swarms 1 – 14.....	141
C.2.	Swarm epicenter maps for swarms 15 - 28.....	142
C.3.	Swarm epicenter maps for swarms 29 - 42.....	143
C.4.	Swarm epicenter maps for swarms 43 - 56.....	144

C.5.	Swarm epicenter maps for swarms 57 - 70.....	145
C.6.	Swarm epicenter maps for swarms 71 - 84.....	146
C.7.	Swarm epicenter maps for swarms 85 - 98.....	147
C.8.	Swarm epicenter maps for swarms 99 - 112.....	148
C.9.	Swarm epicenter maps for swarms 113 - 126.....	149
C.10.	Swarm epicenter maps for swarms 127 - 140.....	150
C.11.	Swarm epicenter maps for swarms 141 - 154.....	151
C.12.	Swarm epicenter maps for swarms 155 - 168.....	152
C.13.	Swarm epicenter maps for swarms 169 - 182.....	153
C.14.	Swarm epicenter maps for swarms 183 - 196.....	154
C.15.	Swarm epicenter map for swarms 197 - 204.....	155

## LIST OF TABLES

### Table

3.1.	Earthquake magnitude statistics for the Yellowstone region from 1973-2002.....	16
4.1.	Definition of quality classes for earthquake locations of the Yellowstone earthquake catalog.....	26
5.1.	Summary of deswarming results.....	38
5.2.	Magnitude of completeness ( $M_{COMP}$ ) values for selected spatial and temporal areas.....	47
5.3.	Earthquakes used to calculate $b$ -values.....	47
6.1.	Earthquake arrival data (Level 1 (raw) data) .....	66
A.1.	Table of Yellowstone earthquake swarms.....	87

## ACKNOWLEDGEMENTS

I would first like to thank my wonderful wife Nicole for her unending patience and understanding as I pursued my master's degree. Without her support and encouragement none of this would be possible. I would also like to thank my wonderful family for all their words of encouragement as well.

Numerous individuals deserve recognition in helping me with my master's research while here at the University of Utah. First and foremost I would like to thank Robert B. Smith for his leadership and guidance. He not only helped me become a better scientist but he taught me how to be a better person. Learning from his work ethic and love of Yellowstone will help me throughout my career as a geophysicist. He has always provided me with the funding needed to carry out my research to the best of my ability and I thank him immensely for that.

Stephan Husen has also been instrumental in the completion of this project. Without his help with earthquake relocation and *b*-value calculations, this project probably would not have been completed. Stephan taught me not only how to approach and solve many problems, but he also made sure I understood each step along the way. He has been a great example to me and I appreciate it very much.

Chuck Meertens also helped me immensely with data visualization. His suggestions and guidance have enhanced the scope and breadth of my research. He has taught me how to be a true professional and has opened doors to me that will be

invaluable during my career. I would also like to thank him for always being willing to answer my questions during his busy schedule.

Greg Waite provided me with his swarm identification algorithm and also helped me with my research whenever I asked him for it. Michael Jordan provided me with help and insight on this project as well.

I must also thank Randy Keller and Krishna Sinha of the University of Oklahoma and Virginia Tech for their help and guidance throughout this project. Jim Pechmann, Kristine Pankow, Relu Burlacu, Michelle Kline, and Paul Roberson of the University of Utah Seismograph Stations are also much appreciated for providing me with both insight and data when needed. Dave Drobeck has given me multiple opportunities to learn from him on installing and maintaining seismic and GPS equipment in the field and I am grateful for that. Debi Kilb, Atul Nayak, and Evan Morikawa of the University of California, San Diego SCRIPPS Institute of Oceanography have been instrumental in helping me import my data into the Fledermaus software suite. Henry Heasler and Cheryl Jaworski of the National Park Service have greatly aided me in obtaining data from Yellowstone National Park and have also answered many of my GIS questions. Figures were made using the Generic Mapping Tool (GMT) [Wessel & Smith, 1998].

I would also like to thank my fellow students at the University of Utah for all their help as well. To all of my office mates and friends — Greg Waite, Michael Jordan, Christine Puskas, Wu-Lung Chang, Aaron DeNosaquo, Katrina Settles, and Julie Willis — thanks.

Last but not least I would like to thank Mickey Begent, Dan Trentman, Erwin McPherson, and Ali Moeinvaziri for computational support.

This project was funded in part by the NSF funded GEOsciences Network (GEON) project, EAR-0724265; the USGS Yellowstone Volcano Observatory, Volcano Hazards Program cooperative agreement no: 04HQAG0019; Yellowstone National Park; and the University of Utah Department of Geology and Geophysics.

## CHAPTER 1

### INTRODUCTION

#### 1.1. Yellowstone Seismicity

Yellowstone has been one of the most seismically active areas in the Intermountain Seismic Belt (ISB) of the western U.S. with over 26,000 located earthquakes ( $-1.0 < M_C < 6.1$ ) and at rates of up to 883 events per month from 1973 to 2003 [Smith & Arabasz, 1991] (Figure 1.1). Furthermore, the Yellowstone area has experienced the largest historic earthquake in the ISB; the August,  $M_S 7.5$  1959 Hebgen Lake, Montana, earthquake located  $\sim 25$  km northwest of the Yellowstone caldera [Doser, 1985]. The caldera has also experienced a  $M_L 6.1$  earthquake in 1975 southeast of Norris Junction [Pitt et al., 1979, Smith & Arabasz, 1991].

Overall, seismic activity in Yellowstone is characterized by swarms of small, generally shallow earthquakes. The most intense seismicity extends from the Hebgen lake area east to the northern caldera boundary near Norris Junction. Although this area only constitutes 16% of the area, it contains 75% of the epicenters. Linear bands of epicenters within and adjacent to the caldera are aligned generally north-northwest parallel to alignments of postcaldera volcanic vents and large regional faults. These normal faults are cut by the 0.64 Ma caldera and are believed to once be continuous Basin-Range faults [Smith & Seigel, 2000] (Figure 1.1).

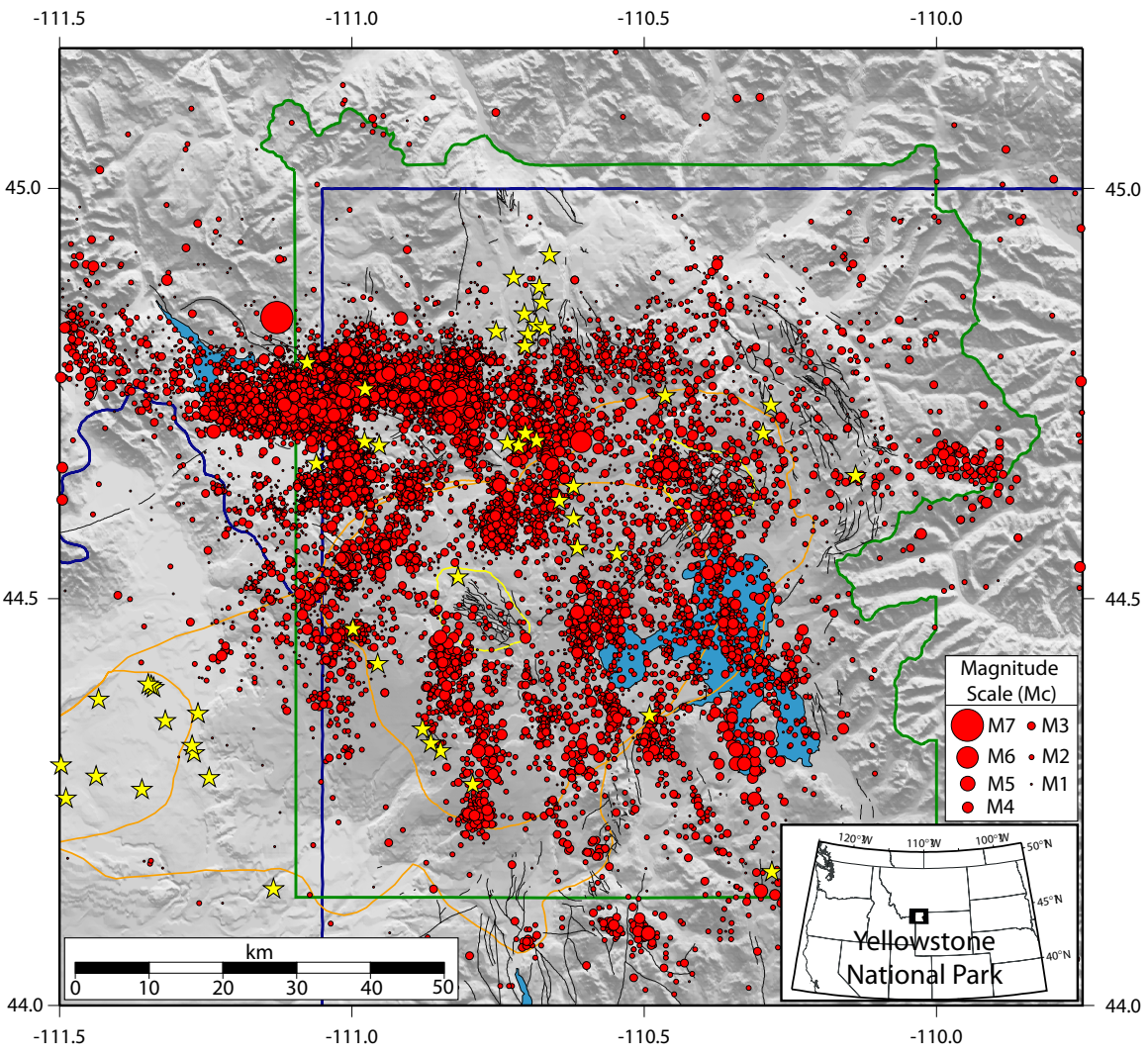


Figure 1.1. Earthquakes in Yellowstone from 1973 - 1981 and 1984 - 2003. Epicenters are shown as red dots, postcaldera vents are shown as yellow stars, and Quaternary faults are shown as black lines. The outlines of the calderas from the last major Yellowstone eruptions are shown in orange. The two resurgent domes are outlined in yellow.

## 1.2. Objectives

The main objectives of this study are (1) to determine the frequency of occurrence of earthquakes, parameterized by the frequency of occurrence parameter called the *b*-value and (2) to develop a GEON (NSF funded Geology in Cyberstructure) GIS database and related graphical tools for geographical, geological, and geophysical datasets related to the Yellowstone hotspot.

Yellowstone is a seismically active area of the western U.S., experiencing the largest historic earthquake in the western U.S. interior of M 7.5 and dominant earthquake swarms that are considered the product of the interaction between Yellowstone's active volcanic processes and large Basin-Range normal faults. However, it is not well understood how the volcanic and the tectonic stresses interact.

The large amount and relatively high quality of the Yellowstone earthquake data make it possible to calculate the *b*-value distribution in the Yellowstone region. Mapping the *b*-values allows one to estimate the relative stress patterns in the area as well as correlate results with previous studies.

The Yellowstone area is a geologically and geophysically well-studied volcanic-tectonic system and is centered at Yellowstone National Park with about 3 million visitors per year. Yellowstone is also a dynamic silicic volcanic system as well so studies are repeated year after year to update results. It can be difficult to focus on a particular topic when searching the literature due to the high amount of data available. The development of a Yellowstone GIS database allows for a central location of data pertaining to the Yellowstone system. Researchers as well as laypersons can access the database anytime and from virtually anywhere and get the datasets that they wish.

Integration of different types of data is needed to better understand what is driving the Yellowstone system. This database allows a researcher to find datasets of different types and to also access the required metadata and references that explain the origin of the data. Studies that use integration of different datasets will help to answer some of the more in depth questions and help us understand how the Yellowstone volcanic system works. For example, although much can be learned from seismic studies and GPS studies alone, integrating these data helps to explain the physics of the volcanic system much better.

## CHAPTER 2

### YELLOWSTONE VOLCANO-MAGMATIC SETTING

#### 2.1. Regional Geology

The crustal structure of the Yellowstone region has been modified by volcanism and lithospheric compression and extension throughout geologic time from the Precambrian to the present. More recent episodes of deformation are superimposed on those that are older. Rocks dating back to the Precambrian are present in Yellowstone in the form of gneisses and schists exposed in parts of the Gallatin Mountain Range. However, it was not until the Laramide that forces began shaping the land into what we see today in Yellowstone. During the Laramide orogeny the middle and southern Rocky Mountains that border the Yellowstone Plateau to the north, east, and south were formed. The Laramide was a period of folding and thrusting which culminated at about 65 Ma. Large crustal blocks were forced up along thrust faults and folded, creating ranges. A period of andesitic volcanism in and around the Yellowstone region followed the end of the Laramide orogeny from 55 Ma to 40 Ma ago and formed the Absaroka Range (Figure 2.1).

The Basin and Range epeirogeny, a broad zone of intraplate extension, formed during the Miocene and consists of a series of N-S trending subparallel mountain ranges bounded by normal faults spaced at roughly 25 km intervals separated by alluvial-filled

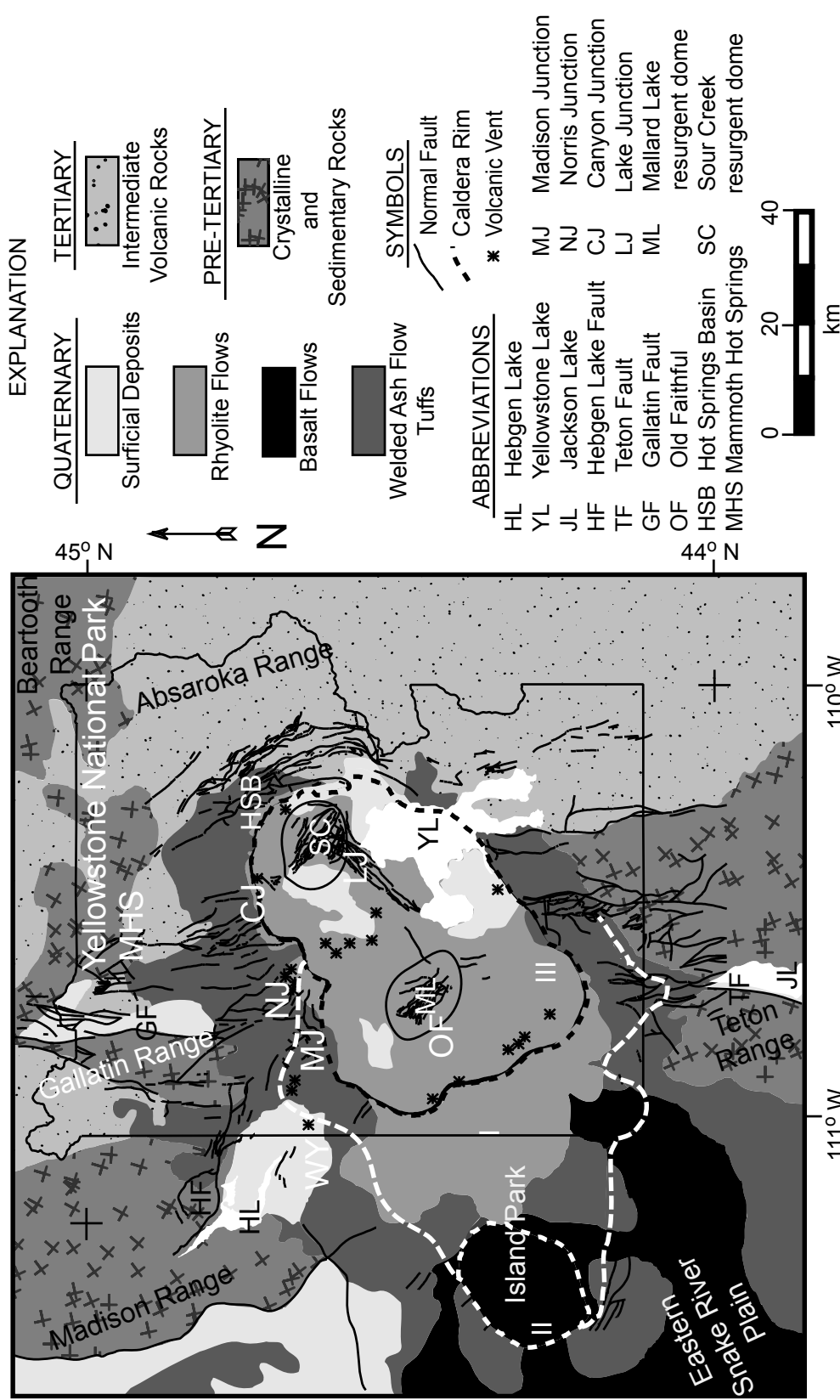


Figure 2.1. General geologic map of the Yellowstone Plateau modified from Miller [1994]. Quaternary normal faults, volcanic vents, and major surface rock types are shown including the rhyolite caldera fill, welded ash flows, and the basalt flows of the Snake River Plain. Roman numerals refer to the calderas shown in Figure 1.1. Mountain ranges are labeled.

basins. The Basin and Range system is characterized by relatively high topography (averaging 1,250 m), high regional heat flow of  $\sim 90 \text{ mW m}^{-2}$ , a history of late Cenozoic silicic-basaltic volcanism, Quaternary normal faulting, and historic earthquake activity exceeding magnitude 7 [Dickinson, 2006; Smith et al., 1989a]. The continued stretching of the crust in the Basin and Range has resulted in a crustal thickness of about 30 km in the central portion of the province as opposed to a crustal thickness of  $\sim 40$  km in the Colorado Plateau [Smith & Arabasz, 1991]. The stretching and thinning of the Basin and Range lithosphere amplified extension and reduced horizontal stress that allowed the Yellowstone plume to ascend buoyantly, penetrate the crust and reach the surface.

The Snake River Plain volcanic field begins in SE Oregon-Southern Idaho and extends northeast 800 km to Yellowstone. It is a bimodal rhyolite-basalt volcanic province that is considered the result of southwest movement of the North America Plate across a mantle magma source. The Yellowstone - Snake River Plain (YSRP) is composed of rhyolite and basalt flows that were erupted as the North American Plate moved over the hotspot that now lies below Yellowstone [Smith and Braille, 1994]. Silicic volcanic centers decrease in age from 16 Ma at the southwestern end of the Snake River Plain to 0.64 Ma in Yellowstone [Armstrong et al., 1975; Pierce & Morgan, 1992; Perkins & Nash, 2002; Christiansen, 2001] (Figure 2.2). Ashfall deposits analyzed by Perkins & Nash [2002] suggest there were 142 caldera-forming eruptions, in a dozen volcanic centers, along the track of the Yellowstone hotspot.

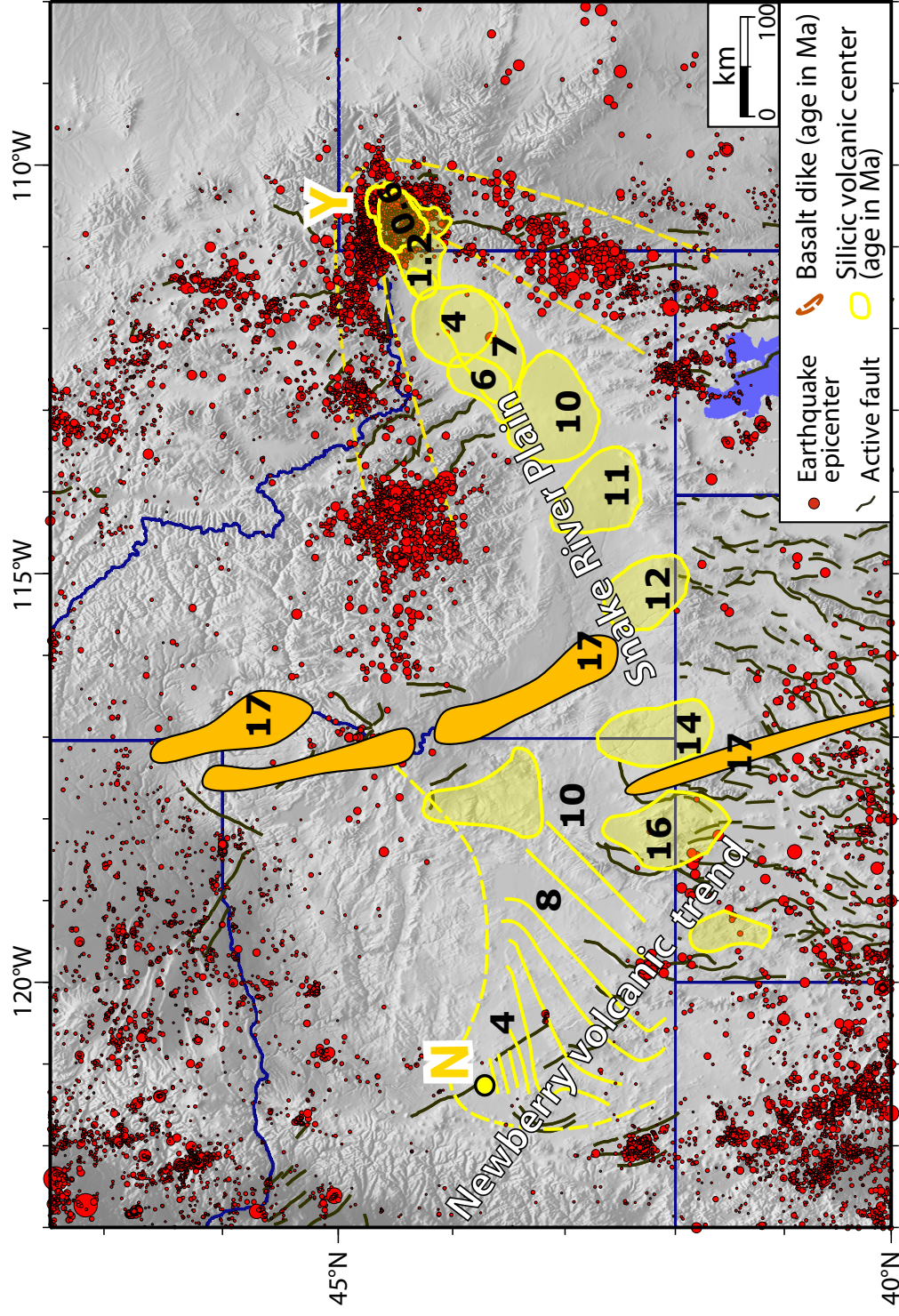


Figure 2.2. Map of the Yellowstone-Snake River Plain-Newberry system modified from Smith and Siegel [2000]. Earthquakes are shown as red circles. Caldera forming events are shown as yellow circles with their corresponding age in millions of years. N and Y mark the spots of the Newberry and Yellowstone hotspots respectively.

## 2.2. Volcanic History

The Yellowstone volcanic system centered at the Yellowstone National Park, Wyoming is one of the largest and most active silicic volcanic systems in the world [Christiansen, 2001]. It forms a topographically high plateau of ~500 m excess elevation as the result of hotspot tumescence. The youthful volcanic history of Yellowstone is dominated by three cataclysmic caldera-forming eruptions in the past two million years [Christiansen, 2001]. The first and largest of the three caldera-forming eruptions occurred 2.0 Ma and ejected a volume of more than 2,500 km<sup>3</sup> of material that formed the Huckleberry Ridge Tuff [Christiansen, 2001]. The Mesa Falls Tuff was erupted at 1.2 Ma and the youngest of the three caldera-forming events erupted ~1,000 km<sup>3</sup> of material at 0.64 Ma and erupted the Lava Creek Tuff [Christiansen, 2001]. This latest eruption created what we refer to as the Yellowstone caldera, which measures roughly 40 x 60 km long. After the latest caldera-forming eruption (0.64 Ma) the Mallard Lake resurgent dome formed in the southwest portion of the caldera. At around 0.16 Ma the Sour Creek resurgent dome formed in the northeast portion of the caldera (Figure 2.3). In the last 640,000 years, at least 30 much smaller rhyolitic and basaltic flows as young as 70,000 years old have covered much of Yellowstone today.

## 2.3. Geophysical Characteristics

Bouguer gravity measurements show a large negative, -60 mGal, anomaly centered over the Yellowstone caldera with an additional -20 mGal anomaly north of Sour Creek dome [Lehman et al., 1982] (Figure 2.4). Crustal models based on the Bouguer gravity anomaly by Lehman et al. [1982] reveals: (1) an upper 2.4-2.5 g/cm<sup>3</sup>

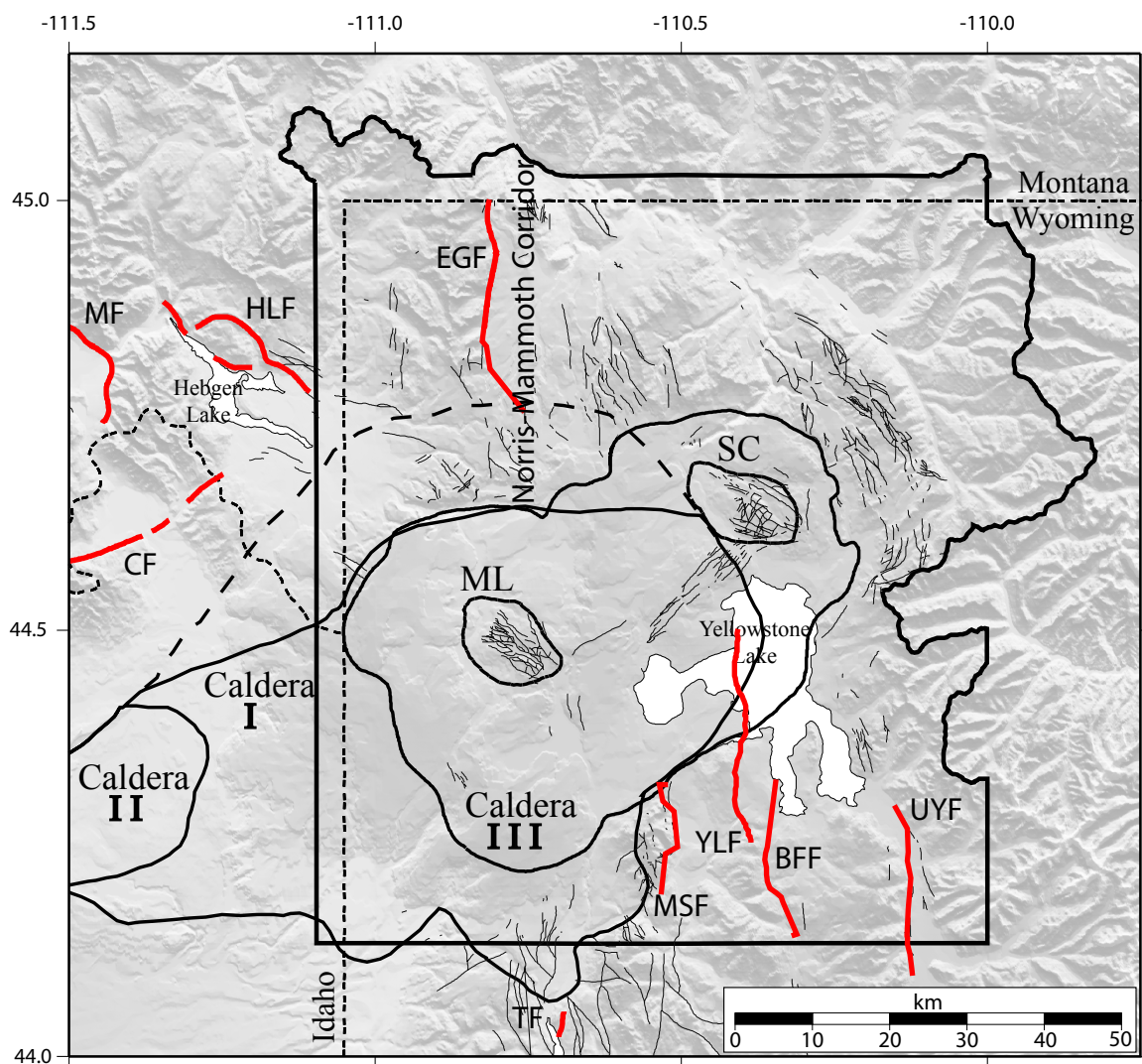


Figure 2.3. A topographic map of the Yellowstone volcanic field showing the three calderas and Cenozoic faults as mapped by Christiansen [2001]. Major faults are shown in red. MF = Madison fault, HLF = Hebgen Lake fault, CF = Centennial fault, EGF = East Gallatin fault, TF = Teton fault, MSF = East Mt. Sheridan fault, YLF = Yellowstone Lake fault, BFF = Buffalo Fork fault, and UYF = Upper Yellowstone Valley fault. The calderas are shown by age: I-2.0 Ma, II-1.2 Ma, and III-0.64 Ma. The dashed line outlines a region of highly fractured crust and high seismicity that may mark the extent of caldera I. The northern boundary of that region is highlighted by a topographic contrast that may have resulted from the 2.1 Ma catastrophic eruption. ML and SC represent the Mallard Lake and Sour Creek resurgent domes which are outlined with a dashed line (modified from Waite [1999]).

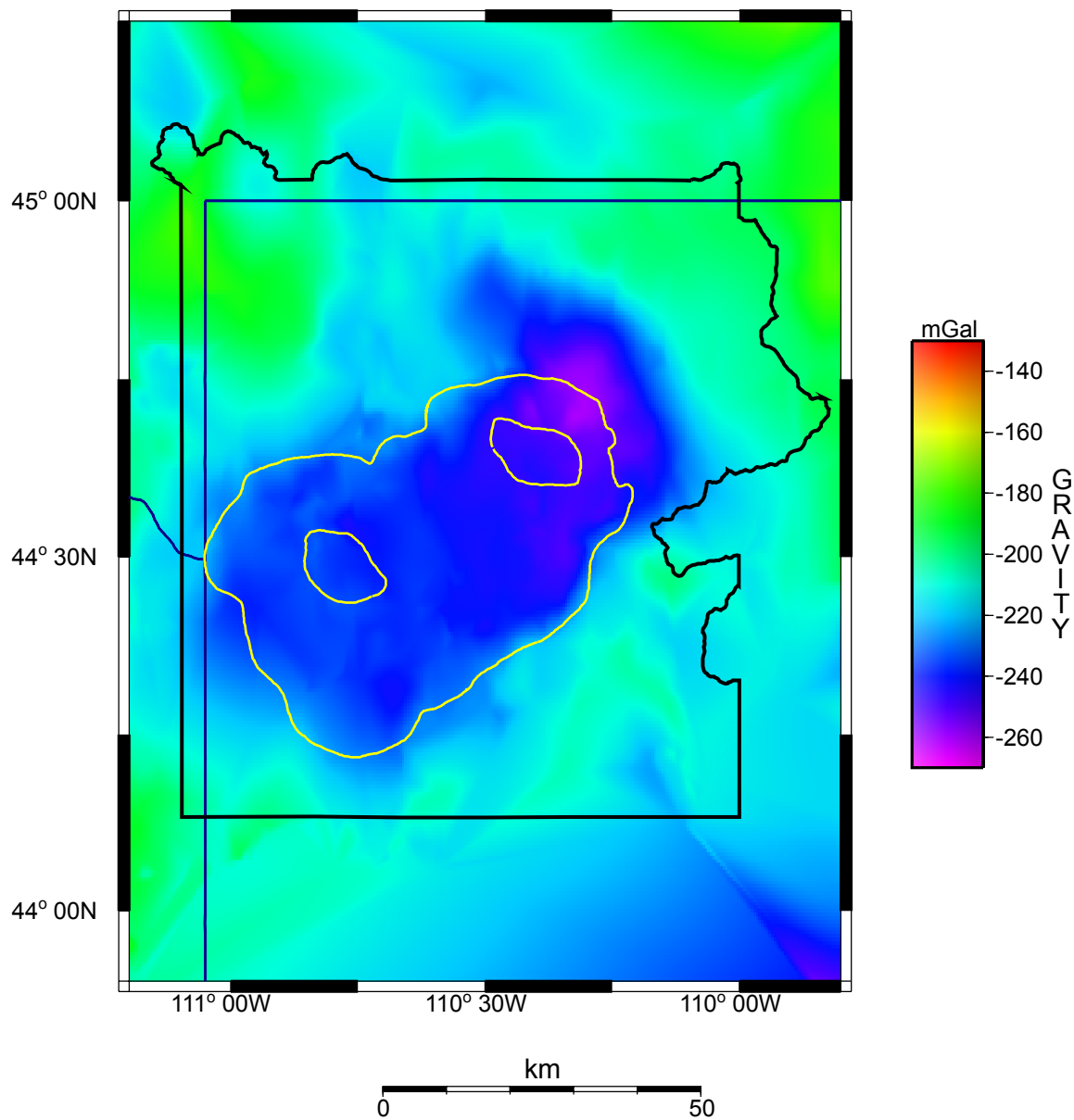


Figure 2.4. Complete Bouguer gravity anomaly map of Yellowstone National Park modified from Krukoski [2002]. Black outline is the National Park boundary. Yellow outlines the 0.64 Ma caldera and resurgent domes, Mallard Lake (SW) and Sour Creek (NE).

layer, 1-2 km thick corresponding to caldera sediment fill and rhyolite flows; (2) a 2.6-2.7 g/cm<sup>3</sup> upper-crustal layer beneath most of the caldera which is interpreted to be a hot but generally solid, granitic layer; and (3) an unusually low-density body of 2.4 g/cm<sup>3</sup> at depths of 1 to ~10 km beneath the northeast caldera which is consistent with models ranging from thick sediment fill, to hydrothermally altered near-surface material underlain by a body dominated by hydrothermal fluids or silicic partial melts of up to 15% [Lehman et al., 1982].

With over 10,000 geysers, hot springs, and fumaroles, Yellowstone has the world's highest concentration of hydrothermal features (Figure 2.5). This large hydrothermal system is, in general, the result of hot water circulating along fractures in the crust heated from below by crystallizing magma (Fournier, 1989).

The crustal structure of Yellowstone has a magmatic and shallow gas system identified by seismic tomographic imaging [Husen et al., 2004a]. A low P-wave velocity ( $V_P$ ) body in the upper crust beneath the caldera at  $\geq 8$  km has been imaged by local earthquake tomography (Benz & Smith, 1984; Miller & Smith, 1999; Husen et al., 2004a) and has been interpreted to be a hot body with up to a few percent partial melt. An additional low  $V_P$  and  $V_P/V_S$  body is resolved in the northwestern part of the Yellowstone volcanic field at shallow depths of  $< 2.0$  km. Theoretical calculations of changes in P- to S-wave velocity ratios indicate that this anomaly can be interpreted as porous, gas-filled rock [Husen et al., 2004a].

Perhaps one of the most striking features of the Yellowstone hotspot is its extraordinarily high heatflow. The presence of crystallizing magma at shallow depths (~8km) feeds the regional heat flow at Yellowstone, estimated at more than 2,000

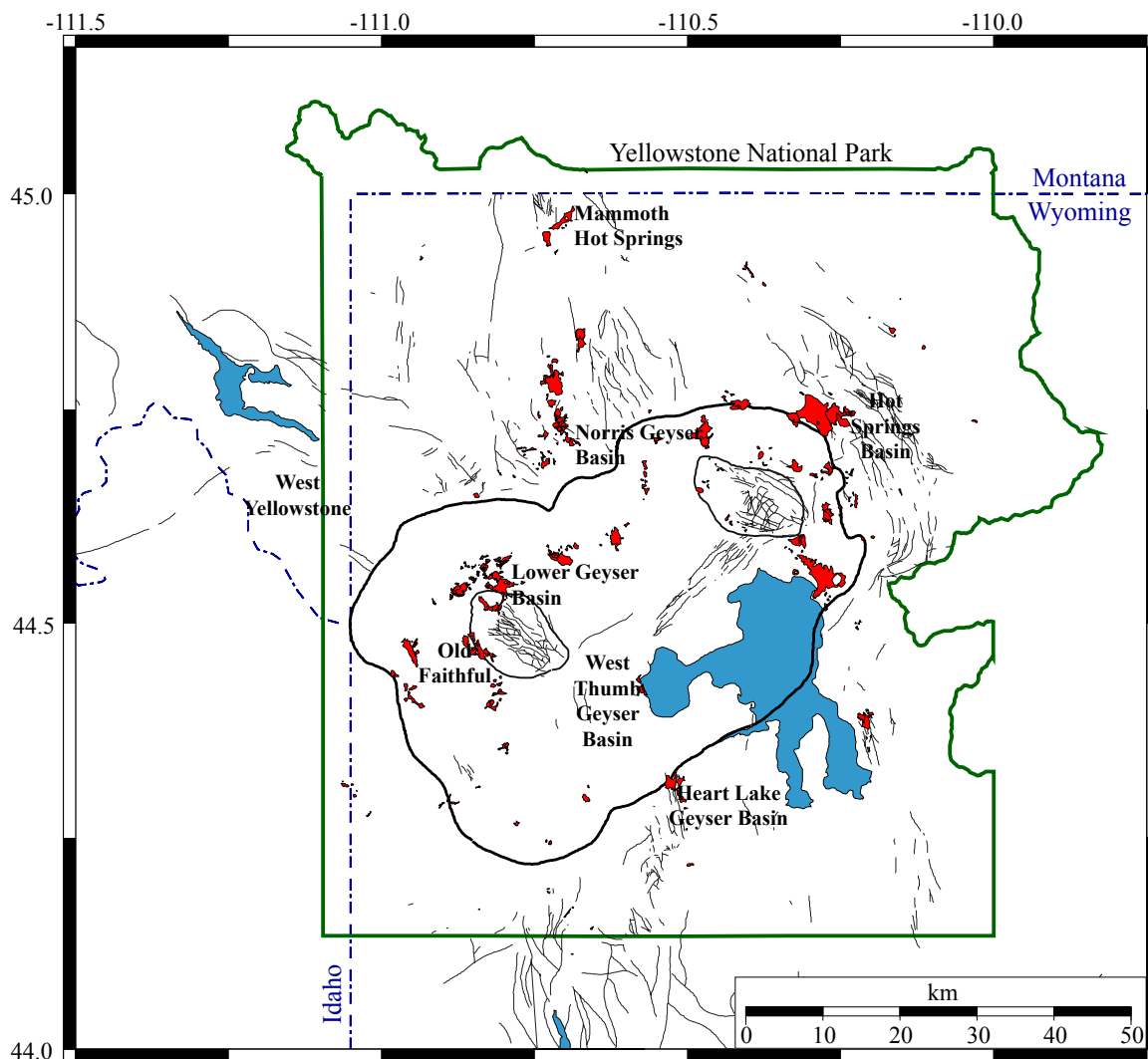


Figure 2.5. Index map of Yellowstone showing hydrothermal features as well as Quaternary faults mapped by Christiansen [2001]. Areas of hydrothermal activity are shown in red. The boundary of Yellowstone National Park, major lakes, and the 0.64 Ma caldera boundary are shown. Major hydrothermal areas are labeled.

$\text{mW/m}^2$  [Blackwell, 1969; Fournier, 1989] that is more than 30 times the continental average. Given a conductive heat flow of  $\sim 200 \text{ mW/m}^2$ , the Nusselt number for the Yellowstone caldera is  $\sim 10$ . This compares to values of  $\sim 6$  to 8 for the Long Valley caldera in eastern California [Hill, 1992].

## CHAPTER 3

### SEISMICITY AND DEFORMATION OF THE YELLOWSTONE REGION

#### 3.1. Yellowstone Earthquakes

Over 26,000 earthquakes were recorded in the Yellowstone region during the time period 1973 to 2003, making it one of the most seismically active areas in the western U.S. interior. [Smith & Arabasz, 1991]. Moreover, the Yellowstone area has experienced the largest historic earthquake in the western U.S. interior; the August,  $M_S 7.5$  1959 Hebgen Lake, Montana, earthquake, that was located ~25 km northwest of the Yellowstone caldera [Doser, 1985] and the 1975  $M_L 6.1$  Norris Junction earthquake [Pitt et al., 1979]. Overall, earthquake activity in Yellowstone is characterized by swarms of small, generally shallow earthquakes, especially northwest of the caldera (Figure 1.1).

In general, swarms are defined as clusters of earthquakes in time and space characterized by an increase in the seismicity rate followed by a decrease in seismicity rate without a mainshock. Essentially all the earthquakes in the catalog have magnitudes less than or equal to  $M_c = 4.0$ ; 99.0% have  $M_c \leq 3.0$ ; 90.3% have  $M_c \leq 2.0$ ; and 50.9% have  $M_c \leq 1.0$  (Table 3.1).

Table 3.1

Earthquake magnitude statistics for the  
Yellowstone region from 1973-2002

$M_C$	% of Earthquakes $\leq M_C$
4.0	99.9
3.0	99.0
2.0	90.3
1.0	50.9

The area where the majority of Yellowstone earthquakes occur extends from the Hebgen lake area east to the northern caldera boundary near Norris Junction (Figure 1.1). Linear bands of seismicity within and adjacent to the caldera are aligned north-northwest parallel to alignments of postcaldera volcanic vents and large regional normal faults. The normal faults are truncated by the caldera boundary faults and are believed to once be continuous Basin-Range faults before the 0.64 Ma old eruption [Christiansen, 2001].

The largest earthquake swarm recorded in Yellowstone occurred in October of 1985, which consisted of over 3000 earthquakes ( $M_C < 5$ ) and spanned more than 3 months [Waite & Smith, 2002]. The temporal pattern of epicenters of the 1985 swarm suggests migration laterally, NW, away from the 0.64 Ma caldera at an average rate of 150 m/d. The swarm occurred around the same time the caldera changed from uplift to subsidence (see Geodetic Data from GPS, InSAR, and Leveling section below). Waite and Smith [2002] suggested that the subsidence was partially accommodated by the migration of magma-derived fluids out of the caldera toward the northwest. The most likely scenario explaining this process involves the rupture of a self-sealed hydrothermal layer and subsequent migration of hydrothermal fluids through a preexisting fracture

zone out of the caldera causing the earthquakes of the 1985 swarm [Waite & Smith, 2002].

### 3.2. Remotely Triggered Earthquakes in Yellowstone

Earthquakes are considered to be triggered if they were induced by either dynamic or static stress changes from the rupture of another earthquake. Static stress changes are measured as the difference in the stress field from just before an earthquake to shortly after the seismic waves have decayed. Dynamic stresses are generally thought to be induced by the seismic waves, usually surface waves, from a large earthquake [Hill et al., 2002].

For example, static stress changes decay rapidly, as  $1/r^3$ , where  $r$  is the distance from the earthquake epicenter. Static stress changes are generally limited to distances of just a few fault lengths from the initial earthquake and lag times of months to years [Hill et al., 2002]. Dynamic stress changes in general have lag times of minutes to hours and decay with distance as roughly  $1/r^2$  to  $1/r$  for seismic body waves and surface waves respectively [Hill et al., 2002].

Triggered earthquakes have been recorded in Yellowstone for both the  $M_w$  7.3 1992 Landers, CA earthquake, located ~190 km west of Los Angeles, CA (1250 km away) [Hill et al., 1993] and the  $M_w$  7.9 2002 Denali fault, Alaska earthquake (3100 km away) [Husen et al., 2004b, 2004c].

Following the Landers earthquake 16 remotely triggered earthquakes were detected in Yellowstone [Hill et al., 1993]. However, in 1992 the Yellowstone seismic network consisted of only short period seismometers whose signals were saturated by the

high amplitude surface waves due to their limited dynamic range. Therefore, it was difficult to identify events during the passage of the surface waves. Within the first 24 hours after the arrival of the Denali fault earthquake surface waves, 250 earthquakes were located in Yellowstone including 11 earthquakes with  $M_C > 2.5$  compared to nine earthquakes with  $M_C > 2.5$  in all of 2002 prior to the Denali fault earthquake [Husen et al., 2004b, 2004c]. Within the first 2 hours following the Denali fault earthquake, triggered earthquakes clustered close to three major hydrothermal areas in Yellowstone: (1) at Upper geyser basin (swarm 179 in Appendix A, B, & C), (2) at West Thumb geyser basin (swarms 180 and 187 in Appendix A, B, & C), (3) and at the north end of Yellowstone Lake basin (swarm 181 in Appendix A, B, & C). Earthquakes following the Denali fault earthquake gradually decayed by roughly 1.5 events/day over the following weeks and finally returned to background levels 0.7 events/day (of  $M_C \geq 1.5$ ) 30 days after the Denali fault earthquake [Husen et al., 2004b, 2004c]. Dynamic stress transients associated with these low-frequency, large-amplitude surface waves are thought to be the dominating triggering mechanism [Hill et al., 1993; Anderson et al., 1994; Gomberg & Bodin, 1994]. Peak dynamic stresses due to the passage of the Denali fault earthquake surface waves were measured in Yellowstone to be as high as 0.22 MPa [Velasco et al., 2004].

### 3.3. Focal Depth Variations Across the Yellowstone Caldera

Focal depth statistics provide vital information on the thermal and stress state beneath the Yellowstone volcanic system. Smith and Bruhn [1984] observed a correlation between the upper crust brittle-ductile transition zone and the maximum, 80<sup>th</sup>

percentile, depth of earthquakes that occur in the Basin and Range extensional environment. This depth has been shown to correspond to a temperature of  $\sim 400^{\circ}\text{C}$  based on petrologic and geochemical studies [Sibson, 1982; Smith & Bruhn, 1984; Fournier, 1999].

In Figure 3.1, the depth above which 80% of the earthquakes in Yellowstone occur is shown. Vertical cross sections reveal a shallowing of seismicity across the caldera. Most of the earthquakes within the caldera are shallower than 5 km. Outside the 0.64 Ma caldera, to the northwest and southeast, focal depths increase markedly to more than 10 km. The deepest events in the Yellowstone region are in the Hebgen Lake region and are located at 10-15 km depth [Husen & Smith, 2004]. This shallowing of earthquakes within the caldera has been attributed to a decrease in the depth of the brittle-ductile transition zone due to elevated temperatures from the underlying crystallizing magma [Smith & Arabasz, 1991; Miller & Smith, 1999].

#### 3.4. Focal Mechanisms and Stress Orientations

Focal mechanisms provide information on the regional stress pattern. Waite and Smith [2004] computed 346 focal mechanisms for the Yellowstone region for the period 1973-1998 with 300 of the 346 located in the area between the Hebgen Lake fault and the northwest rim of the Yellowstone caldera. Of those, 148 were found to be oblique-normal, 100 normal, 99 strike slip, 12 oblique-reverse, and 5 reverse focal mechanisms. T-axes from focal mechanisms computed by Waite and Smith [2004] show a rotation from approximately N-S in the Hebgen Lake region to ENE-WSW south of the 0.64 Ma Yellowstone caldera (Figure 3.2). This rotation matches the maximum extensional strain

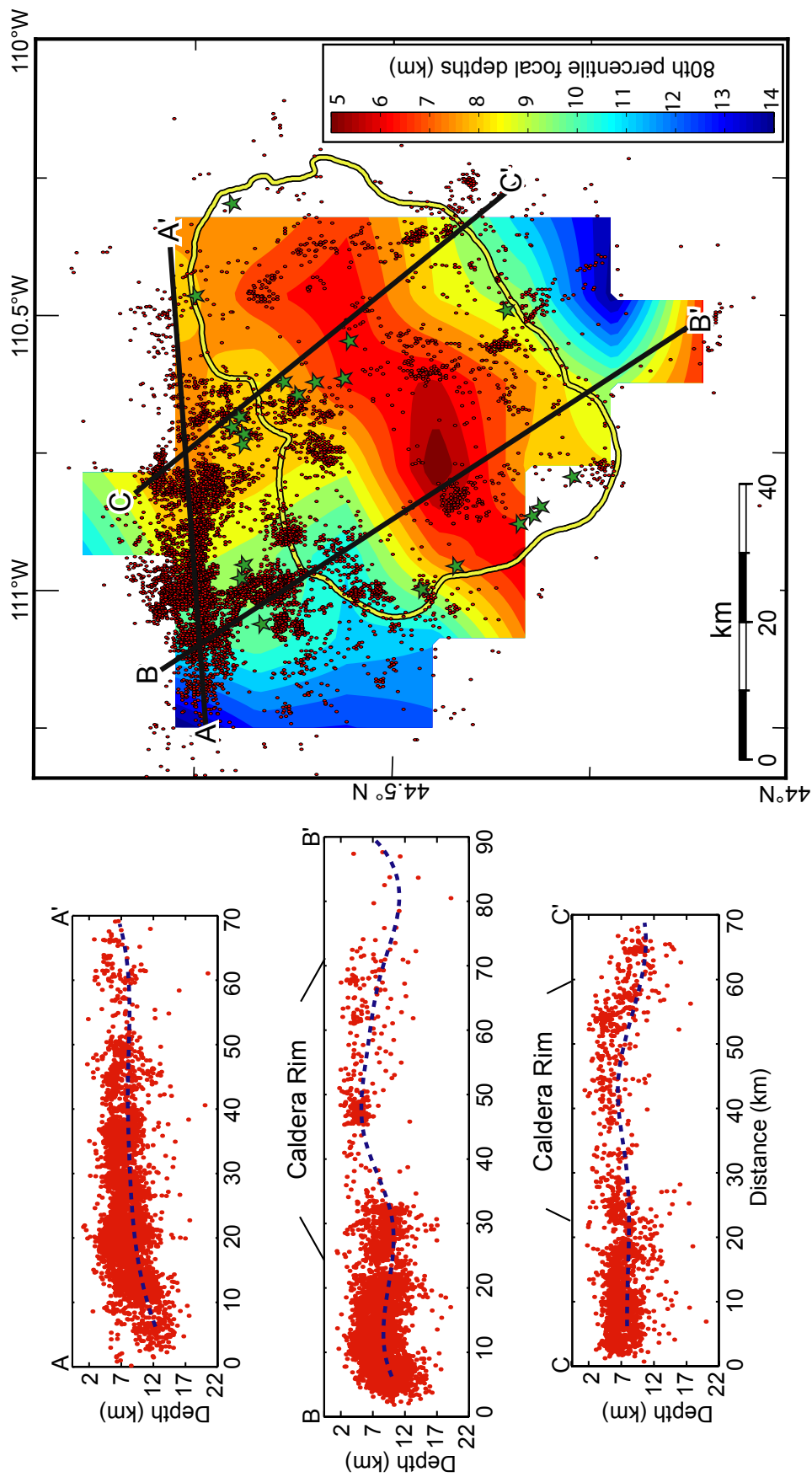


Figure 3.1. Focal depth distribution for A and B quality earthquakes from the years 1973 - 2003 for the Yellowstone region showing the shallowing of hypocenters inside the 0.64 Ma caldera modified from Waite [personal communication]. Color contours in the map as well as the dotted blue lines in the cross-sections are for the 80th percentile focal depths. Locations of the post-caldera volcanic vents are shown as green stars. The 0.64 Ma caldera is outlined in yellow.

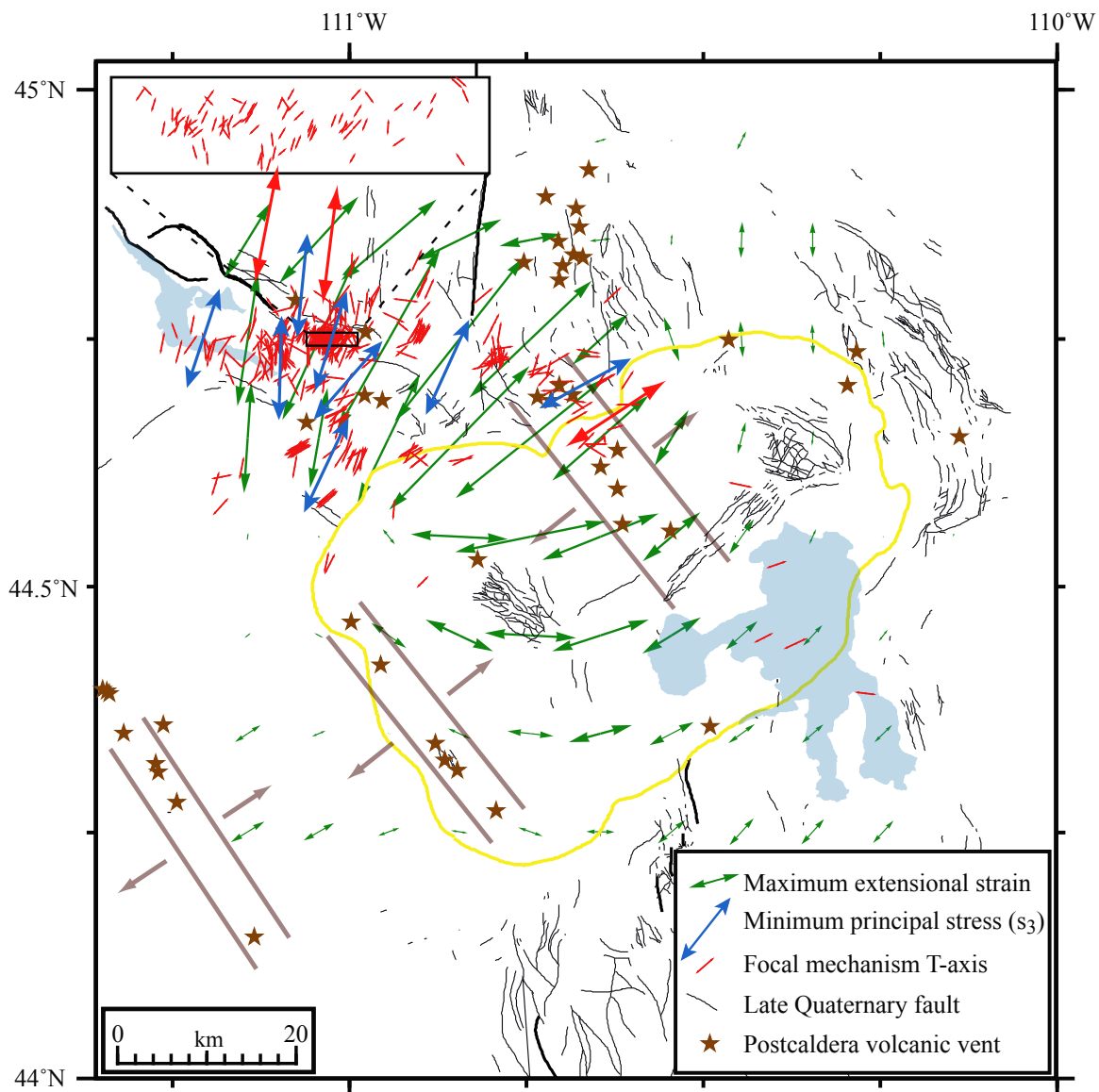


Figure 3.2. Seismic, geodetic, and geologic stress indicators across Yellowstone modified from Waite and Smith [2004].  $T$  axes are shown as small red lines,  $\sigma_3$  directions are shown as large blue arrows, directions of maximum extensional strains from the years 1995-2000, from Puskas et al. [2007], are shown as green arrows. The lengths of the green arrows are proportional to the strain rate. Lines and arrows around the volcanic vents indicate the approximate extension direction that may be inferred from the alignments of the vents.

directions measured by GPS [Puskas et al., 2007]. This rotation occurs in the area just north of the Yellowstone caldera and east of the Hebgen Lake fault where there is the highest amount of seismicity.

### 3.5. Crustal and Mantle Tomography

Four local earthquake tomography studies of Yellowstone [Benz & Smith, 1984; Lynch, 1999; Miller & Smith, 1999; Husen et al., 2004a] have imaged at various resolutions a low (-6%)  $V_p$  body in the upper crust beneath the caldera which has been interpreted as a body of 8-15% partial melt [Miller & Smith, 1999; Husen et al., 2004a]. Due to the addition of several three-component seismographs in the Yellowstone region, Husen et al. [2004a] was able to extend the work of Benz and Smith [1984] and Miller & Smith [1999] by selecting 3,374 local earthquakes between 1995 and 2001, providing 34,538 P-wave times and 5,875 S-P arrival times to image the 3-D  $V_p$  and  $V_p/V_s$  structure of the upper crust beneath Yellowstone. Husen et al. [2004a] imaged a low (-10%)  $V_p$  body at ~2 km depth on the northwest boundary of the caldera as well as a low (-5%)  $V_p/V_s$  body in the same area. This low  $V_p$  and  $V_p/V_s$  body has been interpreted as a CO<sub>2</sub> gas filled body [Husen et al., 2004a].

Two recent teleseismic tomography studies were focused on Yellowstone by Waite et al. [2006] and Jordan et al. [2005]. Teleseismic tomography uses earthquakes at epicentral distances greater than 30° to image the mantle. These teleseismic tomography studies are revealing that low  $V_p$  and  $V_s$  anomalies are present below Yellowstone down to the transition zone (~660 km) [Waite et al., 2006; Jordan et al., 2005]. This low velocity body tilts to the northwest and is about 250 km to the northwest of Yellowstone

in western Montana at its base. The northwest tilt is interpreted to be the result of the plume being entrained in the mantle flow.

### 3.6. Geodetic Data (GPS, InSAR, and Leveling)

Crustal deformation monitoring of Yellowstone by leveling and more recent Global Positioning System (GPS) and Interferometric Synthetic Aperture Radar (InSAR) have shown remarkable ground movement during the last 80 years. This caldera-wide deformation includes uplift of up to 1 m from 1923 to 1984 measured by leveling. Beginning in 1987 the University of Utah began campaign GPS studies in the Yellowstone region. Beginning in 1996 data from continuous GPS stations were used to measure ground deformation as well. From 1987 to the present, all ground velocities were measured from campaign and continuous GPS measurements.

The results show that from 1987-1995 the caldera subsided at a maximum rate of  $-14 \pm 3$  mm/yr centered near the Sour Creek dome (Figure 2.3) for a total of 112 mm. From 1995-2000 the caldera returned to uplift with a maximum rate of  $15 \pm 4$  mm/yr for a total of 75 mm. However the center of uplift during this time period was centered northwest of the caldera in the Norris-Mammoth corridor (Figure 2.3). From 2000-2003 the uplift continued northwest of the caldera at a maximum rate of  $12 \pm 4$  mm/yr for an additional 36 mm of displacement but the central caldera axis returned to subsidence at a maximum rate of  $-9 \pm 6$  mm/yr for an additional 27 mm subsidence [Puskas et al., 2007] (Figure 3.3).

The seismic and ground deformation data are invaluable in interpreting areas of high and low *b*-values in Yellowstone because there are many different scenarios which

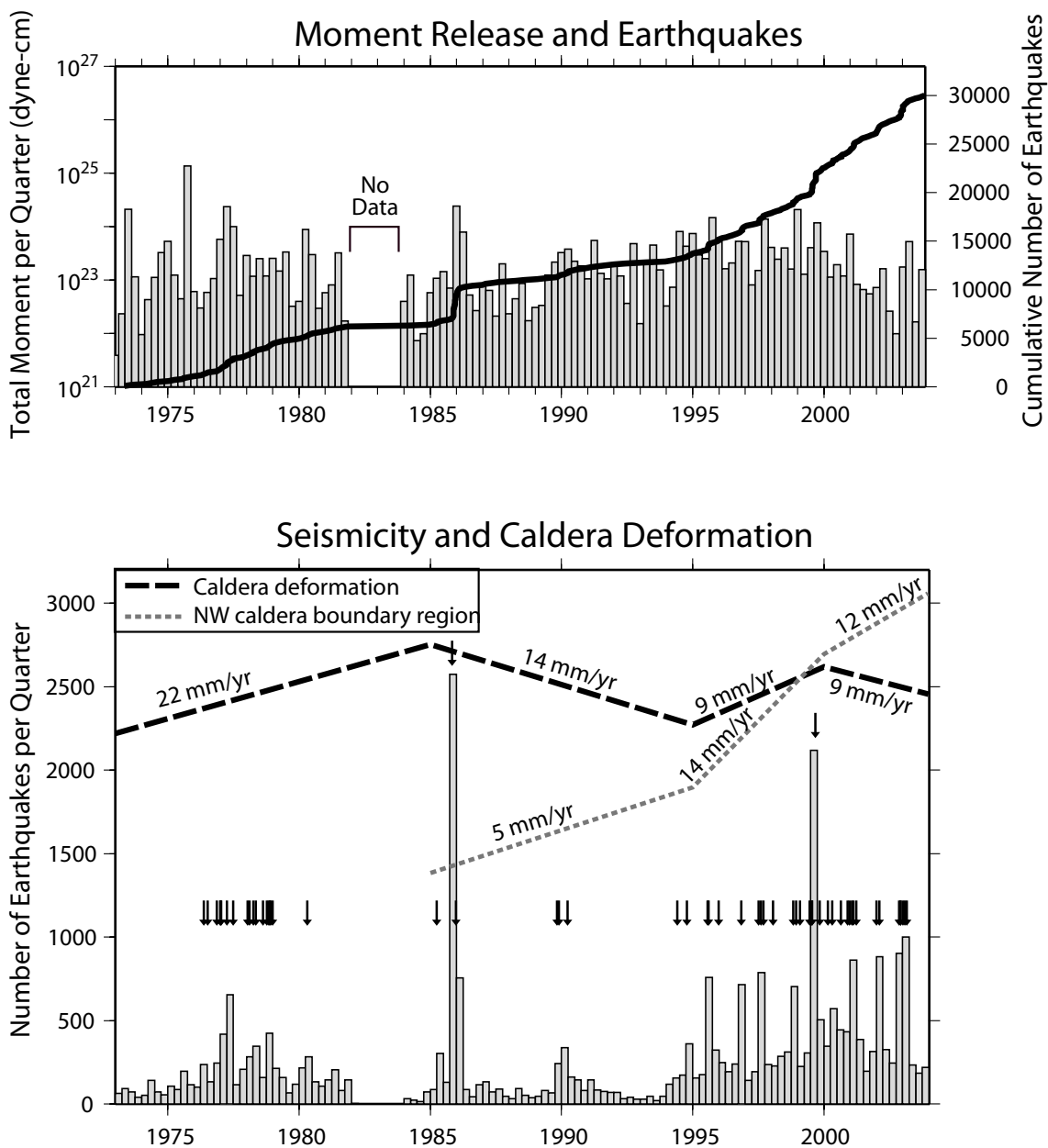


Figure 3.3. Plot of Yellowstone Plateau seismicity, deformation, and moment release. Top histogram shows moment release per quarter and the cumulative number of earthquakes. Bottom histogram shows number of earthquakes per quarter and trends in caldera deformation from leveling and GPS campaigns. Earthquake swarms are marked by arrows. Modified from Puskas et al. [2007].

cause changes in  $b$ -values. The additional data helps to better understand the physical processes that are causing the changing rate of seismicity in certain areas.

## CHAPTER 4

### CALCULATION OF EARTHQUAKE RECURRENCE RATES

#### 4.1. Earthquake Data

Key information can be gained about crustal structure and the state of stress in the crust from analyzing recorded earthquakes. The data used here are the high precision earthquake data from Husen and Smith [2004] of relocated hypocenters from a new three-dimensional P-wave velocity study for the period 1973 – 2002 (Figure 1.1). Hypocenters for 2003 were relocated using the same velocity structure and technique of Husen and Smith [2004] for this study and added to the catalog giving a total number of earthquakes of 26,020. All the events have been classified into four quality classes A, B, C, and D (Table 4.1) [Husen & Smith, 2004].

Table 4.1

#### Definition of quality classes for earthquake locations of the Yellowstone earthquake catalog

Quality Class	Selection Criteria
A (excellent)	rms < 0.5 sec, DIFF < 0.5 km, average error < 2.0 km
B (good)	rms < 0.5 sec, DIFF < 0.5 km, average error $\geq$ 2.0 km
C (questionable)	rms < 0.5 sec, DIFF $\geq$ 0.5 km
D (poor)	rms $\geq$ 0.5 sec

Using the criteria in Table 4.1, 5,323 events are of quality A category, 6,668 are of quality B, 12,559 are of quality C, and 1,470 are of quality D. Husen and Smith [2004] also recalculated coda magnitudes ( $M_C$ ) from the year 1984 to 2003 using available instrument calibrations and an improved coda magnitude equation from Pechmann et al. [2001].

$$M_C = -2.60 + 2.44 \log \tau + 0.0040\Delta$$

where  $\tau$  is signal duration in seconds measured on a short-period vertical component seismogram, and  $\Delta$  is epicentral distance in kilometers. Due to the removal of previous systematic time-dependent magnitude shifts, these recomputed  $M_C$  values are more consistent and more reliable and are comparable to  $M_L$  estimations. The average  $M_C$  for the time period of 1984 to 2003 is 0.9, and only 6% of the earthquakes have  $M_C > 2.0$ .

Because of the importance of good locations and well-constrained magnitudes in calculating  $b$ -values, only events with qualities of A, B, or C were used because they have RMS values less than 0.5 seconds. Also, only earthquakes from 1984 – 2003 were used because of the more consistent and reliable nature of the magnitudes. This leaves 19,741 events in the catalog (Figure 4.1).

#### 4.2. Identification of Earthquake Swarms

There are generally three different types of earthquake sequences, summarized by Mogi [1963]: (I) a mainshock followed by a number of aftershocks of decreasing magnitude and frequency (Figure 4.2A); (II) a slow build up of seismicity (foreshocks) leading to a type I sequence (Figure 4.2B); and (III) a gradual increase and decay of

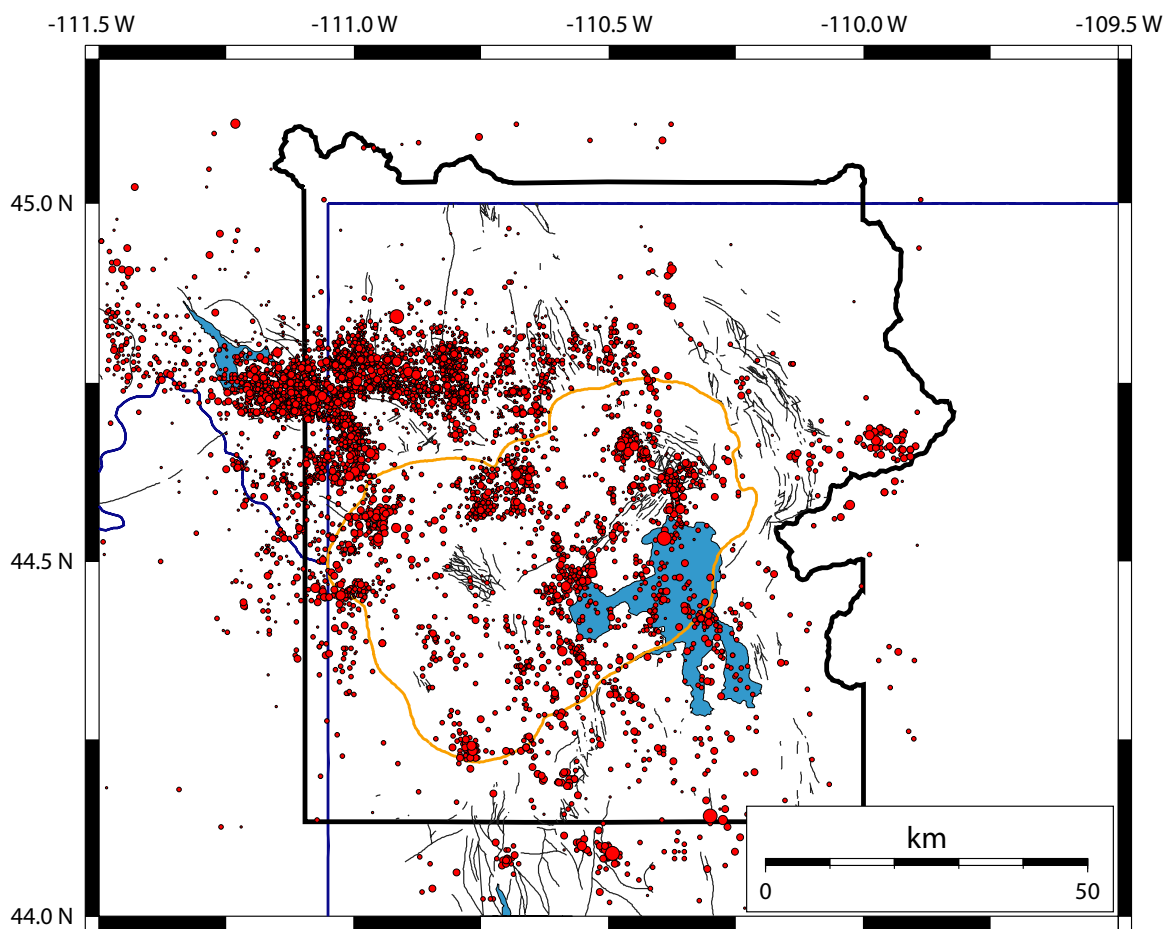
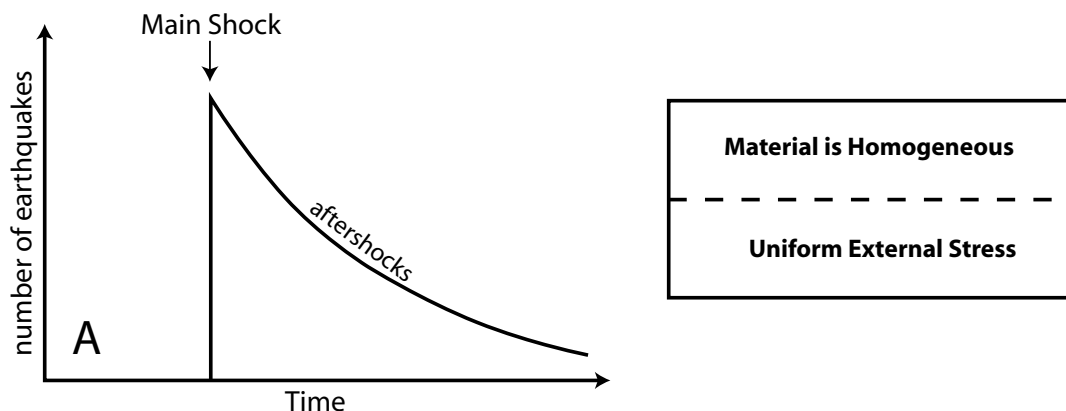
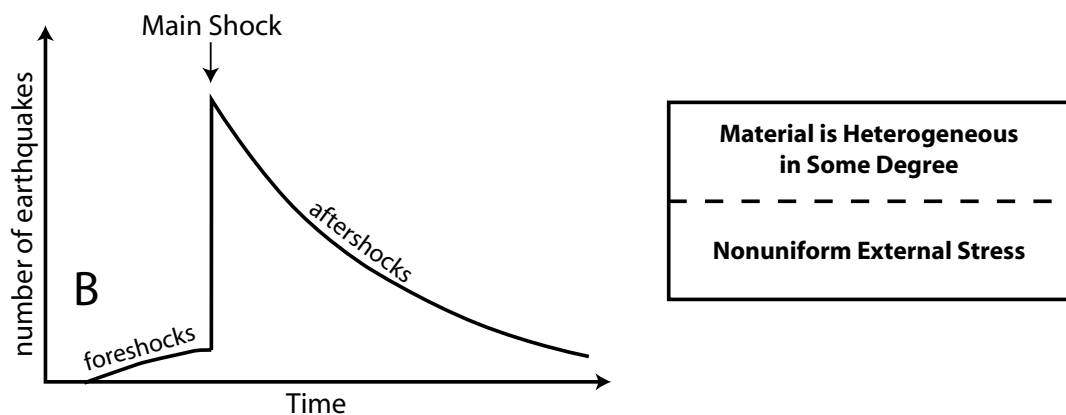


Figure 4.1. Seismicity map showing the locations of A, B, and C quality events from 1984 - 2003. Earthquake epicenters are shown as red circles. The 0.64 Ma caldera is outlined in orange and Quaternary faults mapped by Christiansen [2001] are shown as black lines.

### Type I: Main shock and aftershocks



### Type II: Foreshocks, main shock and aftershocks



### Type III: Swarm

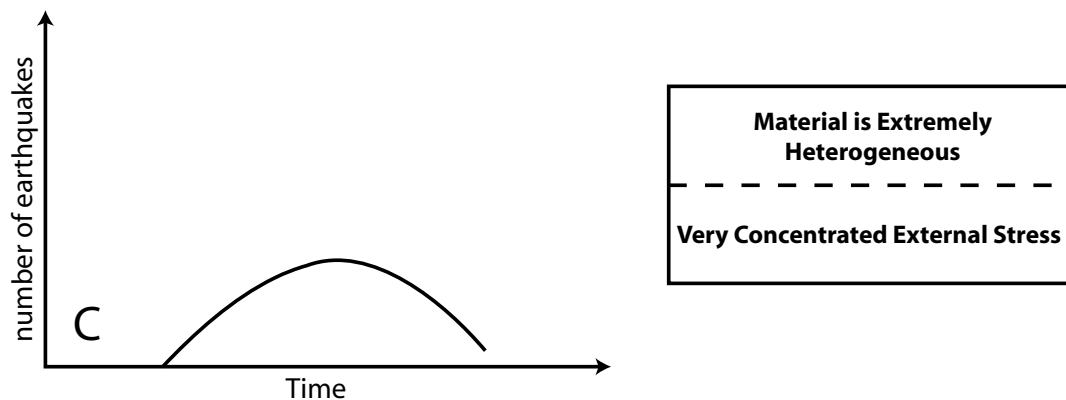


Figure 4.2. Generalized plots of number of earthquakes vs. time for the three types of earthquakes sequences after Mogi [1963]. Type I consists of a main shock and aftershocks and occurs in regions with homogeneous structure and uniform stress. Type III (swarm) consists of gradual build-up and decrease in activity with no significant main event. Type III occurs where the structure is highly fractured or the stress is extremely concentrated. Type II has some foreshocks leading to the main shock-aftershock sequence and occurs in regions intermediate to the first and third types.

seismicity in time without a distinct mainshock (Figure 4.2C) [also see Sykes, 1970].

Type III sequences are also known as earthquake swarms and are often found in volcanic areas or other remarkably fractured regions or areas where there is a concentrated application of stress such as intruding magma [Mogi, 1963].

Sequence I typically occurs in homogeneous material with a uniform external stress. Sequence II tends to occur in material that is heterogeneous to some degree, or a moderate fracture density, with a nonuniform external stress. Sequence III, or swarms, occurs in material that is extremely heterogeneous, or have high fracture density, with a very concentrated external stress (Figure 4.2).

Hill [1977] suggested the following physical process to explain earthquake swarms: A series of dikes oriented with their long dimension parallel to the regional greatest principal stress. Shear failures along oblique fault planes connecting adjacent tips of en echelon or parallel dikes occur when a critical combination of fluid pressure in the dikes and the difference between  $\sigma_1$  and  $\sigma_3$  is reached. More recently, Vidale et al. [2006] suggested that swarms are due to a variable component of background seismicity driven by seismically invisible forces such as aseismic slip and fluid pressure variations.

There are different algorithms available to detect the foreshock, main shock, aftershock sequence [Reasenber, 1985; Youngs et al., 1987], but there are few algorithms written to detect earthquake swarms [Waite, 1999]. In this study, Reasenber's [1985] code was first used to identify swarms in the Yellowstone region. However this approach put events that were clearly not related temporally into a swarm. For example, events up to 5 years apart were classified as members of the same swarm simply because of their spatial relationship. In order to identify swarms in the

Yellowstone catalog an algorithm designed by Waite [1999] was used. This algorithm identifies swarms based on the interevent times and distances.

A definition of an earthquake swarm used in this study was modified from Mogi [1963] and contained the following criteria: (i) the maximum of the daily number of events in the sequence ( $N_d$ ) is greater than twice the square-root of the swarm duration in days ( $T$ ):

$$N_d > 2\sqrt{T}$$

and (ii) the total number of earthquakes in a sequence  $E_T$  is at least 10. Swarms were identified using an  $E_T$  value of 10, 30, and 50 to see which criteria best identified both large and small swarms.

All swarm events were then removed from the catalog to give a de-swarmed data set. Furthermore, all events triggered by the  $M7.9$  Denali Fault earthquake [Husen et al., 2004b; Husen et al., 2004c] were removed as well.

Wiemer and Wyss [2000] state that a careful estimate of the spatial and temporal homogeneity of the magnitude of completeness ( $M_{COMP}$ ) is needed before deviations from a power law behavior for small magnitudes can be made. Therefore,  $M_{COMP}$ , which is the minimum magnitude in which the catalog is complete, was then calculated. In other words, all the earthquakes with magnitudes less than  $M_{COMP}$  are not being recorded by the network. It is well known that  $M_{COMP}$  changes with time in most earthquake datasets, usually decreasing, because the number of seismographs increases and the methods of analysis improve [Wiemer & Wyss, 2000].

The Yellowstone seismicity rate seems to increase around the year 1995; however, this is attributed to upgrades to the network and therefore the catalog was

broken into two time periods, 1984-1994 and 1995-2003. Also, due to the high density of seismographs and earthquakes, the area that extends from Hebgen Lake east to the northern caldera boundary near Norris Junction was separated from the rest of the catalog.  $M_{COMP}$  values were then calculated for the four different subsections. In order to keep  $M_{COMP}$  consistent throughout the entire catalog the highest value of  $M_{COMP}$  was selected and the catalog was cut there. The remaining events were used to calculate  $b$ -values.

#### 4.3. Calculating $b$ -Values

The  $b$ -values determined in this study were calculated using the algorithm in ZMAP [Wiemer, 2001]. Maximum-likelihood  $b$ -values were computed using the following equation [Utsu, 1965; Aki, 1965; Bender, 1983].

$$b = \frac{1}{\bar{M} - M_{\min}} \log e ,$$

where  $\bar{M}$  is the mean magnitude and  $M_{\min}$  the minimum magnitude of the given sample.

The sample is considered complete down to the minimum magnitude  $M_{\min}$ . The magnitude of completeness ( $M_{comp}$ ) has to be corrected by  $\Delta M/2$  to compensate the bias of rounded magnitudes to the nearest  $\Delta M$  bin, thus  $M_{\min} = M_{comp} - \Delta M/2$  [Utsu, 1965; Guo & Ogata, 1997]. The confidence limit of this  $b$ -value estimation is given by [Shi & Bolt, 1982]

$$\sigma(b) = 2.30b^2 \sqrt{\sum_{i=1}^n (M_i - \bar{M})^2 / n(n-1)} ,$$

where  $n$  is the total number of events of the given sample.

For volumetric sampling of earthquakes, we use cylindrical volumes centered at nodes spaced at  $0.01^\circ \times 0.01^\circ$  ( $\sim 0.8\text{km} \times \sim 1.1\text{km}$ ) with varying radii for the cylinders. For cross-sections, sampling is done on a  $0.5 \times 0.5$  km grid with varying radii. For each node a minimum number of events with  $M \geq M_{comp}$ ,  $N_{min}$ , is required in order to determine a reliable  $b$ -value. For samples that contain less than  $N_{min}$  events, a  $b$ -value is not calculated.  $N_{min}$  is set to 50 in this study because below this value the uncertainty in  $b$  increases rapidly. Radii were varied from 3 to 10 km and results were compared. The radius that produced robust results with the greatest spatial extent was chosen.

To compare  $b$ -values for different criteria for removing swarms and with the full catalog,  $b$ -values are spatially mapped for both types of data. If in both instances, the sample size is greater or equal to  $N_{min}$  and thus  $b$  can be computed, the probability  $P_b$  of the hypothesis that the  $b$ -values of the two catalogs are coming from the same population is computed. This probability is derived from the Akaike Information Criterion (AIC) [Akaike, 1974]. Comparing the  $AIC_0$  for both catalogs having the same  $b$ -value  $b_0$  and the  $AIC_{12}$  for both catalogs having two different  $b$ -values  $b_1$  and  $b_2$  leads to the difference  $\Delta AIC$  of these two AIC scores as given by Utsu [1992]:

$$\Delta AIC = -2(N_1 + N_2) \ln(N_1 + N_2) + 2N_1 \ln\left(N_1 + \frac{N_2 b_1}{b_2}\right) + 2N_2 \ln\left(\frac{N_1 b_2}{b_1} + N_2\right) - 2$$

The probability  $P_b$  that the  $b$ -values are not different is given by

$$P_b = e^{\left[\frac{-\Delta AIC}{2}\right]}$$

Using the criteria from Utsu [1999], the difference in  $b$ -values is considered not significant if  $\Delta\text{AIC} < 2$ . If  $\Delta\text{AIC} > 2$ , the difference is significant.  $\Delta\text{AIC} = 2$  corresponds to  $P_b \approx 0.05$ . The difference is considered highly significant if  $\Delta\text{AIC} > 5$ . This value corresponds to  $P_b \approx 0.01$ . Applying the logarithm leads to log-probabilities of  $\log P_b \leq -1.3$  for significantly different  $b$ -values and  $\log P_b \leq -1.9$  for highly significant differences in  $b$ -values [Schorlemmer & Wiemer, 2004; Schorlemmer et al., 2005].

#### 4.4. How is the $b$ -value Interpreted?

The frequency-magnitude distribution (Ishimoto & Iida, 1939; Gutenberg & Richter, 1944) derives from the power-law relationship between the frequency of occurrence and the magnitude of earthquakes:

$$\log N = a - bM,$$

where  $N$  is the cumulative number of earthquakes having magnitudes larger than  $M$ , and  $a$  and  $b$  are constants. It has been shown in laboratory studies, mines, and numerical simulations that the slope of the frequency-magnitude distribution curve, or  $b$ -value, depends on stress conditions.

Statistically significant variations of  $b$ -values have been measured in laboratory experiments, mines and various tectonic regimes such as subducting slabs, near magma chambers, along fault zones and in aftershock zones [Wiemer & Wyss, 2002]. There are several different factors that can cause changes in  $b$ -values such as: (I) increased material heterogeneity, such as a large number of randomly oriented cracks, results in high  $b$ -values [Mogi, 1962]; (II) an increase in applied shear stress [Scholz, 1968; Urbancic et

al., 1992; Schorlemmer et al., 2004; Schorlemmer et al., 2005], or an increase in effective stress [Wyss, 1973], decreases the  $b$ -value and ; (III) an increase in the thermal gradient causes an increase in  $b$  [Warren & Latham, 1970].

In tectonic areas, the  $b$ -value is generally around 1.0 [Frolich & Davis, 1993]. In contrast, volcanic areas show  $b$ -values greater or much less than 1.0. Wiemer & Benoit [1996] first used a dense spatial grid to study  $b$ -values at subduction zones. These studies were later extended to volcanic areas. Due to the proximity to magma systems, all the aforementioned criteria that favor high  $b$ -values are present in volcanic areas such as high heterogeneity due to layering of lava flows and ash, the presence of cooling cracks, dikes and sills as well as high thermal gradients. Due to the dynamic nature of volcanic areas,  $b$ -values tend to change with changing stress conditions through both time and space.

Seismicity associated with magma chambers have been studied using  $b$ -values at several volcanoes including Mt. St. Helens and Mt. Spurr [Wiemer & McNutt, 1997], Off-Ito volcano [Wyss et al., 1997], Long Valley Caldera and Mammoth Mountain [Wiemer et al., 1998], Montserrat [Power et al., 1998], Mt. Etna [Murru et al., 1999], Katmai [Jolly & McNutt, 1999], Mt. Redoubt [Wiemer & Wyss, 2000], Kilauea [Wyss et al., 2001], and Mt. Pinatubo [Sanchez et al., 2004]. These volcanoes studied have shown high spatial variability of  $b$ , with regions of normal  $b$  (1.0) adjacent to regions with anomalously high  $b$  (up to 3.0). Most studies have found that in general,  $b$  is high at depths of 7-0 km where the earthquakes are adjacent to inferred magma bodies identified by other techniques. However, some studies also show significant high  $b$  anomalies at depths of 3-4 km. This is the approximate depth at which magma with 4 wt% gas starts

to exsolve the gas, and further, is near the depth at which open cracks may exist in the host rock [McNutt, 2005].

*b*-values have also been used to infer the state of stress on faults [Scholz, 1968; Wyss, 1973; Urbancic et al., 1992; Schorlemmer et al., 2004; Schorlemmer et al., 2005]. Schorlemmer et al. [2005] show that there is an inverse relationship between differential stress and *b* and later conclude that the *b*-value can therefore be interpreted as a ‘stressmeter’ in the Earth’s crust. This idea is supported by the magnitude 6.0 Parkfield, California, event in 2004, which almost exclusively ruptured areas of the San Andreas fault previously mapped as regions of low *b* [Wiemer & Wyss, 1997; Schorlemmer & Wiemer, 2005].

## CHAPTER 5

### RESULTS

#### 5.1. Earthquake Swarm Analyses

Employing algorithms used to identify the foreshock-mainshock-aftershock sequence [Reasenber, 1985] showed that most earthquake sequences do not follow this pattern because the seismicity in Yellowstone is dominated by swarms. Numerous combinations of interevent times (from 0.5 to 5 days) and distance values (from 2 to 15 km) were tried in the swarm identification algorithm of Waite [1999]. In addition, various definitions of minimum number of earthquakes, from 5 to 50, that constituted a swarm were tried. The combination of an interevent time of 2 days and a distance of 5 km most reliably identified both large and small swarms in the Yellowstone region and the results are summarized in Table 5.1.

Two hundred and four individual swarms were identified (Figure 5.1A, Appendices A, B, C) using the criteria in which a swarm must have at least 10 events (10 minimum). These swarms varied in duration from 1 to 46 days; number of events from 10 to 722; and maximum number of events per day from 5 to 283. The average number of events per swarm for all 204 swarms is 50.8. The total number of events for all 204 swarms is 10,365 which is 52.5% of the original 19,741 events (Figure 5.1B). Magnitudes of swarm events range from  $-1.04 \leq M_C \leq 4.82$  with 99.98% of the swarm

Table 5.1 Summary of deswarming results using various definitions of a swarm

Swarm Definition	# of swarms	duration (days)	# of events	max # of events/day	avg. # of events/swarm	total # of events	% of original catalog
10-min	204	1 to 46	10 to 722	5 to 283	50.8	10,365	52.5
30-min	57	1 to 46	30 to 722	9 to 283	138.7	7,906	40.0
50-min	41	2 to 46	50 to 722	11 to 283	177.9	7,292	36.9

Swarm Definition	magnitude ( $M_C$ ) range	% of events with $M_C \leq 4.0$	% of events with $M_C \leq 3.0$	% of events with $M_C \leq 2.0$	% of events with $M_C \leq 1.0$	% of swarms located north of the caldera	% of swarms located in the caldera
10-min	-1.04 to 4.82	99.98	99.67	95.29	64.17	70.6	27.9
30-min	-1.04 to 4.82	99.97	99.72	96.00	67.21	84.2	15.8
50-min	-1.01 to 4.19	99.99	99.74	96.01	66.02	82.9	17.1

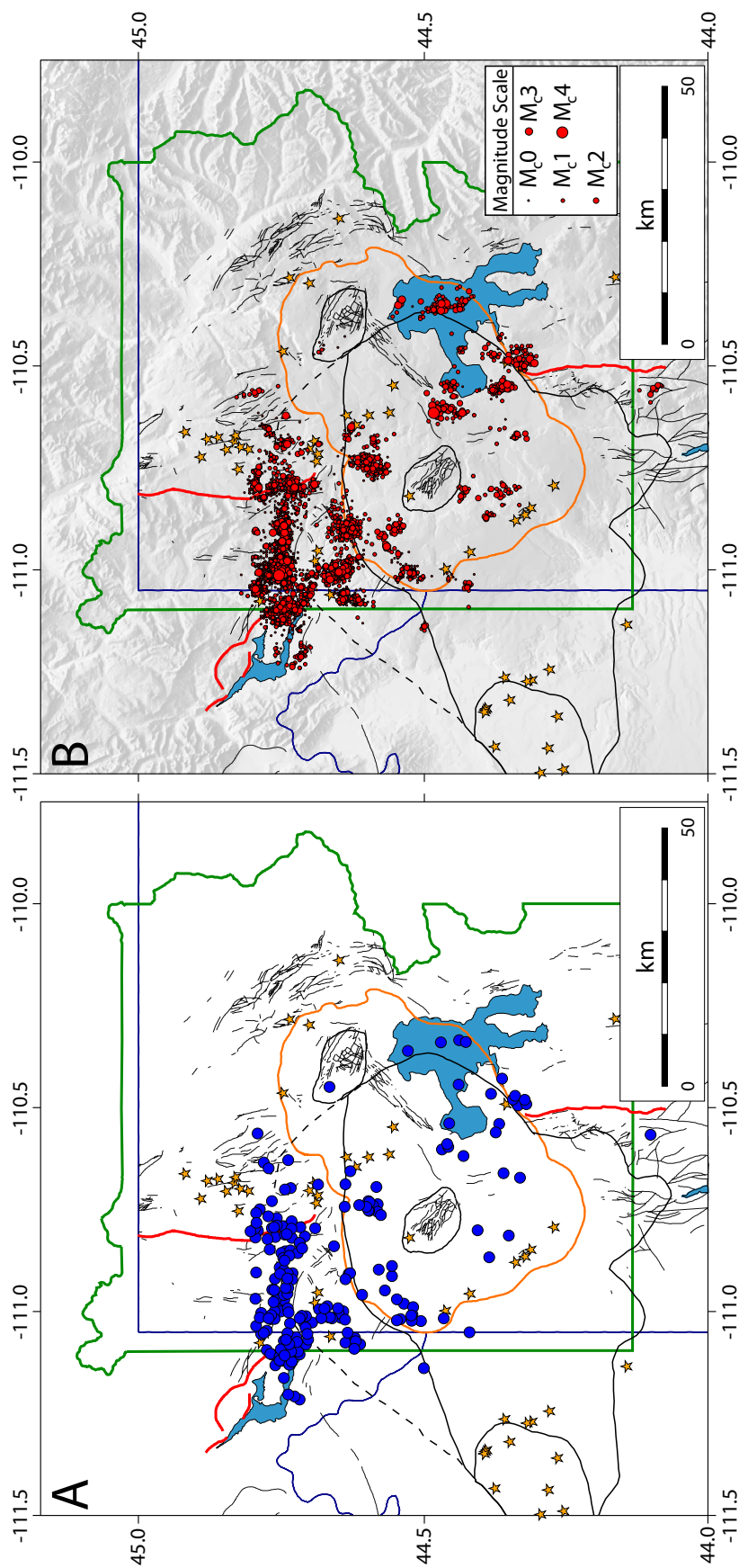


Figure 5.1. Swarm locations identified while using the 10 minimum definition of a swarm. (a) shows mean locations for the 204 swarms shown by blue circles and (b) shows all events from the 204 swarms shown in red circles. Postcaldera volcanic vents are shown as orange stars. The 0.64 Ma caldera is outlined in orange and the 1.2 Ma as well as the 2.0 Ma caldera boundaries are outlined in black with the possible northern extent of the 2.0 Ma caldera shown with a dashed black line. Quaternary faults mapped by Christiansen [2001] are shown as thin black lines. Major Quaternary faults are shown as thick red lines.

events having magnitudes less than or equal to  $M_C = 4.0$ ; 99.67% having  $M_C \leq 3.0$ ; 95.29% having  $M_C \leq 2.0$ ; and 64.17% having  $M_C \leq 1.0$ . One hundred forty-four (70.6%) of the 204 swarms are located in the region just north and northwest of the caldera. Fifty-seven (27.9%) are located within or on the boundary of the 0.64 Ma caldera. Three (1.5%) are located outside the 0.64 Ma caldera to the east or south.

Fifty-seven individual swarms were identified (Figure 5.2A, Appendices A, B, C) using the criteria in which a swarm must have at least 30 events (30 minimum). These swarms varied in duration from 1 to 46 days; number of events from 30 to 722; and maximum number of events per day from 9 to 283. The average number of events per swarm for all 57 swarms is 138.7. The total number of events for all 57 swarms is 7,906 which is 40.0% of the original 19,741 events (Figure 5.2B). Magnitudes of swarm events range from  $-1.04 \leq M_C \leq 4.82$  with 99.97% of the swarm events having magnitudes less than or equal to  $M_C = 4.0$ ; 99.72% having  $M_C \leq 3.0$ ; 96.00% having  $M_C \leq 2.0$ ; and 67.21% having  $M_C \leq 1.0$ . Forty-eight (84.2%) of the 57 swarms are located in the region just north and northwest of the caldera. Nine (15.8%) are located within or on the boundary of the 0.64 Ma caldera.

Forty-one individual swarms were identified (Figure 5.3A, Appendices A, B, C) using the criteria in which a swarm must have at least 50 events (50 minimum). These swarms varied in duration from 2 to 46 days; number of events from 50 to 722; and maximum number of events per day from 11 to 283. The average number of events per swarm for all 41 swarms is 177.9. The total number of events for all 41 swarms is 7,292 which is 36.9% of the original 19,741 events (Figure 5.3B). Magnitudes of swarm events range from  $-1.01 \leq M_C \leq 4.19$  with 99.99% of the swarm events having magnitudes less

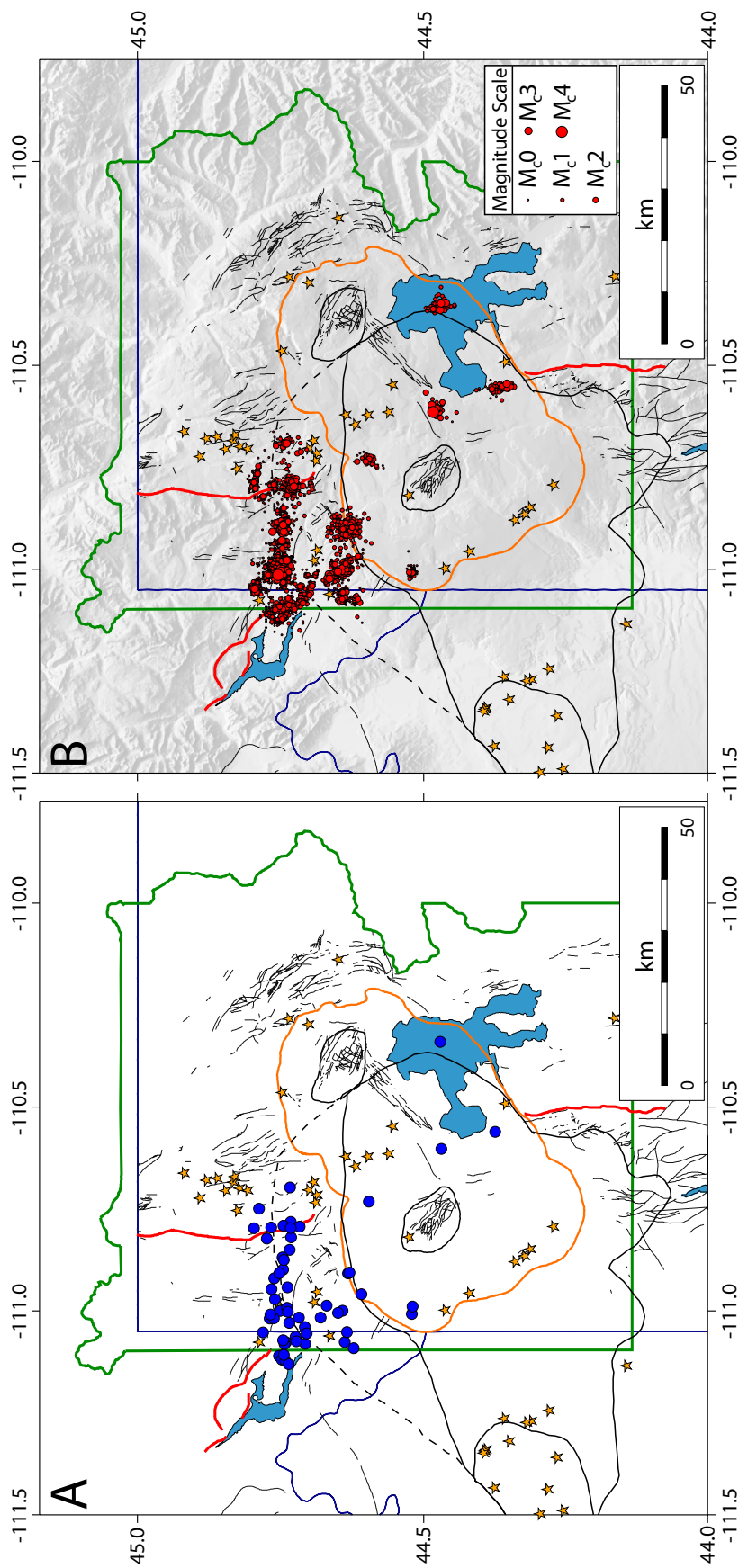


Figure 5.2. Swarm locations identified while using the 30 minimum definition of a swarm. (a) shows mean locations for the 57 swarms shown by blue circles and (b) shows all events from the 57 swarms shown in red circles. Postcaldera volcanic vents are shown as orange stars. The 0.64 Ma caldera is outlined in orange and the 1.2 Ma as well as the 2.0 Ma caldera boundaries are outlined in black with the possible northern extent of the 2.0 Ma caldera shown with a dashed black line. Quaternary faults mapped by Christiansen [2001] are shown as thin black lines. Major Quaternary faults are shown as thick red lines.

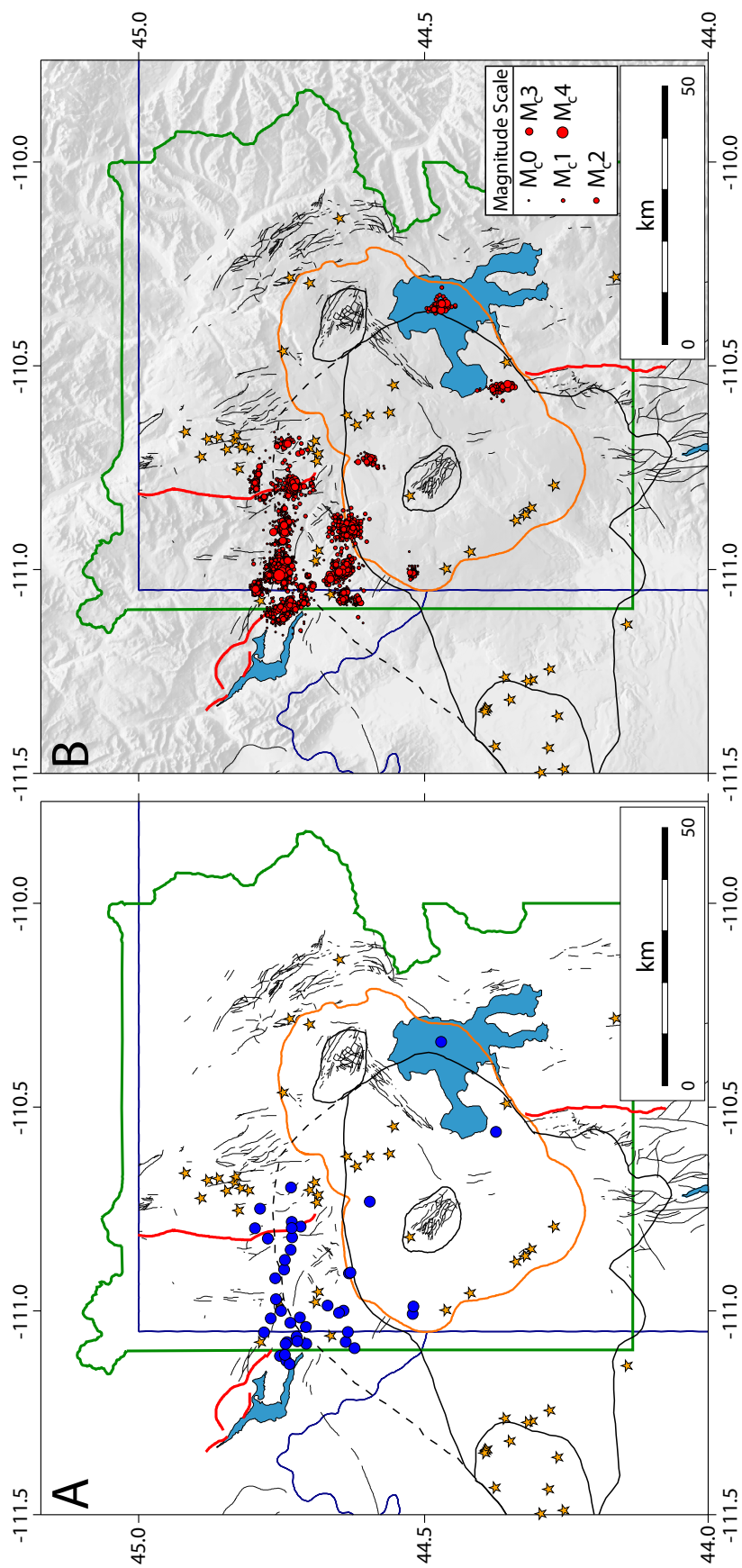


Figure 5.3. Swarm locations identified while using the 50 minimum definition of a swarm. (a) shows mean locations for the 41 swarms shown by blue circles and (b) shows all events from the 41 swarms shown in red circles. Postcaldera volcanic vents are shown as orange stars. The 0.64 Ma caldera is outlined in orange and the 1.2 Ma as well as the 2.0 Ma caldera boundaries are outlined in black with the possible northern extent of the 2.0 Ma caldera shown with a dashed black line. Quaternary faults mapped by Christiansen [2001] are shown as thin black lines. Major Quaternary faults are shown as thick red lines.

than or equal to  $M_c = 4.0$ ; 99.74% having  $M_c \leq 3.0$ ; 96.01% having  $M_c \leq 2.0$ ; and 66.02% having  $M_c \leq 1.0$ . Thirty-four (82.9%) of the 41 swarms are located in the region just north and northwest of the caldera. Seven (17.1%) are located within or on the boundary of the 0.64 Ma caldera.

Waite [1999] identified 72 swarms in the Yellowstone region for the period 1973 to 1997. Although we have identified many of the same swarms in this study, comparisons cannot be made in some cases because Waite [1999] used the original, nonrelocated, earthquake catalog to identify swarms. Here, only the quality A, B, and C earthquakes in the relocated catalog of Husen and Smith [2004] were used and many additional earthquakes were thrown out in the relocation process. For example, Waite [1999] found 3,156 earthquakes in the autumn, 1985 swarm. However, while using the relocated catalog, the swarm consists of only 462 earthquakes. From 1995 to 2003 the swarms identified in this study become more similar to the swarms identified by Waite [1999] in both the number of swarms and the total number of earthquakes in each swarm. This is because the seismic network upgrades improved the quality of the earthquake locations so more earthquakes made it through the relocation process.

For example, Waite [1999] identified a swarm starting in June of 1995 that consists of 581 earthquakes. That same swarm here is actually four smaller individual swarms (swarms 33, 34, 35 and 36 in Appendices A, B, and C). Adding up the total number of earthquakes in these four swarms gives a total of 567. The reason that the swarm is divided up into four different swarms here is because a search radius of 5 km was used in this study while Waite [1999] used a search radius of 15 km.

Although direct comparisons to results from Waite [1999] cannot be made with individual swarms, the patterns of swarms can be compared. The high percentage of swarms located in the region just north and northwest of the caldera (70.6%, 84.2%, and 82.9 % for the 10 minimum, 30 minimum, and 50 minimum definitions, respectively) is comparable to the results shown in Waite [1999]. This suggests that the crust in that area is highly fractured and heterogeneous. The abrupt change in topography in this area suggests that the boundary of the 2.1 Ma caldera (caldera I) is located here (dashed line in Figure 2.3). Swarm epicenters in this area also tend to align in a more east-west fashion which is what we would expect from the orientation of the edge of caldera I. Another explanation for the high rate of seismicity in this region is the increased stress on the area from the 1959 M7.5 Hebgen Lake, MT earthquake (Chang & Smith, 2002).

Swarm earthquake epicenters within and adjacent to the 0.64 Ma caldera are generally aligned in a north-northwest direction. This alignment is parallel and subparallel to alignments of volcanic vents and Quaternary faults (Figure 1.1) and implies that these events could have occurred on preexisting zones of weakness such as buried, but still active Quaternary faults [Christiansen, 1984].

## 5.2. Magnitude of Completeness

The seismicity rate for quality A, B, and C earthquakes in the Yellowstone region increased from ~200 earthquakes per year before 1995 to ~1,500 earthquakes per year after 1995 (Figure 5.4). However, this change in seismicity rate is due to upgrades to the network. Right around the year 1995, three-component short-period and broadband seismometers were added to the network (Figure 5.5). Therefore the catalog data were

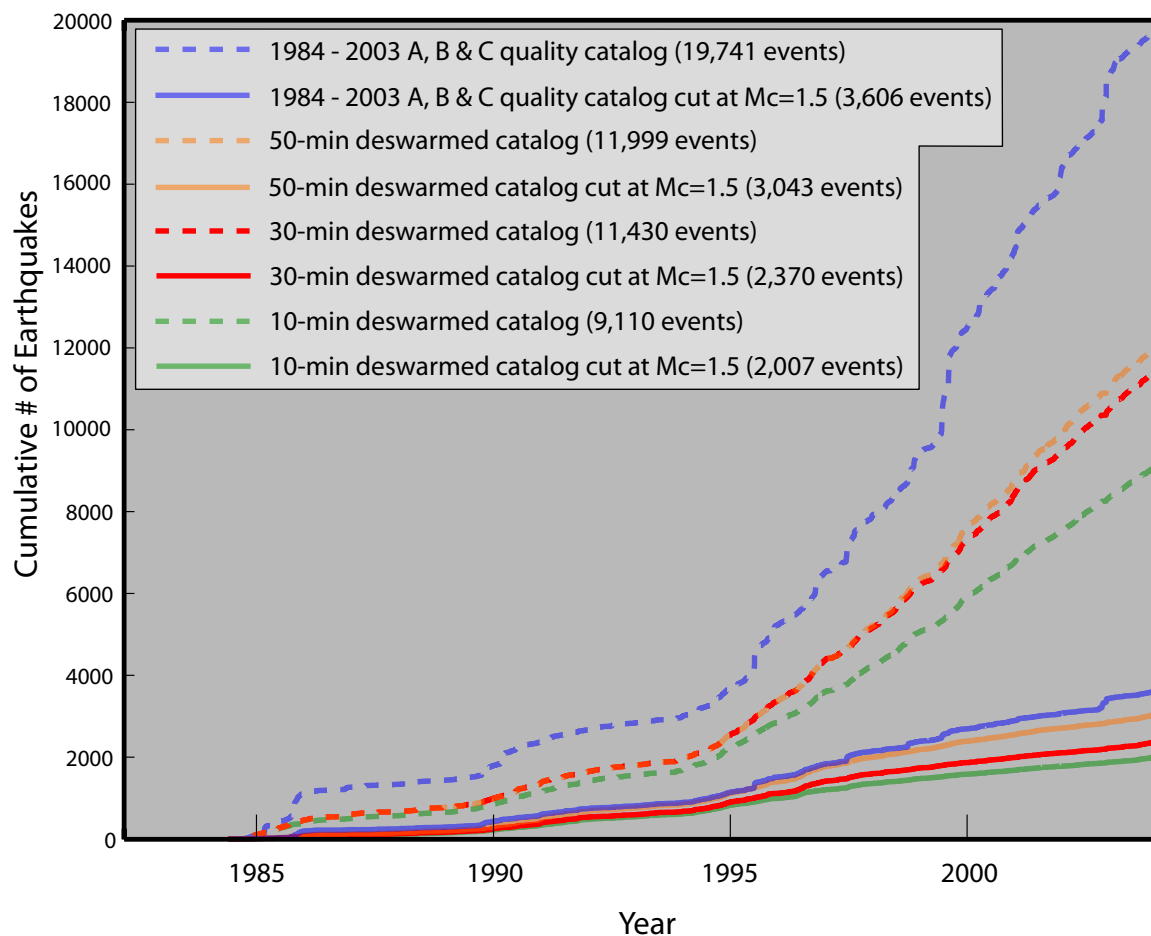


Figure 5.4. Cumulative number of earthquakes vs. time for the different catalogs used to calculate  $b$ -values. Blue dashed line shows the original catalog consisting of A, B, and C quality events from 1984 - 2003. Remaining dashed lines represent the deswarmed catalogs using the various definitions of a swarm. The solid blue line represents the quality A, B, and C events from 1984 - 2003 cut at  $M_{comp}=1.5$ . Remaining solid lines represent the deswarmed catalogs cut at  $M_{comp}=1.5$ .

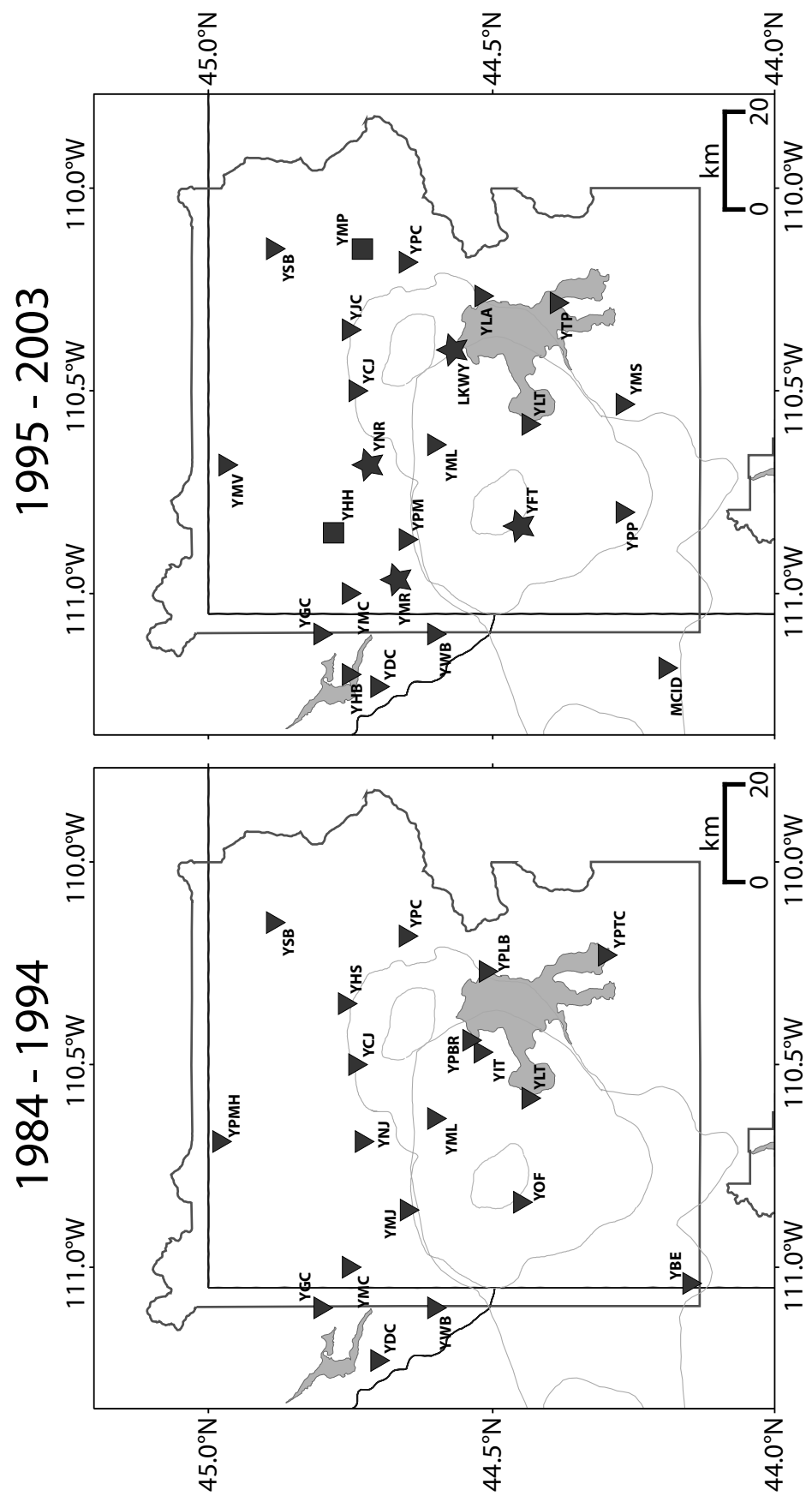


Figure 5.5. Yellowstone seismic network run by the University of Utah Seismograph Stations from 1984 - 1994 and 1995 - 2003. Inverted black triangles represent single (vertical)-component short-period seismographs. Black squares represent three-component short-period seismographs. Black stars represent three-component broadband seismographs.

divided into two time periods, 1984-1994 and 1995-2003. Also, due to the higher density of both seismometers and earthquakes, the area that extends from Hebgen Lake east to the northern caldera boundary near Norris Junction was separated from the rest of the catalog (Figure 5.6). Table 5.2 and Figure 5.6 show the magnitude of completeness values calculated for the various spatial and temporal areas. The highest value of  $M_{COMP}$  was selected ( $M_{COMP} = 1.5$  in the 1984-1994, Remaining region) and the catalog was cut there and the remaining events were used to calculate  $b$ -values to ensure that  $M_{COMP}$  is consistent throughout the time period of the catalog as well as throughout the entire area covered by the catalog. Table 5.3 shows the number of earthquakes remaining to calculate  $b$ -values after a.) deswarming, b.) removing triggered events from the 2002 M7.9 Denali fault earthquake, and c.) cutting the catalog at  $M_{COMP} = 1.5$ .

Table 5.2

Magnitude of completeness ( $M_{COMP}$ ) values for selected spatial and temporal areas.

Area	$M_{COMP}$
1984-1994, North	1.4
1984-1994, Remaining	1.5
1995-2003, North	1.1
1995-2003, Remaining	1.4

Table 5.3

Earthquakes used to calculate  $b$ -values.

Swarm Definition	# of events
10 minimum	2,007
30 minimum	2,370
50 minimum	3,043
No Deswarming	3,606

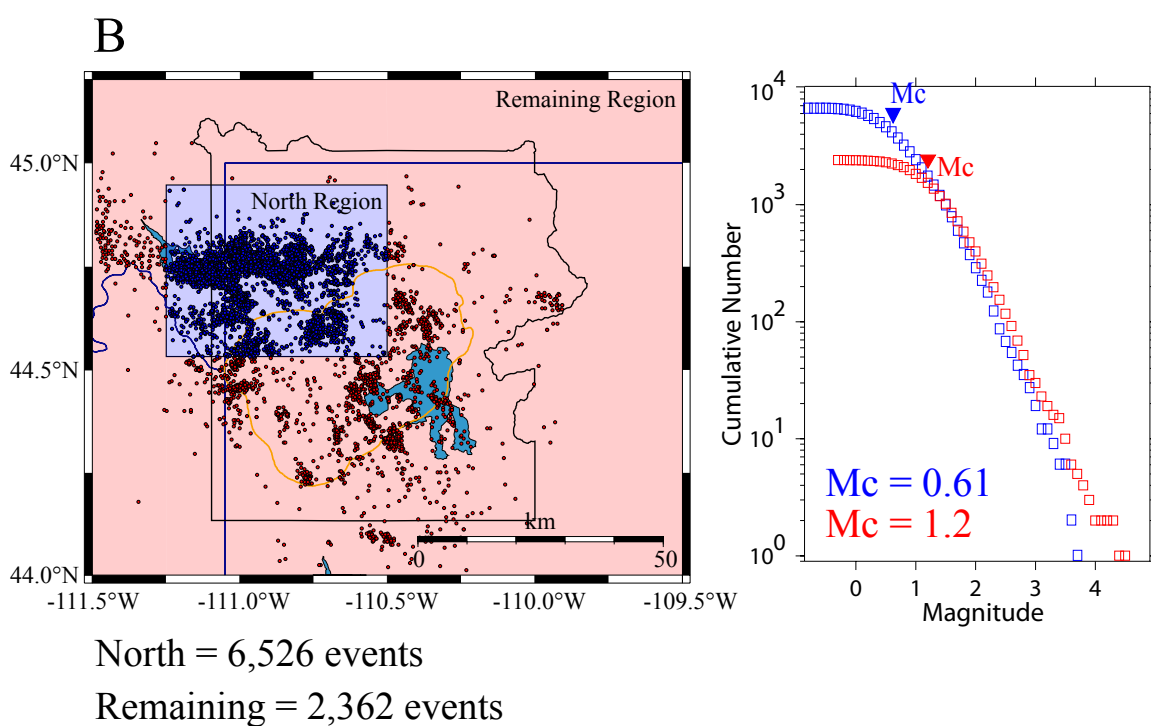
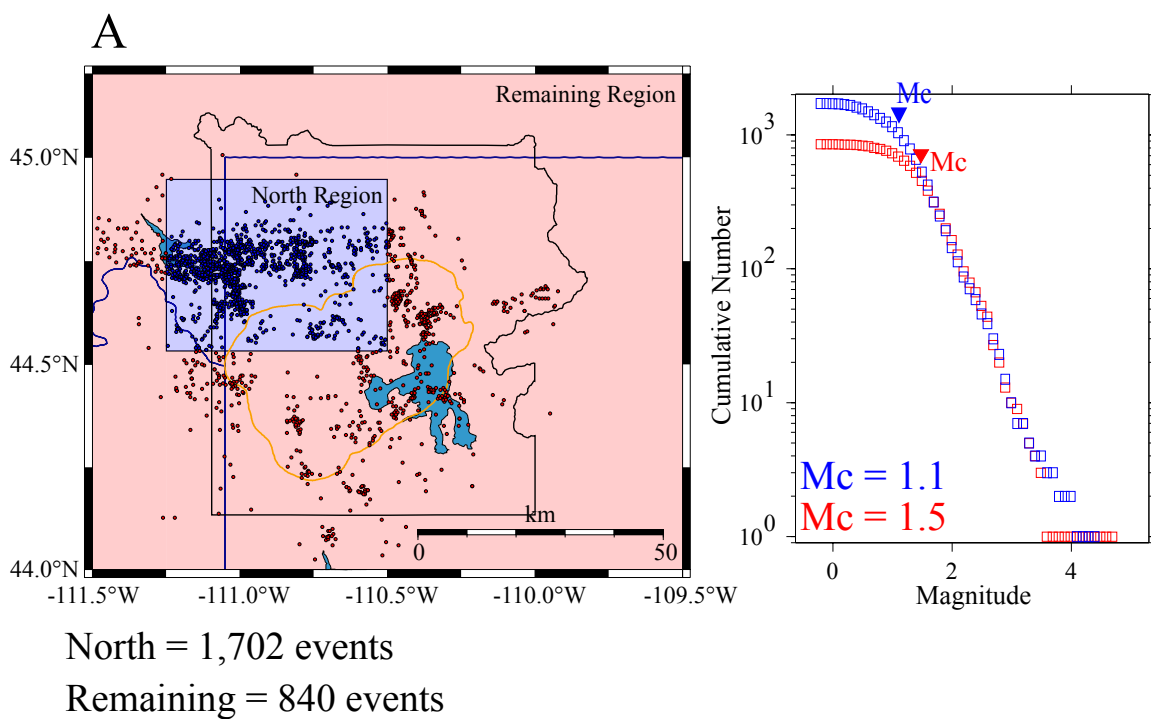


Figure 5.6. Magnitude of completeness ( $M_{comp}$ ) calculations for the 30 minimum deswarmed catalog. (a) shows  $M_{comp}$  values for the years 1984 - 1994 and (b) shows  $M_{comp}$  values for the years 1995 - 2003.

The epicenters used to calculate  $b$ -values for the various swarm definitions are also plotted in Figure 5.7. The timeseries for these catalogs can also be seen in Figure 5.4. As expected, as the minimum number of events that constitute a swarm is increased, more events are left in the catalog to calculate  $b$ -values

### 5.3. $b$ -Value Maps

The spatial distribution of  $b$ -values in Yellowstone shows areas of high and low  $b$ -values and areas of normal crustal values ( $b \approx 1.0$ ) (Figure 5.8) using the different definitions of a swarm as well as using the non-deswarmed catalog. A 10 km radius was chosen to calculate the  $b$ -values because this radius allowed the maximum coverage while still showing details of the areas with both high and low  $b$ -values.

The probability  $P_b$  of the hypothesis that the  $b$ -values of the two catalogs are coming from the same population is computed in order to quantitatively identify the differences between the  $b$ -value maps for the three different deswarmed catalogs as well as the non-deswarmed catalog. In Figure 5.9,  $b$ -values are significantly different when  $\log P_b \leq -1.3$  and the  $b$ -values show highly significant differences for  $\log P_b \leq -1.9$  [Schorlemmer & Wiemer, 2004; Schorlemmer et al., 2005]. Statistically, there is no difference between the  $b$ -values using the deswarmed catalogs from the 10 minimum and 30 minimum definition of a swarm. The 30 minimum catalog is preferred over the catalog from the 10 minimum definition of a swarm due to the fact that using the catalog from the 30 minimum definition of a swarm provides greater spatial coverage for mapping  $b$ -values. When comparing the  $b$ -values from the 30 minimum dataset and the 50 minimum dataset, there are slight differences in the center of the caldera. Overall only

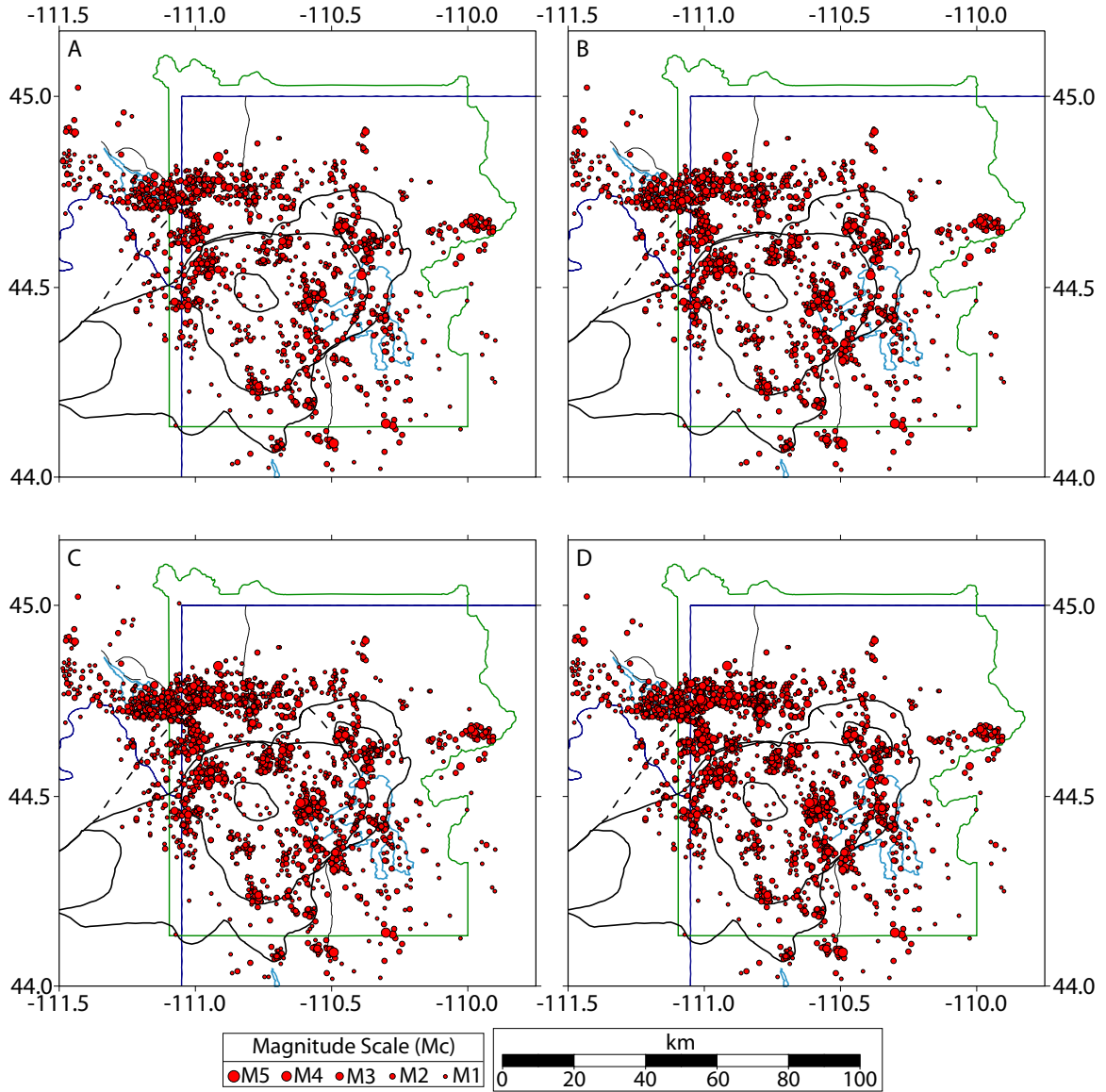


Figure 5.7. Earthquakes used to calculate  $b$ -values for the various deswarmed and non-deswarmed catalogs. (a) shows the 2,007 epicenters for the 10 minimum deswarmed catalog, (b) shows the 2,370 epicenters for the 30 minimum deswarmed catalog, (c) shows the 3,043 epicenters for the 50 minimum deswarmed catalog, and (d) shows the 3,606 epicenters for the non-deswarmed catalog.

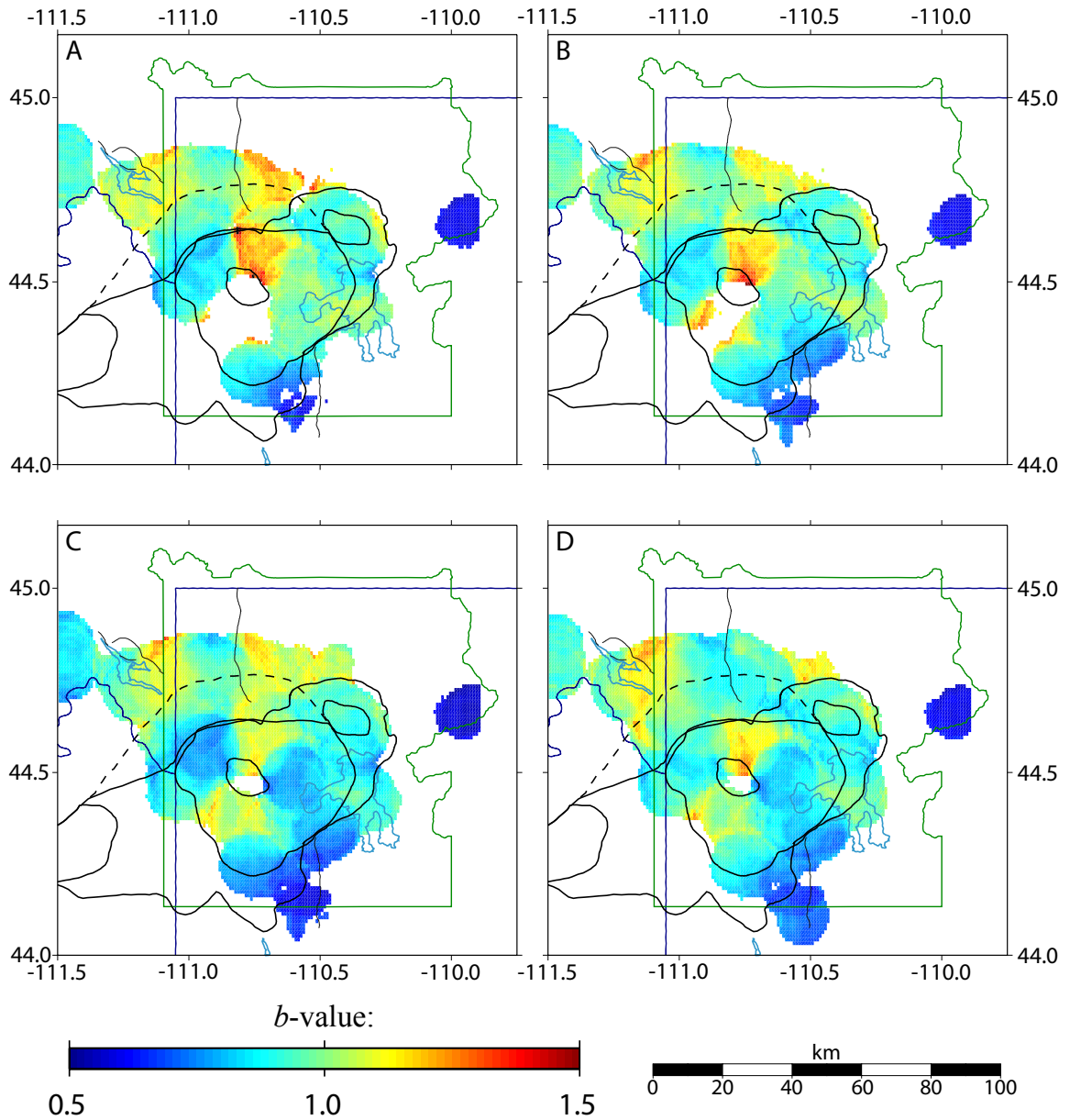


Figure 5.8.  $b$ -value maps for all the various catalogs shown in figure 5.7. (a) shows  $b$ -values calculated for the 10 minimum deswarmed catalog, (b) shows  $b$ -values calculated for the 30 minimum deswarmed catalog, (c) shows  $b$ -values calculated for the 50 minimum deswarmed catalog, and (d) shows  $b$ -values calculated for the non-deswarmed catalog. Hot colors indicate high  $b$ -values and cool colors represent low  $b$ -values.

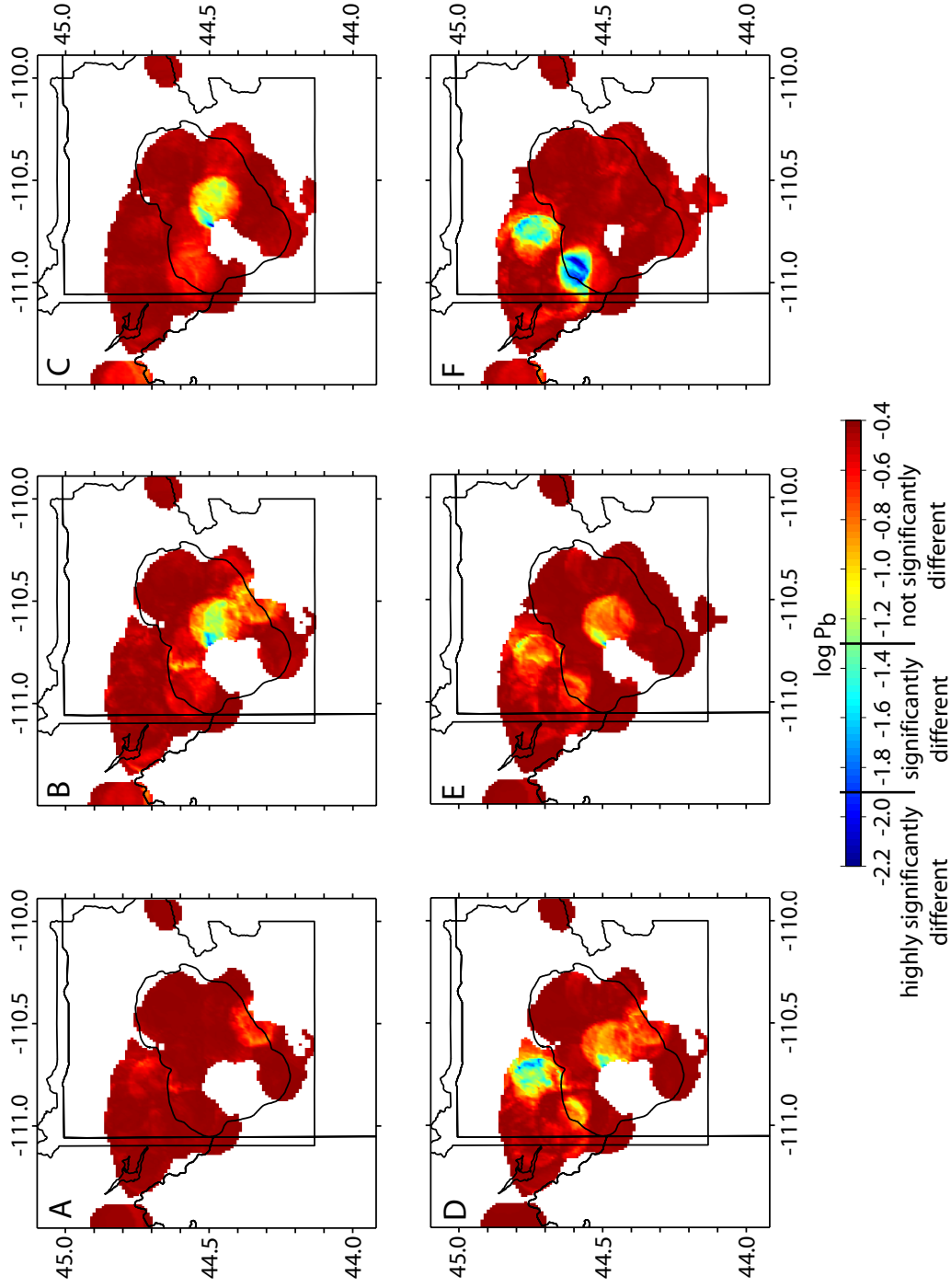


Figure 5.9. Utsu test results comparing the various  $b$ -value maps. (a) 10 minimum vs. 30 minimum, (b) 10 minimum vs. 50 minimum, (c) 30 minimum vs. 50 minimum vs. non-deswarmed, (d) 10 minimum vs. non-deswarmed, (e) 30 minimum vs. non-deswarmed, and (f) 50 minimum vs. non-deswarmed. Hot colors show values that are not significantly different and cool colors show values that are statistically different.

0.4% of the nodes are different between the two datasets. The reason for the differences is a swarm that occurred in August of 1999 (Swarm 109 in Appendices A & B). This swarm consisted of 35 earthquakes so it is only identified and subsequently removed by the algorithm with the 30 minimum definition of a swarm. This swarm contained an earthquake of  $M_C = 4.82$  so when this event remained in the catalog with the 50 minimum definition of a swarm, it single handedly changed the  $b$ -values in that area (Figure 5.10). For this reason, the dataset from the 50 minimum definition of a swarm is discarded.

Only 0.1% of the nodes are significantly different (Figure 5.9) when comparing the  $b$ -values from the 30 minimum dataset with the  $b$ -values from the non-de-swarmed dataset. Some of these differences are due to the same swarm event that was just discussed. Just to the north of the caldera is another area that shows significantly different  $b$ -values. The differences here are due to five earthquakes ranging from  $3.0 \leq M_C \leq 3.8$ . These five earthquakes were detected in two swarms and were removed in the 30 minimum dataset. Because they all occurred in the same area, they all influenced the  $b$ -value calculation for the non-de-swarmed catalog. The non-de-swarmed catalog was discarded and the 30 minimum dataset was chosen as the most stable and best catalog to use when interpreting  $b$ -values due the fact that the  $b$ -value is influenced heavily by just these five events.

There are three areas of relatively high  $b$ -values with values as high as  $1.54 \pm 0.06$  when looking at the spatial distribution of  $b$ -values for the 30 minimum catalog (Figure 5.11). The area with the highest  $b$ -values is under the Mallard Lake Resurgent Dome (MLD) where we see  $b$ -values as high as  $1.54 \pm 0.06$ . This area of high  $b$ -values extends north from the MLD to Madison Junction. A second area with high  $b$ -values, although to

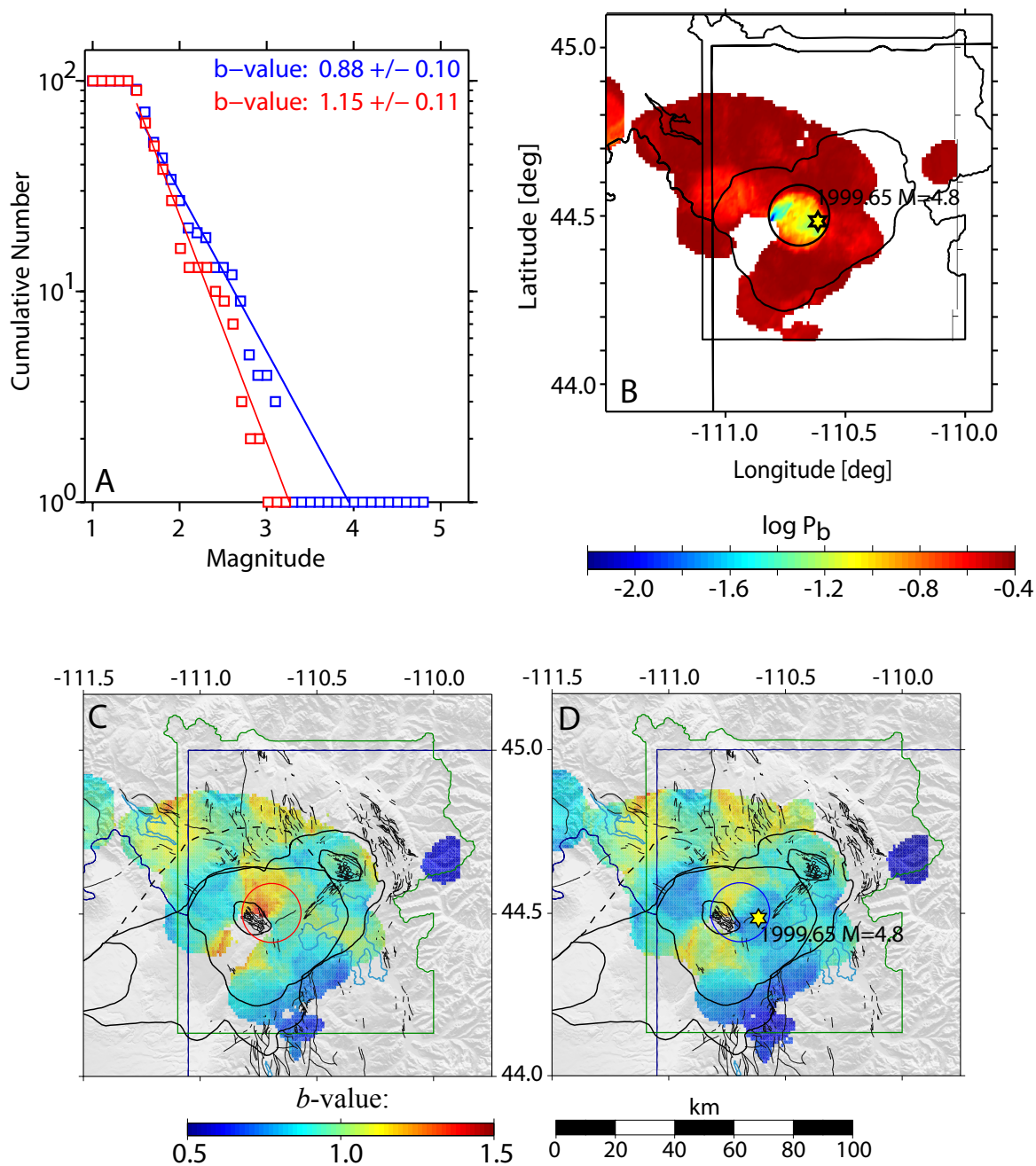


Figure 5.10. Utsu test and frequency-magnitude distribution (FMD) comparison for the 30 minimum  $b$ -value map vs. the 50 minimum  $b$ -value map. (a) shows the FMDs for the two samples shown in c and d. Colors match the colors of the sampling radii shown in c and d. (b) shows the Utsu test results showing the area of significantly different  $b$ -values. (c) shows the  $b$ -value distribution with the sampling radius (red) for the 30 minimum deswarmed catalog. (d) shows the  $b$ -value distribution with the sampling radius (blue) for the 50 minimum deswarmed catalog.

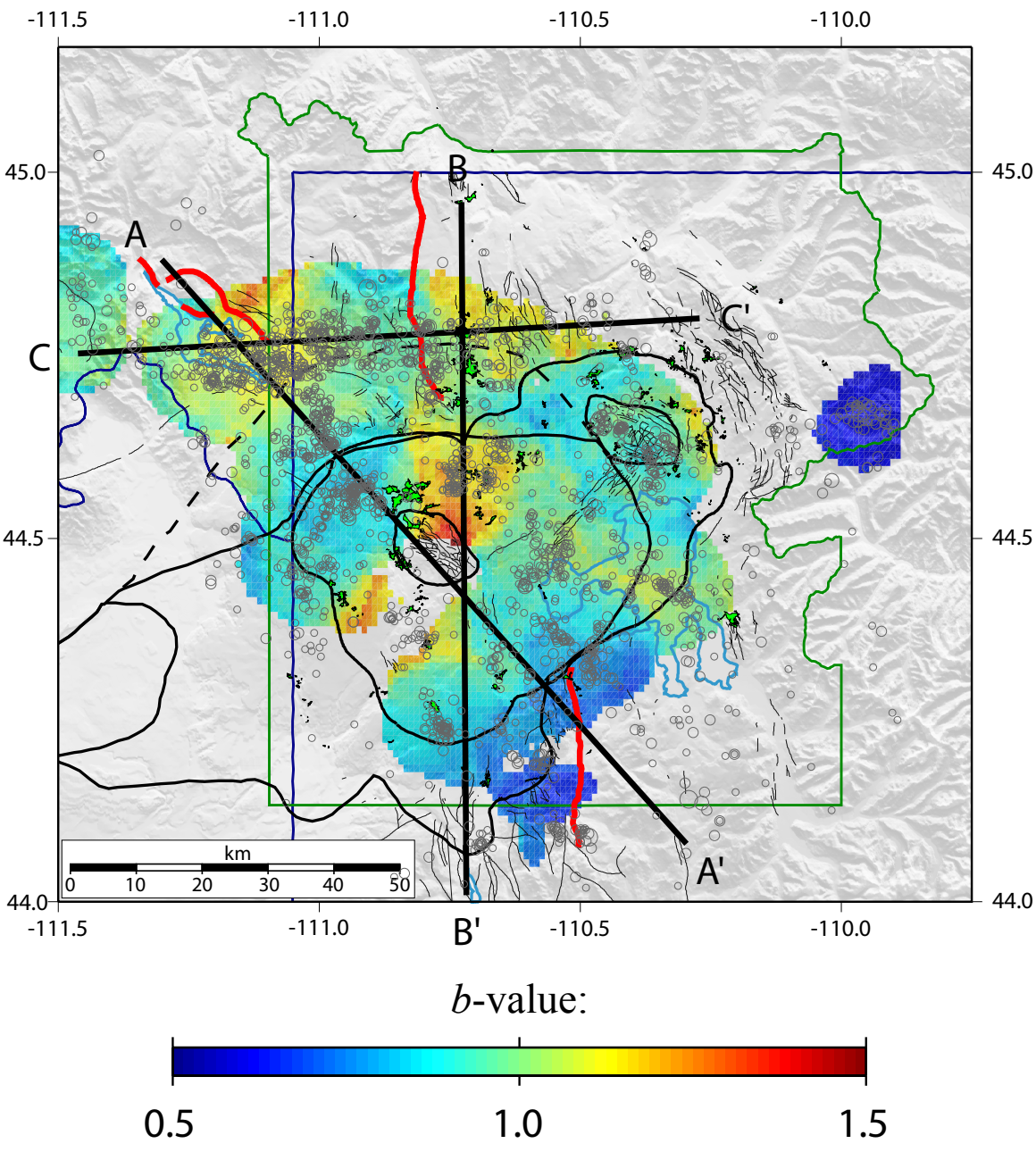


Figure 5.11. Spatial  $b$ -value distribution for the 30 minimum deswarmed catalog. Hot colors represent high  $b$ -values and cool colors represent low  $b$ -values. Earthquakes used in the calculation are shown as open circles. Areas of hydrothermal activity are plotted in green. Lines A-A', B-B', and C-C' represent cross-sections.

a lesser extent, is an area starting near the Norris Geyser Basin (NGB) and extending north in the Norris-Mammoth Corridor and east to the northern boundary of the Yellowstone Caldera. The Gallatin fault bounds this area of elevated  $b$ -values to the west. Here we see values of  $b$  up to  $1.25 \pm 0.06$ . The third area where we see elevated  $b$ -values is in the Hebgen Lake area just west of the Yellowstone National Park border. This area is also the site of the M 7.5 Hebgen Lake earthquake in 1959. The highest  $b$ -value in the Hebgen Lake area is  $1.34 \pm 0.13$  just to the northeast of the Red Canyon fault.

Two areas show relatively low  $b$ -values in addition to areas of high  $b$ -values. In the area to the east of the Sour Creek Resurgent Dome (SCD) on the park border, there are  $b$ -values as low as  $0.56 \pm 0.09$ . This is an area that has experienced persistent seismic activity throughout the entire time span of the catalog. The second area of low  $b$ -values is located at the southern portion of Yellowstone National Park near the East Mt. Sheridan fault (ESF) and the northern extent of the Teton fault. In this area  $b$ -values are as low as  $0.63 \pm 0.09$ . Errors in the  $b$ -value calculations are shown in Figure 5.12.

In cross section,  $b$ -values were calculated using a 0.5 km x 0.5 km grid using varying radii with 20 km wide cross sections.  $b$ -values were only calculated if there were at least 50 earthquakes with  $M_C \geq M_{COMP}$ . A radius of 5 km was selected for the cross sections because beyond this radius there was too much smearing. Although while using a 5 km radius the spatial coverage is limited, there are still some interesting trends in the results (Figure 5.13). Cross section A-A' shows one area of high  $b$ -values located 8 km to the southeast of the Hebgen Lake fault area. Here we note a band of high  $b$ -values extending downward to at least 10 km with values as high as  $1.31 \pm 0.03$ . This feature

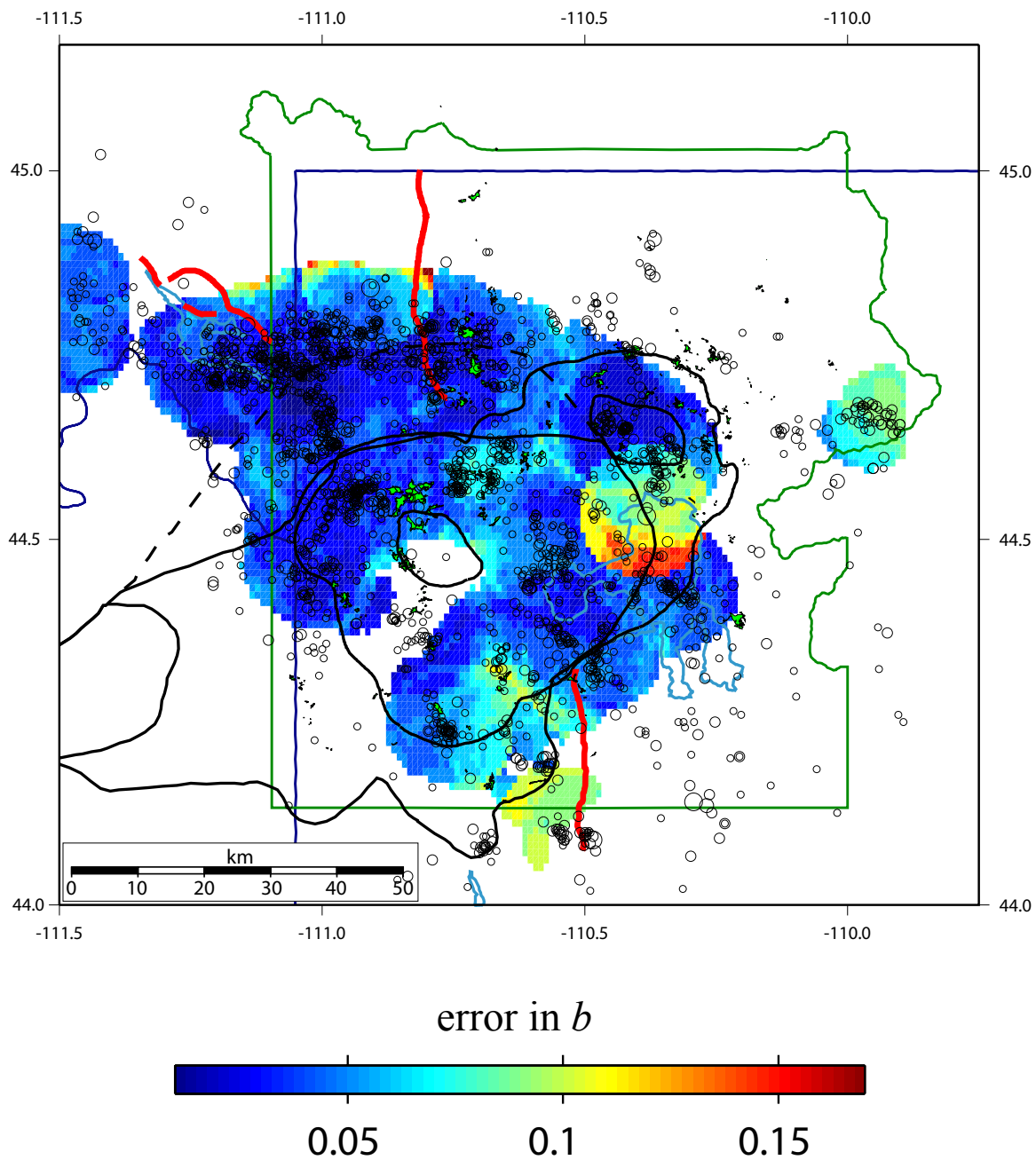


Figure 5.12. Errors in the  $b$ -value calculations. Earthquakes used in the calculations are shown as open circles. Calderas I, II, and III are outlined in black. Areas of hydrothermal activity are shown in green.

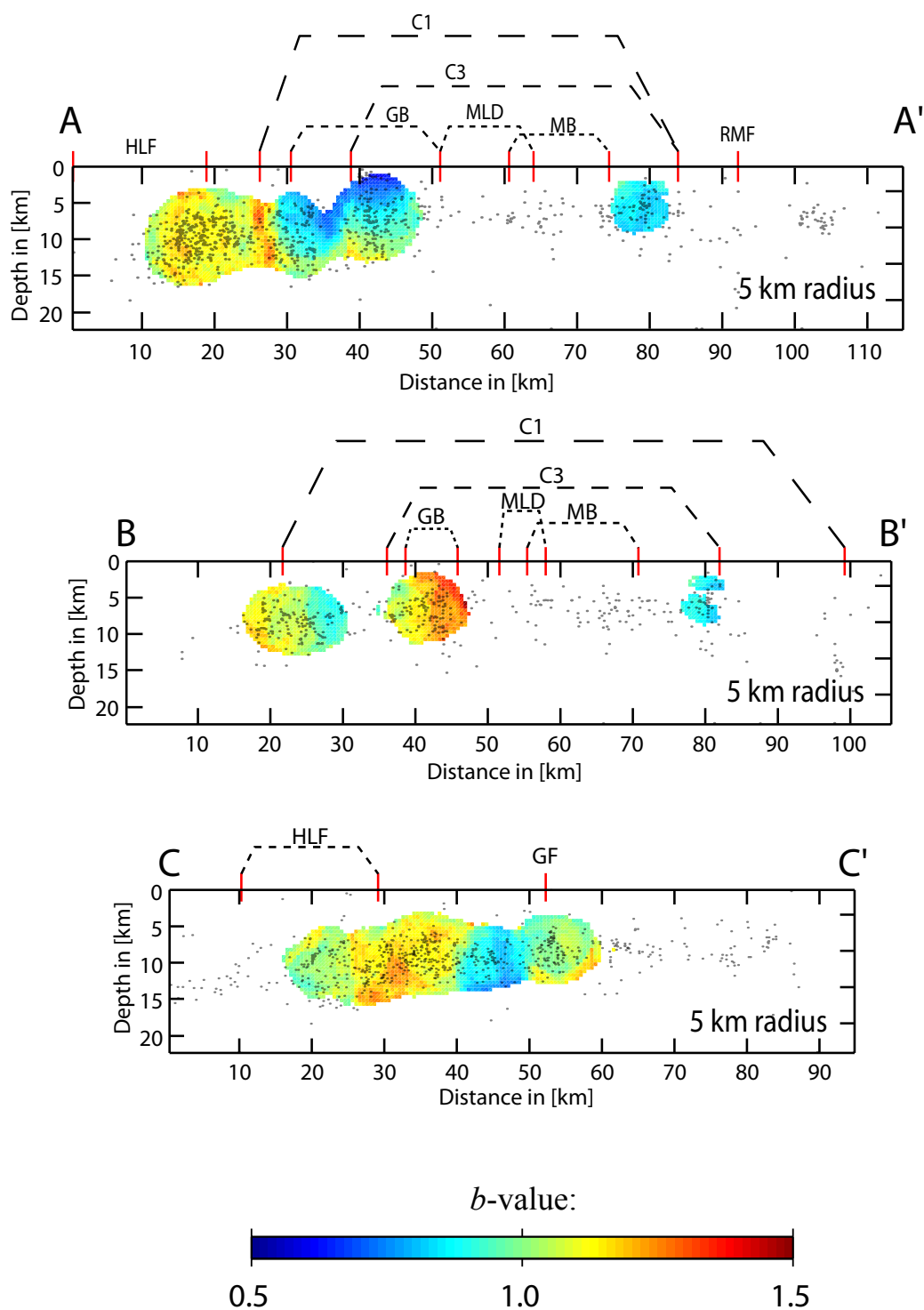


Figure 5.13. *b*-values with depth. Cross-sections are from Figure 5.11. Hot colors represent high *b*-values and cool colors represent low *b*-values. Various geographic features are labeled above each cross-section where c1=caldera I, c2=caldera II, c3=caldera III, MLD=Mallard Lake dome, HLF=Hebgen Lake fault, GF=Gallatin fault, RMF=Red Mountain fault (East Mt. Sheridan fault), GB= CO<sub>2</sub> gas body, and MB=magma body. All *b*-values were calculated using a 5 km radius.

was seen with other values for the radius as well so we are fairly confident that it is not an artifact of the radius selection. An area of low  $b$ -values exists 10 km to the southeast where we see values as low as  $0.61 \pm 0.06$ . The lowest of these  $b$ -values extends to a depth of around 10 km but most are confined within the upper 5 km. In cross-section C-C', an area of high  $b$ -values is located at  $\sim 12$  km depth below the Hebgen Lake fault where  $b$ -values as high as  $1.28 \pm 0.04$  were observed. An area of low  $b$ -values exists 6 km to the west of the Gallatin fault at  $\sim 13$  km depth with values as low as  $0.73 \pm 0.06$ . This area of low  $b$ -values extends from a depth of  $\sim 5$  km to  $\sim 14$  km. Although it is useful to use the cross-sections to see patterns of  $b$ -values, it is not very useful to use them to interpret structures at depth. This is due to the low number of events in the catalog and the larger search radius that had to be used to calculate the values.

$b$ -values were also calculated through time (Figure 5.14). Due to the limited number of earthquakes, the entire catalog had to be used.  $b$ -values were calculated using the Maximum Likelihood method using samples of 150 consecutive events stepped through time by 10 events. Results show that  $b$ -values fluctuate with a high of around 1.7 in late 1990 and a low of about 0.7 in late 1992. Episodes of ground deformation do not seem to correlate with changes in  $b$ -values.

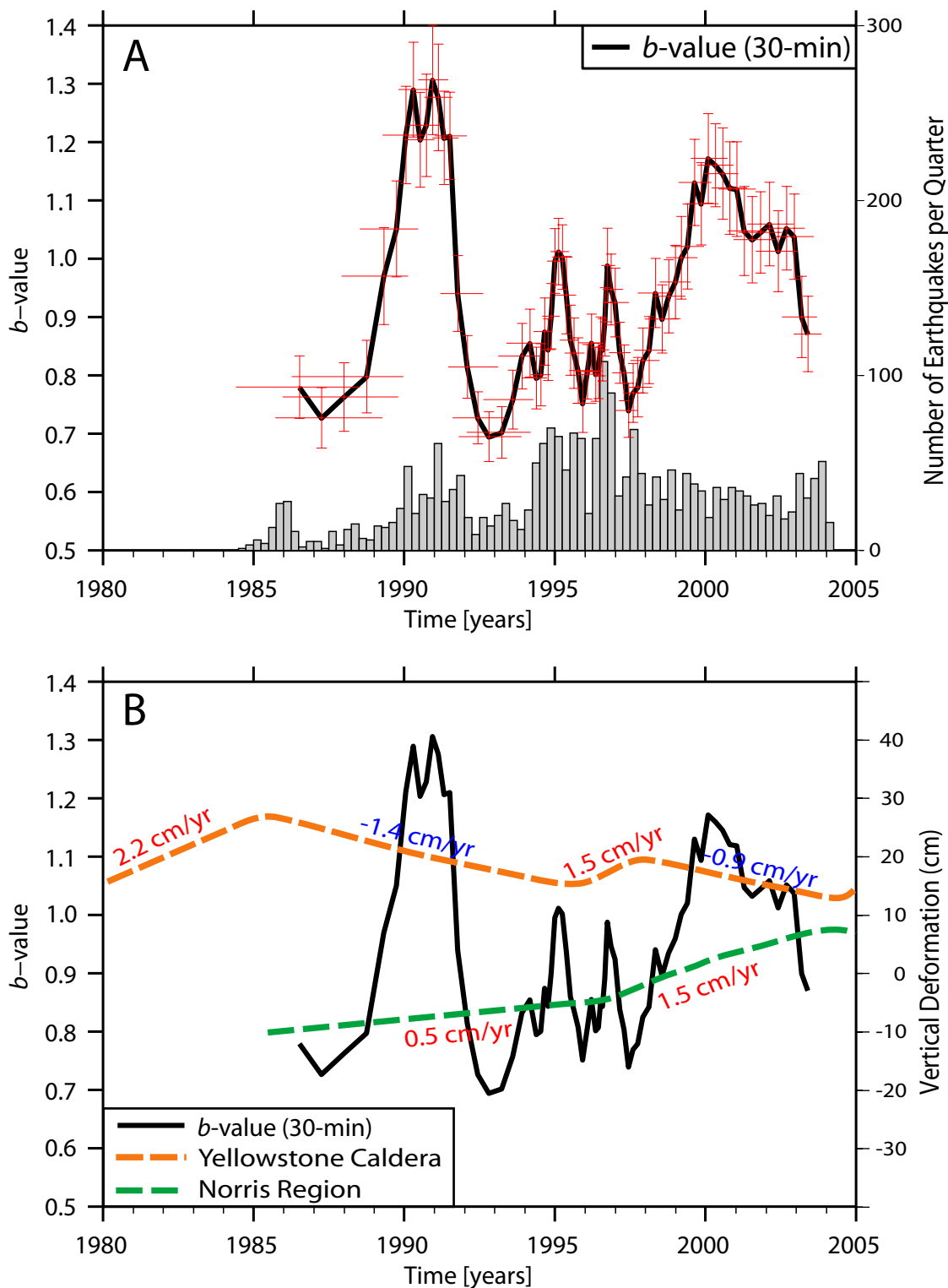


Figure 5.14.  $b$ -values through time. (a)  $b$ -values through time with number of earthquakes through time.  $b$ -value error bars are shown in red. (b)  $b$ -values through time with caldera ground deformation (orange) and Norris area deformation (green). Deformation data are from Puskas et al. [2007].

## CHAPTER 6

### THE YELLOWSTONE GEON-GIS DATABASE

#### 6.1. Objectives

A wide variety of geologic, geophysical, and geographic data for the Yellowstone volcanic system are available from decades of research by various scientists. The scientific community recognized that it was important to organize and distribute these data in a modern data scheme accessible via the Internet. Moreover, integration of different types of data is a key step to integrate disparate data sets that can address larger scope scientific questions about the formation and the continuing processes that keep the Yellowstone system active today. The overall goal of the Yellowstone GIS database is to better facilitate the distribution of geologic, geophysical, and geographical data related to Yellowstone in order to aid in the better understanding of the volcanic system.

Furthermore, the Yellowstone GIS database will serve as a tool to provide information to educate users in the geologic and geophysical nature of the Yellowstone system. To accomplish these goals, the database will be available to the public via a website hosted by the University of Utah.

The Yellowstone system has been widely studied and there exists a variety of data. Not only are there numerous data available, but these data are constantly being updated from year to year because the system is very dynamic in nature. As one can

expect, data pertaining to the Yellowstone volcanic system resides in many different locations. Creating a common place for the storage and distribution of these data provides a valuable asset to the scientific community as well as to the general public. Researchers seeking to gather data on the different aspects of the volcanic and tectonic system will now have to come to only one location and will be able to download the data that they need as well as any metadata that comes with it. This ease in finding data will greatly enhance the integration of data. Potential visitors to Yellowstone National Park who are looking for general knowledge on how the system works will also find information that will enhance their visit to the area.

Researchers are gaining a greater understanding of the processes that drive the volcanic system of Yellowstone. However, to understand how the entire system works and how all the different processes are connected, one needs to integrate all the different types of data. This idea of data integration is the key to answering the “big” questions on how the Yellowstone hotspot came to be and what continues to drive it today. Gaining knowledge on what drives the system will not only help in the understanding of how the system works but will also help immensely on quantifying the hazard that is faced by the many people that visit the Greater Yellowstone Area (GYA).

## 6.2. GEON

The NSF funded Geosciences Network (GEON) project<sup>1</sup> is a collaboration among a dozen PI institutions and a number of other partner projects, institutions, and agencies to develop cyberinfrastructure in support of an environment for integrative geoscience research. GEON is funded by the NSF Information Technology Research (ITR) program.

---

<sup>1</sup> <http://www.geongrid.org>

The goal of GEON is a more quantitative understanding of the 4-D evolution of the North American lithosphere. Furthermore, GEON is required to tackle the extreme heterogeneity among data and tools, across a wide range of earth science sub-disciplines and disciplines.

As a participating institution in the GEON project, a Point of Presence (PoP) node has been installed at the University of Utah as part of the GEON grid computing network. The PoP node is a Dell 2650 PowerEdge server class machine with 750 GB of raw disk space, dual 2.8 GHz Pentium 4 processors, 2 GB of RAM, dual gigabit network interfaces, and redundant power supplies. This machine is one of many machines across the country.

The University of Utah Seismology and Active Tectonics Research Group is part of the Rocky Mountains Testbed of the GEON project, whose goal is the study of lithospheric structure and properties across diverse tectonic environments via the integration of geophysical, petrologic, geochronologic, and structural data and models. Because Yellowstone is such a dynamic and diverse system, the Yellowstone GIS database is being used as a test dataset for this goal.

Researchers can access the data through the GEON portal<sup>2</sup> as the database becomes populated. Researchers can also access a wide variety of tools being built to manipulate data as well. The GEON grid computing network will help researchers access a powerful grid computing scheme to process large amounts of data.

---

<sup>2</sup> <http://portal.geongrid.org>

### 6.3. Geographical Information Systems

A Geographical Information System (GIS) is defined as “a computer system for capturing, storing, checking, integrating, manipulating, analyzing and displaying data related to positions on the Earth's surface” [<http://www.dictionary.com>]. There are many GIS applications available, some of which are open-source. The most popular version of a GIS, and the one used for this project is ArcGIS by the Environmental Systems Research Institute, Inc. (ESRI). There are many advantages and disadvantages to using ArcGIS. The main advantage with ArcGIS is because it is the most used GIS application with a wealth of help and information that both come with the software and is available online. The two main disadvantages are that (1) the software is proprietary which makes it hard for some researchers and most of the general public to use and (2) it is limited to the Microsoft Windows platform.

A GIS is very useful in regards to geological and geophysical data because it uses a Relational Database Management System (RDBMS) in which data are organized across several tables. Tables are associated with each other through common fields. These fields are user defined and can be such features as latitude, longitude, name, depth, magnitude, etc. Because of this, different datasets can be combined and or queried based on their individual attributes.

### 6.4. Data Hierarchy

To organize the data, a hierarchy is used that breaks the data down to the following categories: (1) raw data and metadata, (2) derived products such as maps, cross-sections, etc., (3) interpretive products where there has been an analytic analysis of

the data, (4) knowledge products in which the results have been interpreted in a scientific framework, and (5) education and outreach products.

This organization of the data will help the researcher or layperson to find the exact product that he/she is looking for. In addition the education and outreach section will be a valuable tool to aid in the distribution of learning materials as well as links to other information regarding the Yellowstone volcanic system.

### 6.5. Examples of Data

Table 6.1 shows the phase data for a  $M_C=4.4$  earthquake that occurred in the Yellowstone region on August 21, 2003. This is an example of raw data or level 1 data. Figure 6.1 shows a map of the epicenters from 1973-2003 as well as selected cross-sections; this is an example of a derived product or level 2 data. In this example of level 2 data, a step has been taken to put the epicenters on a map and to create cross-sections to view hypocenters. Figure 6.1 also shows many other types of level 2 data such as faults, topography, caldera outlines, geographic outlines, etc. Figure 3.1 shows the distribution of focal depths in Yellowstone. The 80<sup>th</sup> percentile of focal depths shallow noticeably within the 0.64 Ma Yellowstone caldera. Shallowing of focal depths is due to the higher temperatures within the caldera causing the brittle-ductile transition zone to be shallower beneath the caldera. The higher temperatures are due to the crystallization of basaltic-rhyolitic magma at a depth of about 8 km below the 0.64 Ma caldera [Husen et al., 2004a]. Figure 3.1 is an example of an interpretive product of level 3 data. Figure 6.2 shows low P-wave bodies below Yellowstone as imaged by local earthquake tomography

Table 6.1 - Earthquake arrival data (Level 1 (raw) data)

Station	First Motion	P-qual	P-arrival time (s)	S-qual	S-arrival time (s)	Duration (s)	$\alpha$	$\log(A_0)$	Begin Coda (s)	End Coda (s)	Peak-to-Peak Amp
YSB	c	0	69.9	0	0	642	2.02	6.37	118	334	0
YCJ	c	0	67.29	0	0	323	1.87	5.39	81	172	0
YTP	c	0	60.91	0	0	618	2.15	6.7	124	258	0
YMV	c	0	70.89	0	0	539	1.56	4.96	92	178	0
YPP	c	0	59.89	0	0	229	2.59	6.81	97	187	0
YHHZ	c	0	68.22	0	0	673	1.62	5.28	102	155	0
YPM	c	0	66.77	0	0	546	2.2	6.72	115	240	0
YWB	d	0	67.43	0	0	383	1.99	5.84	94	208	0
YMC	c	0	68.59	0	0	539	1.82	5.67	103	187	0
YDC	?	1	69.48	0	0	267	1.9	5.31	89	129	0
YHB	d	0	69.71	0	0	409	2.21	6.47	120	163	0
YGC	c	0	69.93	0	0	388	1.99	5.85	109	206	0
YML	c	0	64.71	0	0	430	2.18	6.44	103	206	0
YMS	c	0	57.81	0	0	318	2.35	6.58	93	153	0
MCID	c	0	63.86	0	0	546	2.39	7.24	125	241	0
YJCZ	c	0	67.7	0	0	515	1.87	5.77	98	206	0
YPC	c	0	66.05	0	0	345	2.14	6.13	97	180	0
YMPZ	c	0	67.91	0	0	578	1.97	6.14	108	199	0
YNRZ	c	0	66.92	0	0	296	1.91	5.42	88	155	0
yftz	c	0	62.66	0	0	0	0	0	0	0	0
ymrz	c	0	67.18	0	0	0	0	0	0	0	0
imwz	c	0	61.27	0	0	0	0	0	0	0	0
ahiz	c	0	79.95	0	0	0	0	0	0	0	0
bw0z	c	0	81.8	0	0	0	0	0	0	0	0
lkwz	?	0	63.56	0	0	0	0	0	0	0	0

Phase Data for a  $M_c=4.4$  Yellowstone Earthquake Occurring on August 21, 2003 at 1:46 a.m.

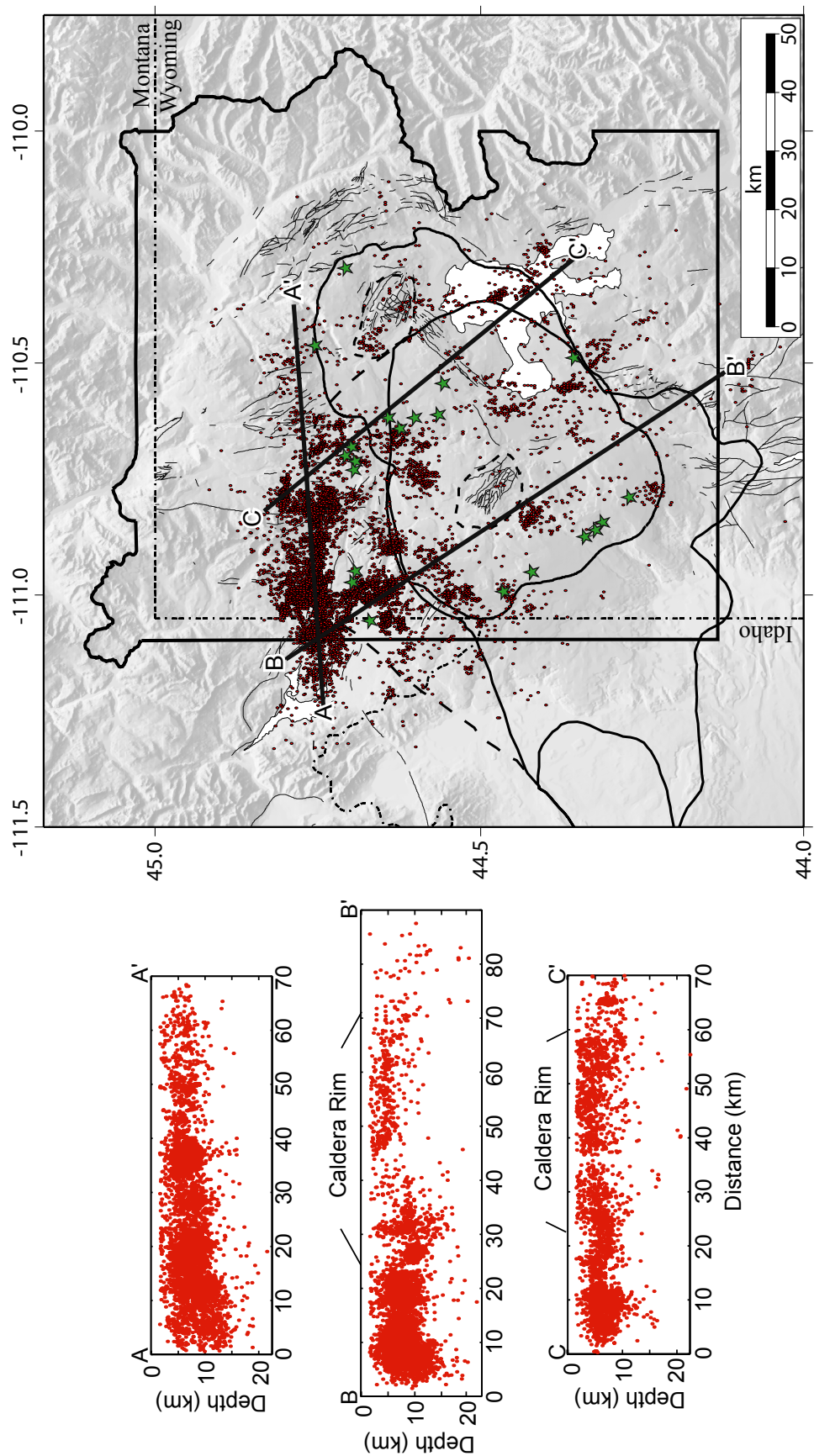


Figure 6.1. Epicenters and hypocenters of the A & B quality earthquakes from 1973 - 1981 and 1984 - 2003. Quaternary faults are shown as thin black lines. The three calderas are outlined as thick black lines. The two resurgent domes are outlined as dashed black lines.

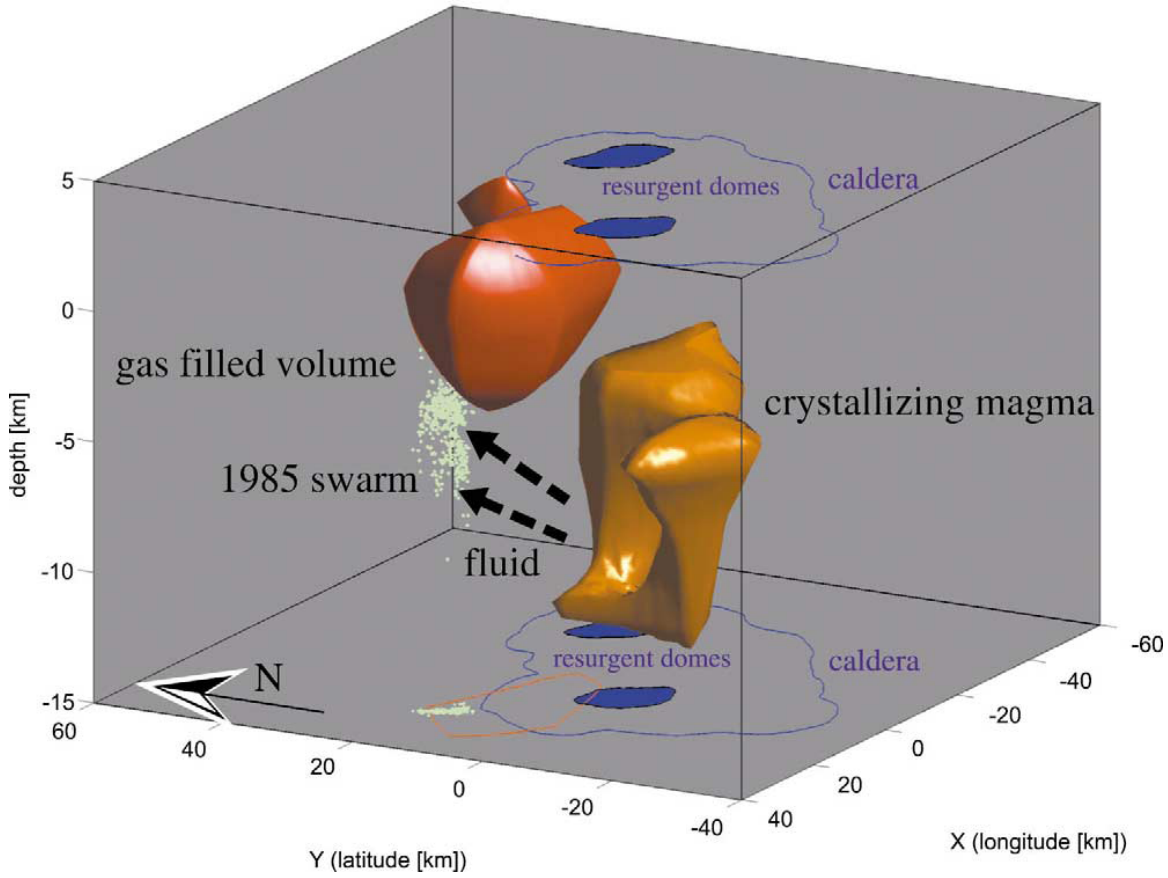


Figure 6.2. Partial melt and CO<sub>2</sub> gas bodies imaged by local earthquake tomography modified from Husen et al. [2004a]. Orange body outlines location of a possible crystallizing magma body beneath the 0.64 Ma caldera; red body outlines location of shallow, possible gas filled volume.

and is an example of a knowledge product or level 4 data. The orange body in Figure 6.2 has been interpreted to be a body of possible crystallizing magma. The red body outlines the location of a shallow, possible CO<sub>2</sub> gas filled body [Husen et al., 2004a]. This figure shows how the autumn, 1985 swarm [Waite & Smith, 2002] could be due to fluids migrating away from the magma body.

## 6.6. Data Visualization

Data visualization is an important tool in understanding the spatial relationships between different aspects of the Yellowstone-Teton volcanic-tectonic system. The Fledermaus suite of tools<sup>3</sup> is used in this study for data visualization. Using Fledermaus Professional edition, we were able to create scenefiles with a variety of the data from the database. Scenefiles are collections of various geographic, geologic, and geophysical objects. The spatial understanding of such things as the Yellowstone magma chamber and earthquake swarms is enhanced while using the 3-D environment to visualize data (Figure 6.3). Fledermaus also allows us to input panoramic pictures and pictures of GPS benchmarks as well (Figure 6.4). Flythroughs can be created and exported as movies. These movies are great tools for the general public to download or view at visitor centers.

Scenefiles from Fledermaus will be available to the public through the website for download. Users can view the data using a free viewer for files in the Fledermaus file format called iView3D<sup>4</sup>.

---

<sup>3</sup> <http://www.ivs3d.com/>

<sup>4</sup> <http://www.ivs3d.com/products/iview3d/>

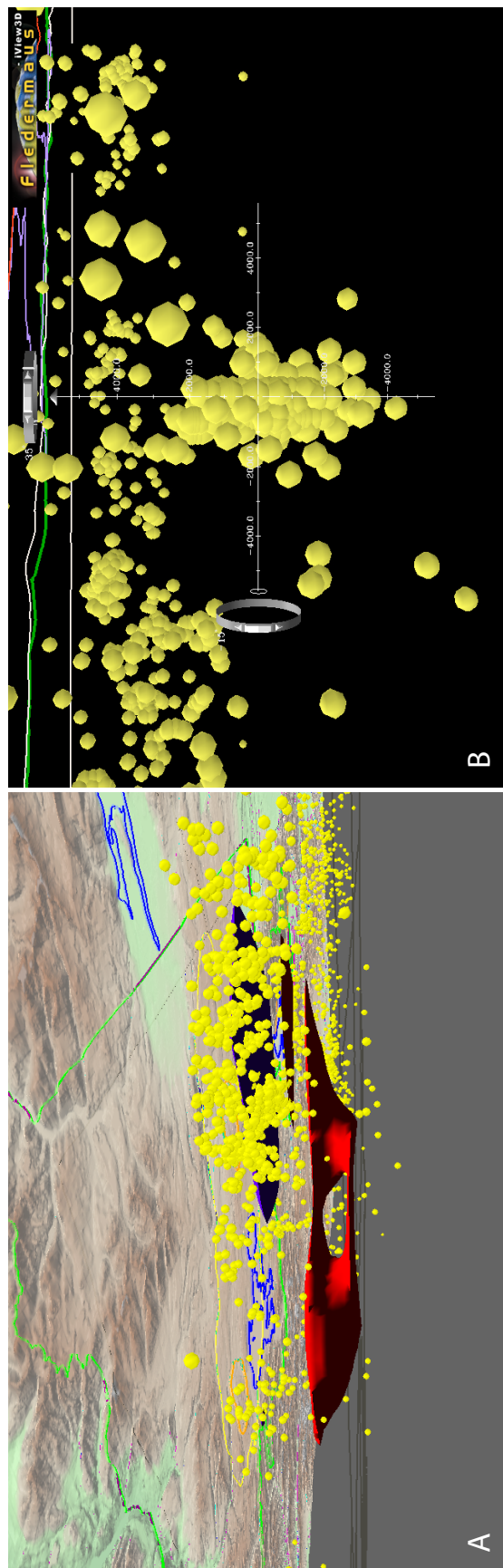


Figure 6.3. Data visualization of Yellowstone's magma chamber and earthquake swarms. Screen captures from Fledermaus showing (A) Yellowstone's magma chamber in red along with earthquake hypocenters shown in yellow and (B) an individual swarm.

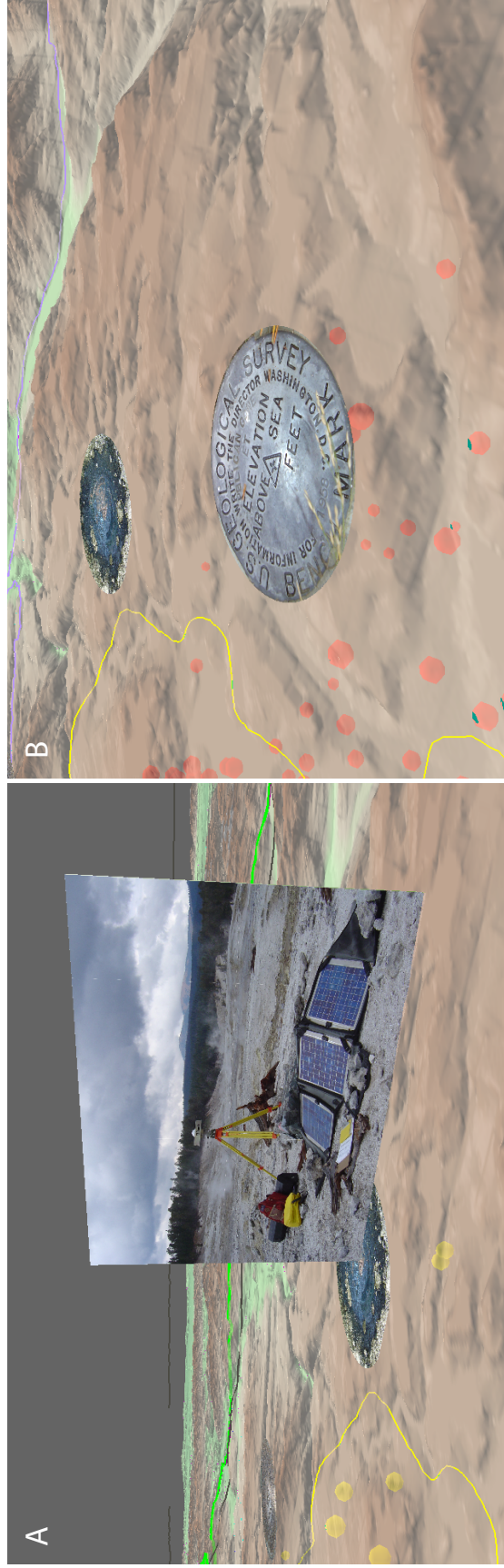


Figure 6.4. Data visualization of panoramic photos and GPS benchmarks. Screen captures from Fledermaus showing (A) a picture of the campaign station HOTS located in Hot Springs Basin in Yellowstone National Park and (B) a benchmark located at the summit of Pelican Cone.

### 6.7. Website

The Yellowstone GIS database is accessible on the World Wide Web at <http://www.yellowstonegis.utah.edu> (Figure 6.5). From the front page, one can navigate to the various aspects of the webpage such as Maps, where you can see different pictures from different places in Yellowstone and Grand Teton National Parks as well as see animated sequences of Yellowstone earthquakes for the years 1973 – 2005. The research tab explains all the different areas of research that are going on within the University of Utah Seismic and Active Tectonics Research Group (UUSATRIG). The Data tab links to the online data that is described in the previous section. The image gallery tab takes the user to a page that shows pictures of different aspects Yellowstone volcanic system. The education and outreach tab takes the user to a valuable page that has numerous links to other sites that provide information on the system. The contact us tab links to information on how to contact the webmaster as well as all the funding institutions. Below the tabs is a link that takes the user to the current seismic and GPS monitoring update published by the Yellowstone Volcano Observatory (YVO). This update provides information such as the level of seismicity in the region (number of earthquakes, biggest magnitude, etc.) as well as information on any unusual ground motions going on as well as links to the data. There is also a spot below this link for any current news that pertains to the area.

Appendix D shows all data that are planned and are currently a part of the Yellowstone GIS database.

# THE YELLOWSTONE-TETON EPICENTER

A central location for Yellowstone-Teton geologic information (GIS)

- OVERVIEW
- MAPS
- RESEARCH
- DATA
- IMAGE GALLERY
- EDU, OUTREACH AND LINKS
- CONTACT Us



**WHAT'S HOT**  
Seismic & GPS Monitoring in the Yellowstone Region, January 2007

**THE UNIVERSITY OF UTAH** Dept. of Geology & Geophysics, 135 S. 1460 E. #719, SLC, UT 84112 801.581.7856

Supported by: The University of Utah, National Science Foundation, GEON: The Geosciences Network, Yellowstone Volcano Observatory, National Park Service, the United States Geological Survey, and the University of Utah Seismograph Stations

Website by: University of Utah Media Solutions

Grand Prismatic Spring, Yellowstone ◀ Play Again

Figure 6.5. The Yellowstone-Teton Epicenter located at <http://www.yellowstonegis.utah.edu>. The website offers a wealth of knowledge updated in a real-time fashion for both the researcher and the layperson looking to gather either data for a research project or just information for an upcoming visit to the region.

## CHAPTER 7

### DISCUSSION

Seismicity in Yellowstone is dominated by swarms. Most swarms occur 5 to 20 km north of the 0.64 Ma Yellowstone caldera between Norris Geyser Basin and Hebgen Lake. Areas of high  $b$ -values within and adjacent to the 0.64 Ma caldera could be indicative of the transport of magmatic fluids out of the caldera and into the areas around Norris Geyser Basin and Hebgen Lake.

#### 7.1. Earthquake Swarm Identification

Using the definition that a swarm has to be at least 30 events, ~40% of the recorded seismicity in the Yellowstone region is due to swarm activity (Figure 5.2B). Of the 57 swarms identified, 48 (84.2%) are located in the region just north and northwest of the caldera while 9 (15.8%) are located within or on the boundary of the 0.64 Ma caldera (Figure 5.2A). Because a high number of swarms were identified in the east-west band of seismicity extending from the Hebgen Lake fault to the Norris Geyser Basin, it is interpreted that the crust is highly fractured in this area because the large number of small magnitude earthquakes occur on numerous small cracks. This stems from the fact that earthquake swarms are often found in volcanic areas or other remarkably fractured regions or areas where there is a concentrated application of stress such as intruding

magma [Mogi, 1963]. There is also an abrupt change in the topography in this region and the east-west alignment of swarm epicenters here indicates that this is the location of the northern rim of the 2.0 Ma caldera (caldera I, dotted line in Figure 2.3) which is about 15 km north of the mapped caldera rim of Christiansen [2001]. It is believed that the Gallatin range was once continuous with the Teton range to the south. During the eruption 2.0 million years ago, the mountain range was either destroyed by the eruption itself or destroyed during the caldera collapse [Smith & Seigel, 2000]. The east-west alignment of swarm epicenters in this area is significant in that the swarms may be occurring on preexisting zones of weakness from the 2.0 Ma caldera eruption.

Shallowing of focal depths within the caldera where the 80<sup>th</sup> percentile focal depth decreases from around 10 km north of the caldera rim and about 14 km south of the caldera rim to about 5 km inside the caldera suggests that the temperature is too high to sustain most brittle failure. The shallowest earthquakes occur at a depth of about 3 km immediately beneath the Mallard Lake Resurgent Dome (Figure 3.1). There is also a significant decrease in the number of swarms within the 0.64 Ma caldera (caldera III).

## 7.2. *b*-value Distribution

We interpret the area of high *b*-values (up to  $1.54 \pm 0.06$ ) in the area located near the Mallard Lake Resurgent Dome (MLD) (Figure 5.11) to be influenced by high crustal heterogeneity and a high thermal gradient. This high heterogeneity is due to numerous small cracks in the crust oriented in all directions due to recent episodes of uplift. Under these conditions, the likelihood of large earthquakes occurring is decreased because a rupture terminates when it encounters an existing crack orientated unfavorably for failure.

In such a highly fractured crust, many small ruptures would be observed but fewer larger ones, which is what is seen in the frequency-magnitude distribution [Wiemer et al., 1998]. The average magnitude of events in this area is  $\sim 1.5$ . This translates to an average rupture length of about 70 m [Wiemer & McNutt, 1997; Kanamori & Anderson, 1975]. These small cracks produce only small earthquakes due to their short length. A high thermal gradient could be due to the presence of magma below the surface. This is consistent with results from the Long Valley Caldera in eastern California, which is a similar large silicic volcanic center. Wiemer et al. [1998] found high b-values ( $b > 1.5$ ) in the area near the resurgent dome and interpreted these to be the result of a highly fractured crust.

Puskas et al. [2007] measured uplift by GPS just north of the caldera near the Norris geyser basin beginning in 1987 and continuing until 1995 at a rate of 5 mm/yr. GPS measurements from the years 1995-2003 show uplift significantly increased on the northern caldera rim just south of Norris Geyser Basin (NGB). During this period the uplift continued at a higher rate of  $15 \pm 4$  mm/yr for a total of 75 mm. In 2000-2003, uplift continued on the northern caldera rim at  $12 \pm 4$  mm/yr for an additional 36 mm of displacement, while subsidence resumed in the central caldera axis [Puskas et al., 2007].

In addition to GPS, Satellite Interferometric Synthetic Aperture Radar (InSAR) studies also measured uplift on the north caldera rim from the years 1995-2002 [Wicks et al., 1998; Wicks et al., 2006]. Wicks et al. [2006] suggest that the uplift is due to variations in the movement of molten basalt into and out of the Yellowstone volcanic system. More specifically, they state that basaltic magma is being fed into the volcanic system beneath the Sour Creek Resurgent Dome (SCD) (Figure 2.3). The basaltic

magma then spreads horizontally at a rheological boundary before escaping the caldera system at the three-way intersection of the northern caldera boundary, the west-northwest-striking seismic belt east of the Hebgen Lake fault, and the north-trending Norris-Mammoth corridor. Before exiting the volcanic system, magma accumulated beneath the north caldera boundary, leading to continued uplift in the area [Wicks et al., 2006] (Figure 7.1).

This emplacement of magma and the accompanying expansion would give rise to many of the factors that tend to cause high  $b$ -value measurements such as high heterogeneity of the crust due to numerous cracks from the increased stress and a high thermal gradient which is also supported by focal depth distribution. The shallowest earthquakes in the area occur beneath the MLD (Figure 3.1) where the depth of 80% of the hypocenters is  $\sim 5$  km. As stated before, this depth is interpreted as the brittle-ductile transition zone with a temperature of  $\sim 400^\circ\text{C}$  [Sibson, 1982; Smith & Bruhn, 1984; Fournier, 1999]. This gives a thermal gradient of  $\sim 80^\circ\text{C}/\text{km}$  for the area beneath the Mallard Lake resurgent dome. If the average 80<sup>th</sup> percentile depth of 8 km inside the 0.64 Ma caldera is used, an average thermal gradient of  $\sim 50^\circ\text{C}/\text{km}$  is determined. Smith & Braile [1994] estimated an average thermal gradient for the Yellowstone region of  $\sim 45^\circ\text{C}/\text{km}$ . This supports the results of [Warren & Latham, 1970] in which they show that an increase in the thermal gradient causes an increase in  $b$ . Given that the period of uplift and the period of high  $b$ -values occur during the same time, these could be the underlying reasons for the high  $b$ -values measured in this study.

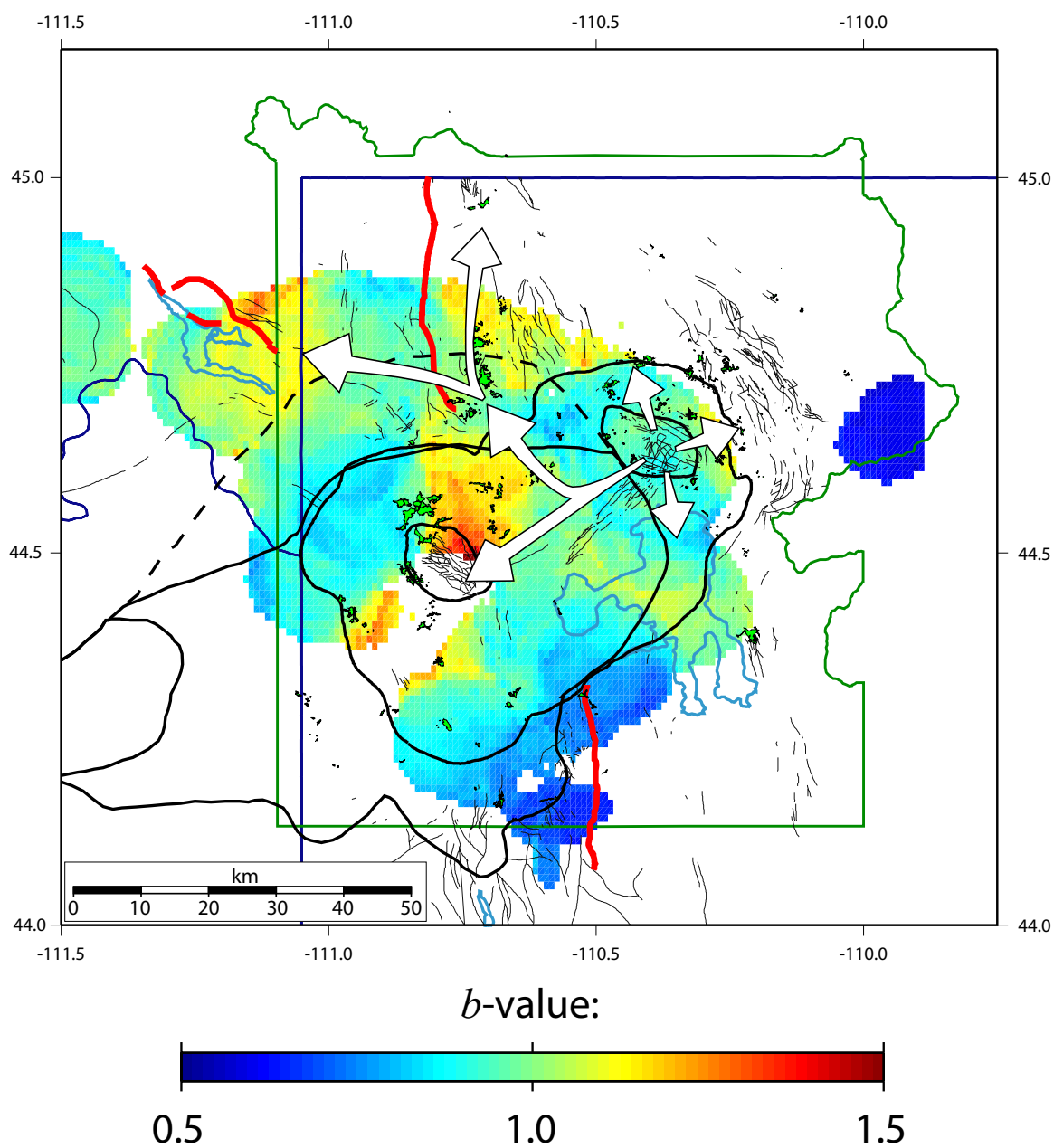


Figure 7.1. High  $b$ -value areas indicative of the presence of magmatic fluids. Arrows show interpreted magma migration paths from Wicks et al., 2006. Color background shows  $b$ -values. Hot colors represent high  $b$ -values and cool colors represent low  $b$ -values. Areas of hydrothermal activity are plotted in green.

The area of high  $b$ -values of up to  $1.25 \pm 0.06$  north of the caldera rim extending from Norris Geyser Basin can also be a result of magmatic fluids escaping the caldera and moving north into the Norris-Mammoth Corridor [Wicks et al., 2006] (Figure 7.1). Again, the presence of magma gives rise to all the contributing factors causing higher  $b$ -values, mainly high heterogeneity, and high thermal gradient. This is because the presence of partial melt would cause higher temperatures which intern would create a zone of relatively lower stress around the area of partial melt. Numerous cracks would form as the area of partial melt pushed up through the crust as well.

The area of high  $b$ -values located near Hebgen Lake exhibiting values up to  $1.34 \pm 0.13$  could also be the result of magma escaping the caldera (Figure 7.1). However, high  $b$ -values in this area could also be a reflection of a relatively low stress regime as a result of the 1959 Hebgen Lake earthquake. Chang and Smith [2002] show that the 1959 M7.5 Hebgen Lake earthquake caused a decrease in the Coulomb static stress of about 4 bars in the areas immediately north and south of the fault plane where we see elevated  $b$ -values.

Another explanation for the higher  $b$ -values could be because of the high concentration of hydrothermal features in the area. Hydrothermal waters of Yellowstone circulate through the crust in an intricate system of cracks and are heated from below from a body of crystallizing magma. The fact that there is hydrothermal activity shows that the crust is very heterogeneous. There seems to be a correlation between higher  $b$ -values and the location of hydrothermal activity in the western half of Yellowstone (Figure 5.11). This would indicate that the high  $b$ -values are due to both the highly fractured (heterogeneous) crust and the high temperatures that allow hydrothermal

activity to occur. Therefore, the high  $b$ -values could be an indication of the highly fractured crust that facilitates the movement of hot, hydrothermal fluids. Wall [2005] showed that NE-SW and NW-SE trending fractures in the Lava Creek Tuff provide major flow pathways for hydrothermal fluids at Norris Geysir Basin.

The area of low  $b$ -values in the southern part of the Park where  $b$ -values are as low as  $0.63 \pm 0.09$  (Figure 5.11) is suggested to be attributed to high stress accumulation from large Basin-Range faults south of the caldera. Stress accumulation would take place mainly on the East Mt. Sheridan fault and the Teton fault.

The East Mt. Sheridan fault is a large north-south striking normal fault bounding the east side of Mt. Sheridan (Figure 2.3) and is about 41 km long, has a maximum magnitude ( $M_w$ ) of 6.9, a 1.1 mm/yr slip rate, and dips  $60^\circ$  to the east (Wong et al., 2000). It is believed that prior to the cataclysmic caldera-forming eruptions at Yellowstone, the East Mt. Sheridan fault was continuous across the plateau with the faults to the north of the caldera [Smith & Seigel, 2000]. The ages of the most recent events are not known as no dating has been done on this fault system.

The Teton fault is a major basin and range fault that bounds the eastern margin of the Teton Range. Holocene fault scarps extend for 55 km along the range front and range from 3 to 52 m high [Byrd et al., 1994]. This confirms that the fault has been subject to several postglacial ground rupturing earthquakes [Gilbert et al., 1983; Susong et al., 1987; Smith et al., 1989b, 1993]. There has been  $\sim 2$  km of movement along the fault since the eruption of the Huckleberry Ridge tuff 2.0 Ma [Christiansen & Blank, 1972]. The northern segment of the fault appears to die out under the 70,000-yr-old Pitchstone Plateau rhyolite flows and the eastern segment of the fault merges into the remains of the

ring fracture system from the 2.0 Ma caldera in Yellowstone National Park [Christiansen & Blank, 1972].

Trenching studies on the fault reveal evidence for two major ruptures in the past. The youngest event was a  $M=6.8$  earthquake that occurred 4,700 to 6,000 years ago and produced 1.3 m of offset. The second youngest event was a  $M=7.1$  earthquake that occurred 7,300 years ago and produced 2.8 m of offset [Byrd, 1991]. In addition to the two recorded events from trenching, Byrd [1995] suggests that there were five additional  $M\sim 7.0$  events from 14 ka to 7.9 ka, each producing  $\sim 2.0$  m of offset. The Teton fault is estimated to be about 64 km long, have a maximum magnitude ( $M_w$ ) of 7.2, a 1.5-2.0 mm/yr slip rate, and dips  $60^\circ$  to the east (Byrd, 1995; Wong et al., 2000).

Scholz [1968], Wyss [1973], Urbancic et al. [1992], Schorlemmer et al. [2004], and Schorlemmer et al. [2005] showed that an increase in applied shear stress or an increase in effective stress decreases the  $b$ -value. It is proposed here that the low  $b$ -values in the southern portion of Yellowstone National Park are due to stress buildup from the East Mt. Sheridan fault and the Teton fault. The high stress in the area could be because of the lack of large, scarp forming events in the recent past, allowing stress to build up, or crustal deformation from the volcanic system in Yellowstone could be loading the faults. It is not well known how the large normal faults to the north and south interact with the caldera system, more specifically, whether or not the volcanic system is loading the faults or whether it is absorbing stress. King et al. [1994] state that stress increases of less than one-half bar appear sufficient to trigger earthquakes, and stress decreases of a similar amount are sufficient to suppress them. Therefore, it is possible

that a stress increase on the large normal faults to the north and south of the caldera system could trigger earthquakes.

Imaging the  $b$ -value distribution for different time periods corresponding to crustal deformation would be extremely helpful to understand the underlying cause of the deformation. However, there are not enough earthquakes for the different time periods to calculate  $b$ -values. In addition, using a 10 km radius to calculate  $b$ -values have limited our ability to identify smaller features. As time goes by and more earthquakes are recorded,  $b$ -values will be able to be calculated at finer and finer scales.

## CHAPTER 8

### CONCLUSIONS

A large percentage of earthquakes recorded in the Yellowstone region, estimated at ~40%, are defined as occurring in swarms. This corresponds to about 38% of the total seismic moment. Fifty-seven swarms (Figure 5.2A, appendices A, B, C) were identified during the years 1984-2003, comprising of 7,906 events (Figure 5.2B). Forty-eight of the 57 swarms occur in the east-west band of seismicity that stretches from the Hebgen Lake fault to the Norris Geyser Basin (Figure 5.2A). Swarms vary in duration from 1 to 46 days and have a range of 30 to 722 total events.

Swarm events as well as the 597 triggered earthquakes from the 2002  $M7.9$  Denali fault earthquake [Husen et al., 2004b; Husen et al., 2004c] were removed from the catalog. A magnitude of completeness ( $M_{COMP}$ ) value of  $M_C=1.5$  was calculated for the time period (Figure 5.6) and all events smaller than this were removed from the catalog leaving 2,370 events to calculate  $b$ -values from 1984-2003 (Figure 5.7B).

Significant spatial variations in the frequency-magnitude distribution are well-defined in the Yellowstone region. The spatial distribution of  $b$ -values in Yellowstone shows areas of both high and low  $b$ -values mixed in with areas of normal crustal values ( $b \approx 1.0$ ) (Figure 5.8, Figure 5.11). There are two main areas of anomalous  $b$ -values that are interpreted in this paper. The first is an area of anomalously high  $b$ -values (up to

1.54±0.06) below and just to the north of the Mallard Lake Resurgent Dome and the second is an area of anomalously low  $b$ -values (as low as  $0.63 \pm 0.09$ ) just south of the 0.64 Ma caldera rim (Figure 5.11).

The area of high  $b$ -values just to the north of the Mallard Lake Resurgent Dome occurs in the same area as recent crustal deformation where the area around Norris Geyser Basin was uplifted by as much as 111 mm from the years 1987-2003 [Puskas et al., 2007]. Using InSAR data, Wicks et al. [2006] interpreted this area of uplift as due to the emplacement of basaltic magma at ~15 km below the surface. Magma intrusion as well as the crustal deformation are processes that would alter the frequency-magnitude distribution of earthquakes towards high  $b$ -values. As magmatic fluids are injected into the system, temperatures are expected to rise around the intrusion and the crust would weaken. The high temperature, weakened crust and the expanding sill could cause the formation of numerous small fractures as magma escaped the volcanic system. A relatively large number of smaller magnitude earthquakes are expected to accompany the formation of these small fractures and would alter the frequency-magnitude distribution of earthquakes towards higher  $b$ -values. This supports the hypothesis that the higher  $b$ -values in this region are due to the presence of magmatic fluids.

The area of low  $b$ -values 0 to 14 km south of the 0.64 Ma caldera rim is interpreted to be due to high stress in the crust due to the loading of both the East Mt. Sheridan fault and the Teton fault. This could also be an indication of a relatively strong crust. However, it is unclear if the high stress in the crust is due to the lack of large earthquakes on the East Mt. Sheridan and Teton faults in the recent past or if those faults are being loaded by the crustal deformation from the Yellowstone volcanic system.  $b$ -

values calculated for the Yellowstone region can be used in further studies to better understand the seismic hazard in the area.

Various geologic, geophysical, and geographic data of the Yellowstone-Teton magmatic-tectonic system were compiled and converted to a GIS format. These data were divided into four categories: (1) raw data and metadata, (2) derived products such as maps, cross-sections, etc., (3) interpretive products where there has been analytic analyses of the data and (4) knowledge products in which the results have been interpreted in a scientific framework. Various datasets were registered on the GEON portal for distribution. These data can be viewed and queried using ARCIMS running on our website. These data as well as other geologic and geophysical data pertaining to the Yellowstone volcanic system are available through the Yellowstone GIS database (<http://www.yellowstonegis.utah.edu>). This website will be an aid to researchers by offering a variety of data products relating to the Yellowstone volcanic system all in one place. These data will be from a variety of backgrounds and will be updated in as near real-time a state as resources are available. In addition to researchers, the website will prove to be a wealth of information about the Yellowstone region for the general public as well. Data visualization tools were created and provide a way for the public to better understand the geologic and geophysical workings of the Yellowstone hotspot.

## APPENDIX A

### TABLE OF YELLOWSTONE EARTHQUAKE SWARMS

This appendix consists of a table that lists characteristics of the swarms including swarm start and end date, duration, longitude and latitude, the maximum number of events per day, the maximum magnitude, and the total number of events. Swarms are color-coded based on what definition of a swarm they were identified with. All 204 swarms were identified using the 10 minimum definition of a swarm. The total of the dark gray and light gray swarms constitutes the swarms identified using the 30 minimum definition of a swarm. Swarms shaded light gray were identified using the 50 minimum definition of a swarm. The swarms plotted in the figures in the text and in Appendices B and C use the same numbering system.

Table A.1 - Table of Yellowstone earthquake swarms

#	Start Day	End Day	Dur	Lon	Lat	EQ/Day <sub>max</sub>	Mag <sub>max</sub>	No. EQ
1	3/1/1985	3/11/1985	11	-110.7495	44.7884	71	2.77	148
2	4/23/1985	4/24/1985	2	-111.0945	44.7760	7	1.07	11
3	8/16/1985	8/18/1985	3	-111.0155	44.6465	7	2.17	15
4	9/5/1985	9/7/1985	3	-110.9945	44.6845	9	2.07	15
5	9/19/1985	9/20/1985	2	-110.8140	44.3516	19	2.69	21
6	10/3/1985	11/17/1985	46	-110.9995	44.6422	85	3.72	462
7	11/24/1985	12/10/1985	17	-111.0050	44.6503	11	3.08	52
8	11/13/1986	11/17/1986	5	-111.0170	44.6621	7	2.62	17
9	11/23/1986	11/25/1986	3	-111.0145	44.6677	8	2.83	12
10	11/29/1986	12/1/1986	3	-111.0140	44.6655	5	1.83	11
11	5/21/1988	5/24/1988	4	-111.1205	44.7486	12	2.22	21
12	9/29/1989	10/3/1989	5	-111.0635	44.7243	37	2.16	67
13	10/20/1989	10/20/1989	1	-111.0895	44.7455	11	1.87	11
14	10/24/1989	11/1/1989	8	-111.0770	44.7411	50	2.28	68
15	12/19/1989	12/19/1989	1	-110.3345	44.4387	12	2.19	12
16	2/26/1990	3/9/1990	12	-111.0765	44.6385	84	2.11	233
17	6/16/1990	6/17/1990	2	-110.8160	44.7094	15	2.52	27
18	7/8/1990	7/9/1990	2	-110.4660	44.3827	14	2.11	16
19	12/24/1990	12/25/1990	2	-111.2160	44.7188	18	2.79	23
20	12/31/1990	1/11/1991	12	-111.2085	44.7275	7	2.74	25
21	6/28/1992	6/29/1992	2	-110.7585	44.7947	10	2.30	11
22	5/22/1993	5/23/1993	2	-110.9695	44.7536	9	2.21	14
23	12/14/1993	12/15/1993	2	-111.1320	44.7610	8	1.82	11
24	5/2/1994	5/4/1994	3	-111.0815	44.7436	38	2.26	54
25	7/28/1994	7/30/1994	3	-111.0805	44.6129	9	1.86	17
26	9/9/1994	9/17/1994	9	-111.0295	44.7356	33	2.11	52
27	11/22/1994	11/25/1994	4	-111.0535	44.7399	5	2.10	10
28	11/28/1994	11/29/1994	2	-111.0555	44.7859	9	1.85	12
29	12/13/1994	12/15/1994	3	-110.5635	44.7922	8	2.22	12
30	1/5/1995	1/7/1995	3	-111.0955	44.7306	5	1.52	10
31	4/16/1995	4/17/1995	2	-110.9135	44.5570	6	2.07	10
32	4/25/1995	4/29/1995	5	-110.8885	44.5570	9	2.34	27
33	6/25/1995	7/9/1995	15	-110.9080	44.6329	170	2.84	439
34	7/2/1995	7/5/1995	4	-110.8400	44.6583	8	1.99	22
35	7/2/1995	7/5/1995	4	-110.9920	44.6515	9	2.10	16
36	7/11/1995	7/21/1995	11	-110.9060	44.6303	41	2.35	90
37	8/27/1995	9/3/1995	8	-111.0270	44.7118	6	2.51	20
38	10/7/1995	10/7/1995	1	-110.4945	44.3354	20	3.32	20
39	10/10/1995	10/13/1995	4	-110.4800	44.3441	16	2.92	23
40	11/10/1995	11/13/1995	4	-111.2035	44.7386	7	1.71	11
41	11/20/1995	11/24/1995	5	-110.8920	44.7536	7	1.94	20
42	11/27/1995	12/8/1995	12	-110.8985	44.7461	43	3.05	192
43	12/3/1995	12/7/1995	5	-111.1060	44.7666	7	1.45	12
44	3/14/1996	3/14/1996	1	-111.0200	44.6390	20	2.04	20
45	4/2/1996	4/2/1996	1	-110.6185	44.4312	12	3.34	12
46	5/28/1996	5/28/1996	1	-110.7710	44.7585	10	2.31	10

47	6/16/1996	6/17/1996	2	-111.1005	44.7318	20	1.74	25
48	7/16/1996	7/17/1996	2	-110.9485	44.5694	14	3.20	17
49	7/27/1996	7/29/1996	3	-110.9810	44.5358	12	2.25	23
50	8/30/1996	8/30/1996	1	-110.5385	44.4562	28	2.66	28
51	9/6/1996	9/7/1996	2	-111.1055	44.7188	8	2.23	15
52	9/16/1996	9/16/1996	1	-110.6945	44.5843	22	2.63	22
53	9/16/1996	9/21/1996	6	-111.0655	44.6217	8	1.36	24
54	10/11/1996	11/8/1996	29	-110.7820	44.7331	68	2.83	281
55	10/30/1996	10/31/1996	2	-111.0510	44.4207	11	2.61	16
56	11/26/1996	11/26/1996	1	-110.5400	44.3684	22	2.60	22
57	12/14/1996	12/15/1996	2	-111.0960	44.7368	8	1.45	10
58	12/20/1996	12/22/1996	3	-111.0270	44.6969	11	1.87	12
59	1/2/1997	1/5/1997	4	-110.9810	44.7499	14	2.32	22
60	3/4/1997	3/6/1997	3	-110.9045	44.7947	9	2.91	12
61	4/7/1997	4/8/1997	2	-110.8975	44.5799	9	2.61	14
62	4/27/1997	5/12/1997	16	-110.7910	44.7455	17	2.18	44
63	6/6/1997	6/27/1997	22	-110.8195	44.7324	140	3.76	363
64	6/11/1997	6/14/1997	4	-111.0980	44.7212	10	1.46	13
65	7/7/1997	7/21/1997	15	-110.7935	44.7175	27	2.61	52
66	7/21/1997	7/27/1997	7	-110.9795	44.7574	10	1.31	25
67	7/24/1997	7/30/1997	7	-110.7785	44.7325	6	1.97	25
68	8/12/1997	8/13/1997	2	-111.0810	44.7075	76	1.90	91
69	8/14/1997	8/14/1997	1	-110.7420	44.5930	11	2.13	11
70	9/1/1997	9/4/1997	4	-111.0730	44.6204	5	0.91	14
71	9/1/1997	9/1/1997	1	-111.0035	44.7859	11	3.38	11
72	12/15/1997	12/16/1997	2	-110.6290	44.7386	9	3.15	10
73	12/17/1997	12/19/1997	3	-110.7370	44.5819	10	2.08	14
74	12/25/1997	12/30/1997	6	-111.0395	44.7082	45	2.59	64
75	3/24/1998	3/24/1998	1	-110.6720	44.3317	11	2.58	11
76	4/10/1998	4/12/1998	3	-111.1155	44.7362	14	1.38	20
77	4/11/1998	4/12/1998	2	-111.0690	44.7038	18	1.75	21
78	4/17/1998	4/20/1998	4	-110.4495	44.6664	5	1.37	11
79	4/25/1998	4/27/1998	3	-110.4710	44.3404	5	1.63	10
80	5/26/1998	5/28/1998	3	-110.7955	44.7673	34	2.21	35
81	6/9/1998	6/11/1998	3	-110.8175	44.7610	16	1.80	17
82	6/23/1998	6/26/1998	4	-110.9060	44.7311	14	2.09	21
83	6/27/1998	7/1/1998	5	-110.8115	44.7448	7	1.92	16
84	7/4/1998	7/18/1998	15	-111.0115	44.7075	8	2.02	25
85	9/4/1998	9/4/1998	1	-110.7405	44.5900	11	1.97	11
86	9/27/1998	9/30/1998	4	-111.0550	44.7050	44	2.27	49
87	9/27/1998	10/4/1998	8	-110.3400	44.4711	52	3.80	159
88	11/10/1998	12/1/1998	22	-111.0915	44.6229	50	2.55	189
89	11/26/1998	11/26/1998	1	-110.4915	44.3205	23	3.79	23
90	12/14/1998	12/20/1998	7	-111.1040	44.7698	7	1.57	20
91	12/26/1998	12/28/1998	3	-110.6880	44.6384	8	2.10	10
92	1/1/1999	1/13/1999	13	-110.8225	44.7747	16	2.69	61
93	1/19/1999	1/20/1999	2	-110.7555	44.5819	9	1.57	11
94	3/28/1999	4/5/1999	9	-110.8480	44.7710	8	1.81	20

95	4/20/1999	4/23/1999	4	-110.8670	44.3858	10	2.29	19
96	5/11/1999	5/19/1999	9	-111.0720	44.7461	15	2.34	31
97	5/17/1999	5/31/1999	15	-110.9870	44.6702	19	2.40	70
98	5/23/1999	5/23/1999	1	-110.7960	44.6913	18	3.15	18
99	6/10/1999	6/10/1999	1	-110.7535	44.5968	17	1.78	17
100	6/13/1999	7/16/1999	34	-111.0000	44.7517	112	4.19	722
101	6/13/1999	6/25/1999	13	-111.1105	44.7536	42	2.31	143
102	6/27/1999	7/7/1999	11	-111.1195	44.7486	9	2.07	38
103	7/19/1999	7/25/1999	7	-110.9720	44.7455	18	1.20	23
104	7/20/1999	7/22/1999	3	-110.8525	44.7437	18	1.41	23
105	7/31/1999	7/31/1999	1	-110.7980	44.7959	19	1.21	19
106	7/31/1999	8/28/1999	29	-110.9715	44.7604	119	3.14	586
107	8/7/1999	8/14/1999	8	-111.1225	44.7424	136	2.17	162
108	8/17/1999	8/21/1999	5	-111.1205	44.7536	6	1.60	18
109	8/27/1999	8/27/1999	1	-110.6025	44.4692	35	4.82	35
110	9/11/1999	9/12/1999	2	-110.9595	44.7461	9	1.65	10
111	10/3/1999	10/21/1999	19	-110.9200	44.7617	37	3.03	101
112	10/28/1999	10/28/1999	1	-111.0165	44.6808	48	1.55	48
113	11/3/1999	11/4/1999	2	-110.9995	44.7623	7	1.33	10
114	11/12/1999	11/13/1999	2	-110.4435	44.4399	16	1.92	20
115	11/25/1999	11/27/1999	3	-110.9565	44.7399	11	1.51	19
116	12/21/1999	12/26/1999	6	-110.9465	44.7666	19	2.76	38
117	1/12/2000	1/17/2000	6	-111.1630	44.7461	7	1.74	17
118	1/20/2000	1/21/2000	2	-110.6345	44.7815	18	2.66	14
119	1/25/2000	1/30/2000	6	-111.0745	44.7231	49	2.27	59
120	3/9/2000	3/9/2000	1	-110.7520	44.5980	25	2.05	25
121	3/21/2000	4/13/2000	24	-111.0185	44.7698	40	2.16	278
122	5/24/2000	5/26/2000	3	-110.7910	44.7486	19	2.23	20
123	5/30/2000	5/30/2000	1	-111.0105	44.7150	15	1.36	15
124	6/4/2000	6/5/2000	2	-110.8020	44.7916	9	2.06	10
125	6/19/2000	6/30/2000	12	-110.8185	44.7959	7	1.55	29
126	7/25/2000	8/18/2000	25	-110.7975	44.7971	54	2.72	211
127	9/12/2000	9/14/2000	3	-110.9690	44.7959	8	1.79	10
128	9/22/2000	9/27/2000	6	-110.9770	44.7642	5	2.07	13
129	10/7/2000	10/10/2000	4	-110.8565	44.7505	7	0.72	10
130	10/10/2000	10/11/2000	2	-110.9475	44.7629	11	2.11	13
131	10/24/2000	10/27/2000	4	-111.1305	44.7368	29	2.18	51
132	11/22/2000	11/27/2000	6	-110.8335	44.7182	8	1.96	15
133	11/23/2000	11/26/2000	4	-110.6975	44.7343	82	3.76	93
134	12/1/2000	12/4/2000	4	-110.8035	44.8046	5	1.49	13
135	12/2/2000	12/6/2000	5	-110.7010	44.7443	18	1.85	29
136	12/10/2000	12/10/2000	1	-110.7295	44.7673	25	1.57	25
137	12/10/2000	12/12/2000	3	-111.0930	44.7517	7	1.32	15
138	12/24/2000	12/28/2000	5	-110.8500	44.7349	34	2.51	54
139	12/30/2000	1/4/2001	6	-110.8315	44.7188	9	1.49	16
140	1/1/2001	1/3/2001	3	-111.1230	44.7324	5	1.11	10
141	1/15/2001	1/16/2001	2	-110.4810	44.3236	19	2.23	21
142	1/16/2001	1/25/2001	10	-111.0520	44.6347	130	2.40	320

143	2/2/2001	2/3/2001	2	-110.7295	44.5980	24	2.18	27
144	2/26/2001	3/2/2001	5	-111.0165	44.7188	29	1.94	54
145	3/16/2001	3/22/2001	7	-110.6890	44.6863	6	2.26	15
146	3/16/2001	3/17/2001	2	-111.0980	44.7336	14	0.83	16
147	3/20/2001	3/20/2001	1	-110.9070	44.7393	14	1.68	14
148	3/23/2001	3/27/2001	5	-110.9215	44.7318	6	1.33	11
149	4/19/2001	4/20/2001	2	-110.9210	44.6384	7	0.85	10
150	4/23/2001	4/24/2001	2	-110.7665	44.7735	11	1.23	12
151	4/30/2001	5/4/2001	5	-110.9420	44.7386	17	1.91	37
152	5/11/2001	5/12/2001	2	-111.0185	44.5420	10	1.20	11
153	5/18/2001	5/22/2001	5	-110.7825	44.7940	7	3.09	19
154	5/21/2001	5/24/2001	4	-110.9420	44.7430	5	1.84	10
155	6/19/2001	6/28/2001	10	-110.9075	44.7529	10	2.48	35
156	6/29/2001	6/29/2001	1	-111.0235	44.5059	22	1.95	22
157	9/4/2001	9/6/2001	3	-111.1390	44.5010	19	2.37	22
158	9/6/2001	9/10/2001	5	-111.0180	44.7623	16	0.99	34
159	11/1/2001	11/5/2001	5	-110.7895	44.7585	14	1.14	19
160	11/20/2001	11/22/2001	3	-110.8690	44.7473	18	1.29	31
161	11/25/2001	11/28/2001	4	-111.0470	44.7760	8	1.90	22
162	11/30/2001	1/9/2002	41	-111.0530	44.7815	49	3.13	480
163	1/2/2002	1/3/2002	2	-111.0170	44.4660	9	1.25	10
164	1/7/2002	1/7/2002	1	-110.8570	44.7219	12	1.23	12
165	1/15/2002	1/17/2002	3	-110.7320	44.5961	56	2.78	60
166	1/19/2002	1/21/2002	3	-111.0220	44.5482	8	1.55	11
167	1/29/2002	2/2/2002	5	-111.0090	44.7685	22	0.82	49
168	2/13/2002	2/15/2002	3	-110.7435	44.6017	19	2.15	23
169	3/21/2002	3/26/2002	6	-111.0355	44.7947	6	1.06	13
170	3/29/2002	3/29/2002	1	-110.7430	44.6397	16	1.17	16
171	4/29/2002	5/1/2002	3	-111.0805	44.7368	17	2.49	21
172	5/4/2002	5/7/2002	4	-111.0695	44.7424	5	1.24	11
173	5/7/2002	5/8/2002	2	-110.6490	44.7729	17	1.83	18
174	7/19/2002	7/22/2002	4	-110.8635	44.7368	8	1.34	16
175	8/9/2002	8/15/2002	7	-110.9925	44.7392	10	1.46	30
176	10/8/2002	10/12/2002	5	-110.5610	44.3746	64	3.14	110
177	10/20/2002	10/20/2002	1	-110.7635	44.5762	18	1.99	18
178	11/3/2002	11/6/2002	4	-110.7390	44.6142	22	1.95	26
179	11/3/2002	11/5/2002	3	-110.8010	44.4064	15	2.77	22
180	11/3/2002	11/5/2002	3	-110.5965	44.4580	12	2.57	18
181	11/3/2002	11/4/2002	2	-110.3610	44.5290	9	3.19	15
182	11/3/2002	11/7/2002	5	-110.9590	44.6092	18	2.47	45
183	11/3/2002	11/10/2002	8	-110.7970	44.7330	31	1.54	59
184	11/3/2002	11/10/2002	8	-111.1080	44.7449	48	2.89	67
185	11/4/2002	11/5/2002	2	-110.6610	44.3609	9	1.47	10
186	11/7/2002	11/12/2002	6	-111.0150	44.7884	5	1.55	11
187	11/11/2002	11/11/2002	1	-110.5895	44.4599	23	2.50	23
188	11/13/2002	11/17/2002	5	-110.8450	44.7143	8	0.91	10
189	12/5/2002	12/10/2002	6	-110.8750	44.7449	283	3.32	331
190	12/5/2002	12/6/2002	2	-110.7935	44.7635	9	1.06	10

191	12/5/2002	12/7/2002	3	-110.3390	44.4269	25	2.65	27
192	12/13/2002	12/14/2002	2	-110.9190	44.7399	11	2.54	21
193	12/31/2002	1/4/2003	5	-110.8100	44.7411	7	1.23	12
194	1/3/2003	1/13/2003	11	-111.0075	44.5208	43	2.48	85
195	1/20/2003	1/27/2003	8	-111.0225	44.5221	10	1.36	22
196	1/29/2003	2/13/2003	16	-110.9895	44.5196	31	2.92	79
197	2/5/2003	2/7/2003	3	-111.0020	44.7380	22	1.17	35
198	2/9/2003	2/14/2003	6	-110.6560	44.6298	8	3.55	22
199	2/16/2003	2/21/2003	6	-111.0100	44.5228	6	1.17	19
200	4/15/2003	4/21/2003	7	-110.9930	44.6752	6	2.37	24
201	5/23/2003	5/23/2003	1	-110.4290	44.3634	11	1.40	11
202	8/28/2003	8/30/2003	3	-111.0170	44.7729	12	1.88	23
203	9/29/2003	9/30/2003	2	-110.5665	44.1014	11	2.56	17
204	11/20/2003	11/22/2003	3	-110.9700	44.5482	8	2.21	12

## APPENDIX B

### TEMPORAL DISTRIBUTIONS OF EARTHQUAKES IN YELLOWSTONE SWARMS

This appendix consists of two sets of plots of temporal distributions of swarm earthquakes. The first 34 figures show the number of earthquakes per day for each of the 204 swarm sequences identified in this study. The numbers refer to the order, in time, in which the swarms occurred.

The next 13 figures show the distribution of swarm earthquake magnitudes with time. The swarms plotted in the figures in the text and in Appendices A and C use the same numbering system.

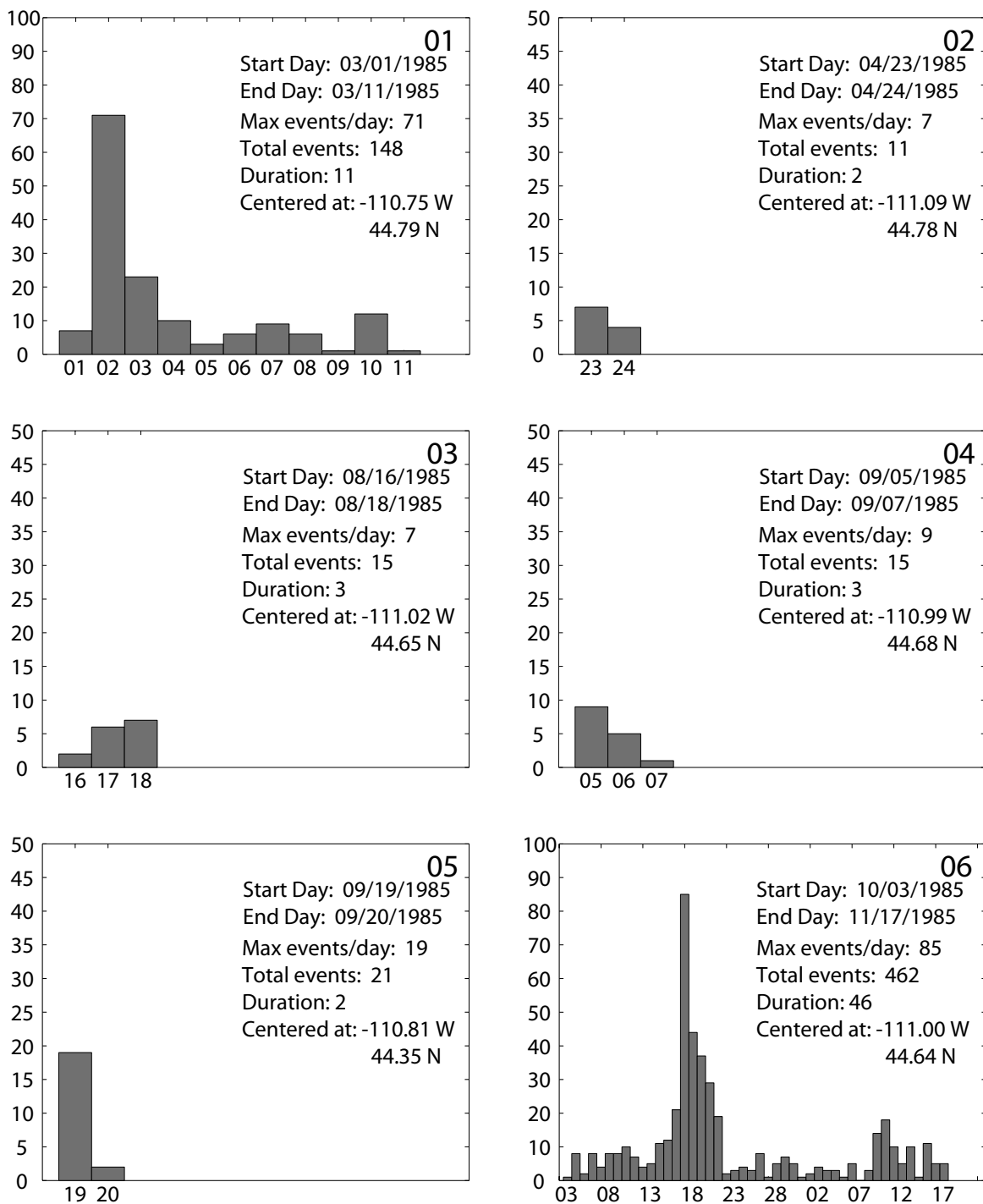


Figure B.1 - Number of earthquakes vs. time for swarm numbers 1 - 6.

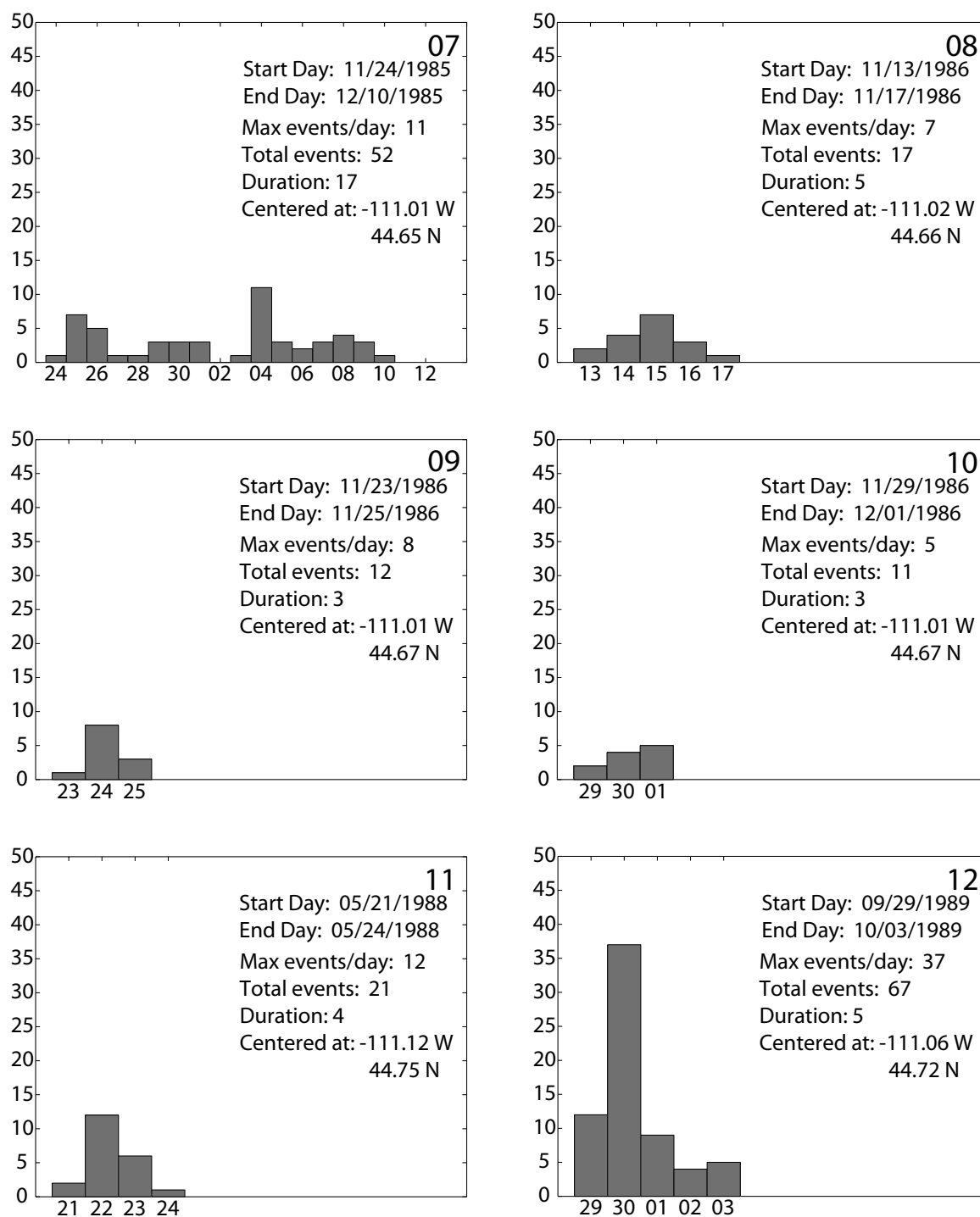


Figure B.2 - Number of earthquakes vs. time for swarm numbers 7 - 12.

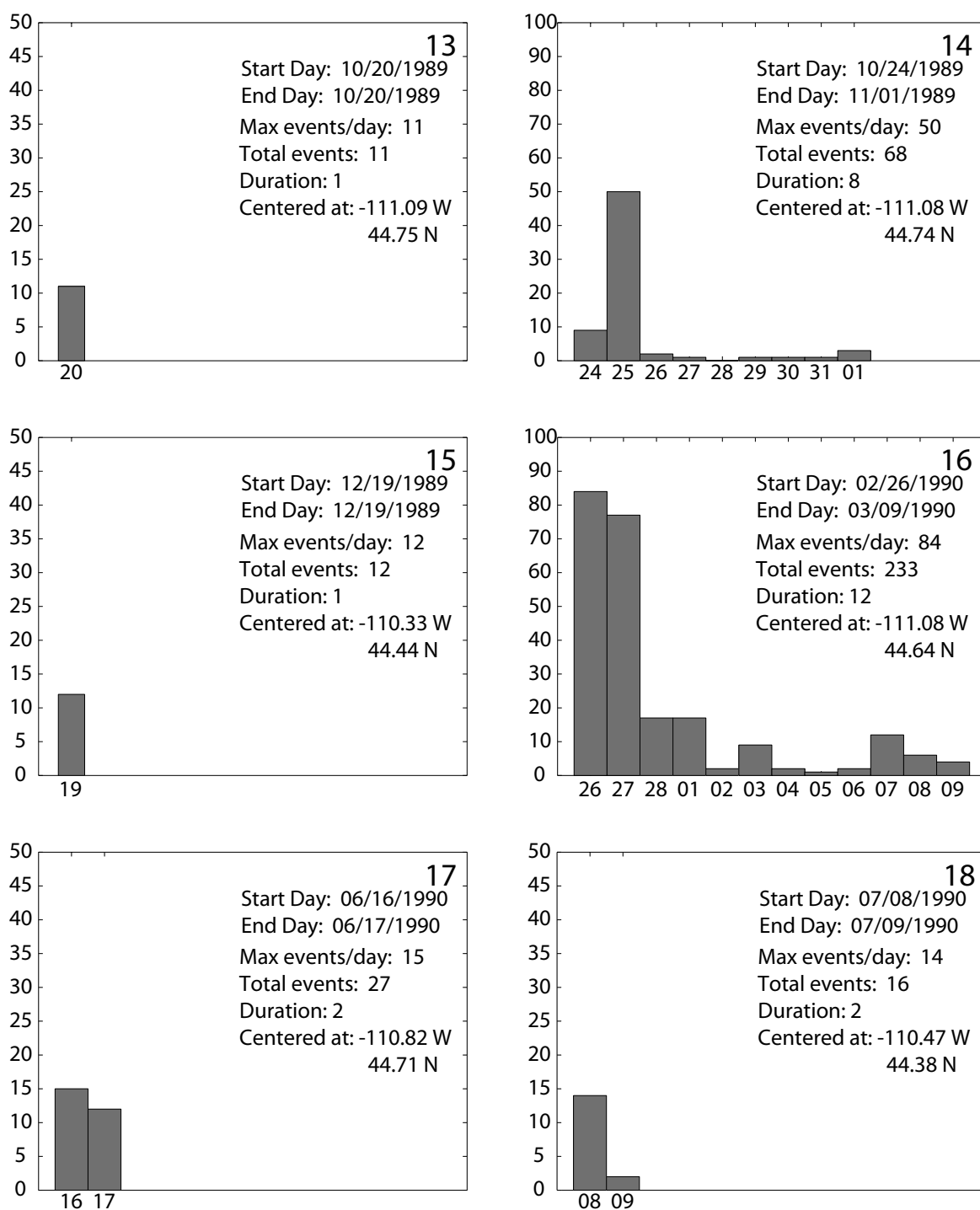


Figure B.3 - Number of earthquakes vs. time for swarm numbers 13 - 18.

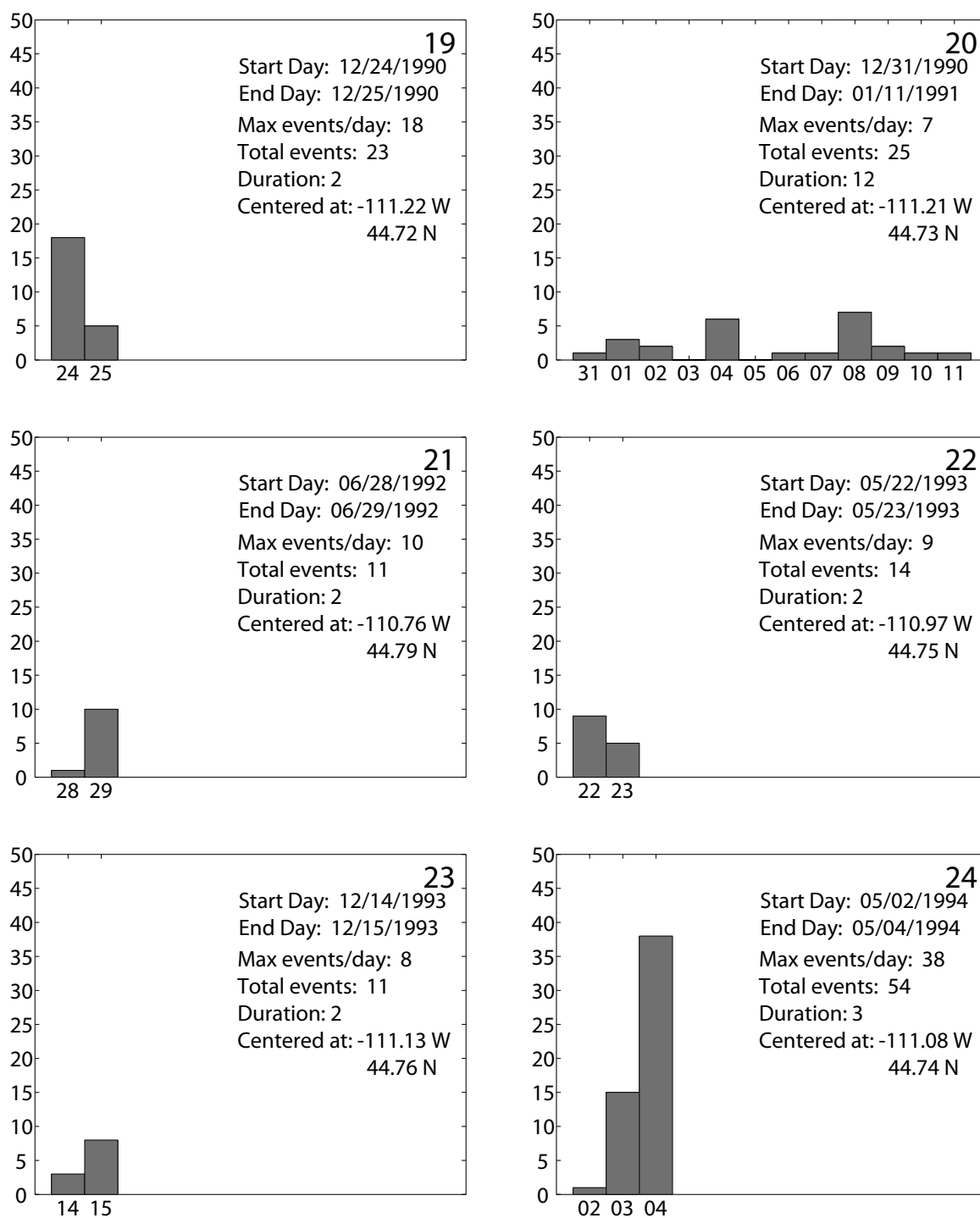


Figure B.4 - Number of earthquakes vs. time for swarm numbers 19 - 24.

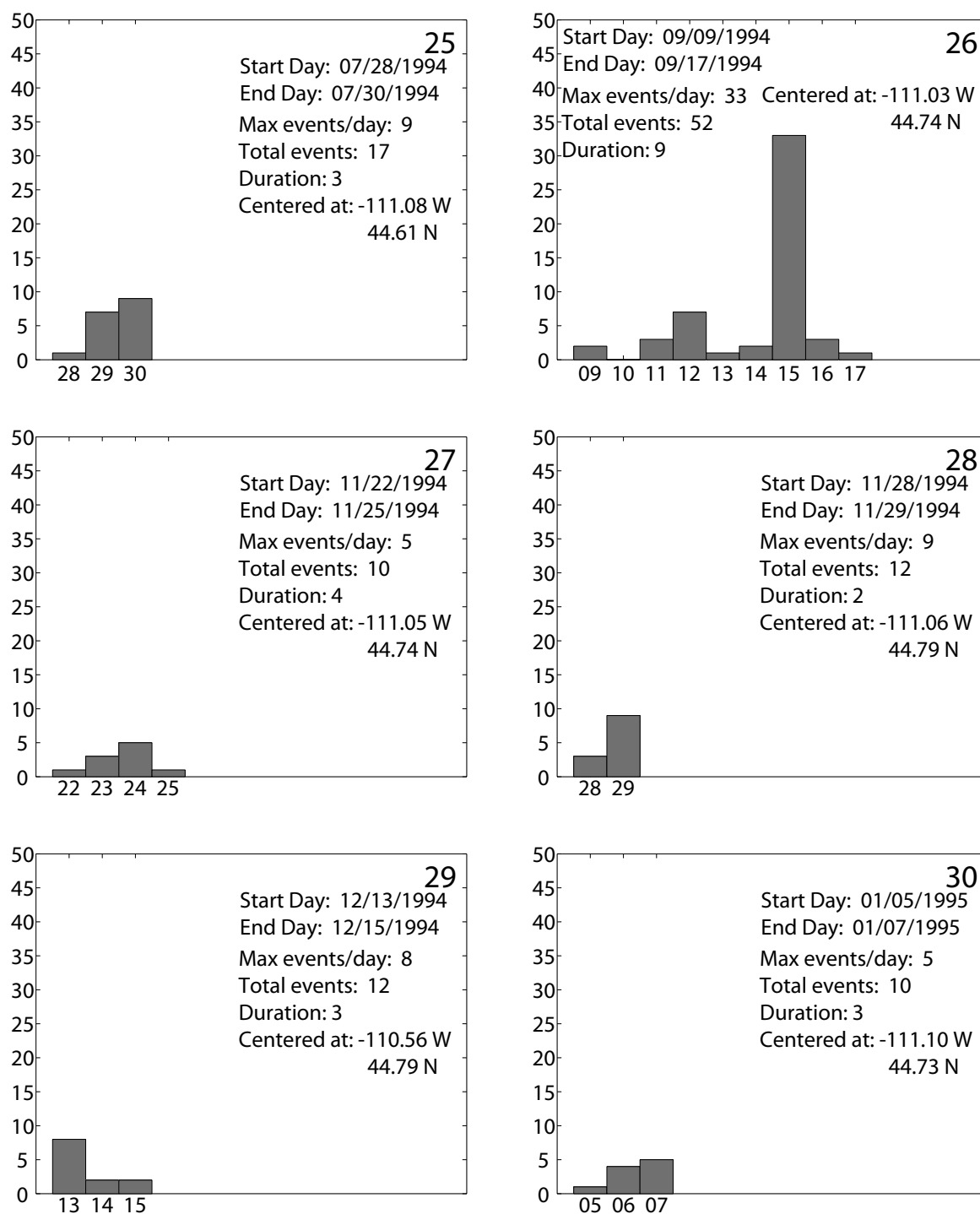


Figure B.5 - Number of earthquakes vs. time for swarm numbers 25 - 30.

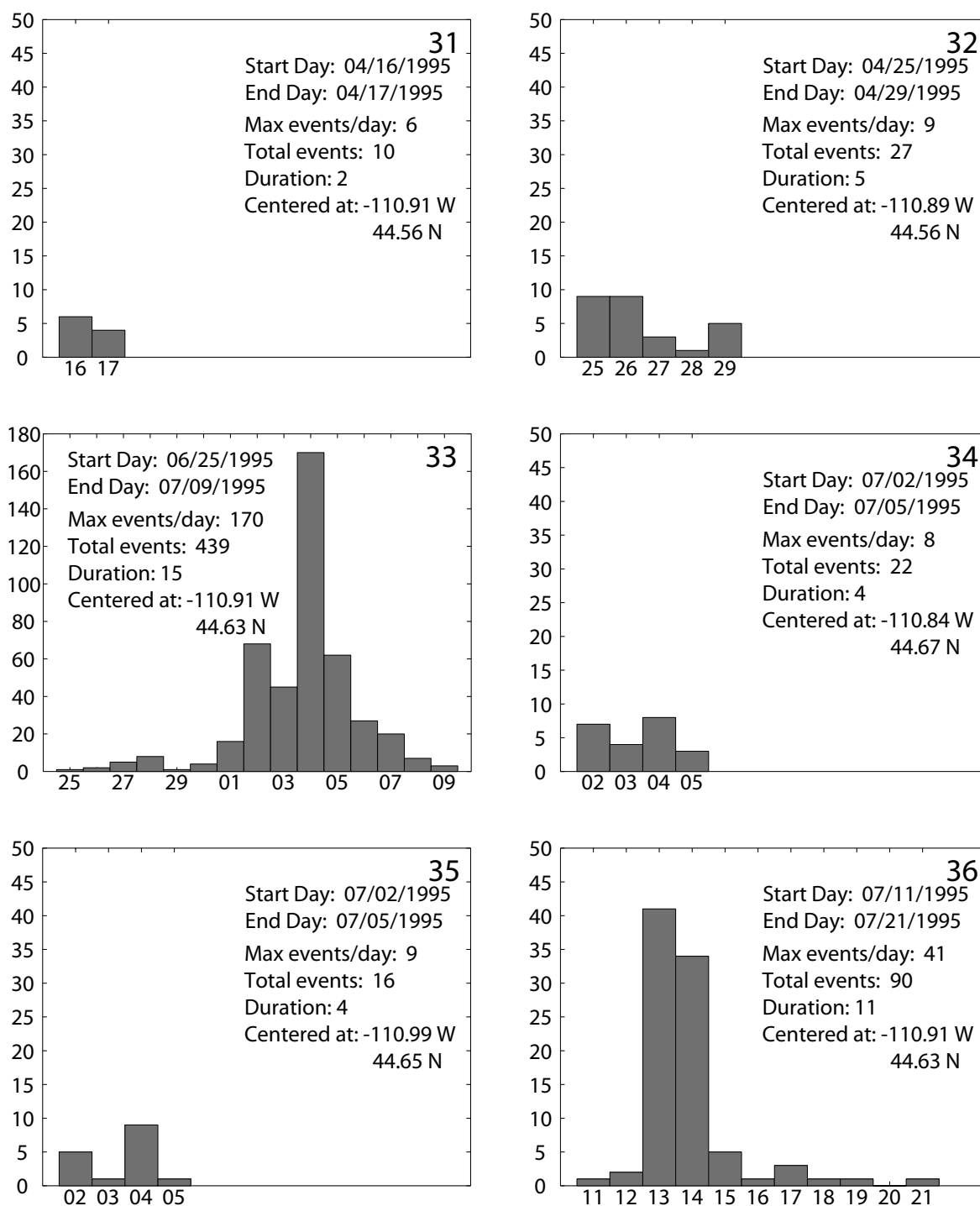


Figure B.6 - Number of earthquakes vs. time for swarm numbers 31 - 36.

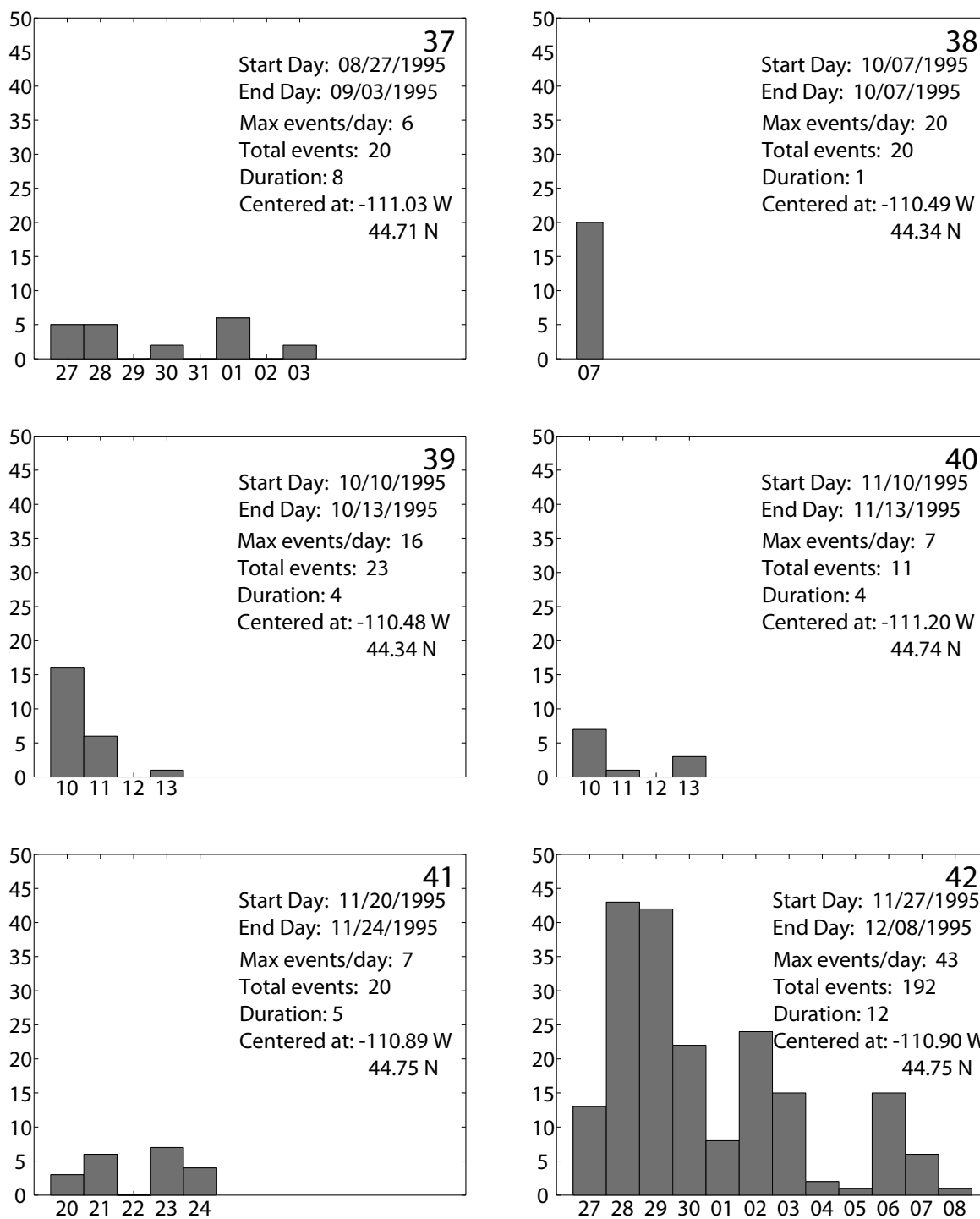


Figure B.7 - Number of earthquakes vs. time for swarm numbers 37 - 42.

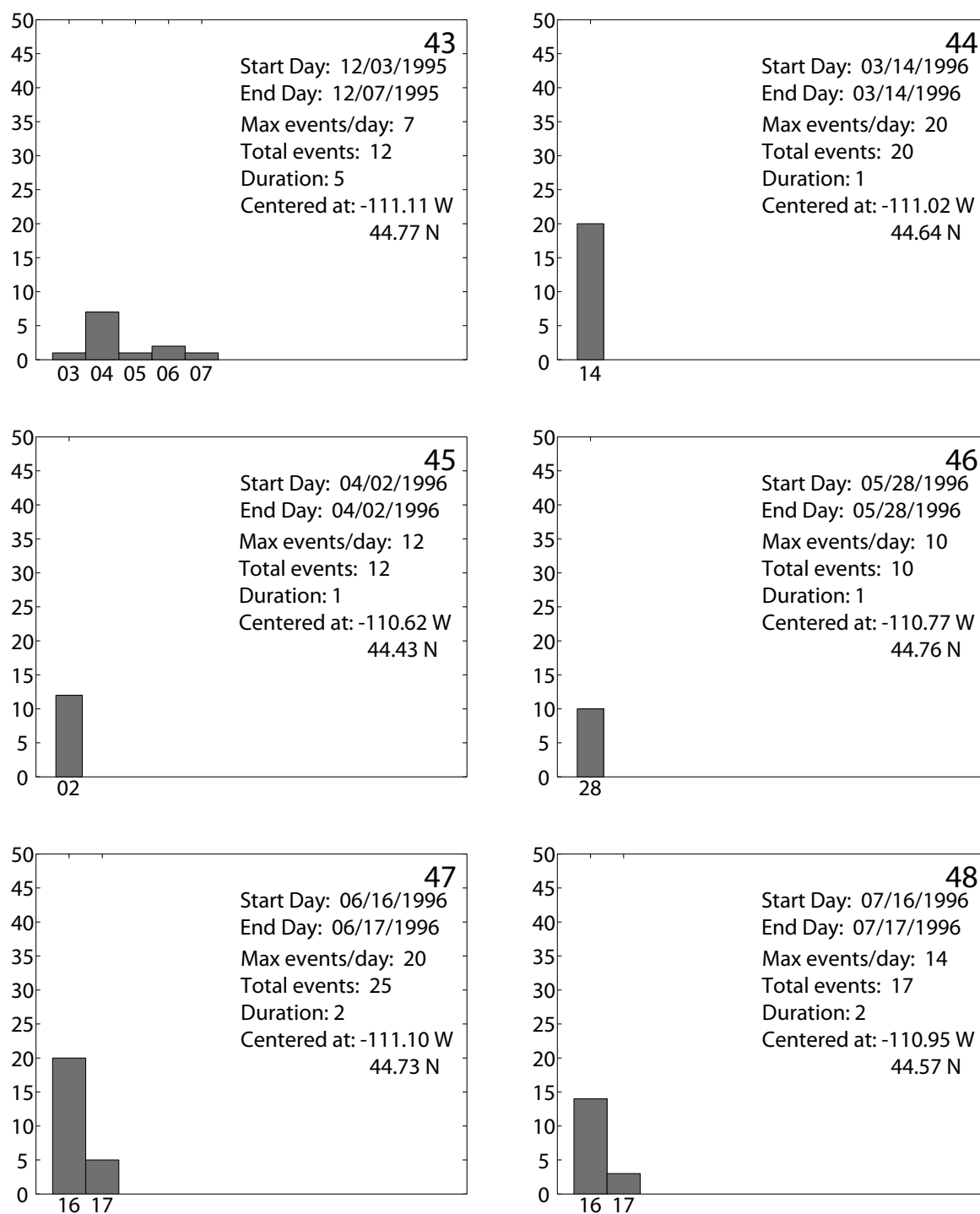


Figure B.8 - Number of earthquakes vs. time for swarm numbers 43 - 48.

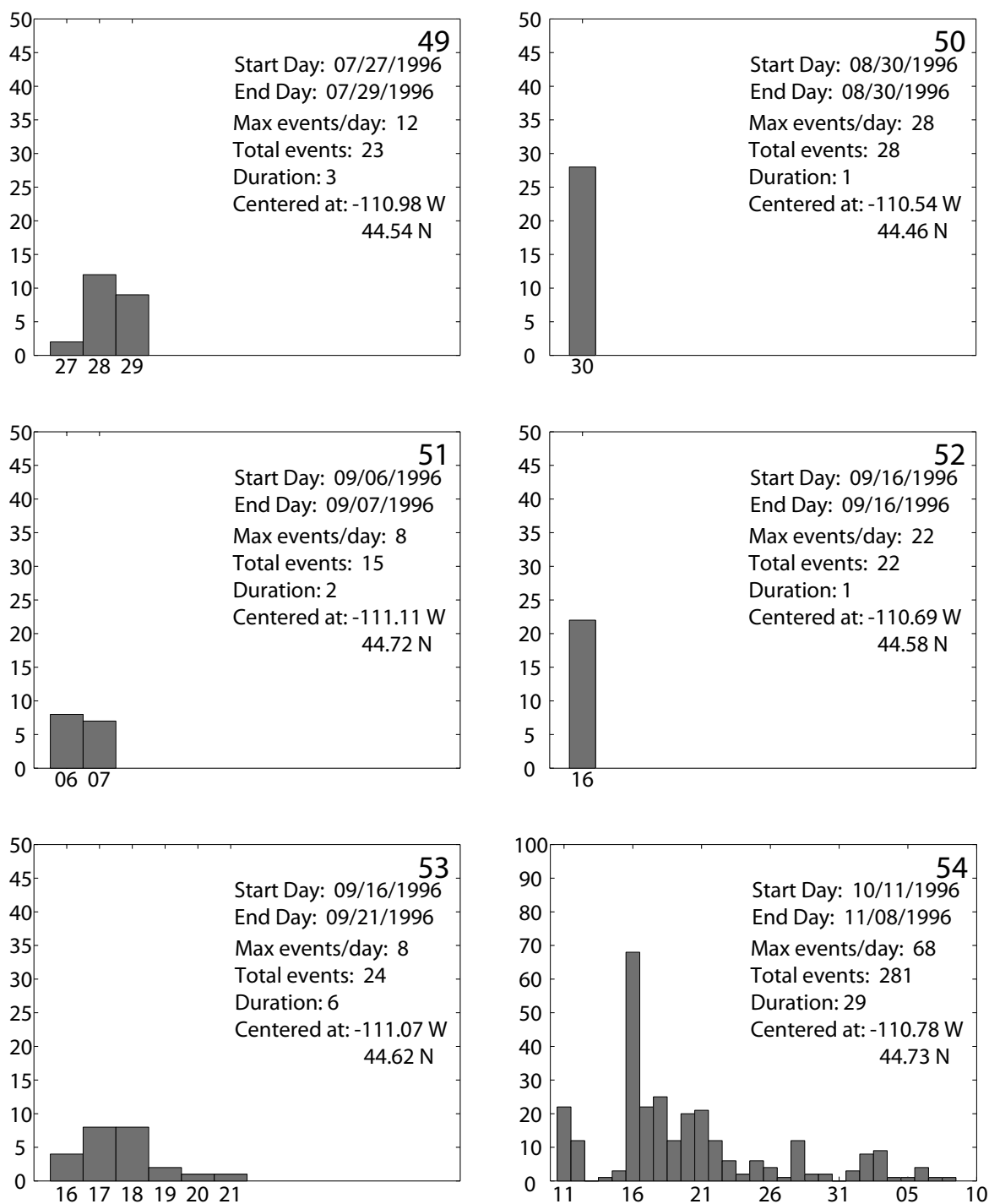


Figure B.9 - Number of earthquakes vs. time for swarm numbers 49 - 54.

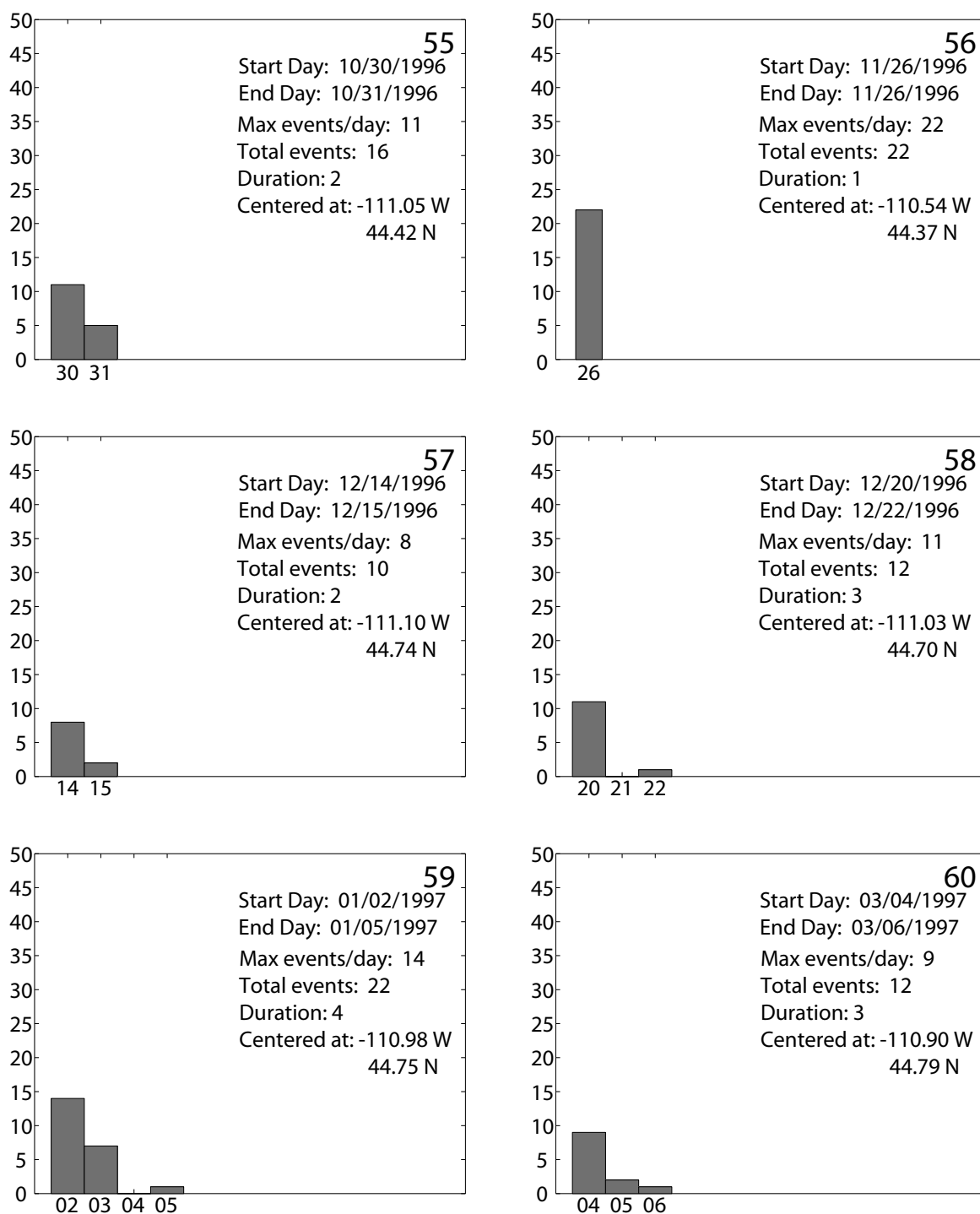


Figure B.10 - Number of earthquakes vs. time for swarm numbers 55 - 60.

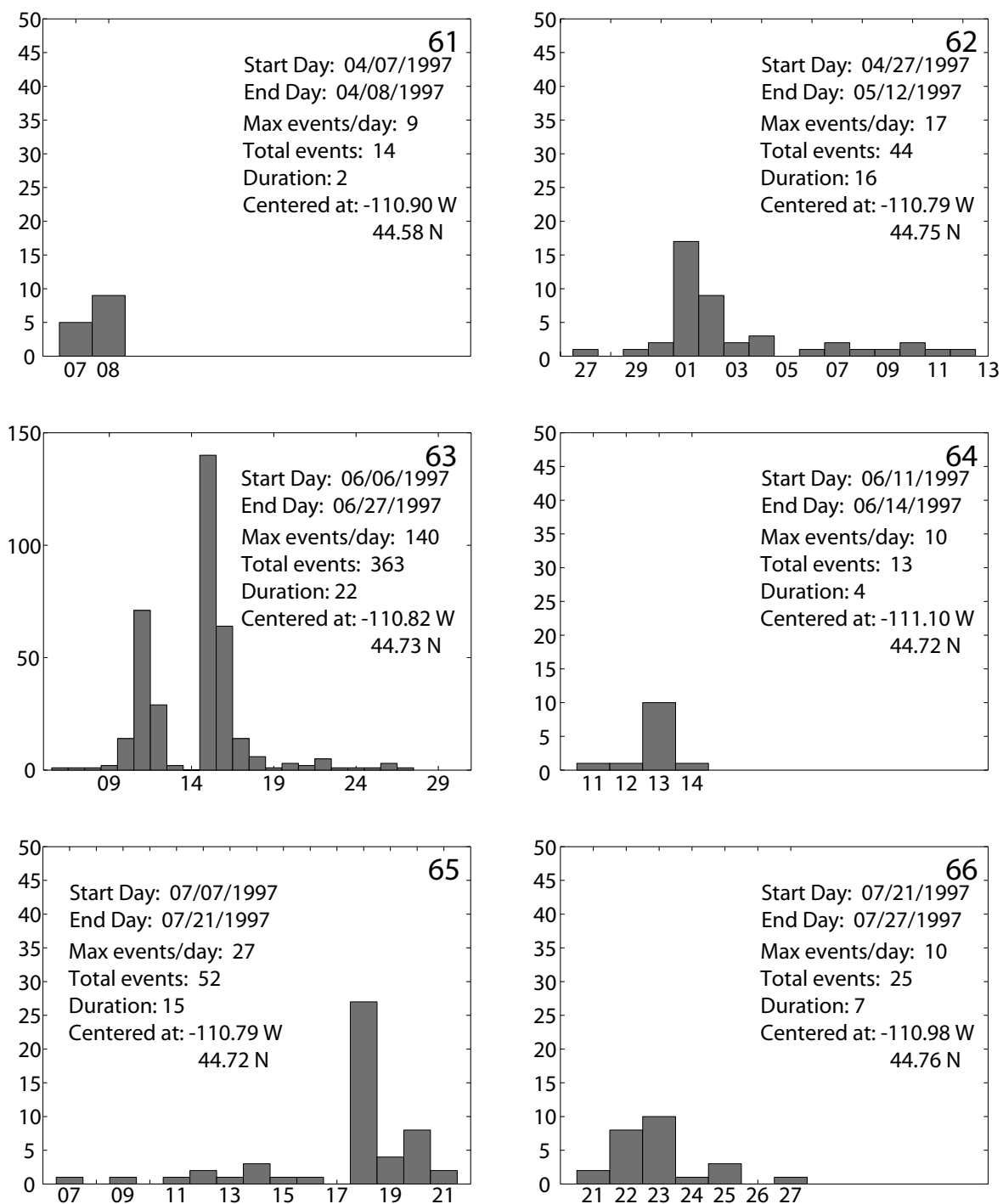


Figure B.11 - Number of earthquakes vs. time for swarm numbers 61 - 66.

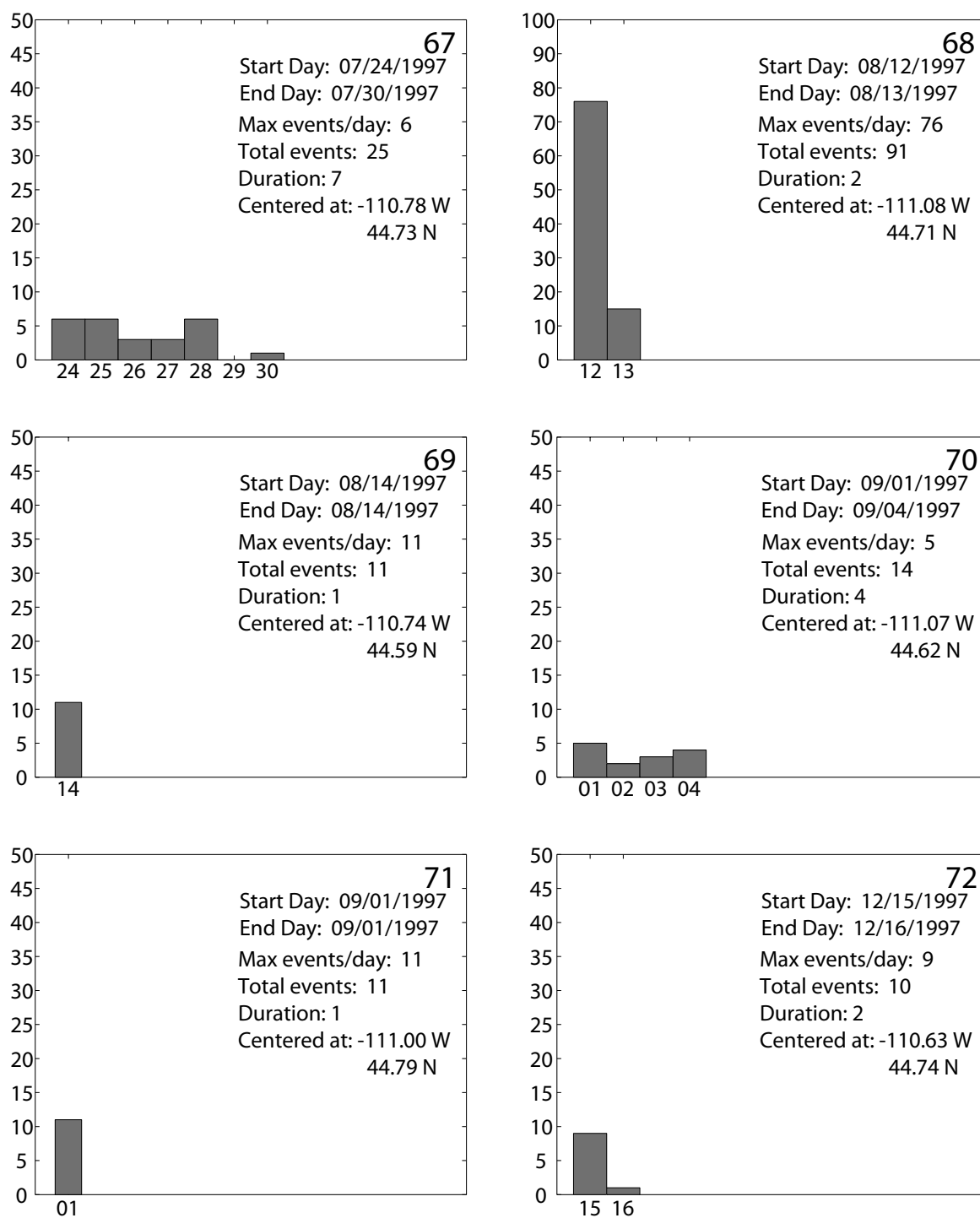


Figure B.12 - Number of earthquakes vs. time for swarm numbers 67 - 72.

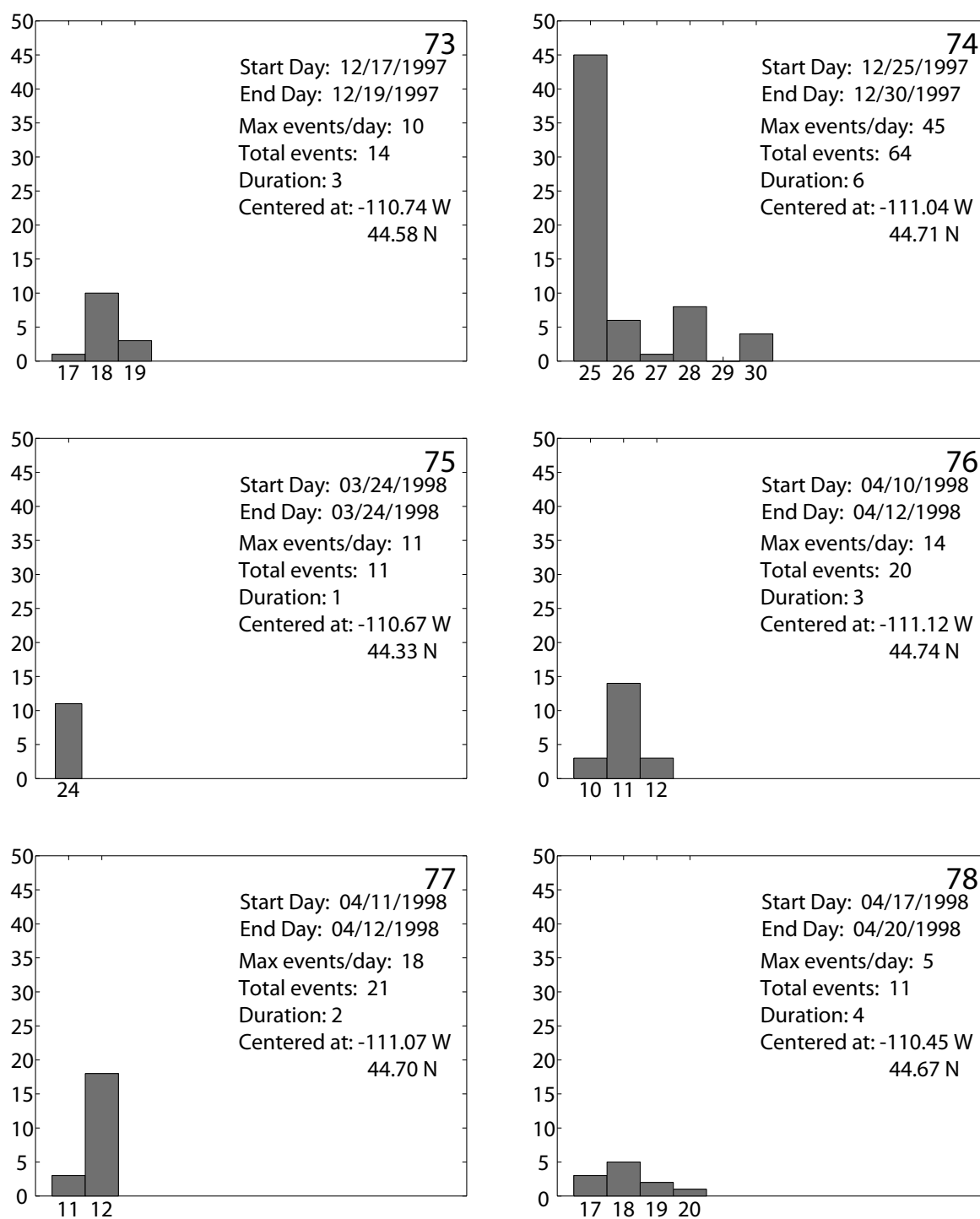


Figure B.13 - Number of earthquakes vs. time for swarm numbers 73 - 78.

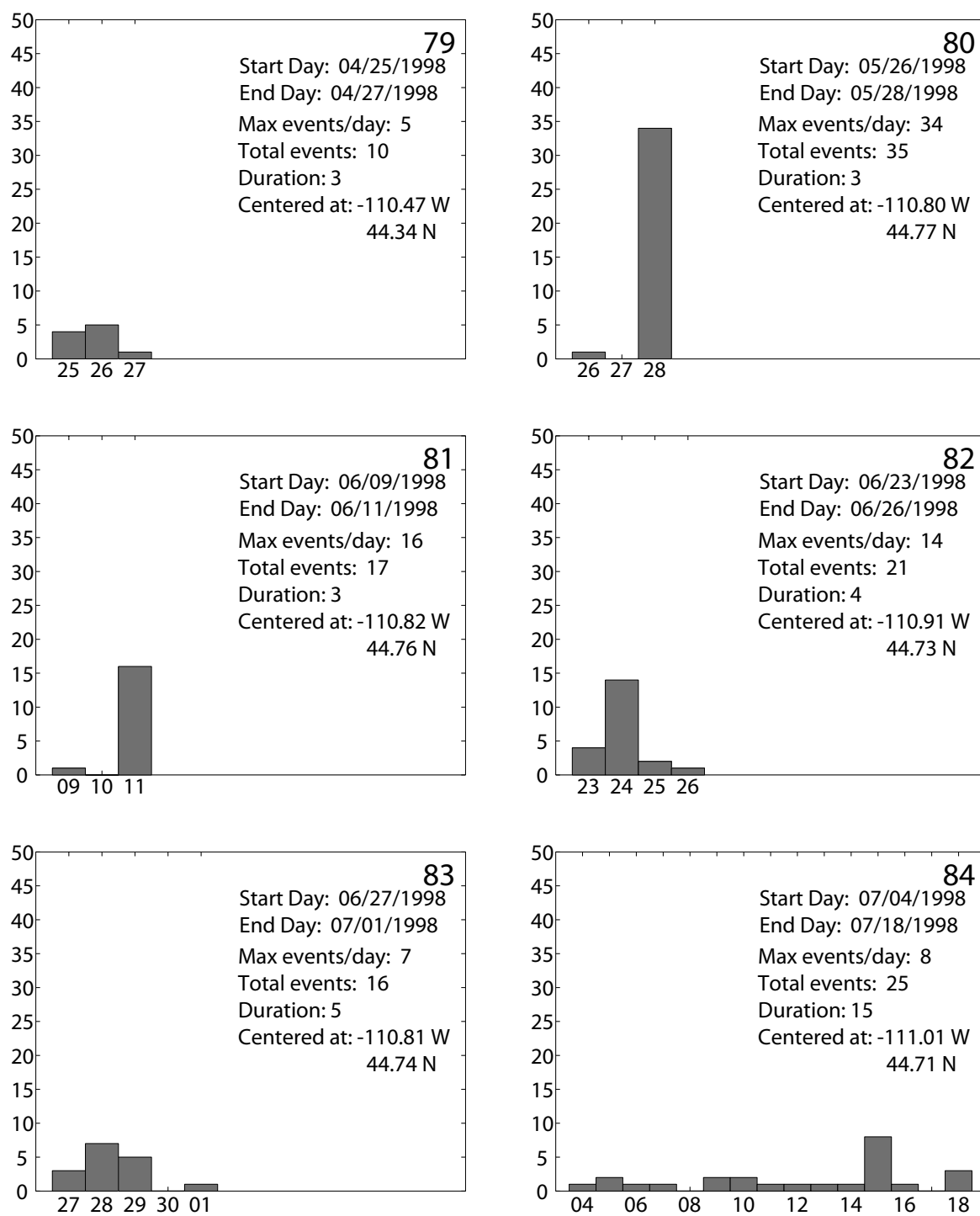


Figure B.14 - Number of earthquakes vs. time for swarm numbers 79 - 84.

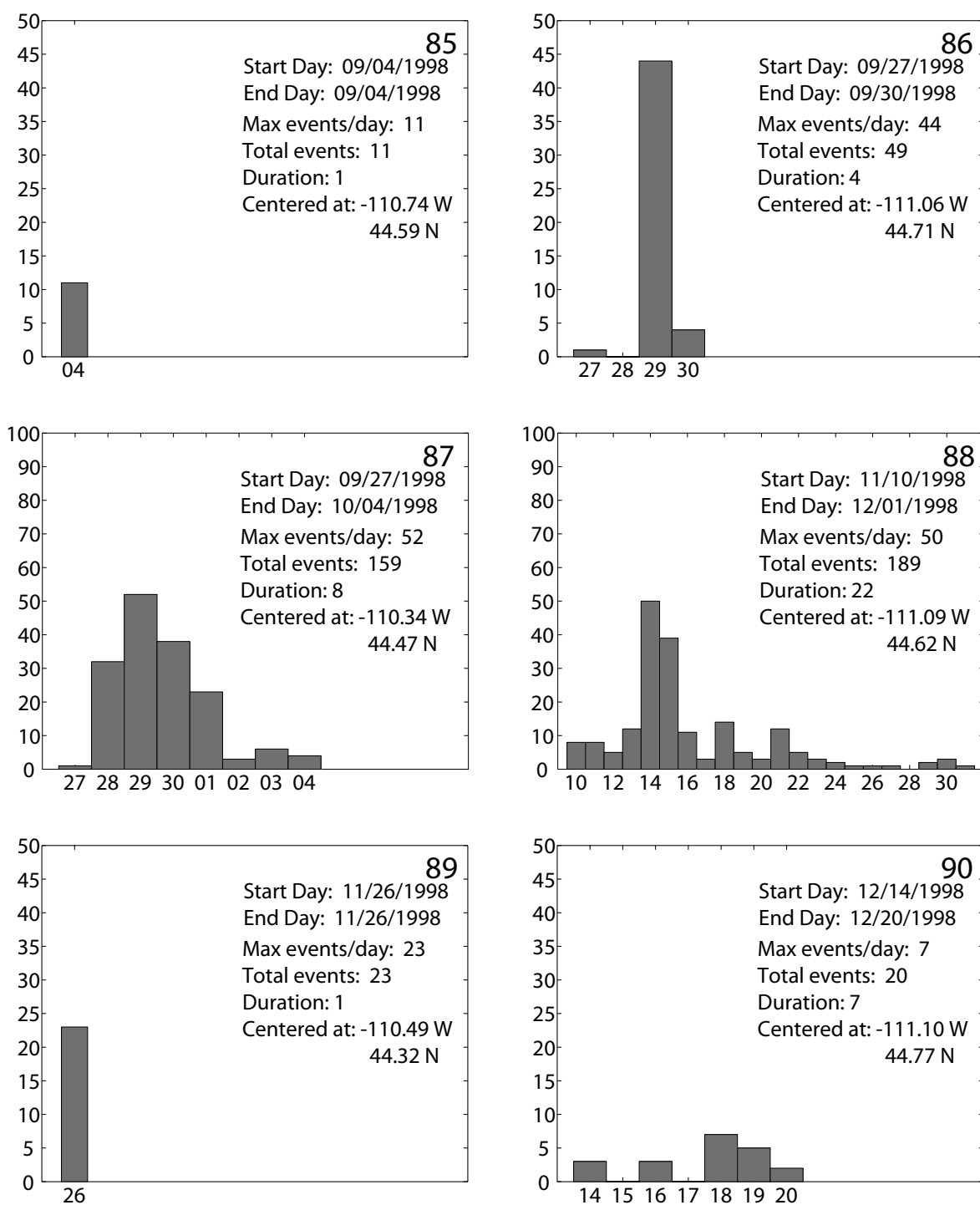


Figure B.15 - Number of earthquakes vs. time for swarm numbers 85 - 90.

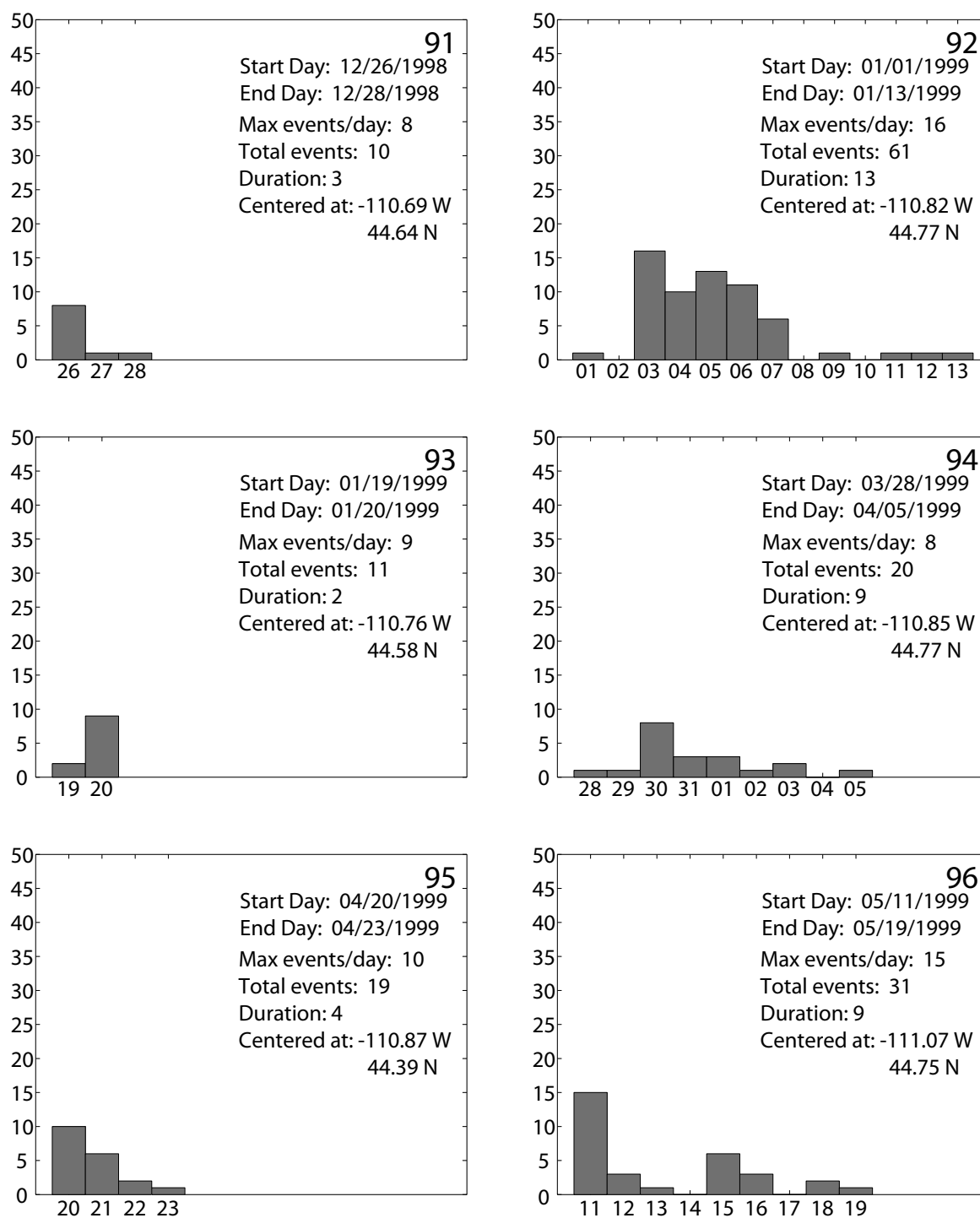


Figure B.16 - Number of earthquakes vs. time for swarm numbers 91 - 96.

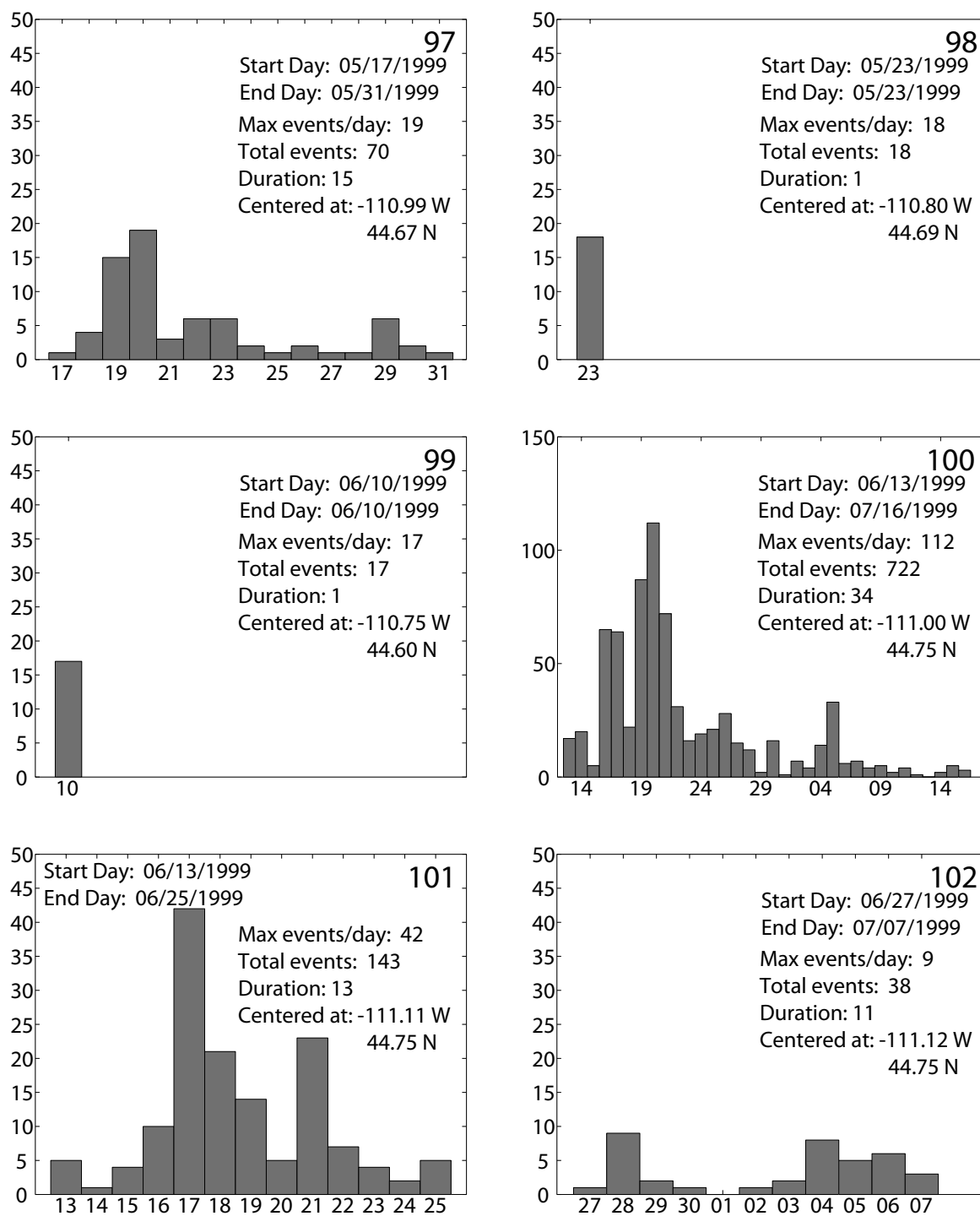


Figure B.17 - Number of earthquakes vs. time for swarm numbers 97 - 102.

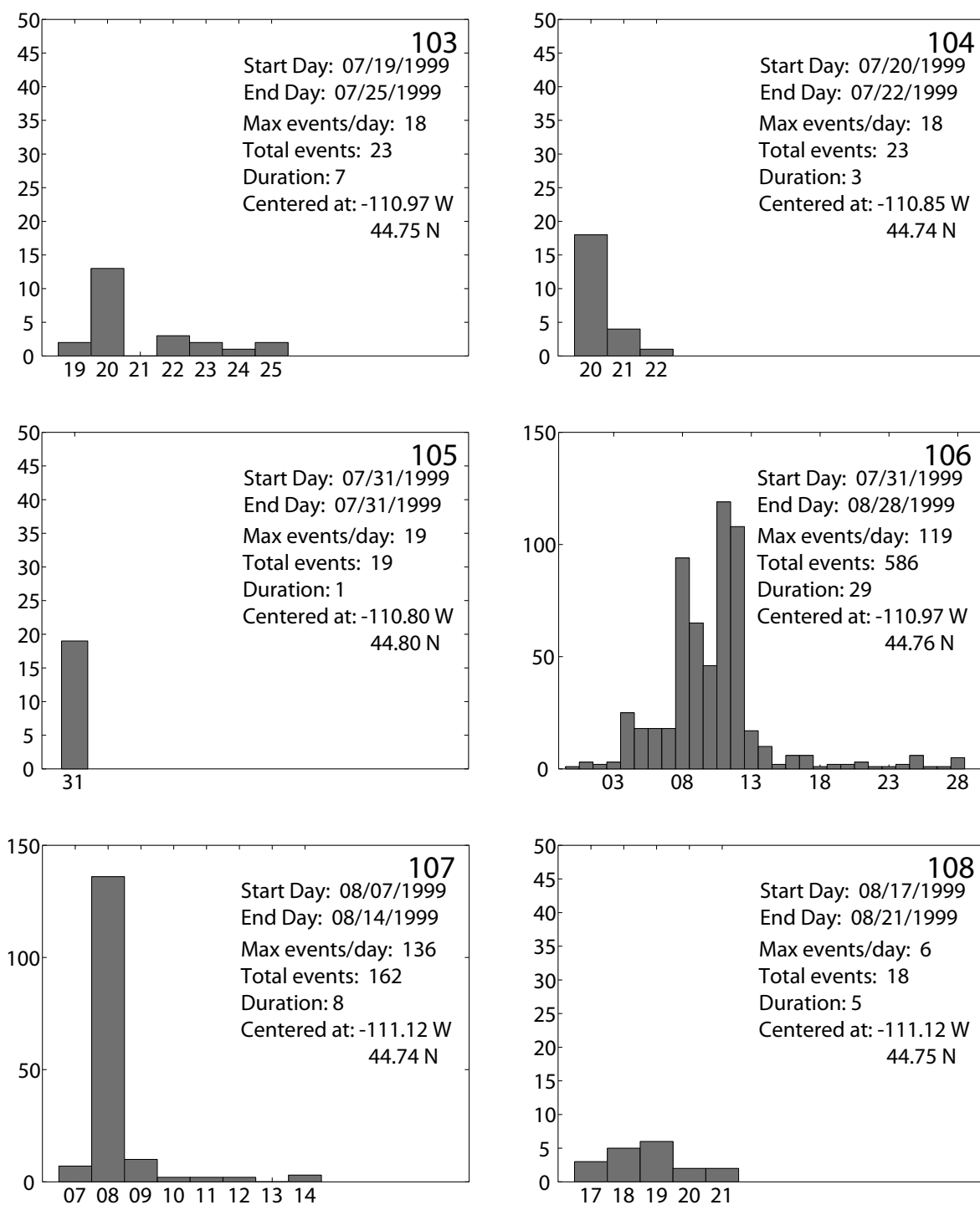


Figure B.18 - Number of earthquakes vs. time for swarm numbers 103 - 108.

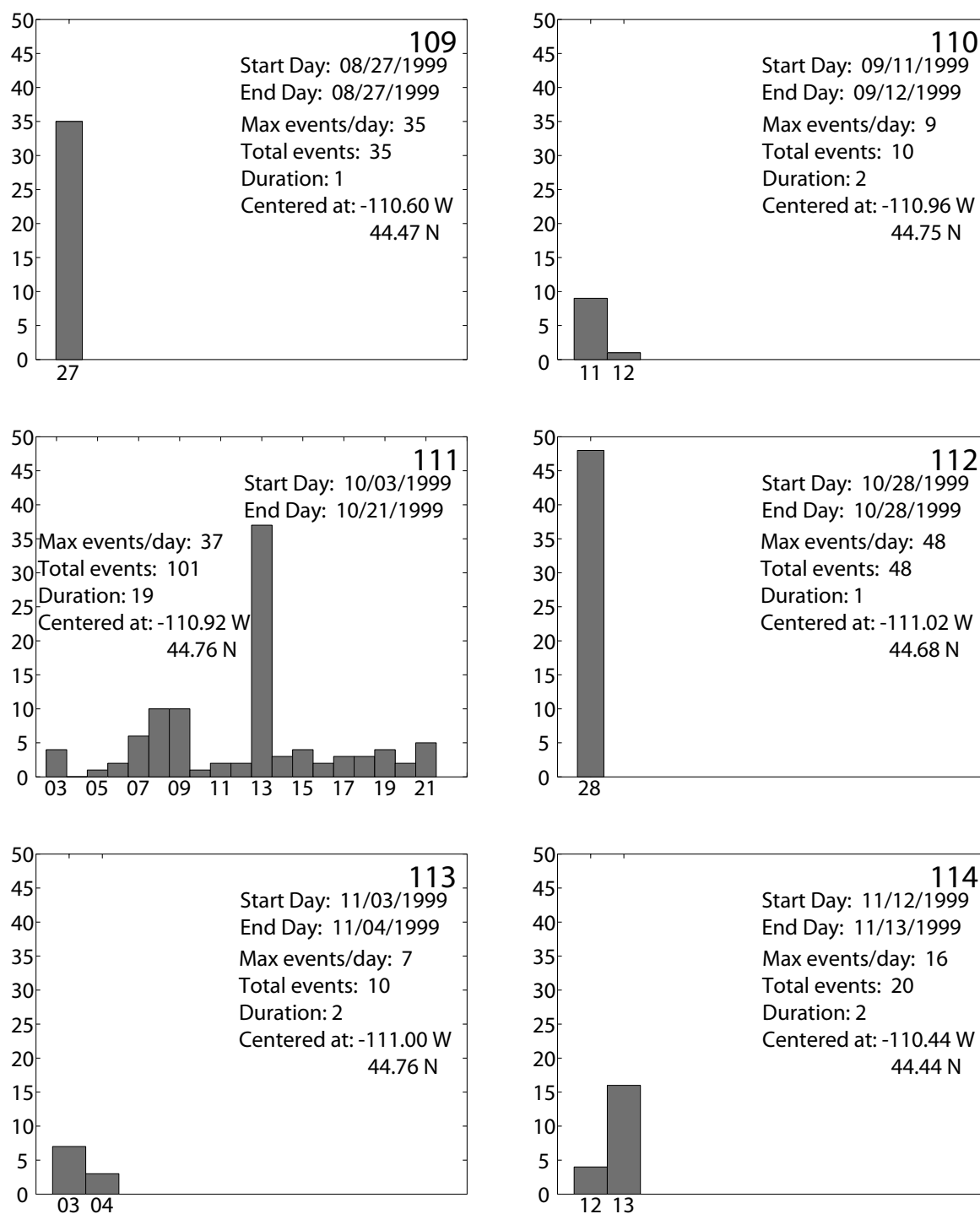


Figure B.19 - Number of earthquakes vs. time for swarm numbers 109 - 114.

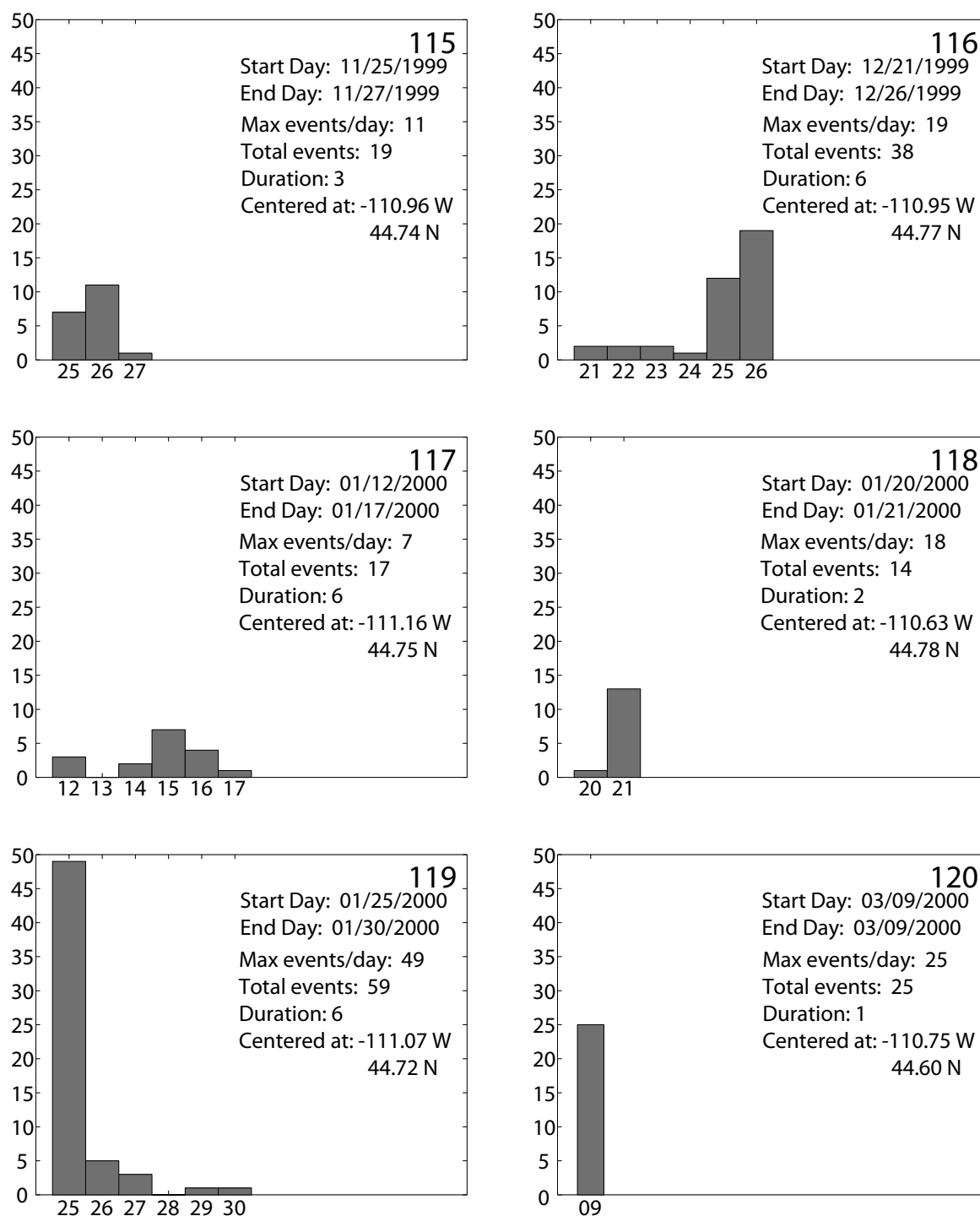


Figure B.20 - Number of earthquakes vs. time for swarm numbers 115 - 120.

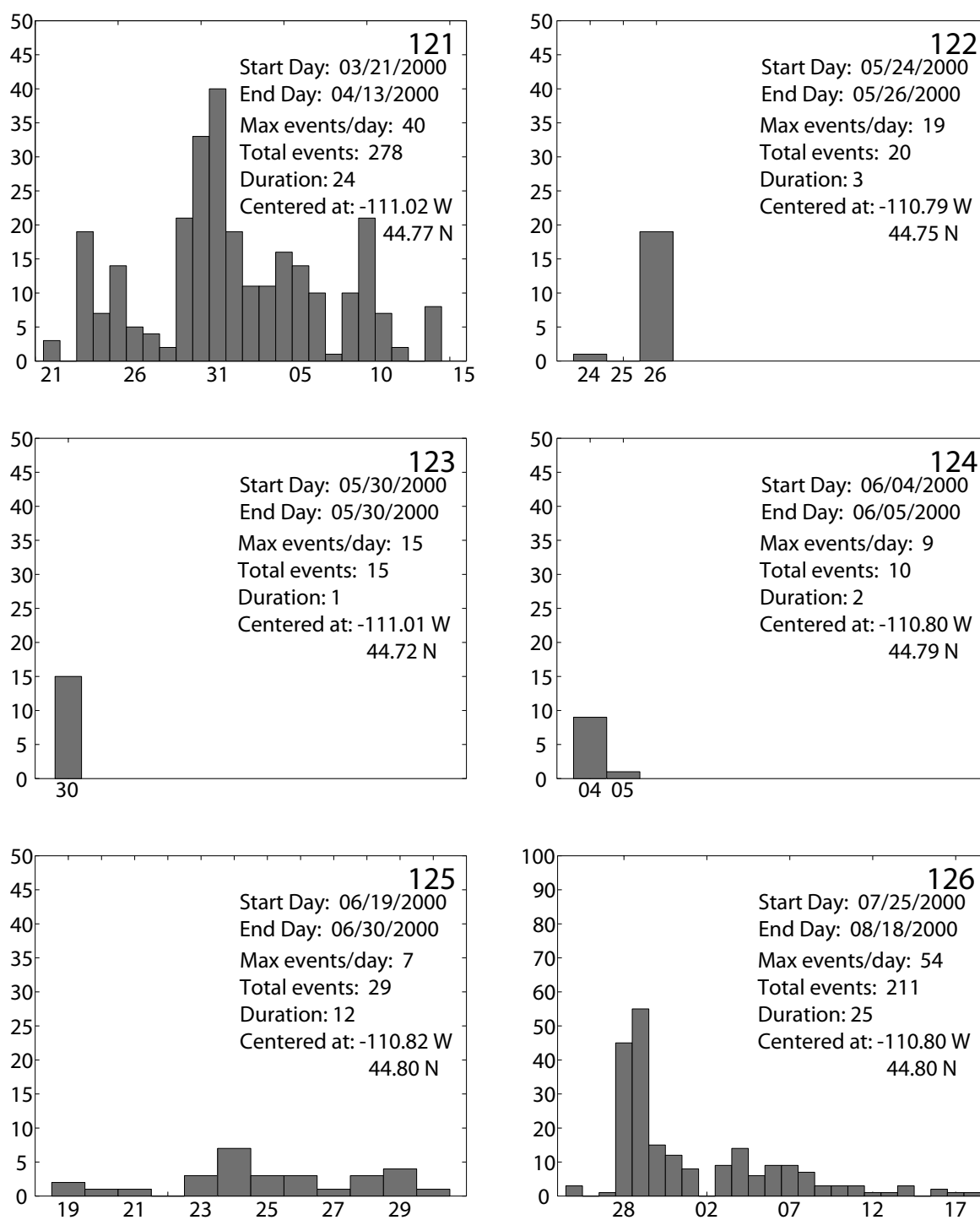


Figure B.21 - Number of earthquakes vs. time for swarm numbers 121 - 126.

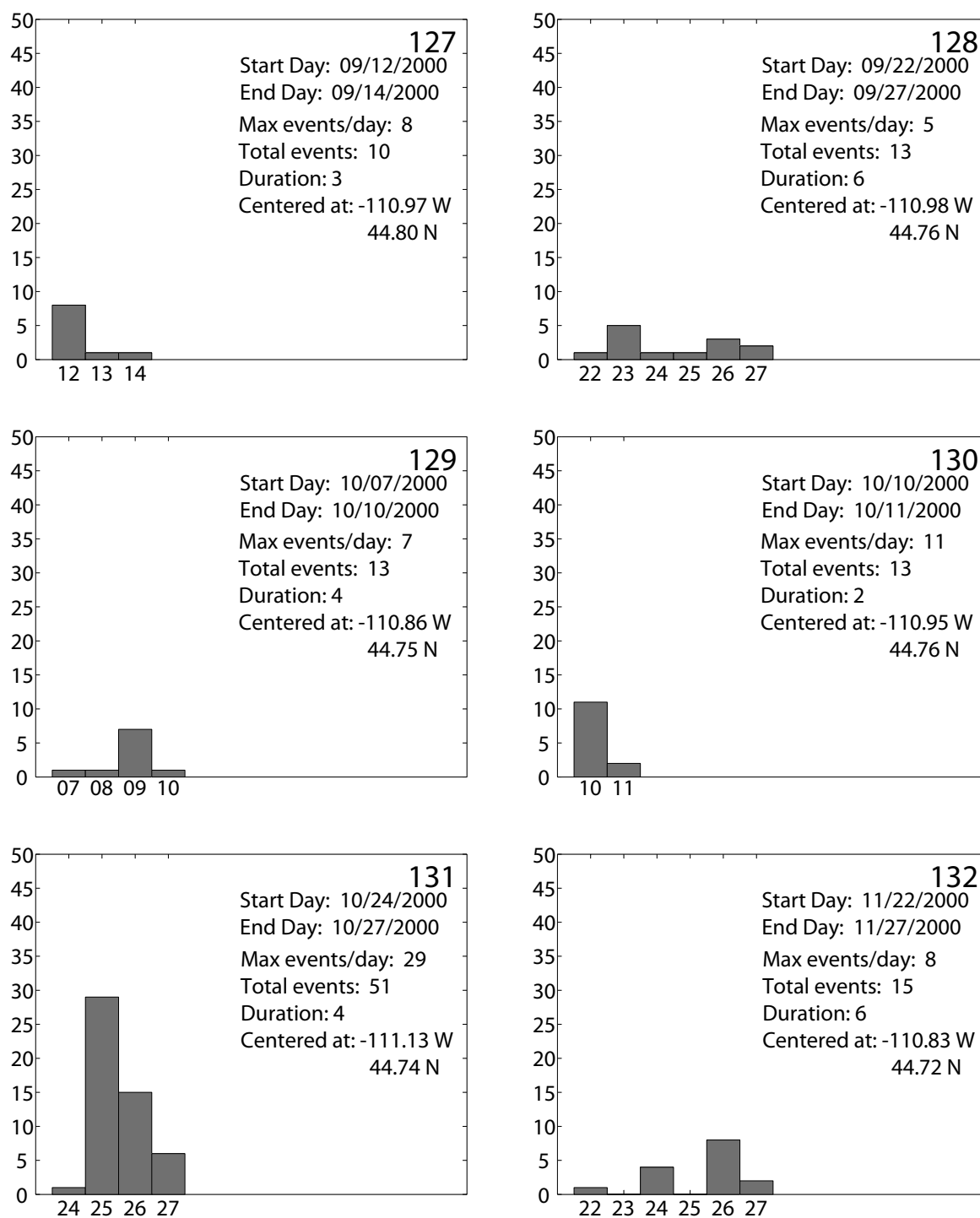


Figure B.22 - Number of earthquakes vs. time for swarm numbers 127 - 132.

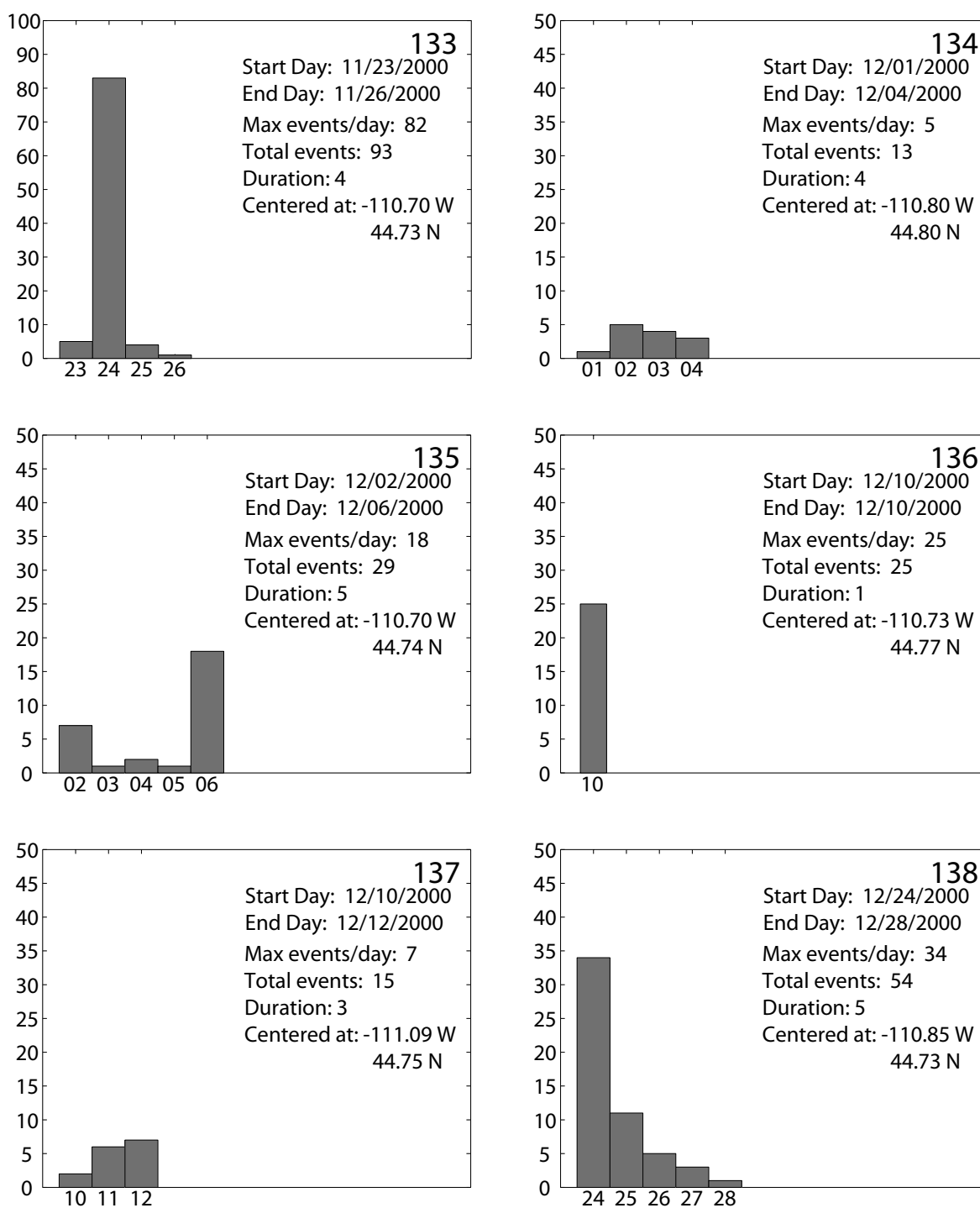


Figure B.23 - Number of earthquakes vs. time for swarm numbers 133 - 138.

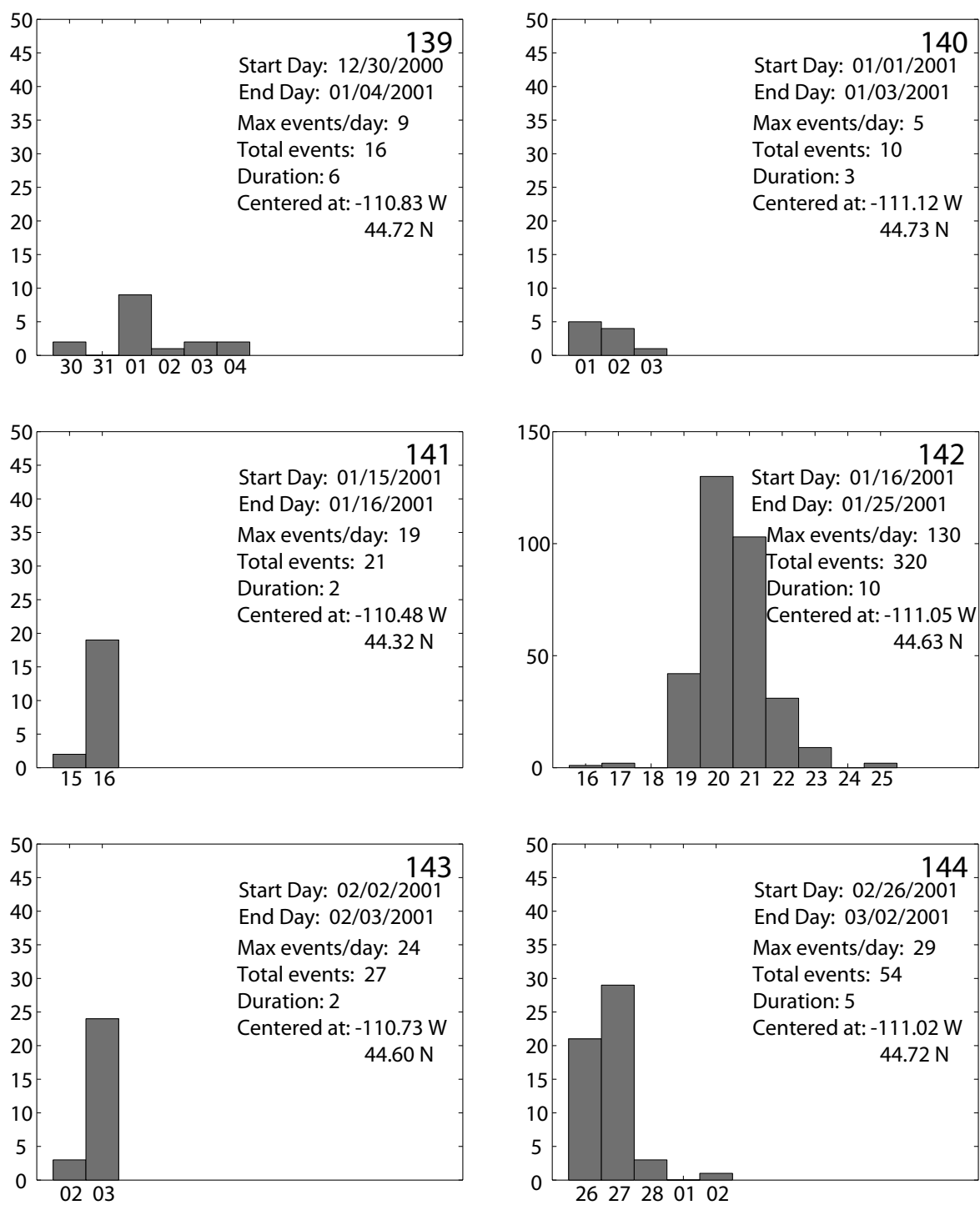


Figure B.24 - Number of earthquakes vs. time for swarm numbers 139 - 144.

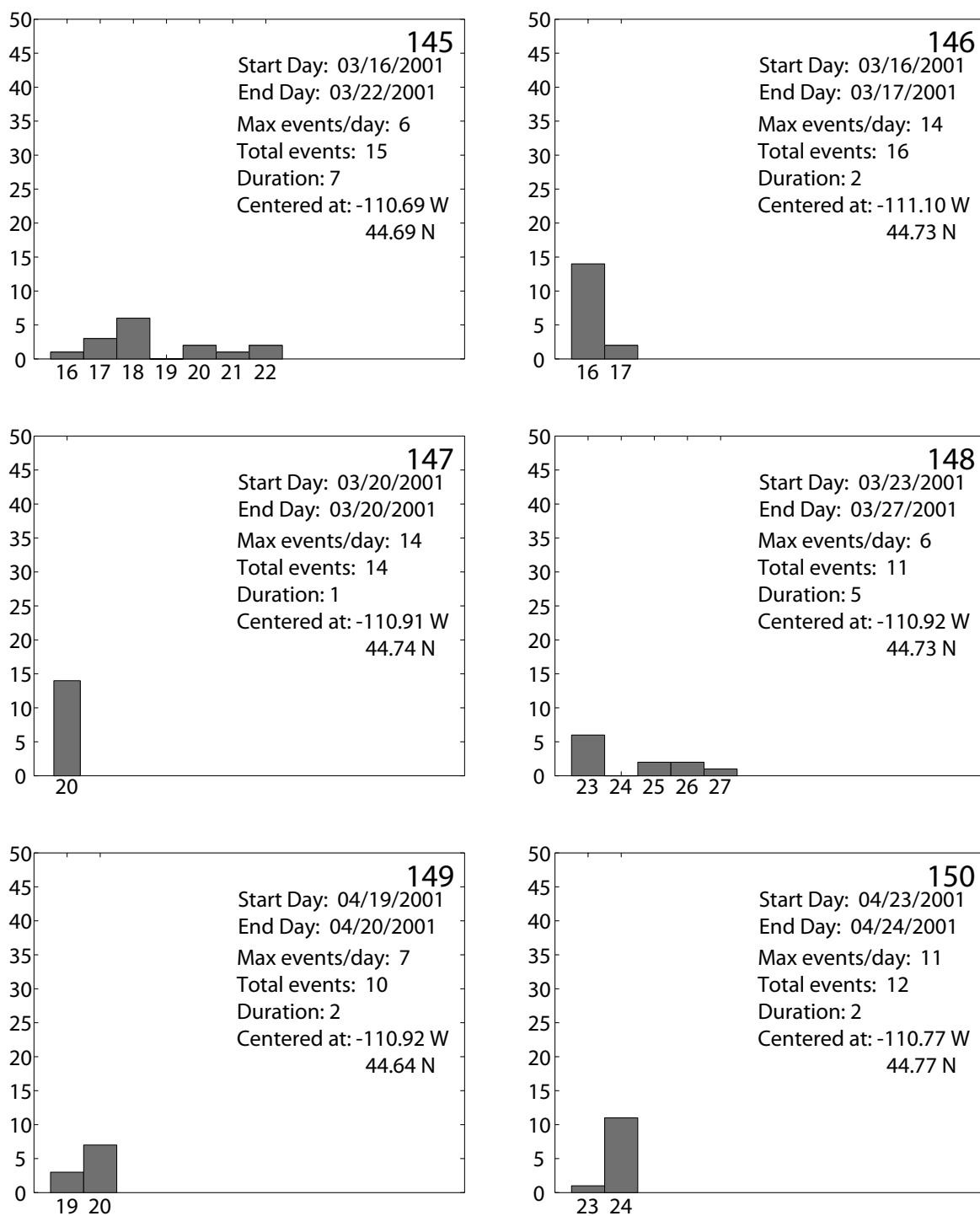


Figure B.25 - Number of earthquakes vs. time for swarm numbers 145 - 150.

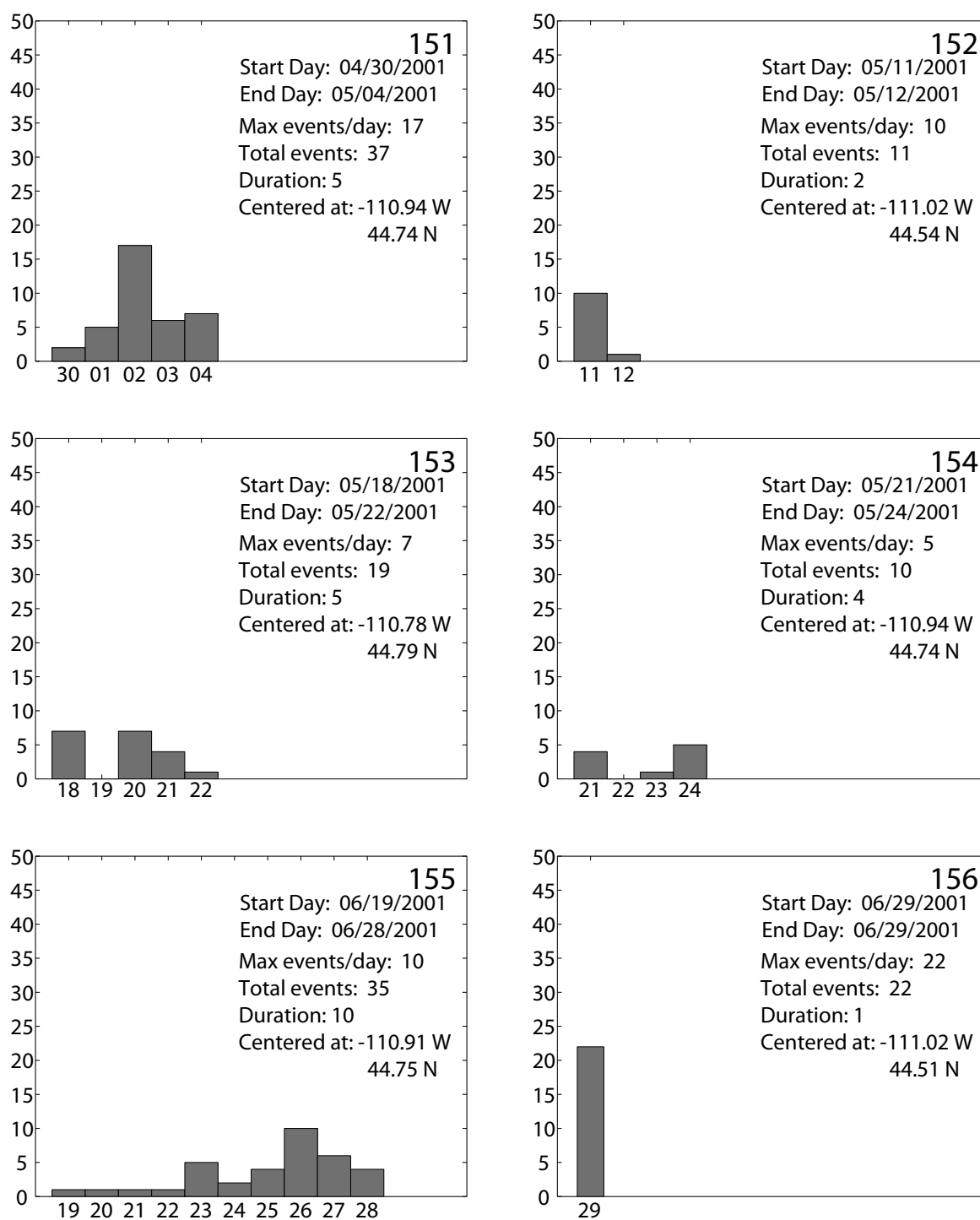


Figure B.26 - Number of earthquakes vs. time for swarm numbers 151 - 156.

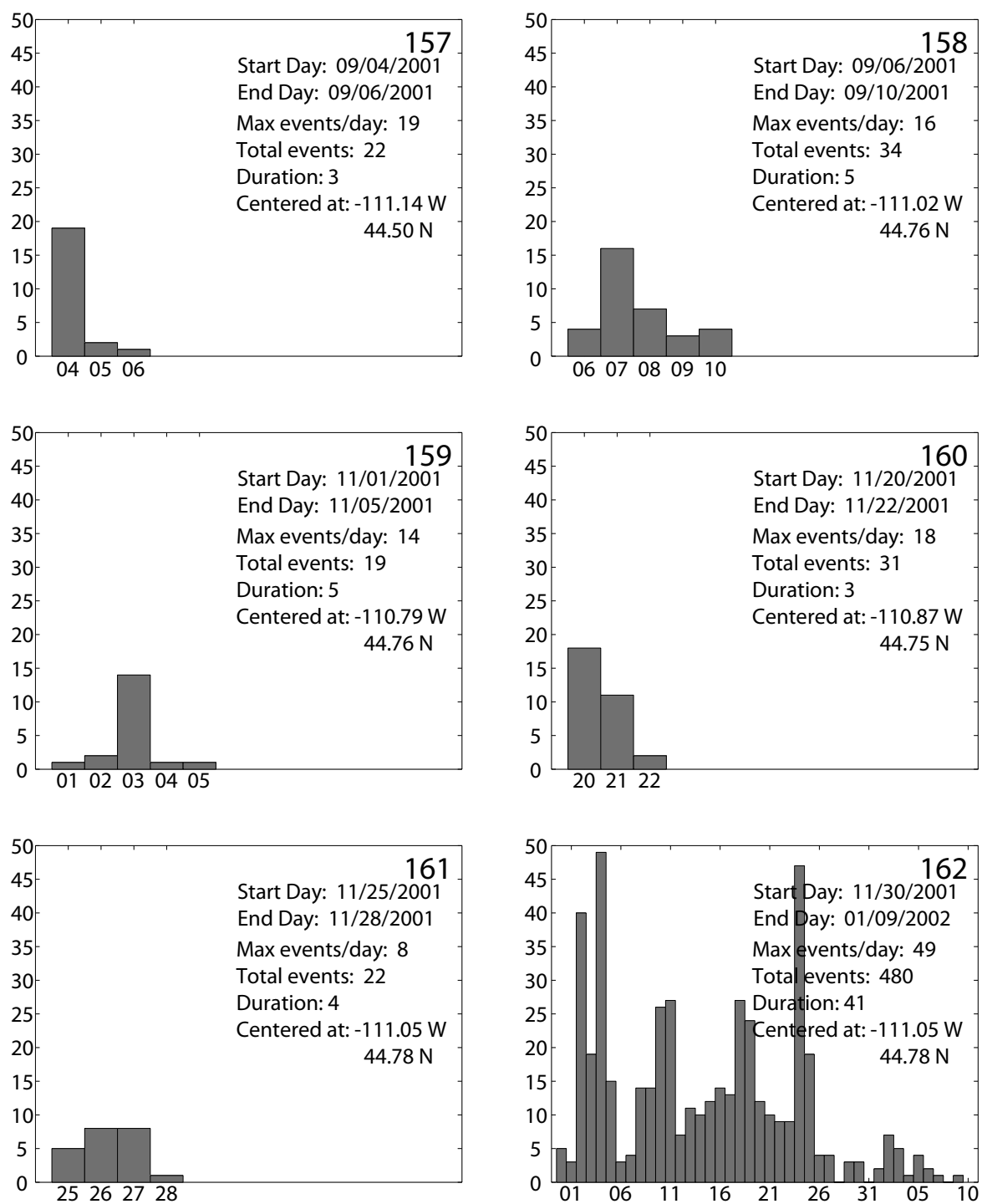


Figure B.27 - Number of earthquakes vs. time for swarm numbers 157 - 162.

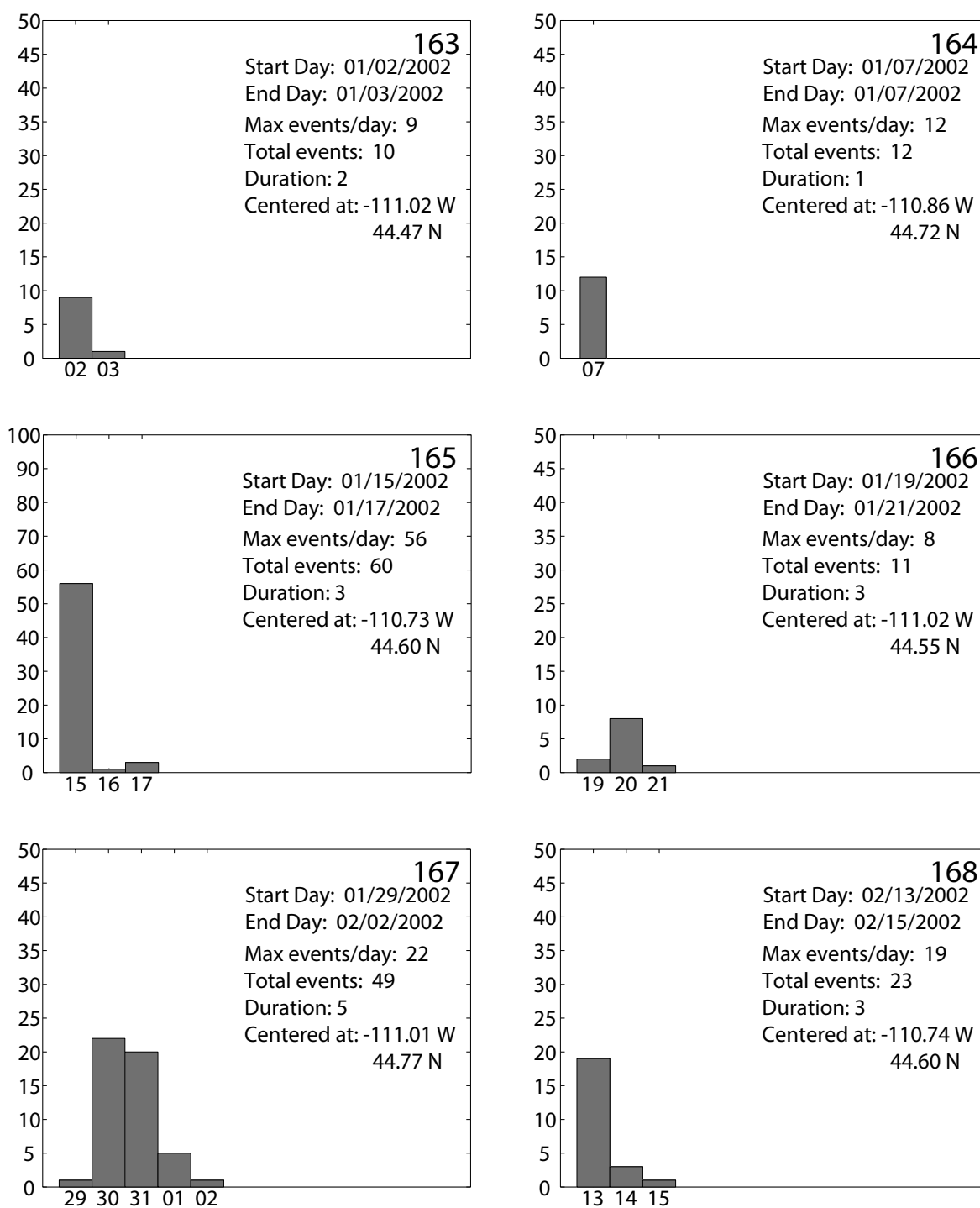


Figure B.28 - Number of earthquakes vs. time for swarm numbers 163 - 168.

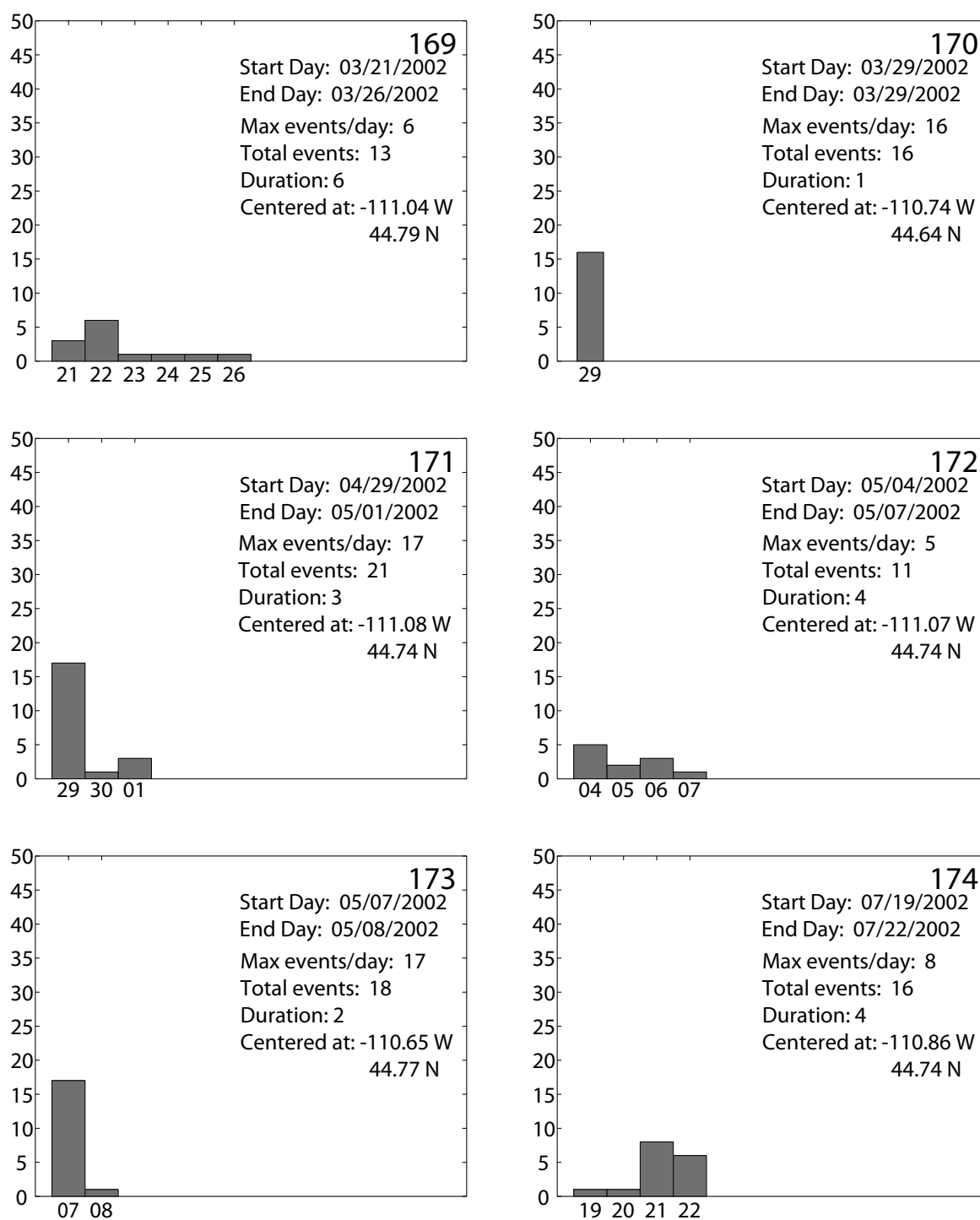


Figure B.29 - Number of earthquakes vs. time for swarm numbers 169 - 174.

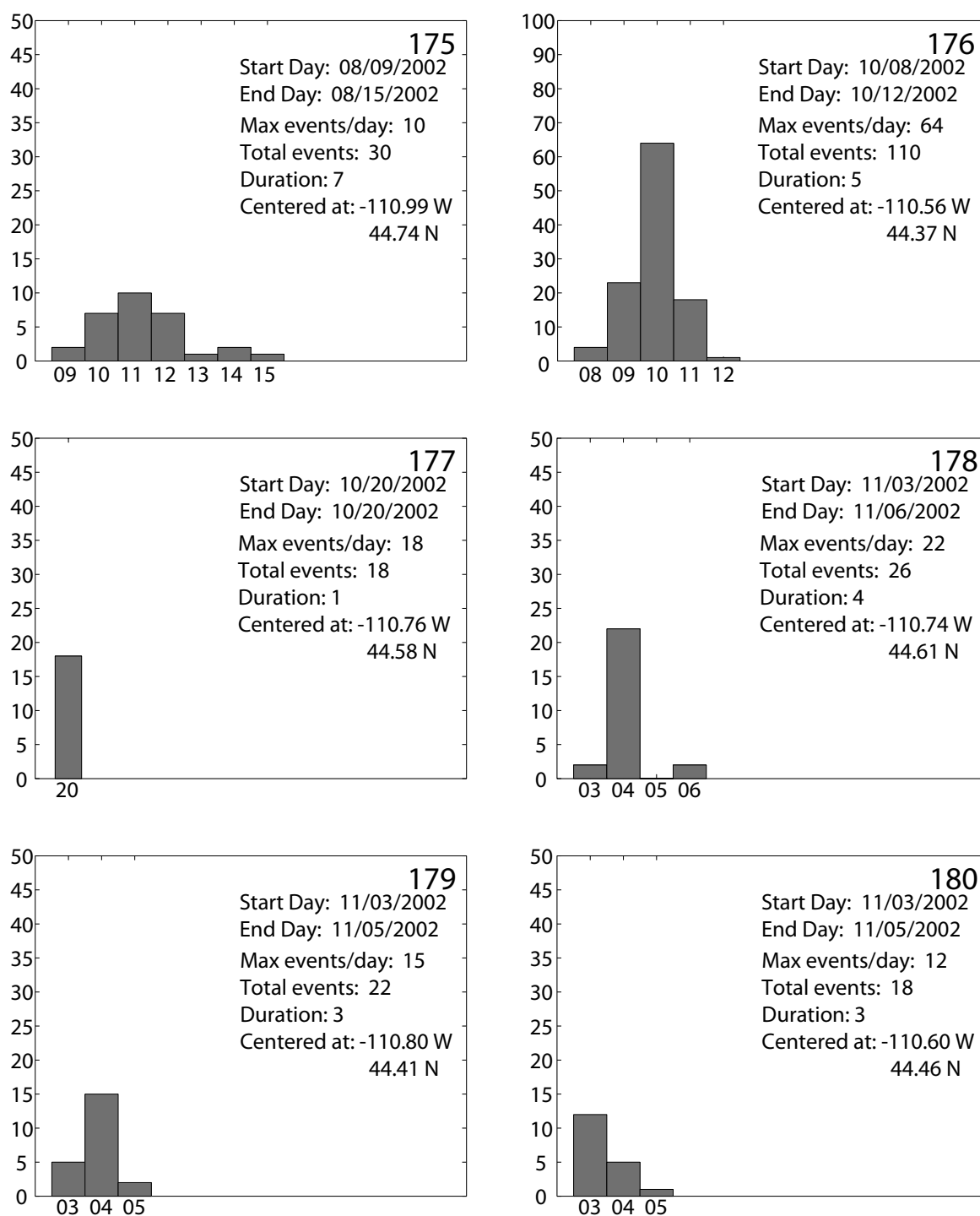


Figure B.30 - Number of earthquakes vs. time for swarm numbers 175 - 180.

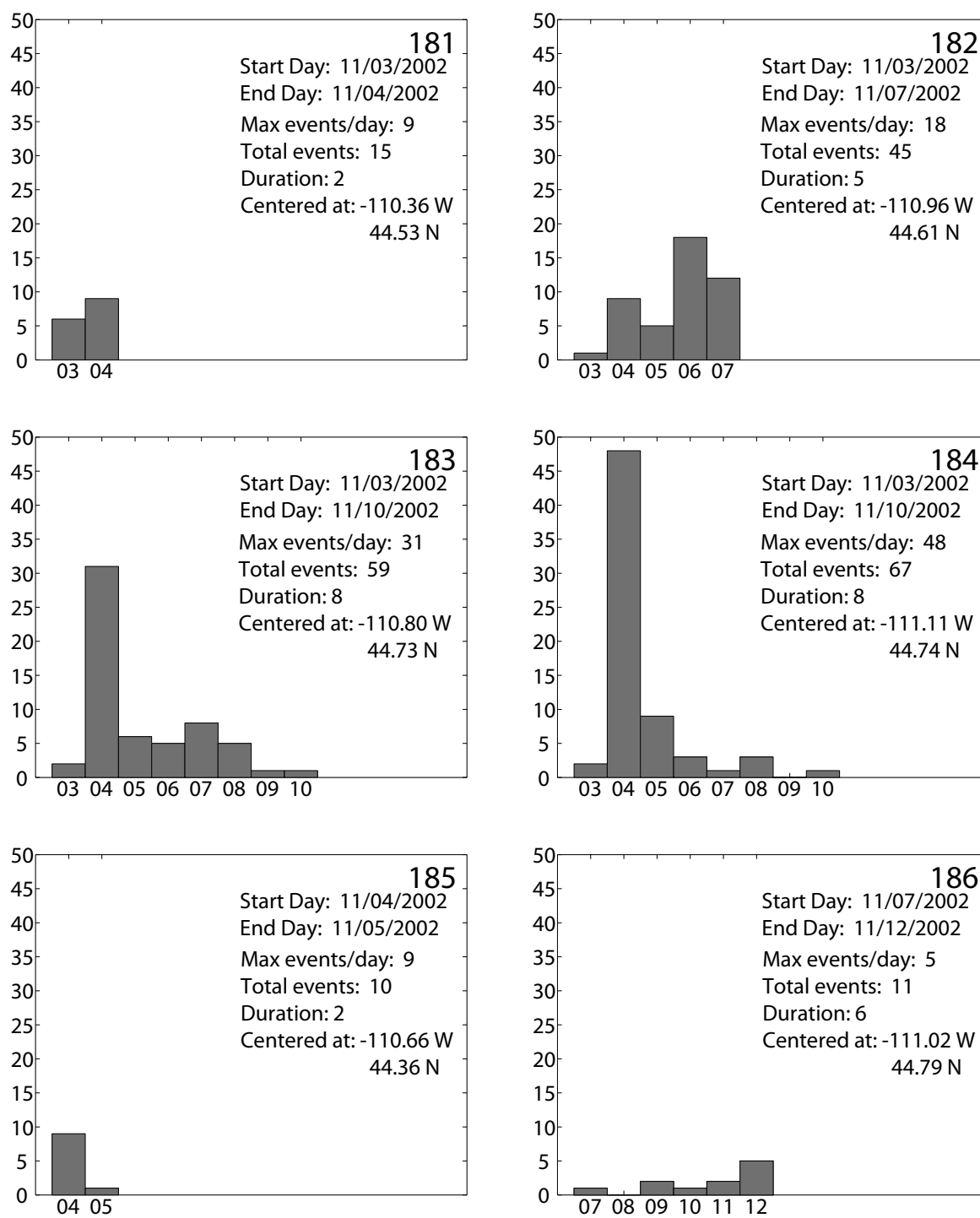


Figure B.31 - Number of earthquakes vs. time for swarm numbers 181 - 186.

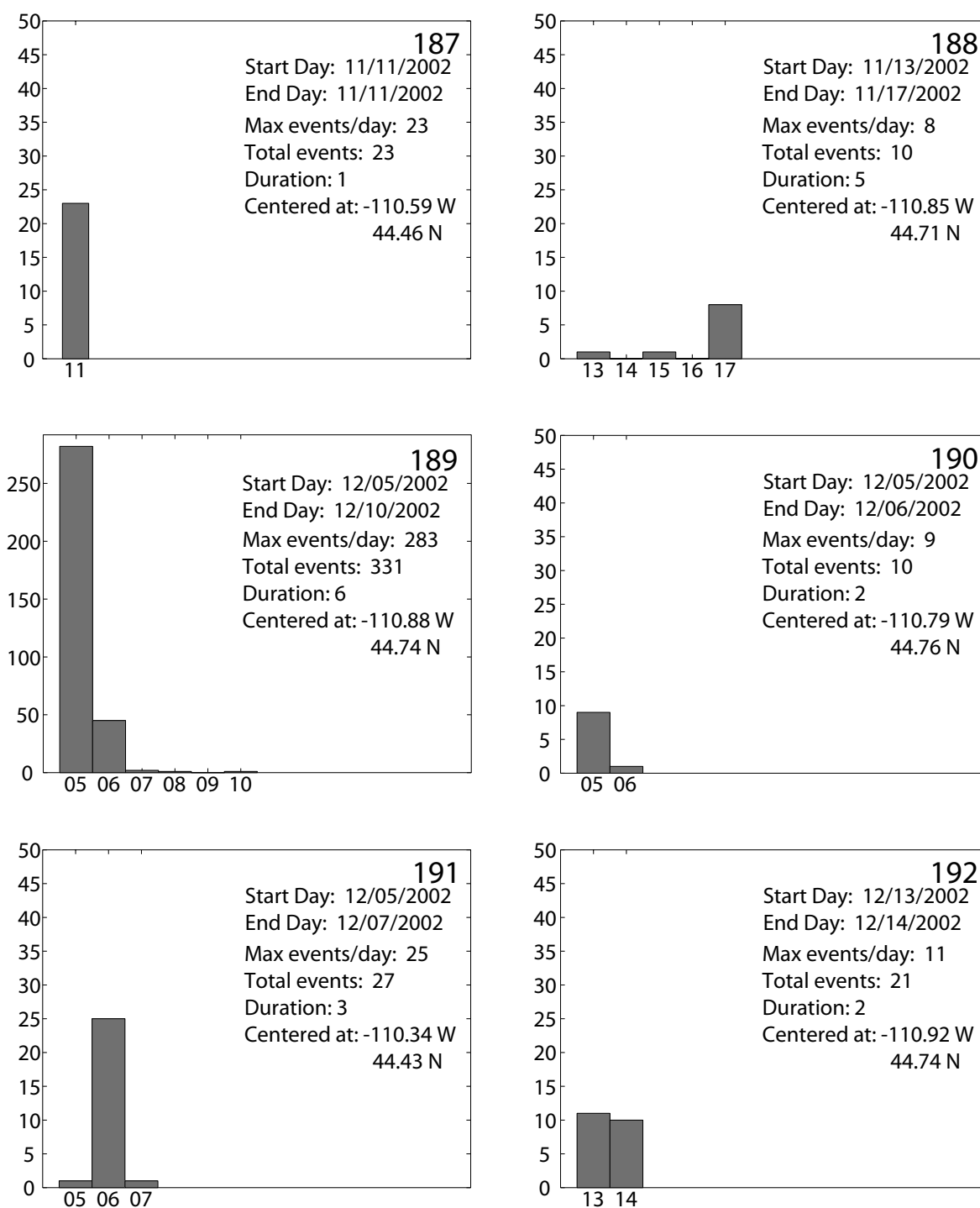


Figure B.32 - Number of earthquakes vs. time for swarm numbers 187 - 192.

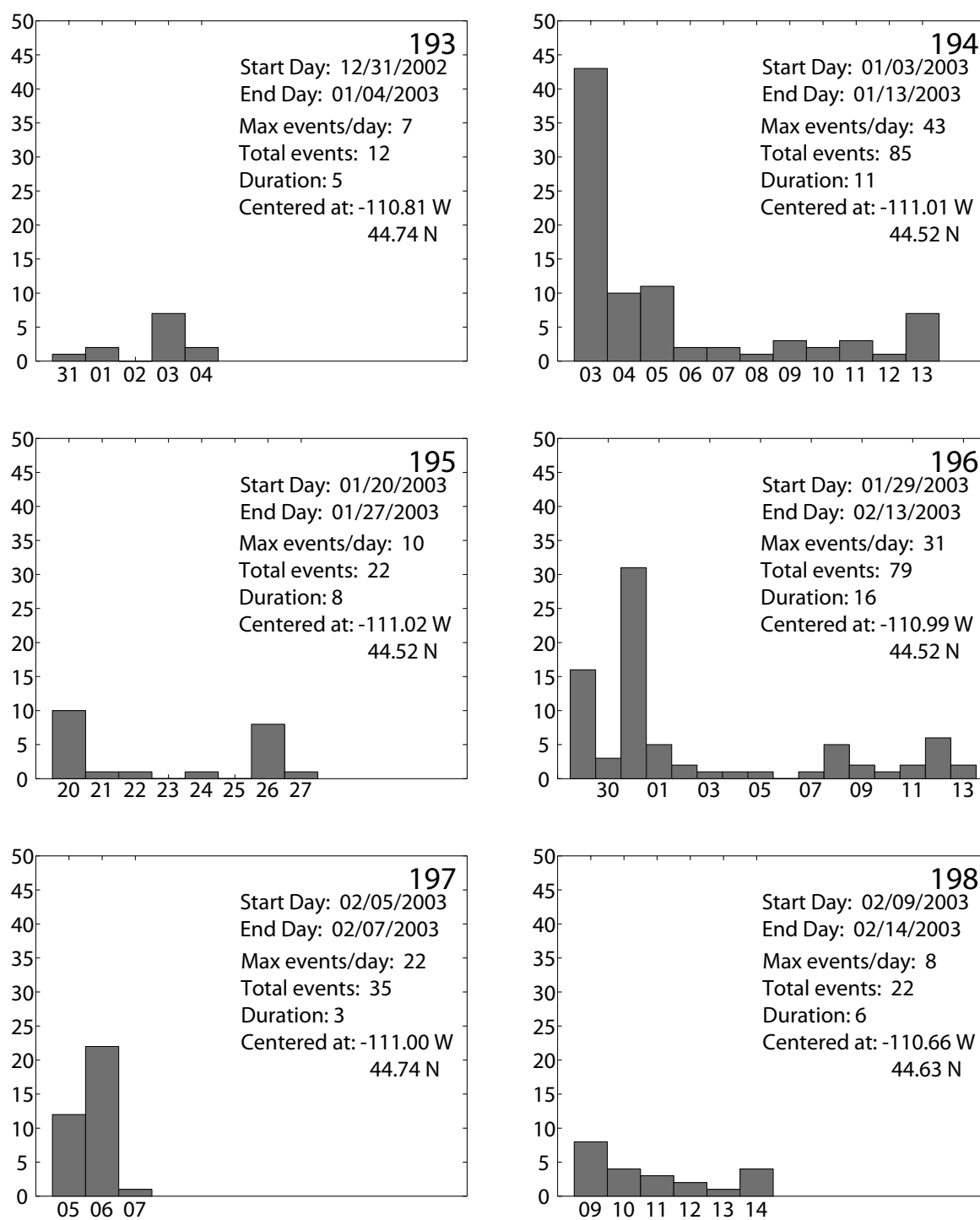


Figure B.33 - Number of earthquakes vs. time for swarm numbers 193 - 198.

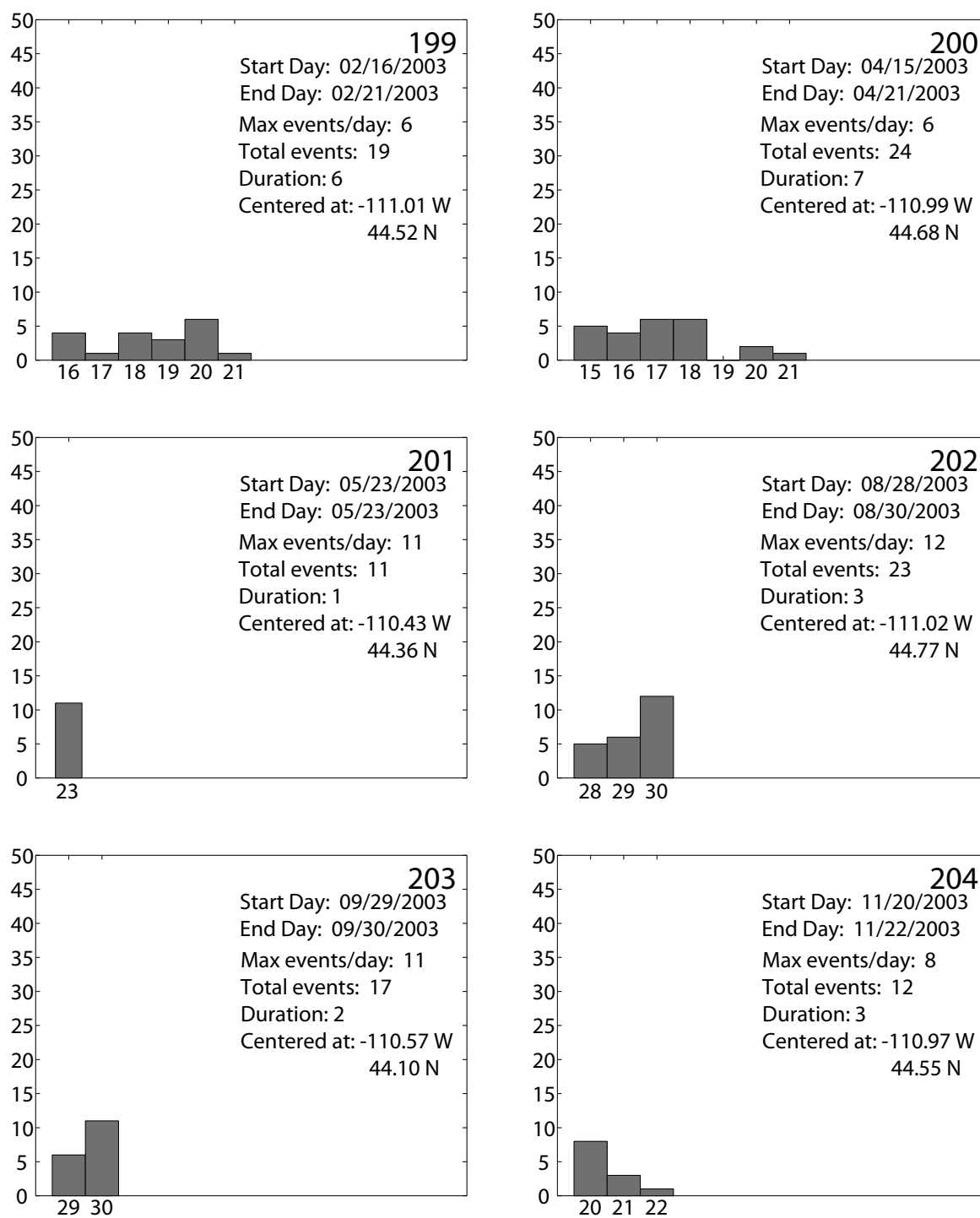


Figure B.34 - Number of earthquakes vs. time for swarm numbers 199 - 204.

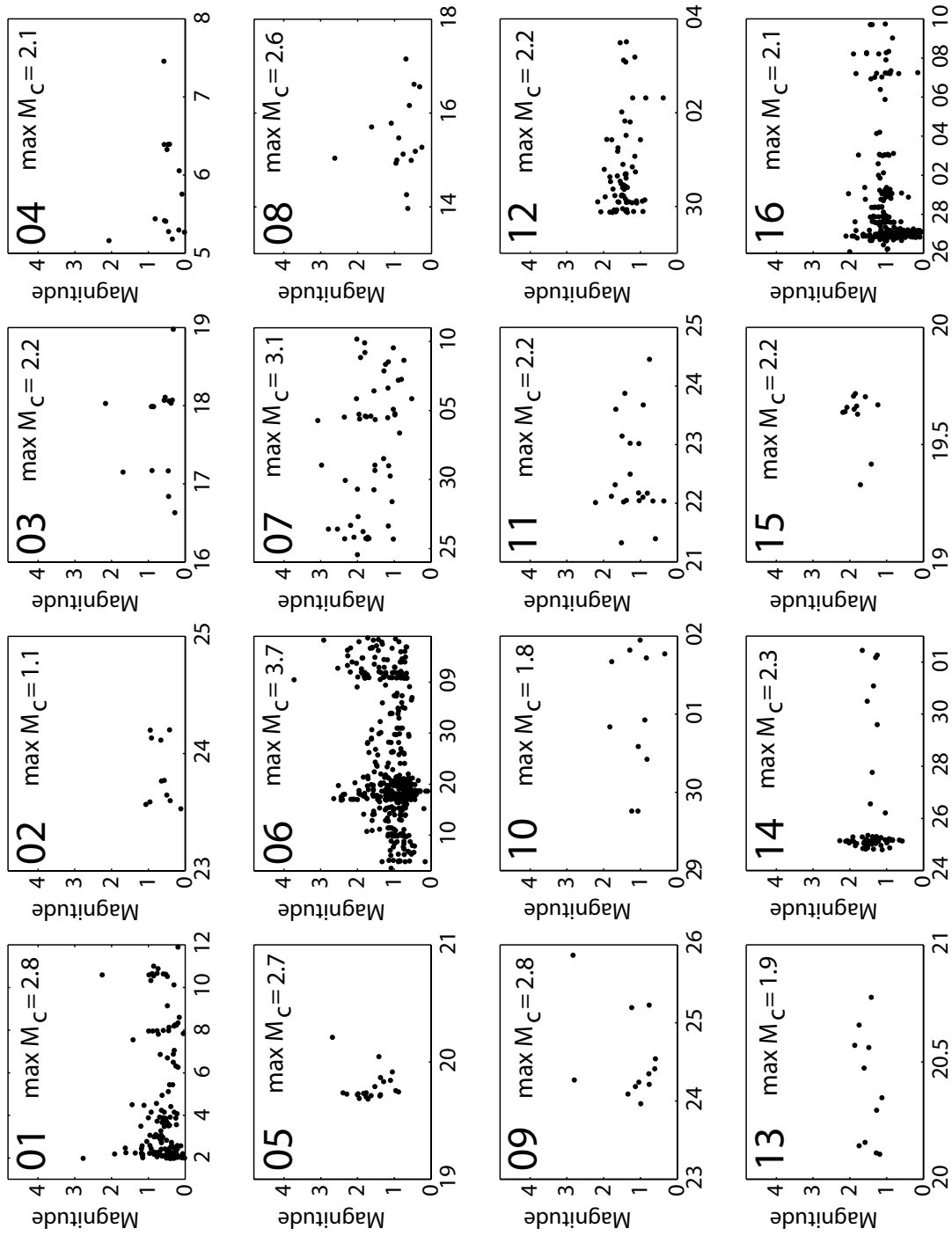


Figure B.35 - Magnitude vs. time for swarm numbers 1 - 16.

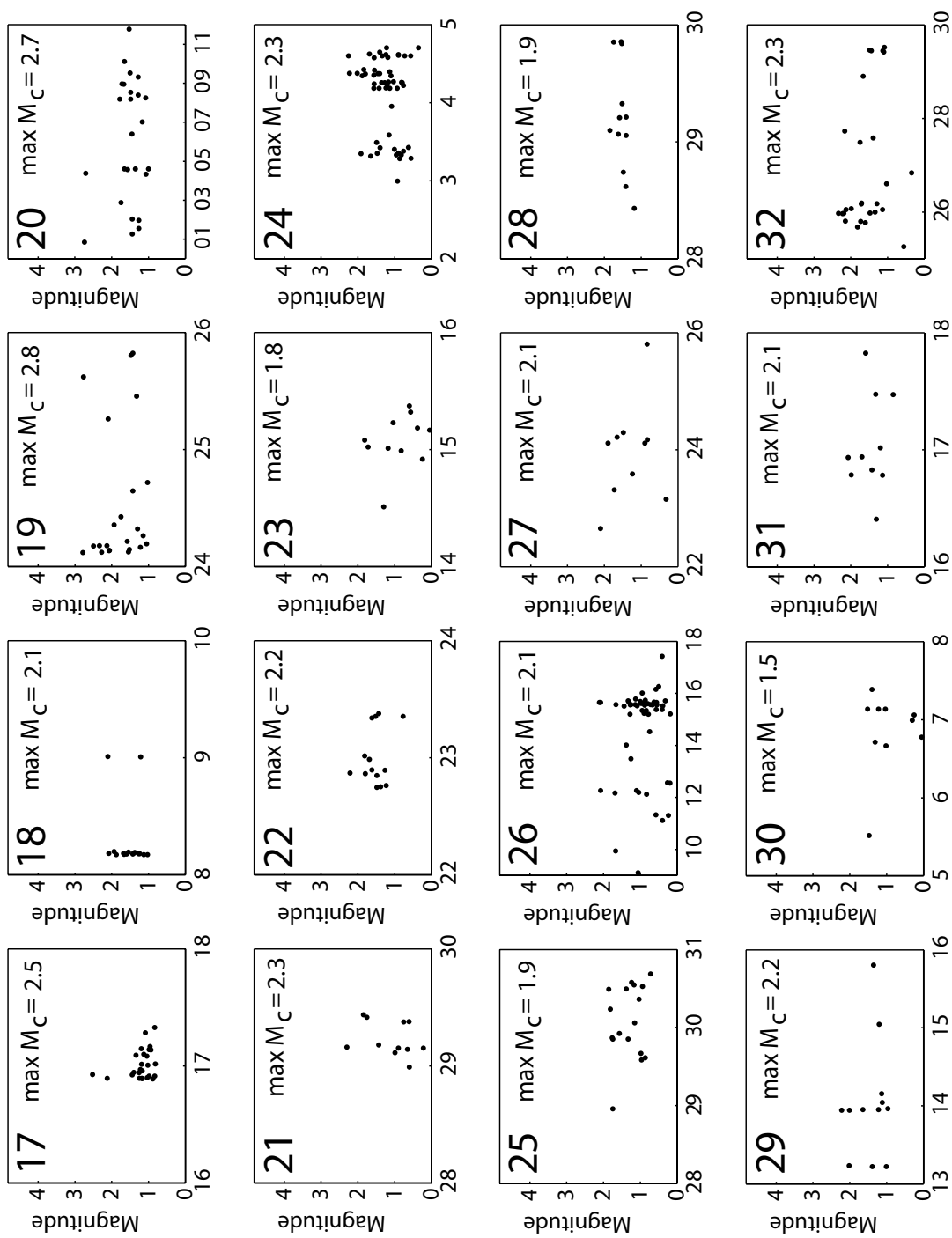


Figure B.36 - Magnitude vs. time for swarm numbers 17 - 32.

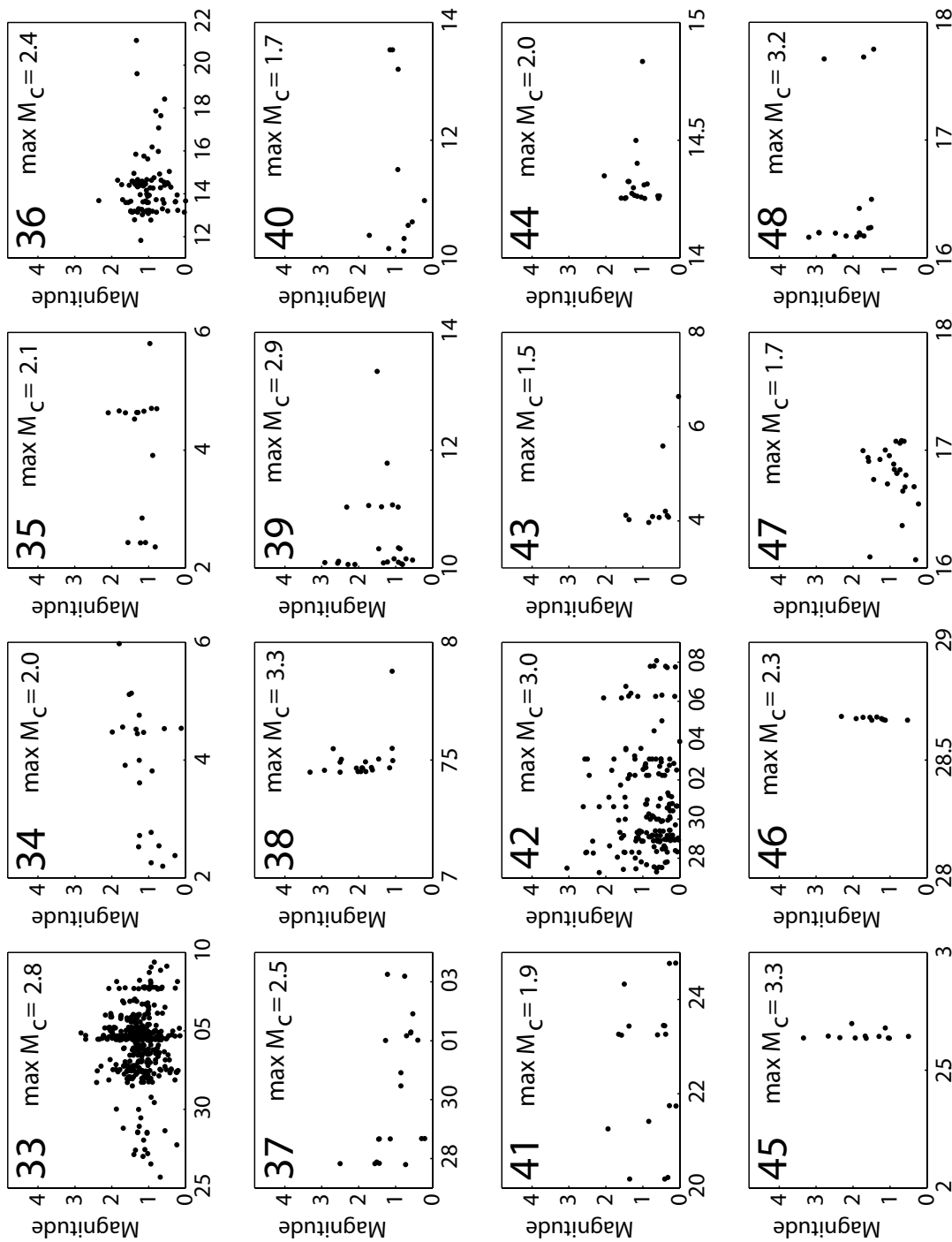


Figure B.37 - Magnitude vs. time for swarm numbers 33 - 48.

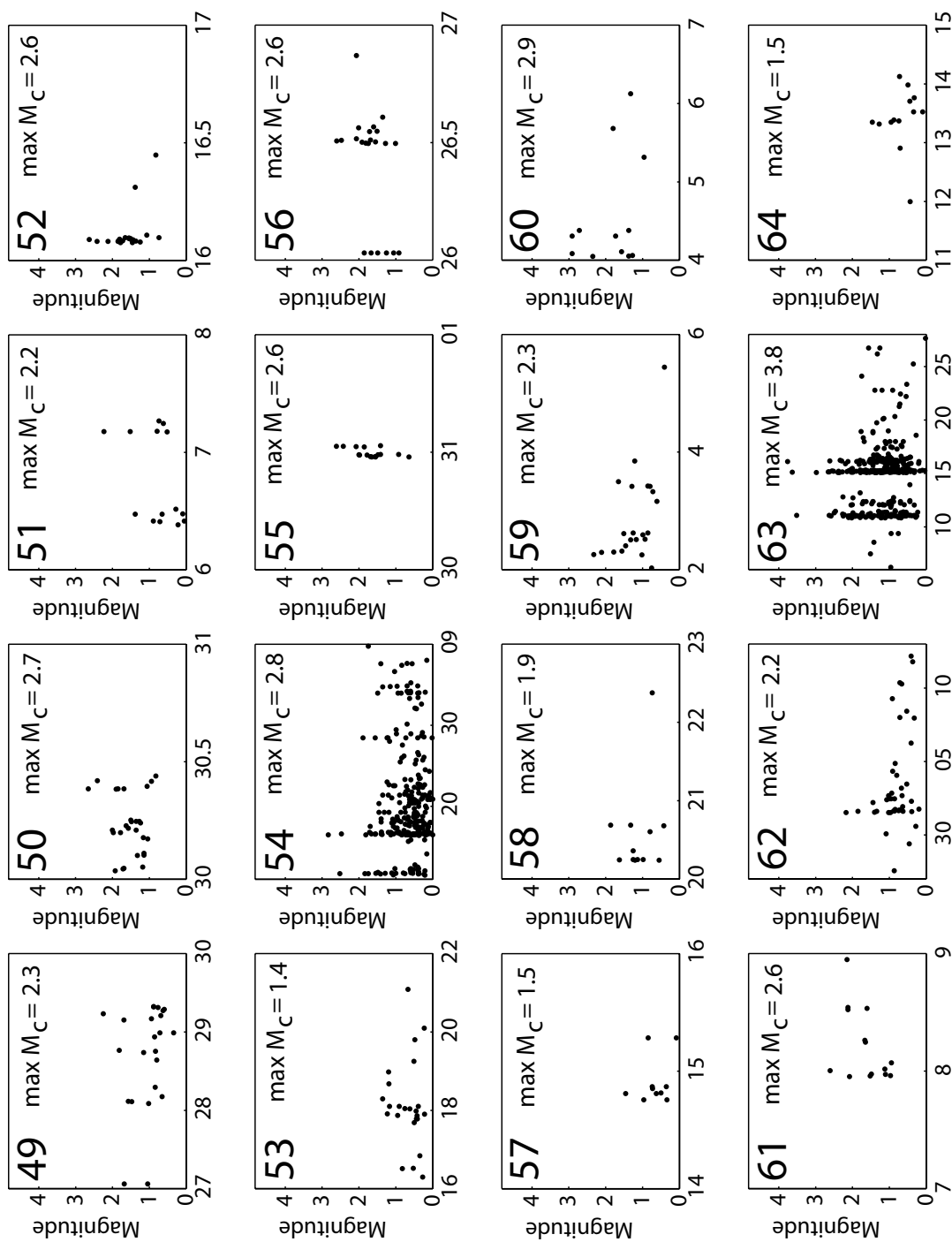


Figure B.38 - Magnitude vs. time for swarm numbers 49 - 64.

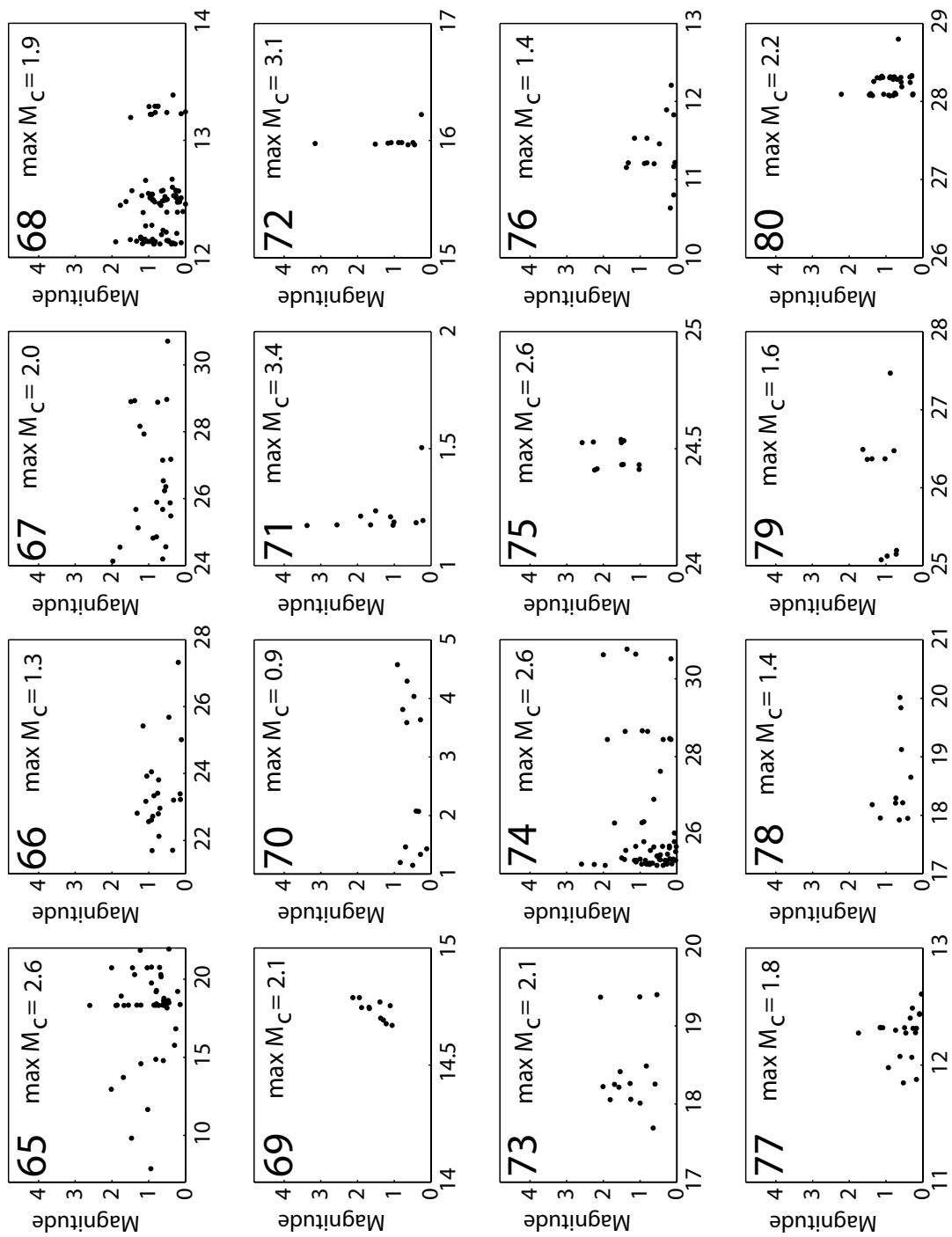


Figure B.39 - Magnitude vs. time for swarm numbers 65 - 80.

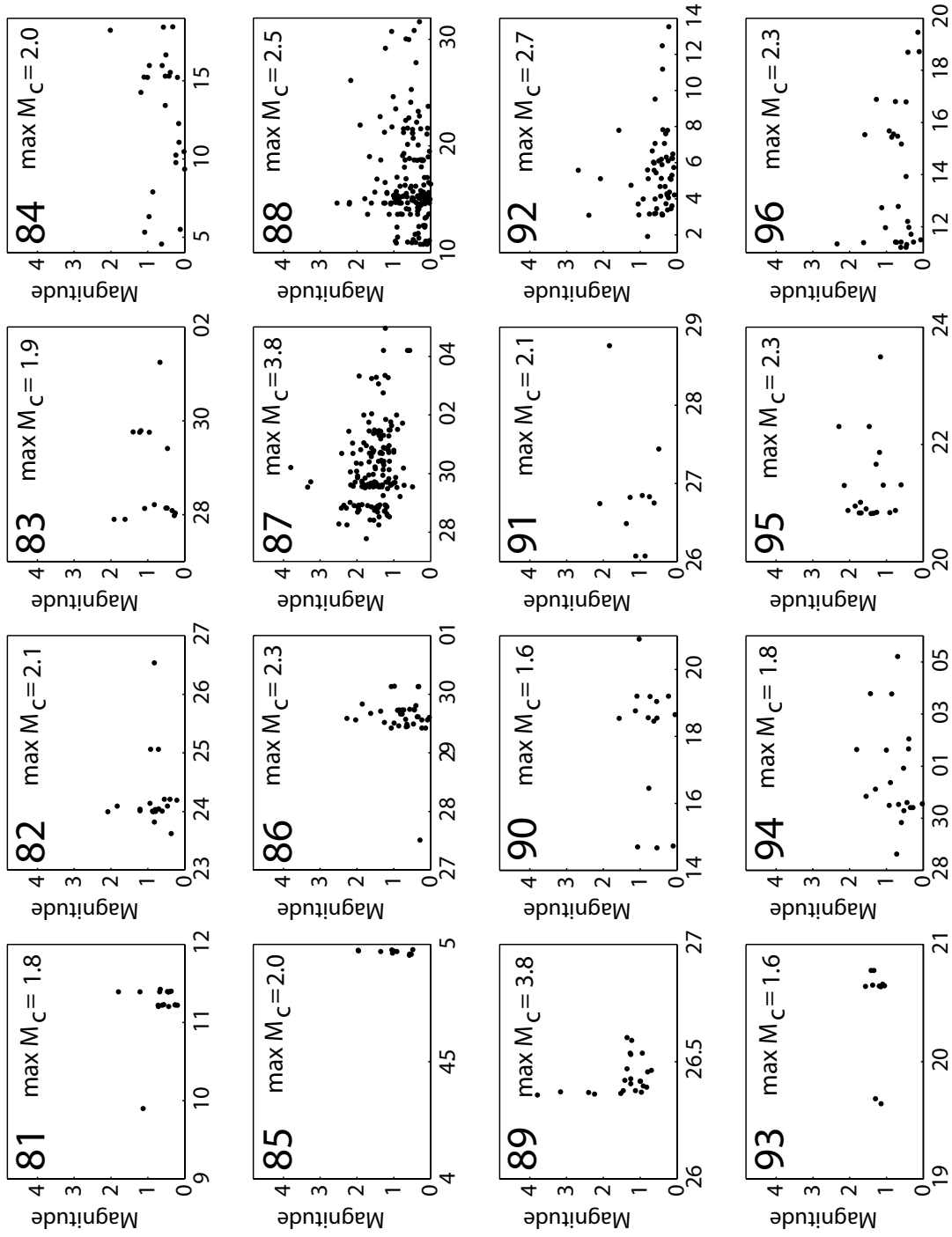


Figure B.40 - Magnitude vs. time for swarm numbers 81 - 96.

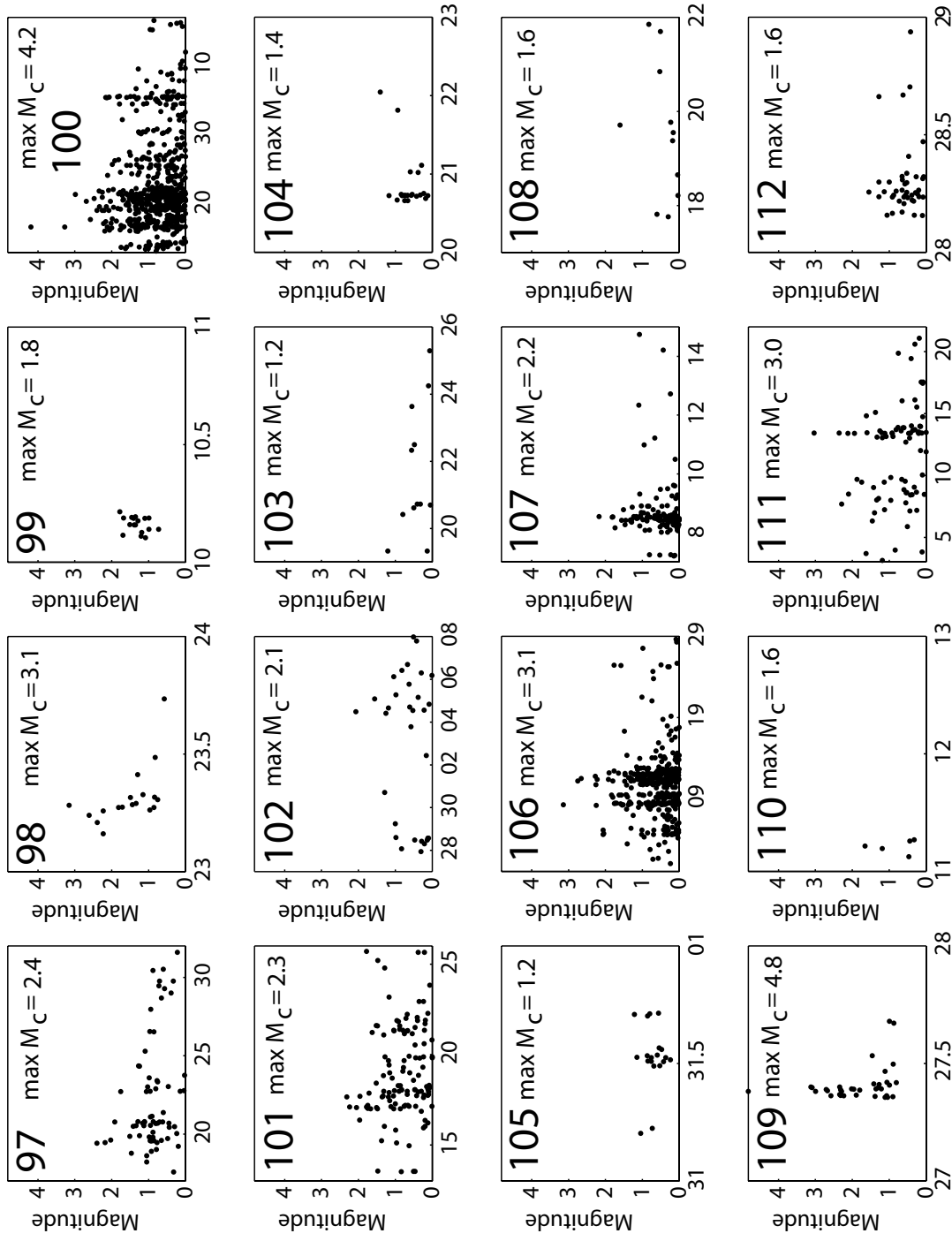


Figure B.41 - Magnitude vs. time for swarm numbers 97 - 112.

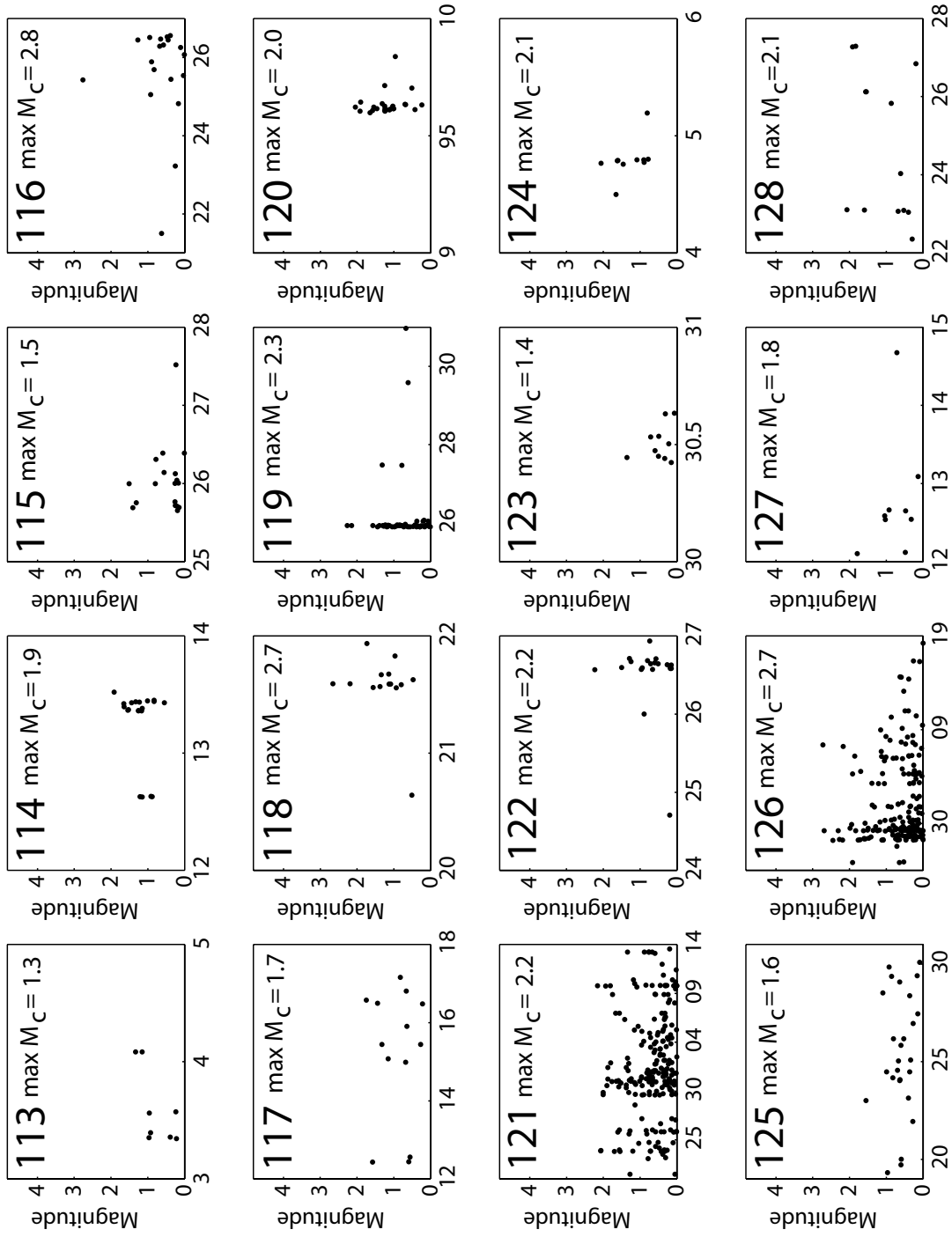


Figure B.42 - Magnitude vs. time for swarm numbers 113 - 128.

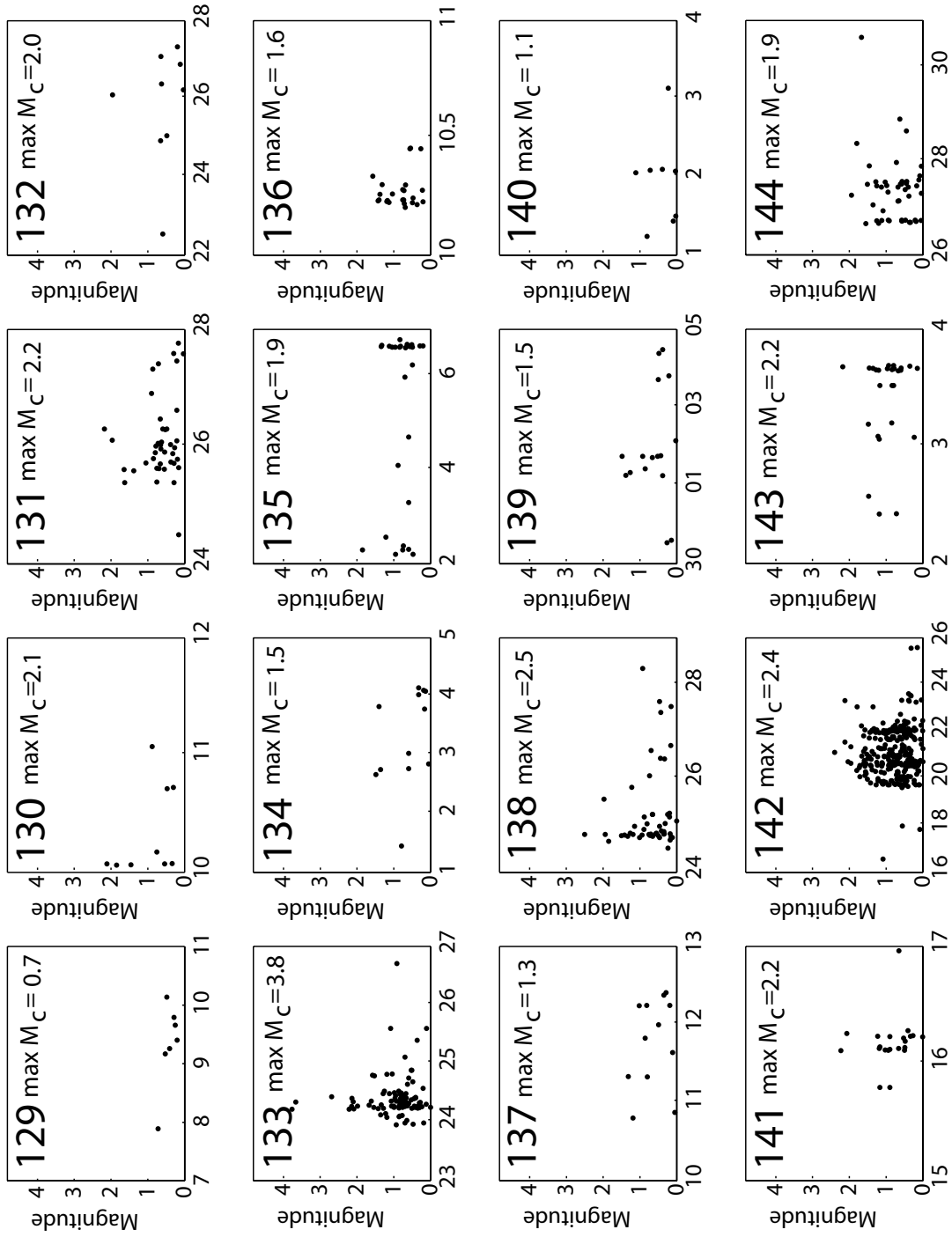


Figure B.43 - Magnitude vs. time for swarm numbers 129 - 144.

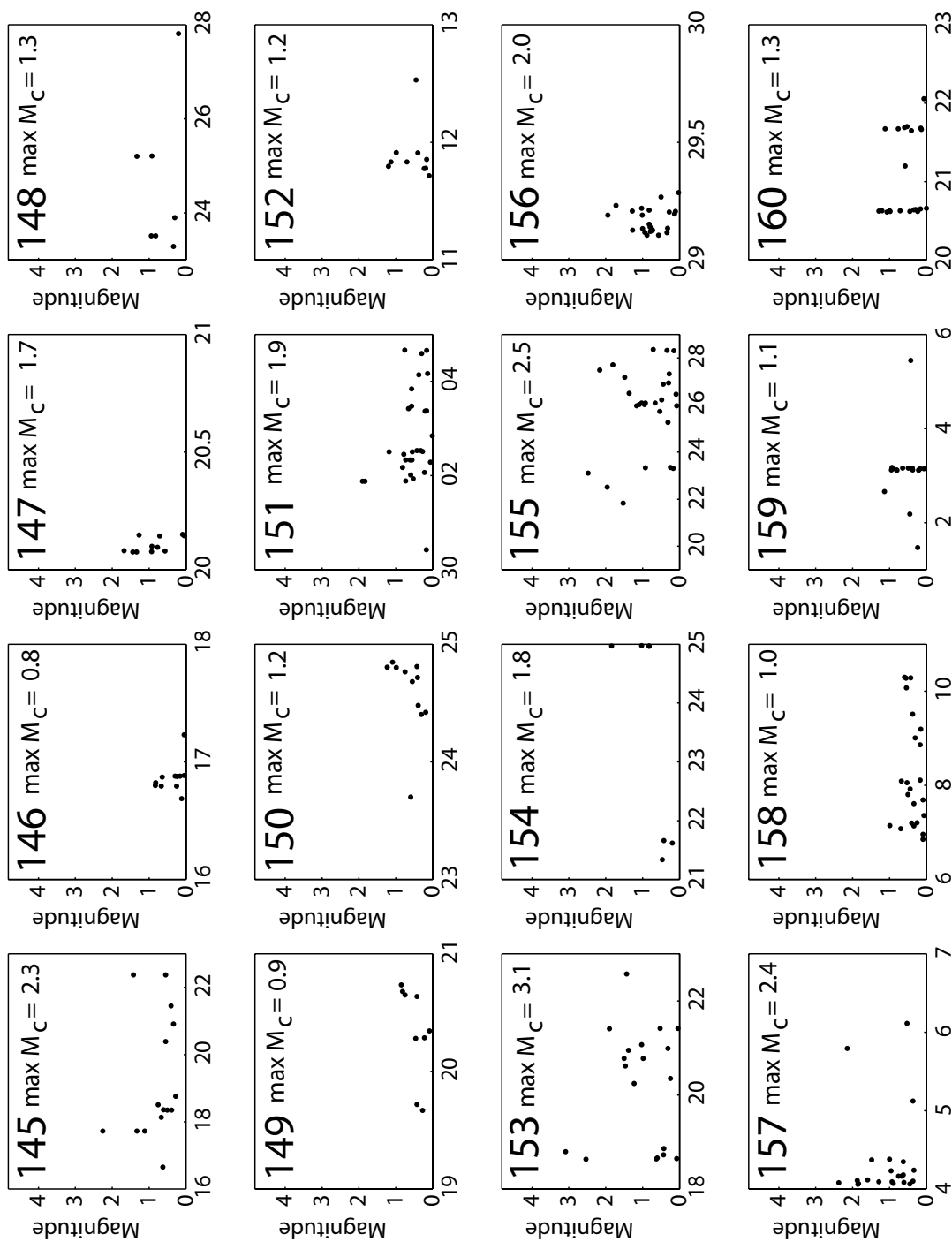


Figure B.44 - Magnitude vs. time for swarm numbers 145 - 160.

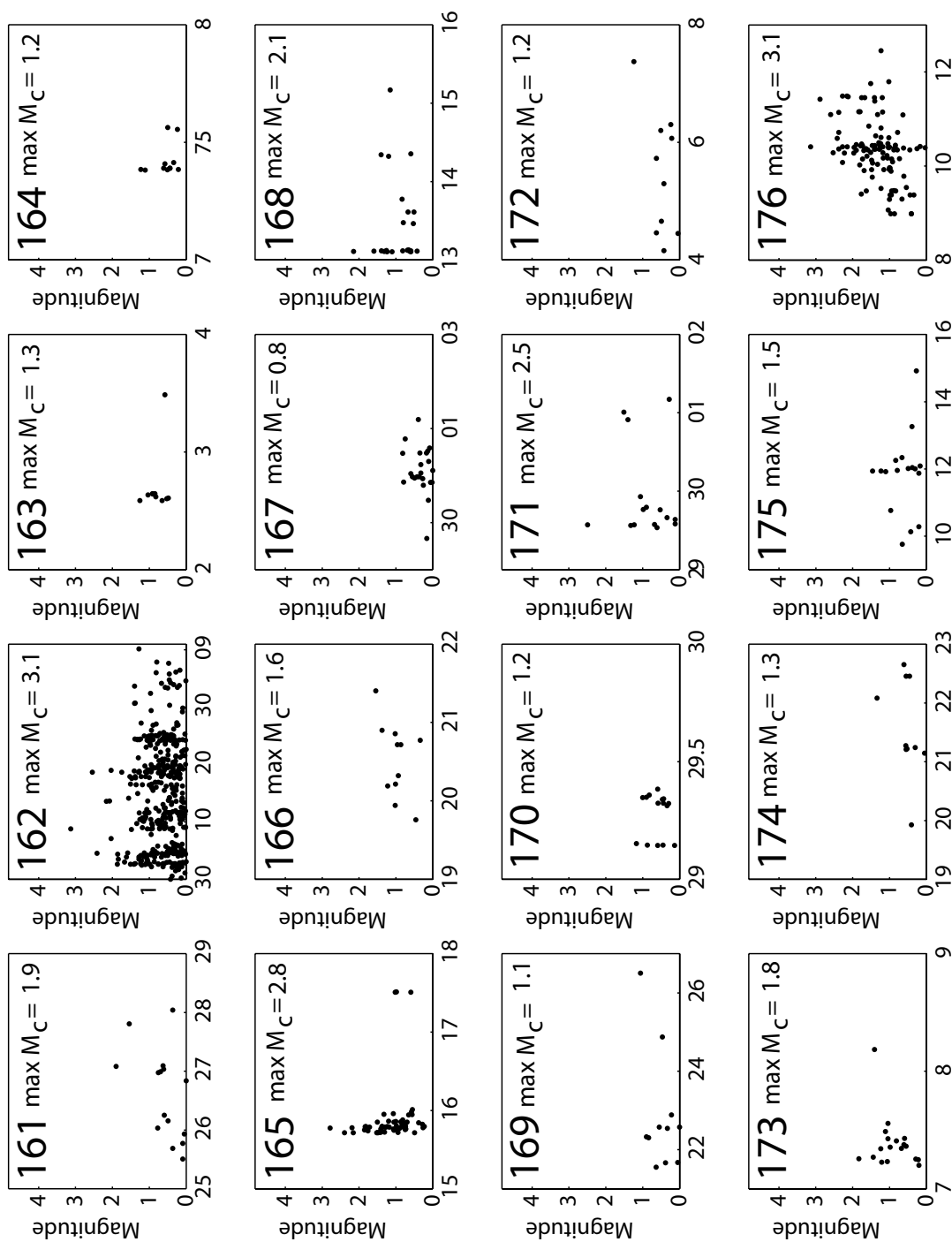


Figure B.45 - Magnitude vs. time for swarm numbers 161 - 176.

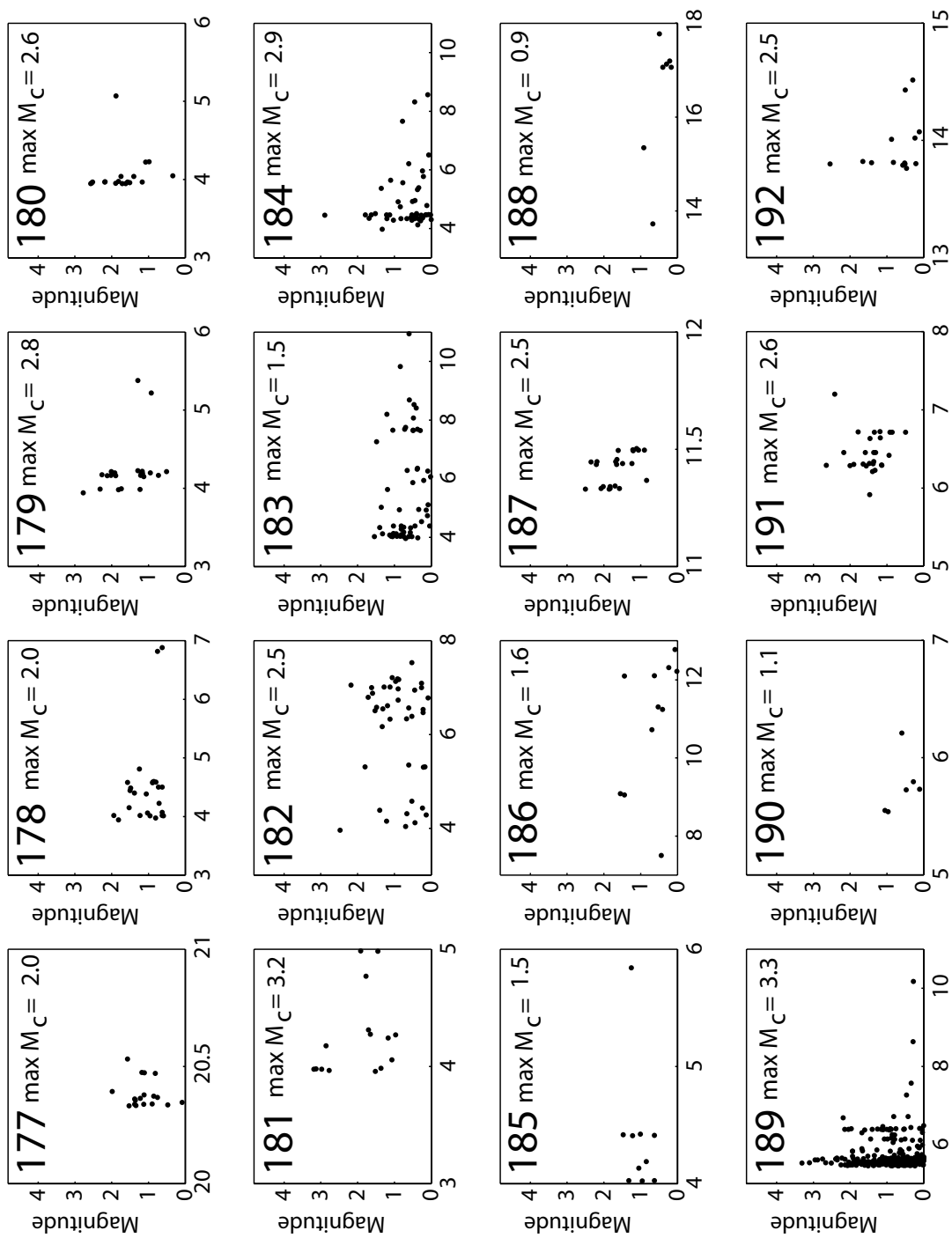


Figure B.46 - Magnitude vs. time for swarm numbers 177 - 192.

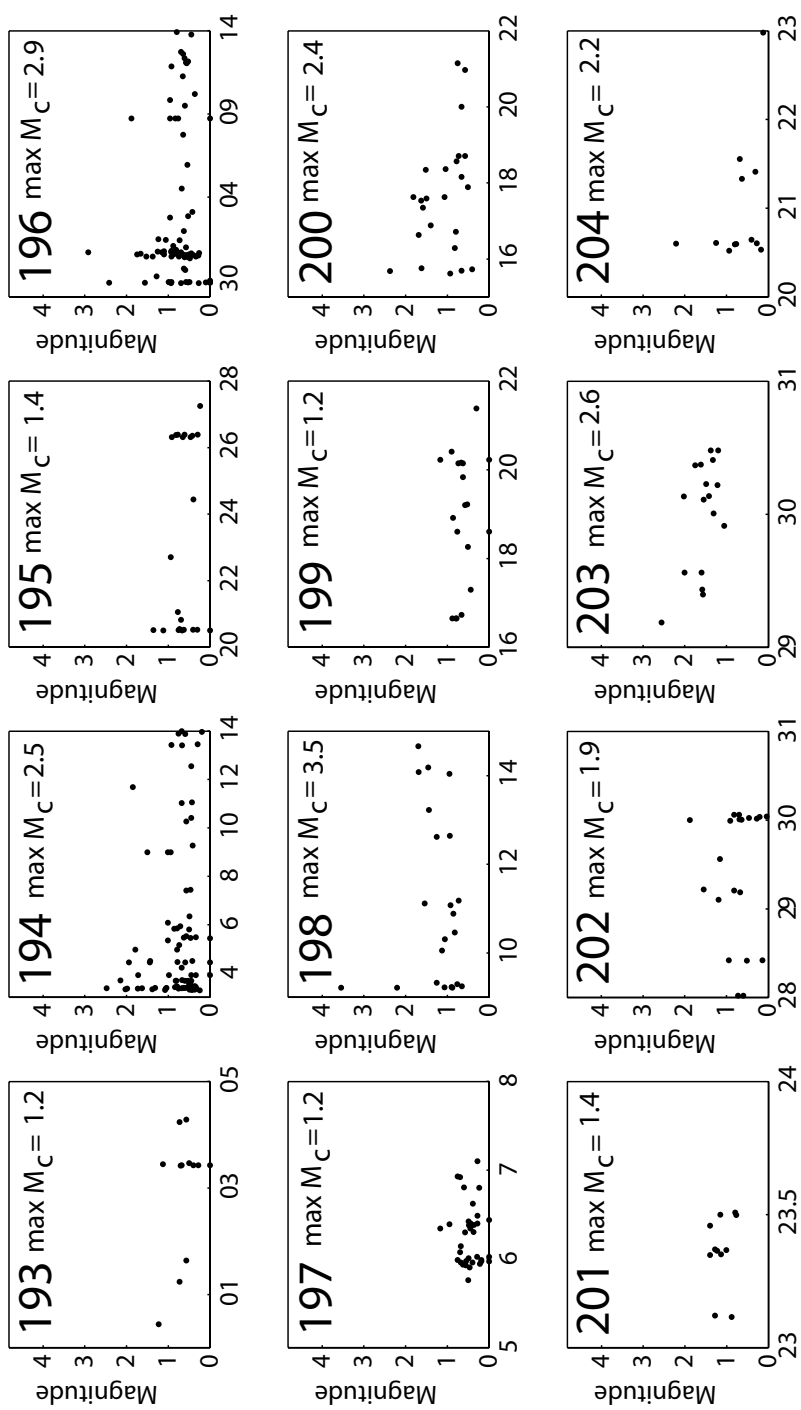


Figure B.47 - Magnitude vs. time for swarm numbers 193 - 204.

## APPENDIX C

### PLOTS OF INDIVIDUAL EARTHQUAKE

#### SWARM EPICENTERS

Swarm epicenters are plotted in this appendix for all definitions of swarms. See Appendix A to identify what definition was used (10 minimum, 30 minimum, 50 minimum) to identify individual swarms. The swarms are color-coded and numbered according to the order of occurrence. The swarms plotted in the figures in the text and in Appendix A and B use the same numbering system.

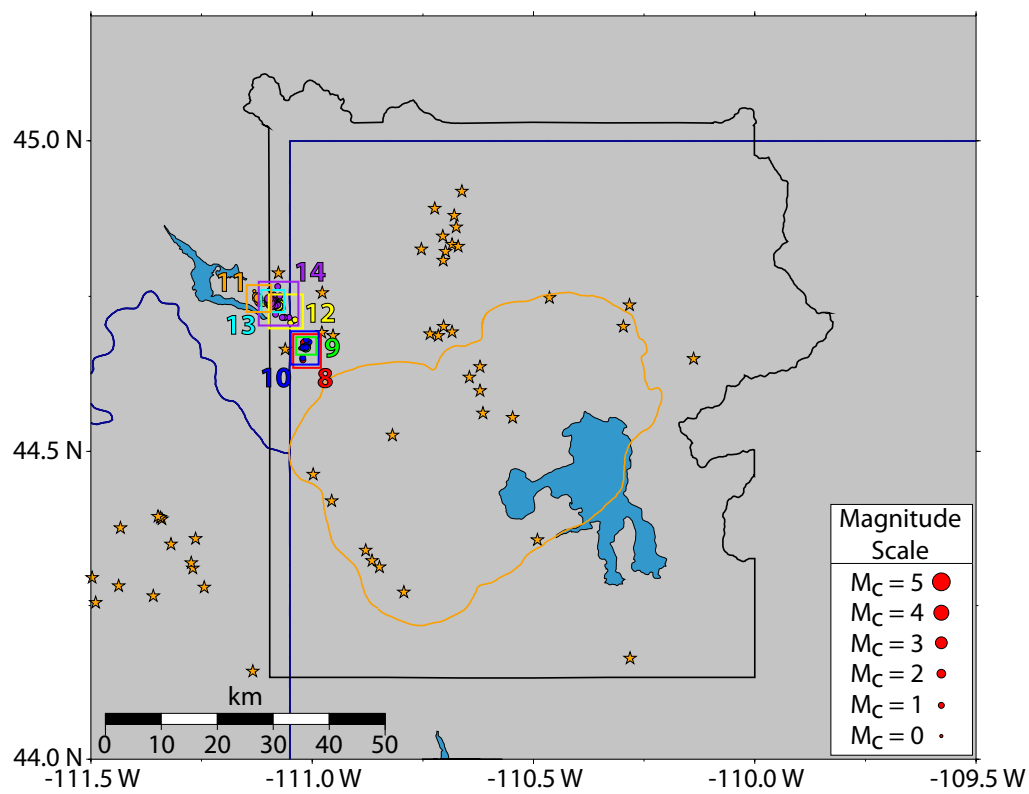
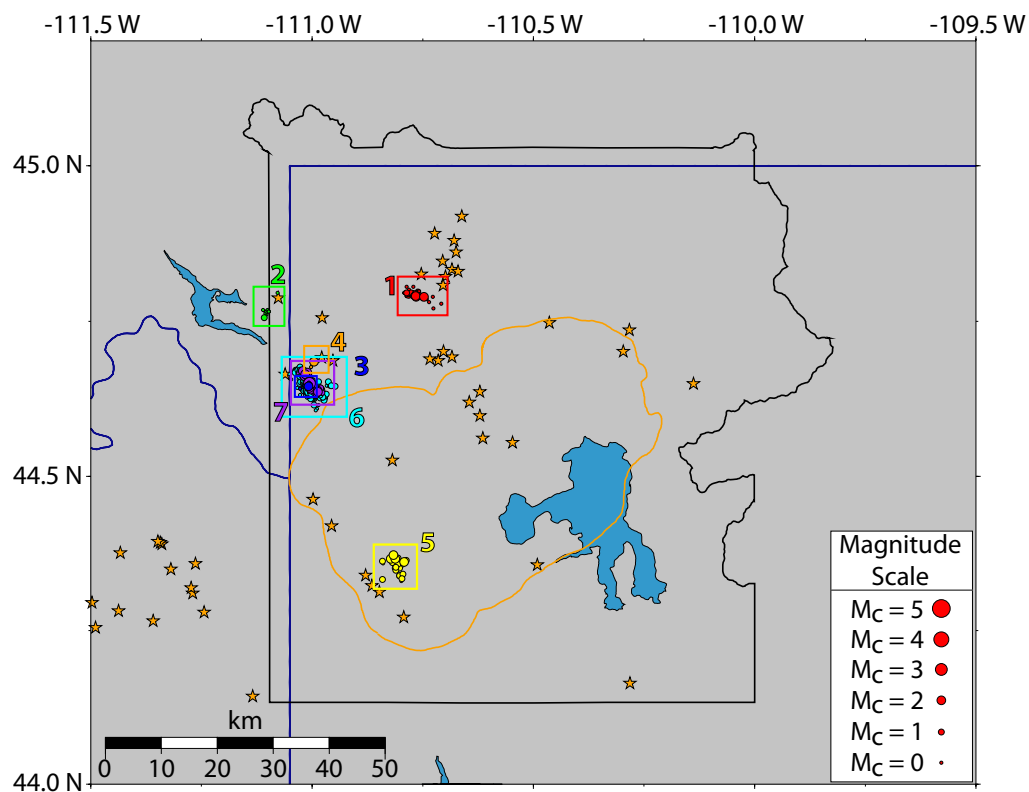


Figure C.1 - Swarm epicenter maps for swarms 1 - 14.

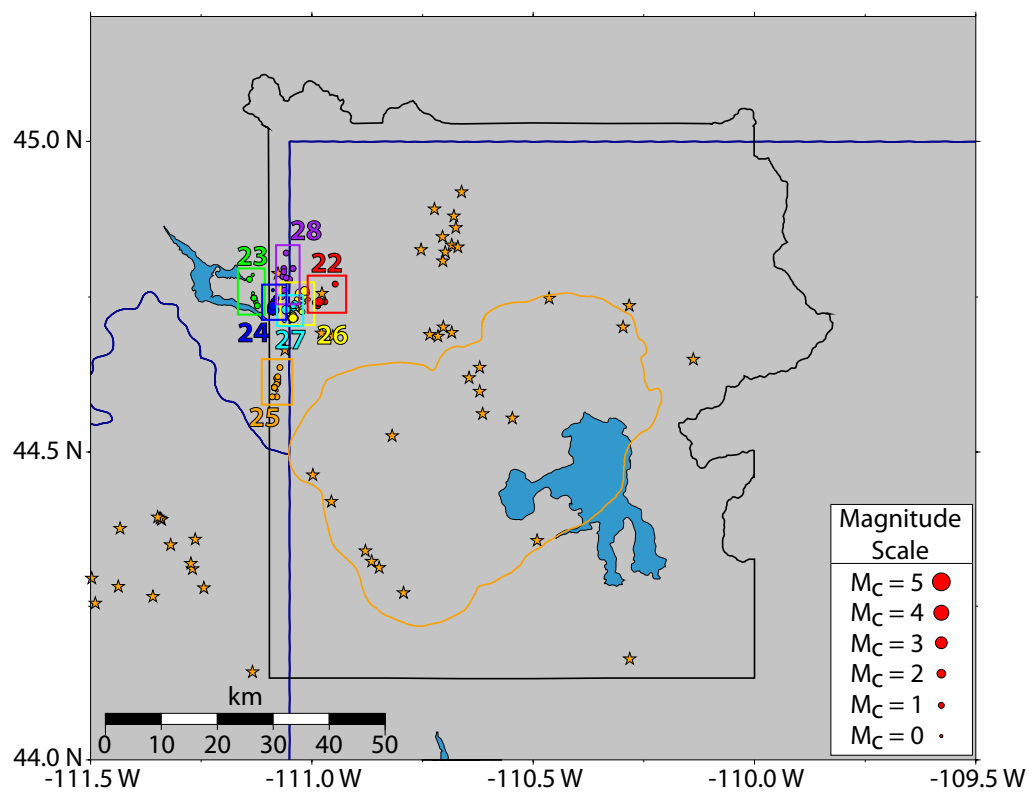
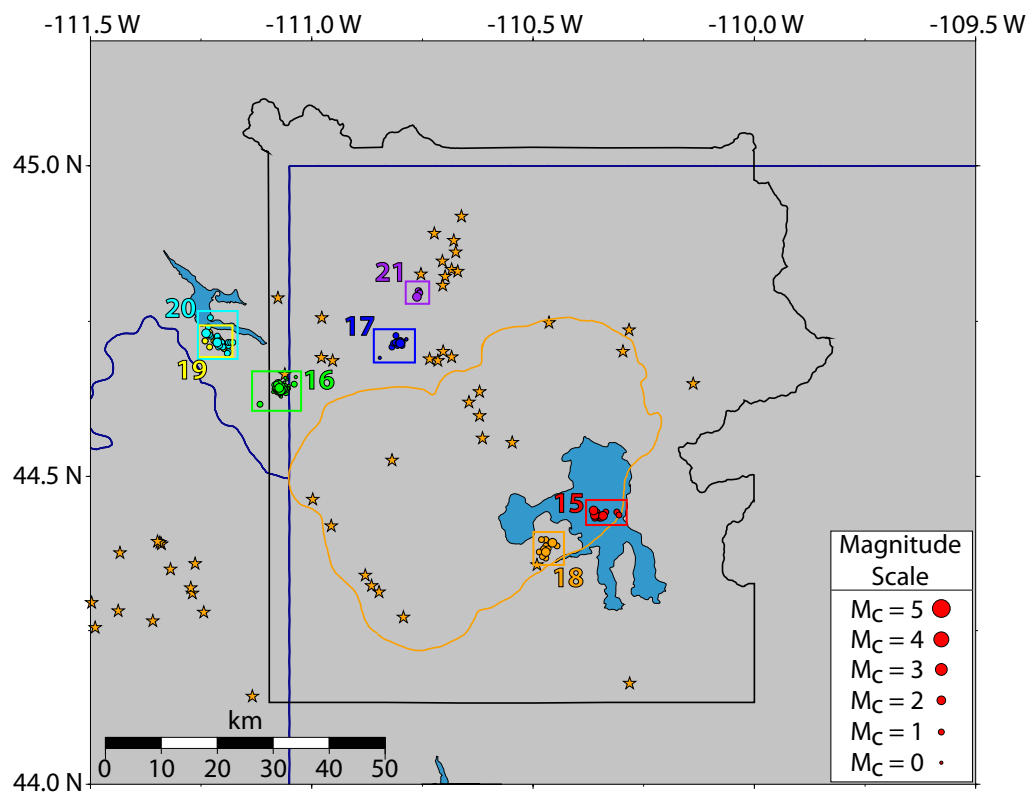


Figure C.2 - Swarm epicenter maps for swarms 15 - 28.

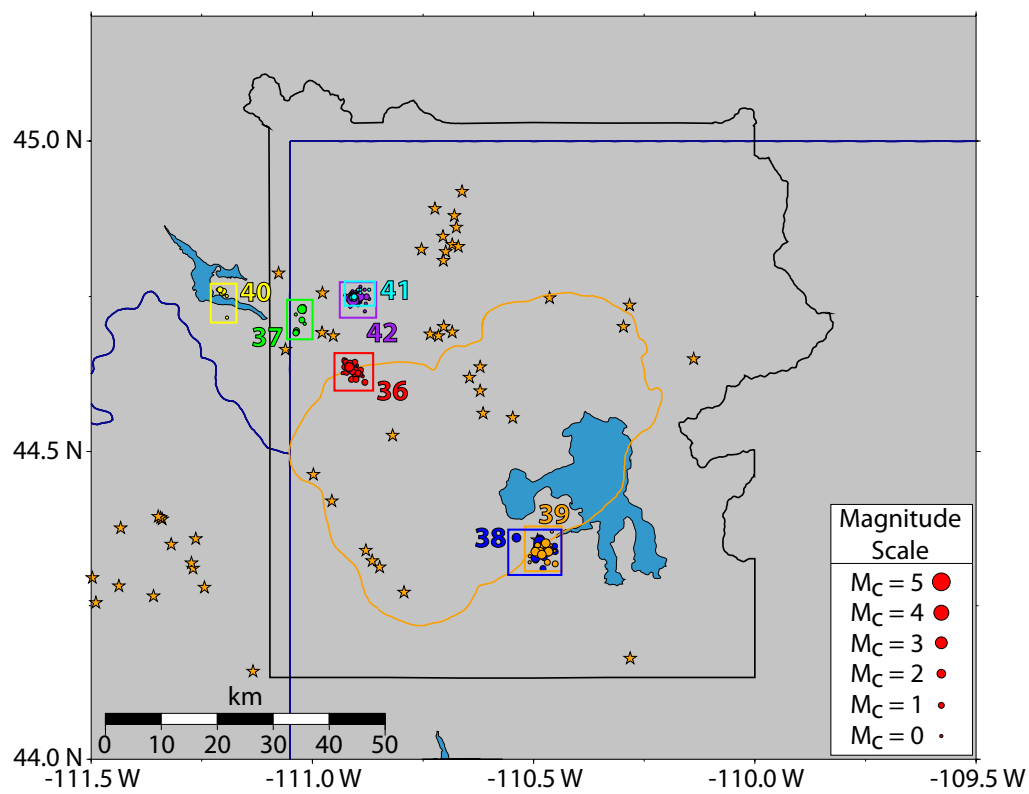
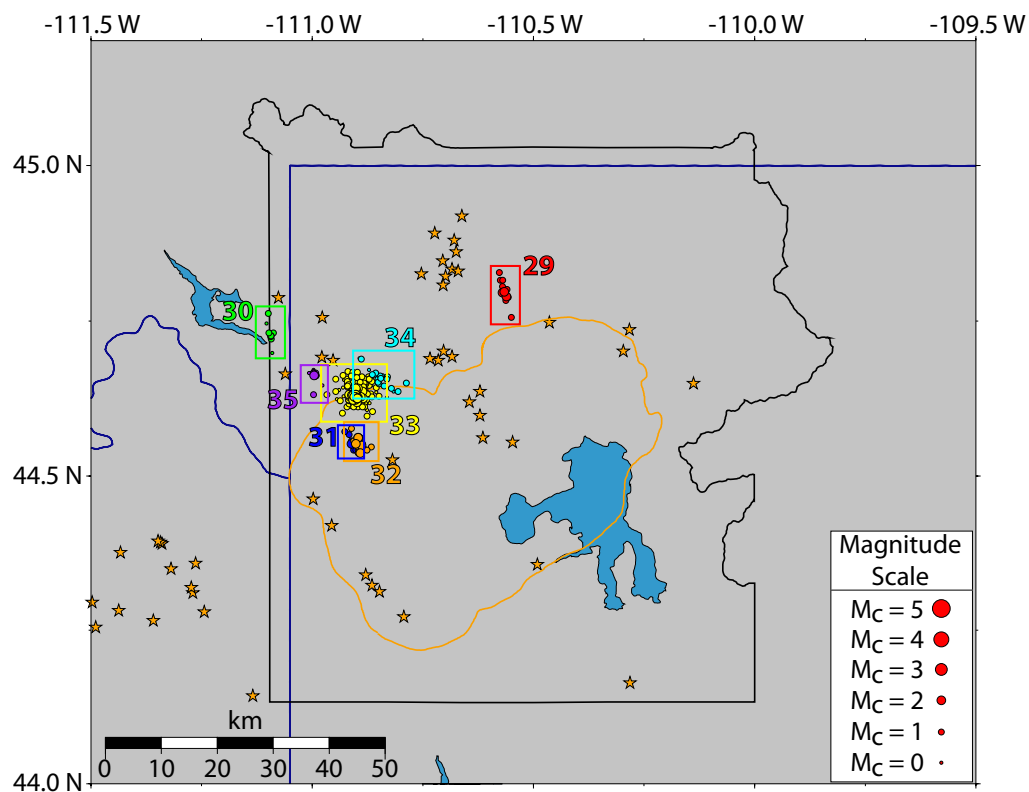


Figure C.3 - Swarm epicenter maps for swarms 29 - 42.

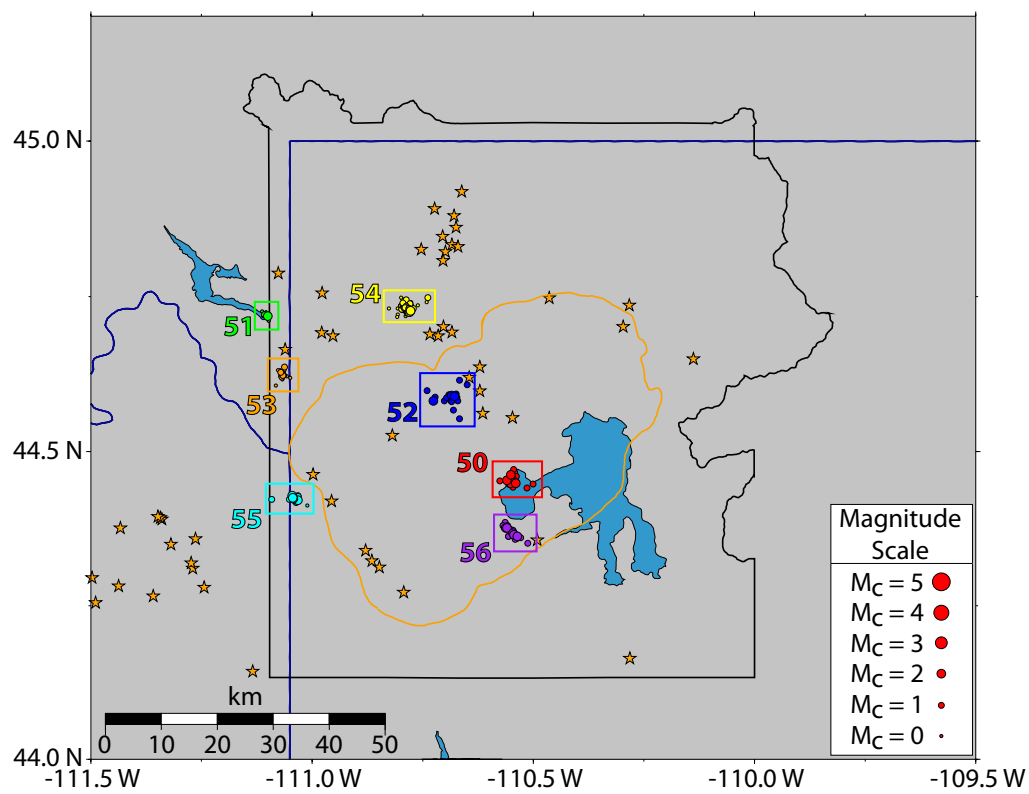
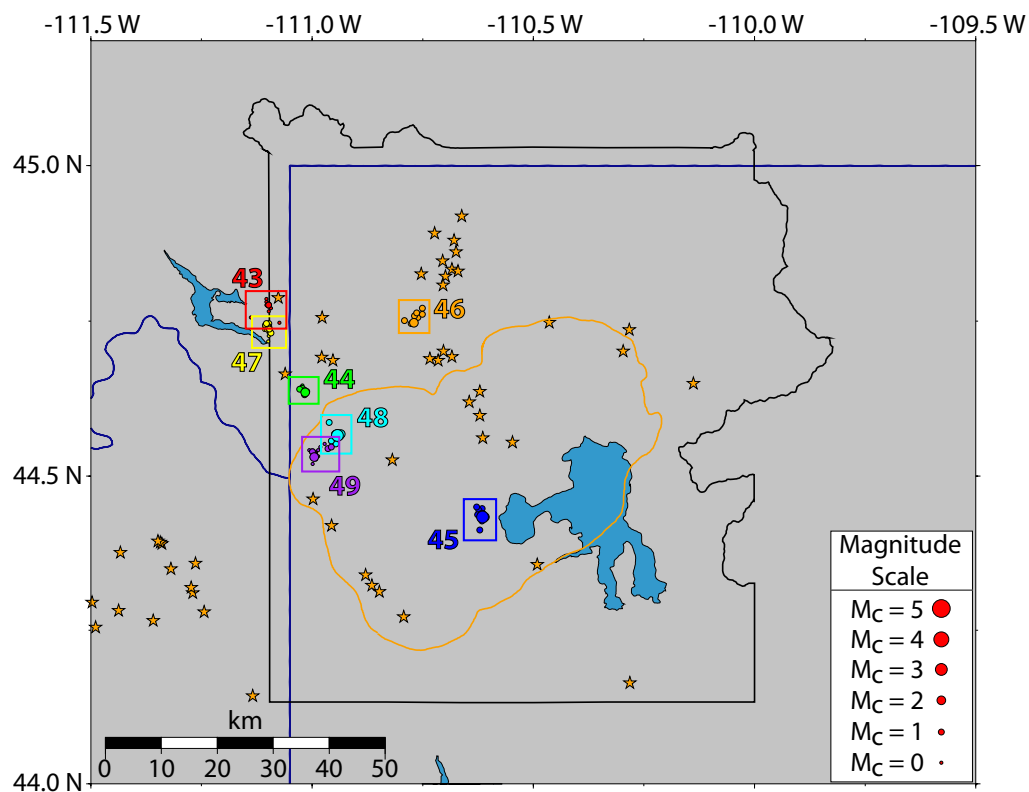


Figure C.4 - Swarm epicenter maps for swarms 43 - 56.

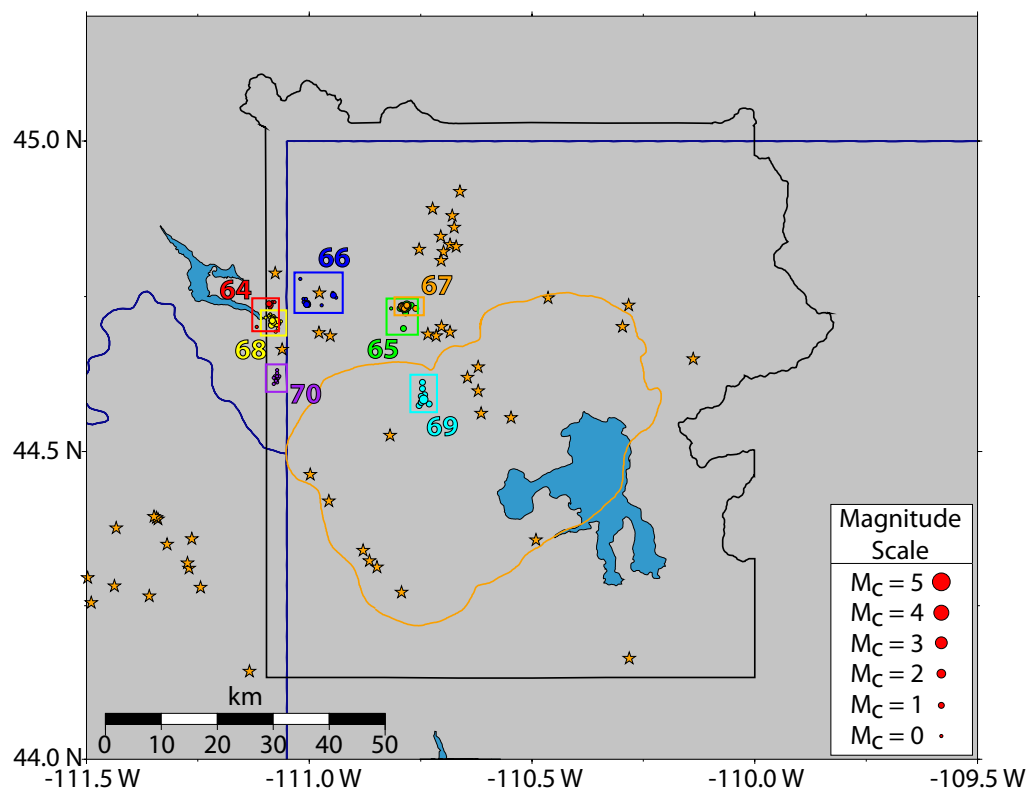
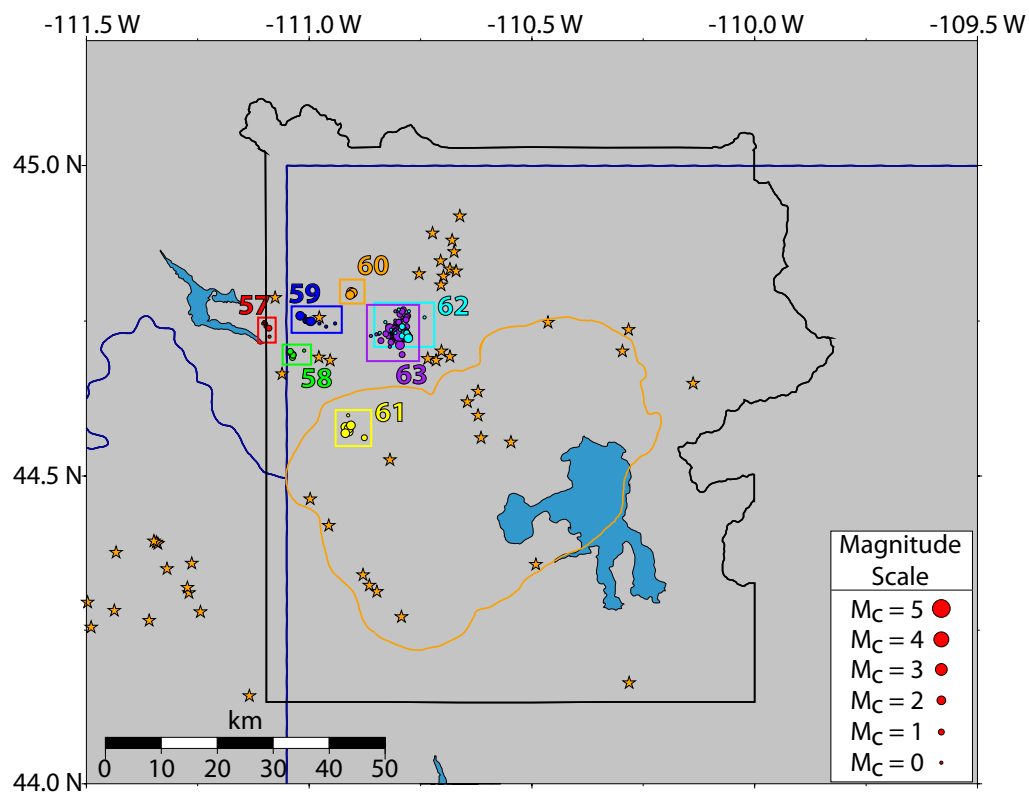


Figure C.5 - Swarm epicenter maps for swarms 57 - 70.

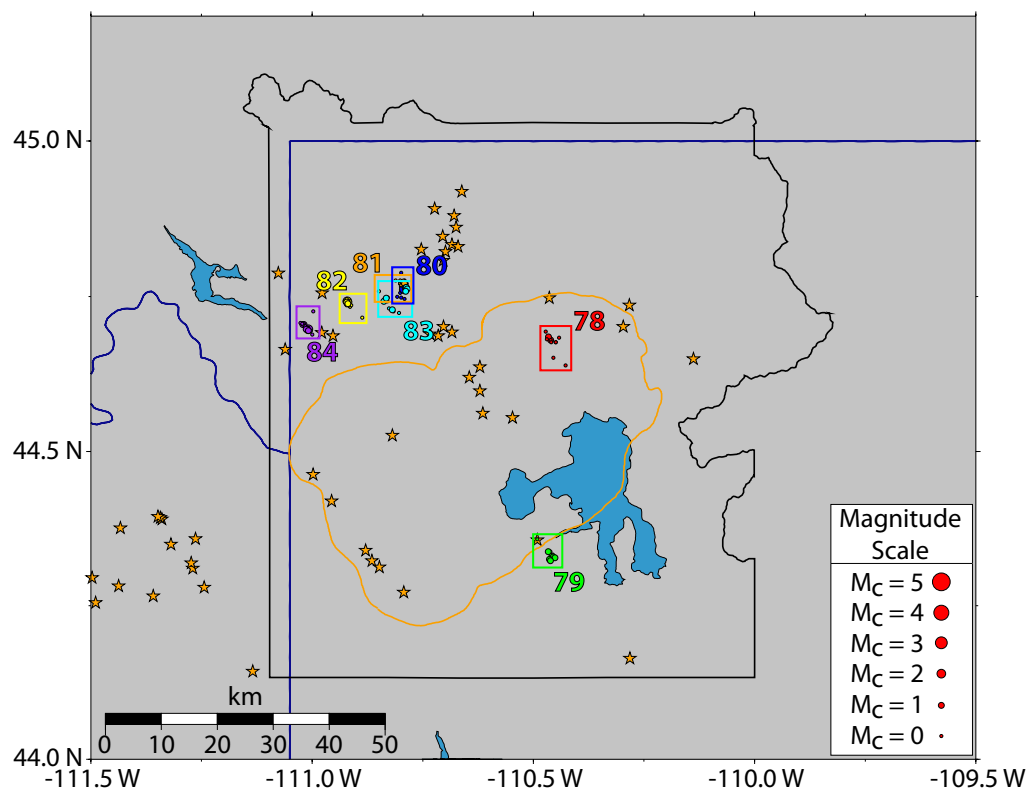
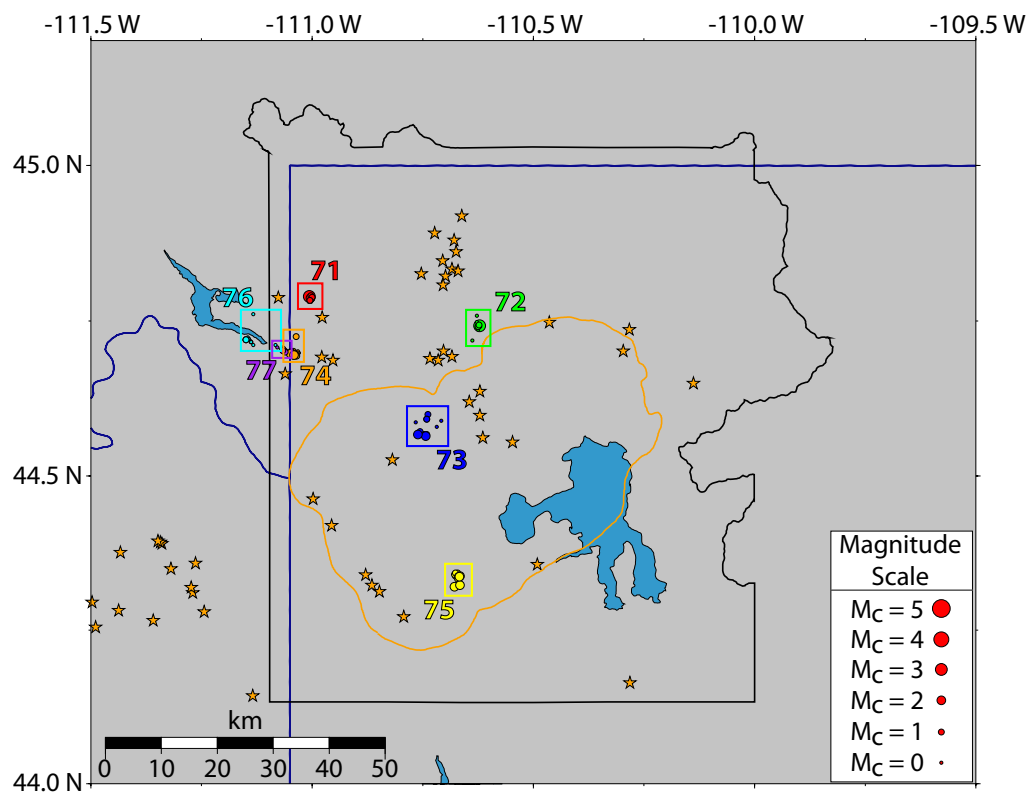


Figure C.6 - Swarm epicenter maps for swarms 71 - 84.

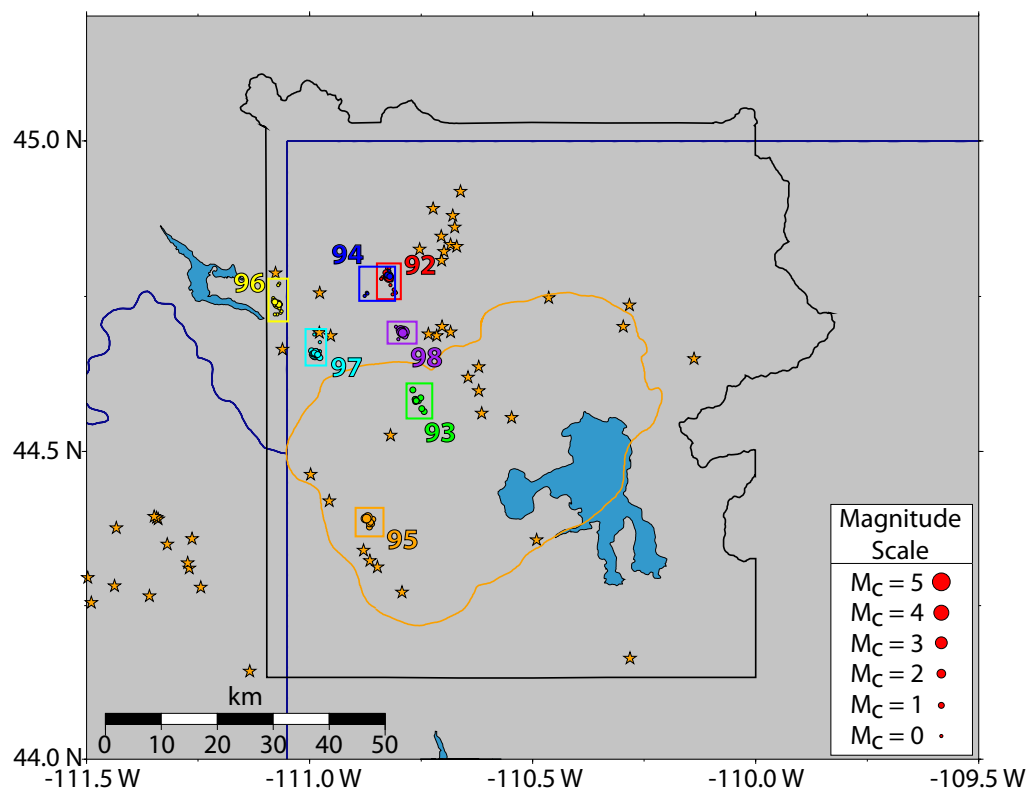
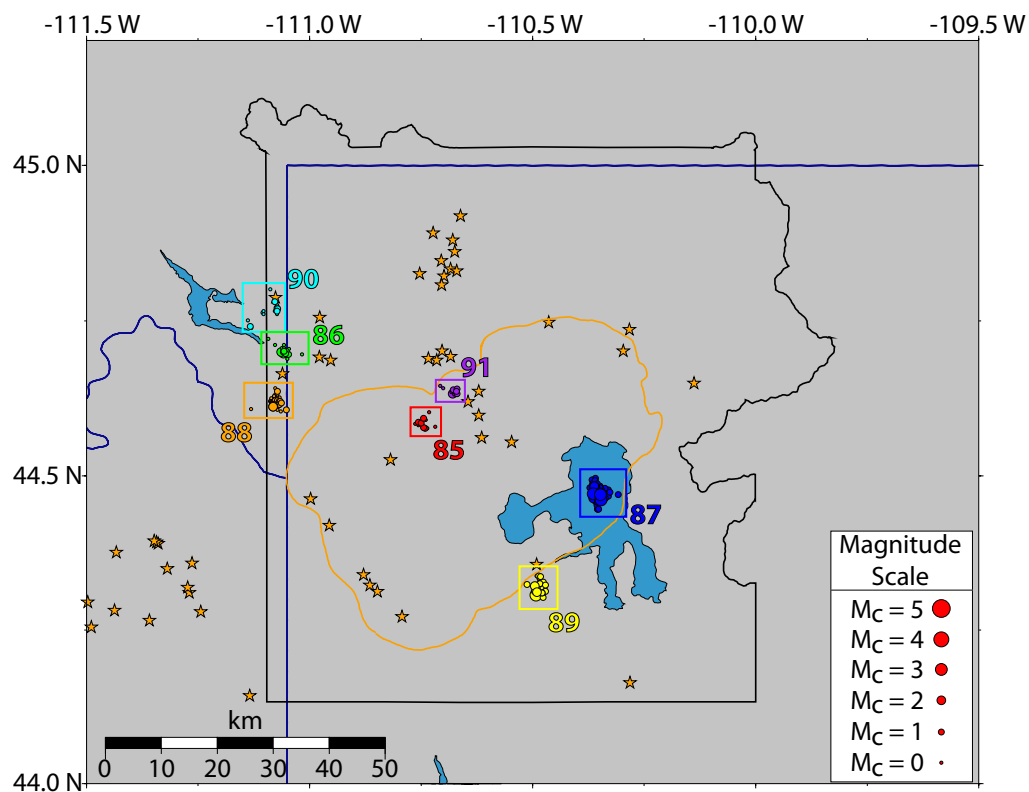


Figure C.7 - Swarm epicenter maps for swarms 85 - 98.

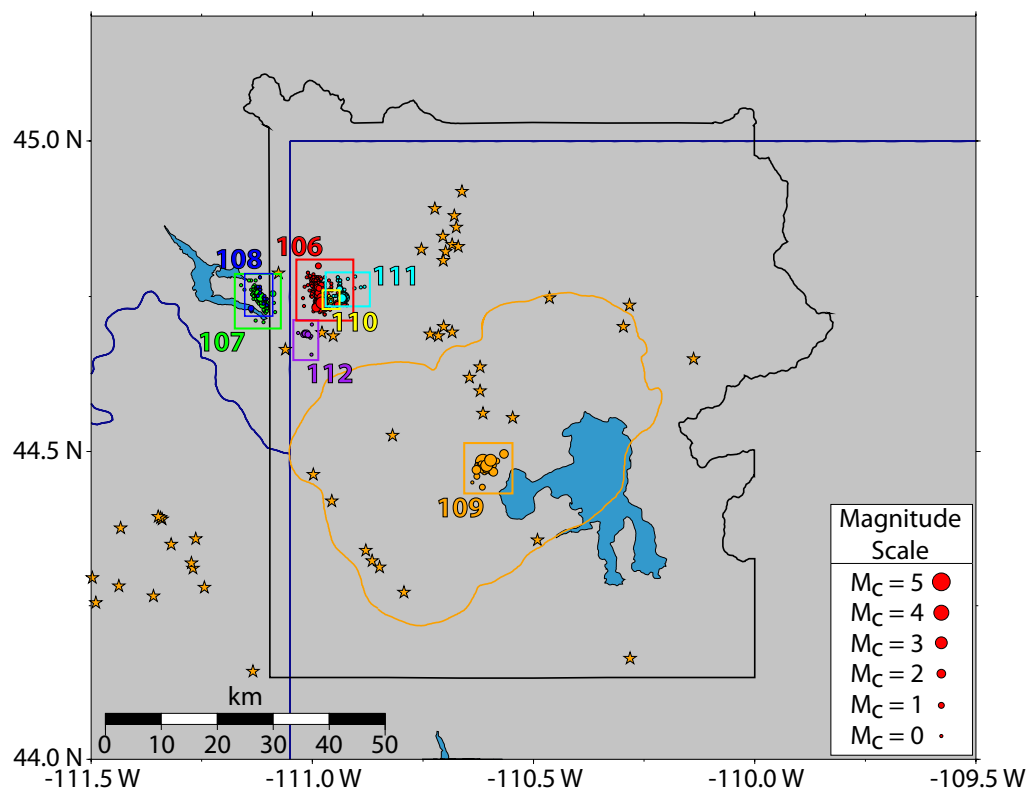
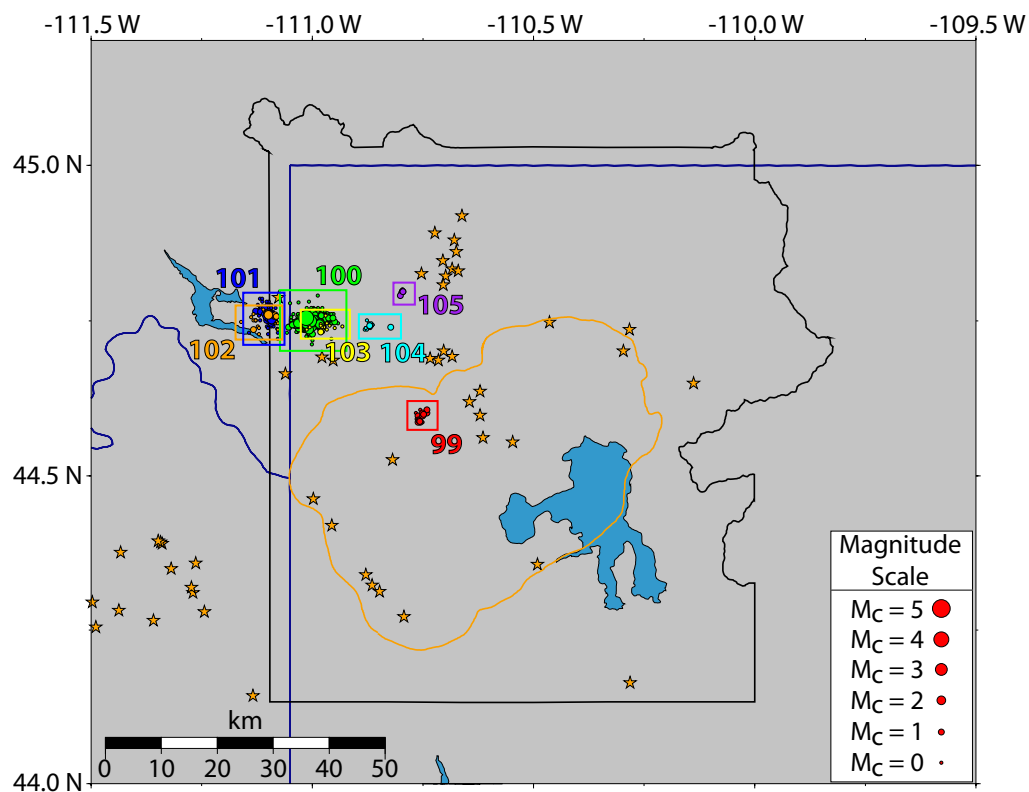


Figure C.8 - Swarm epicenter maps for swarms 99 - 112.

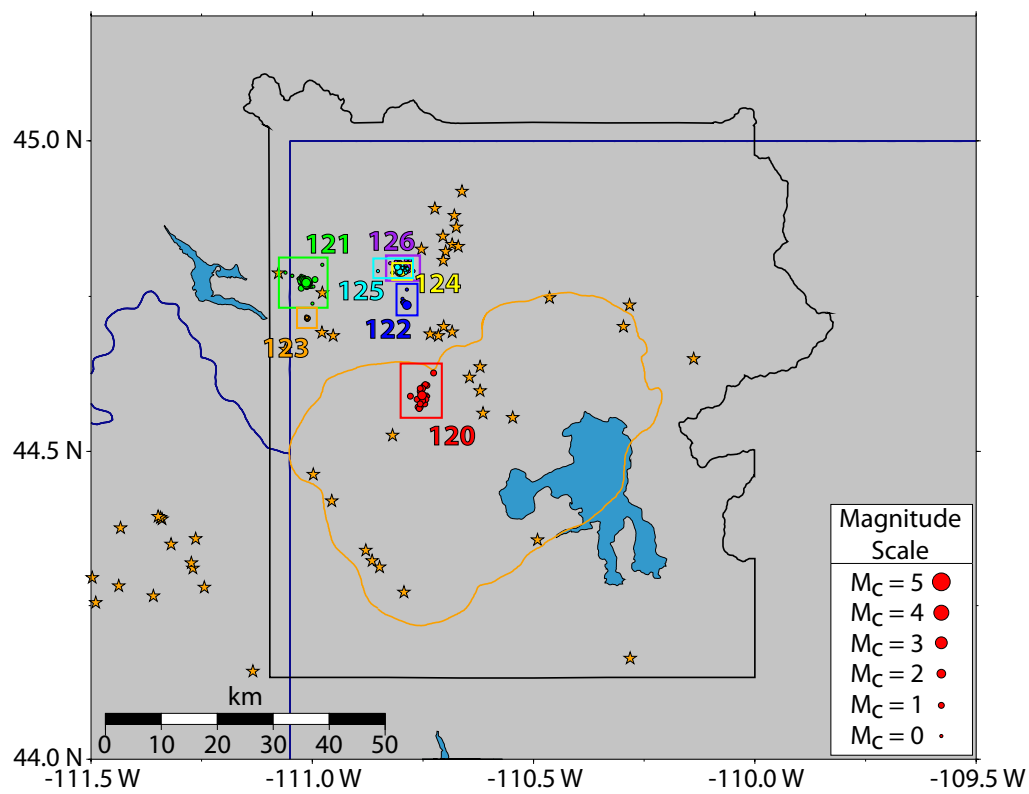
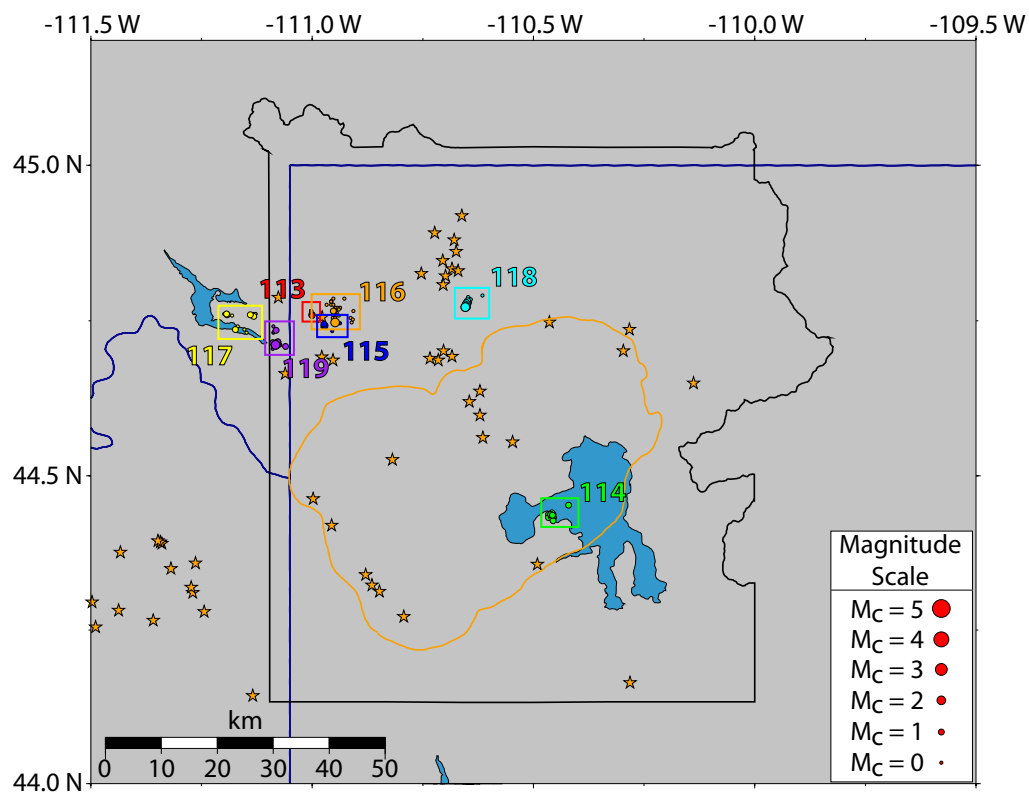


Figure C.9 - Swarm epicenter maps for swarms 113 - 126.

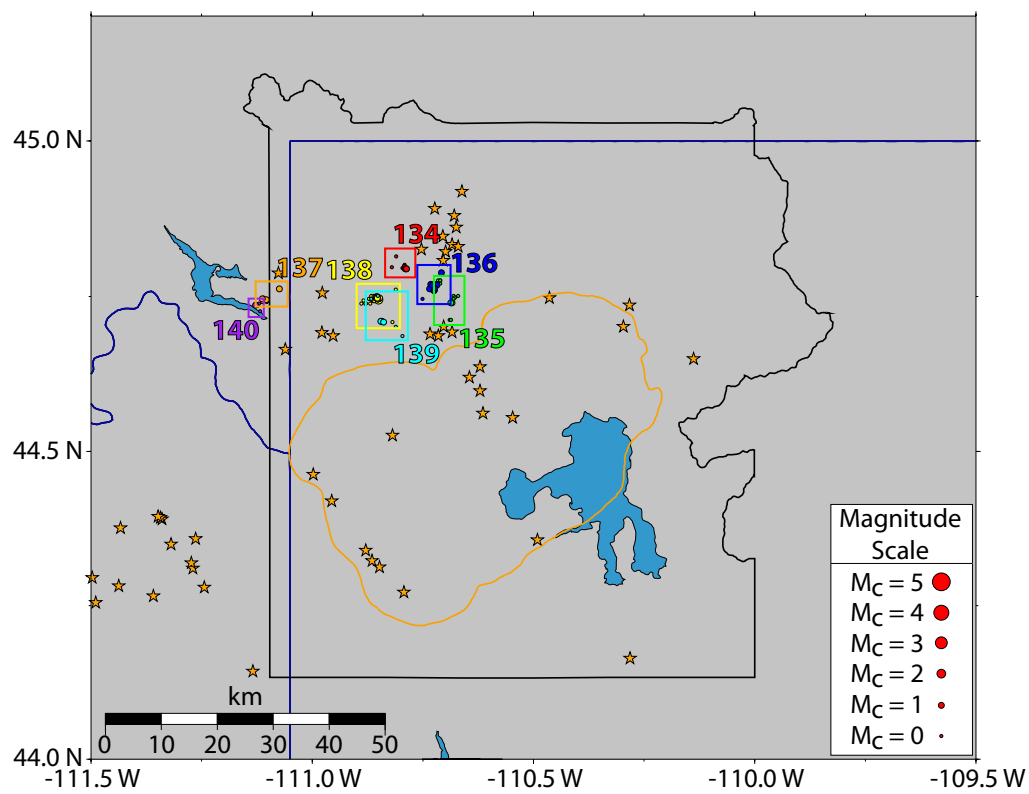
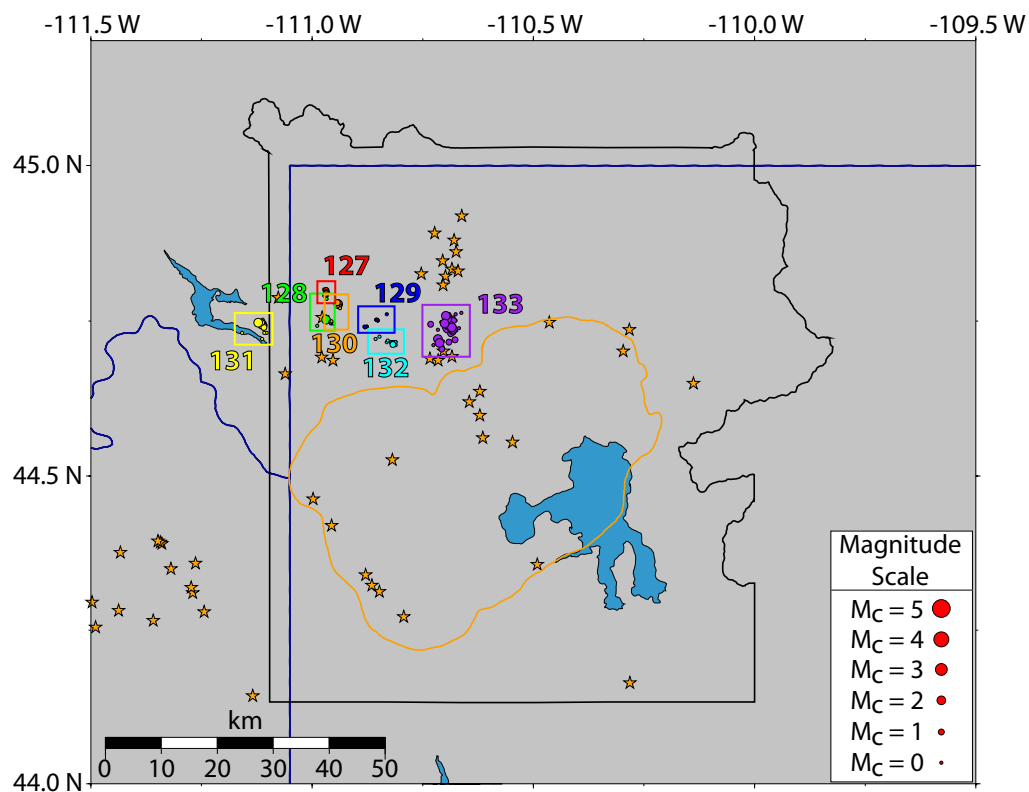


Figure C.10 - Swarm epicenter maps for swarms 127 - 140.

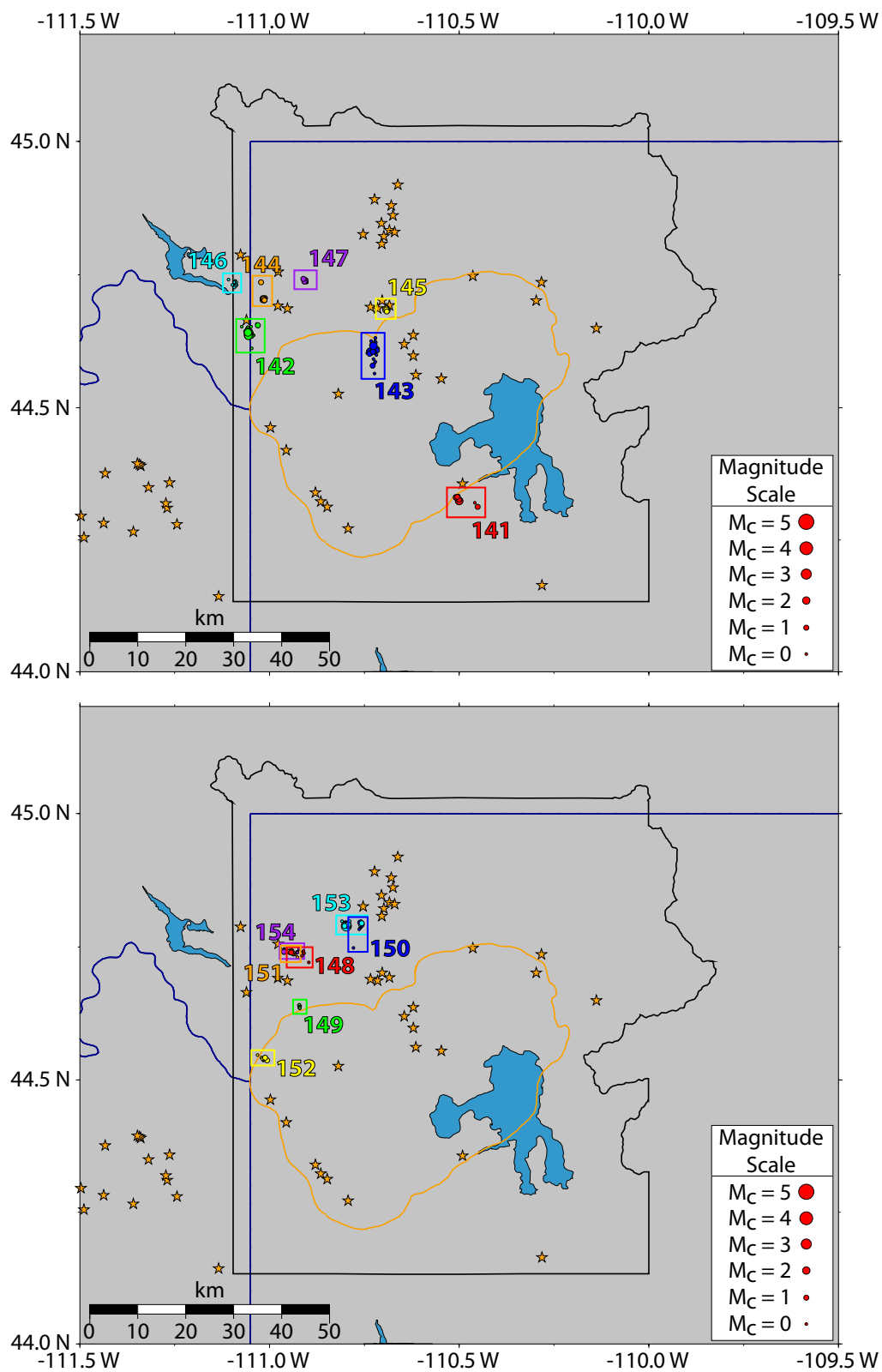


Figure C.11 - Swarm epicenter maps for swarms 141 - 154.

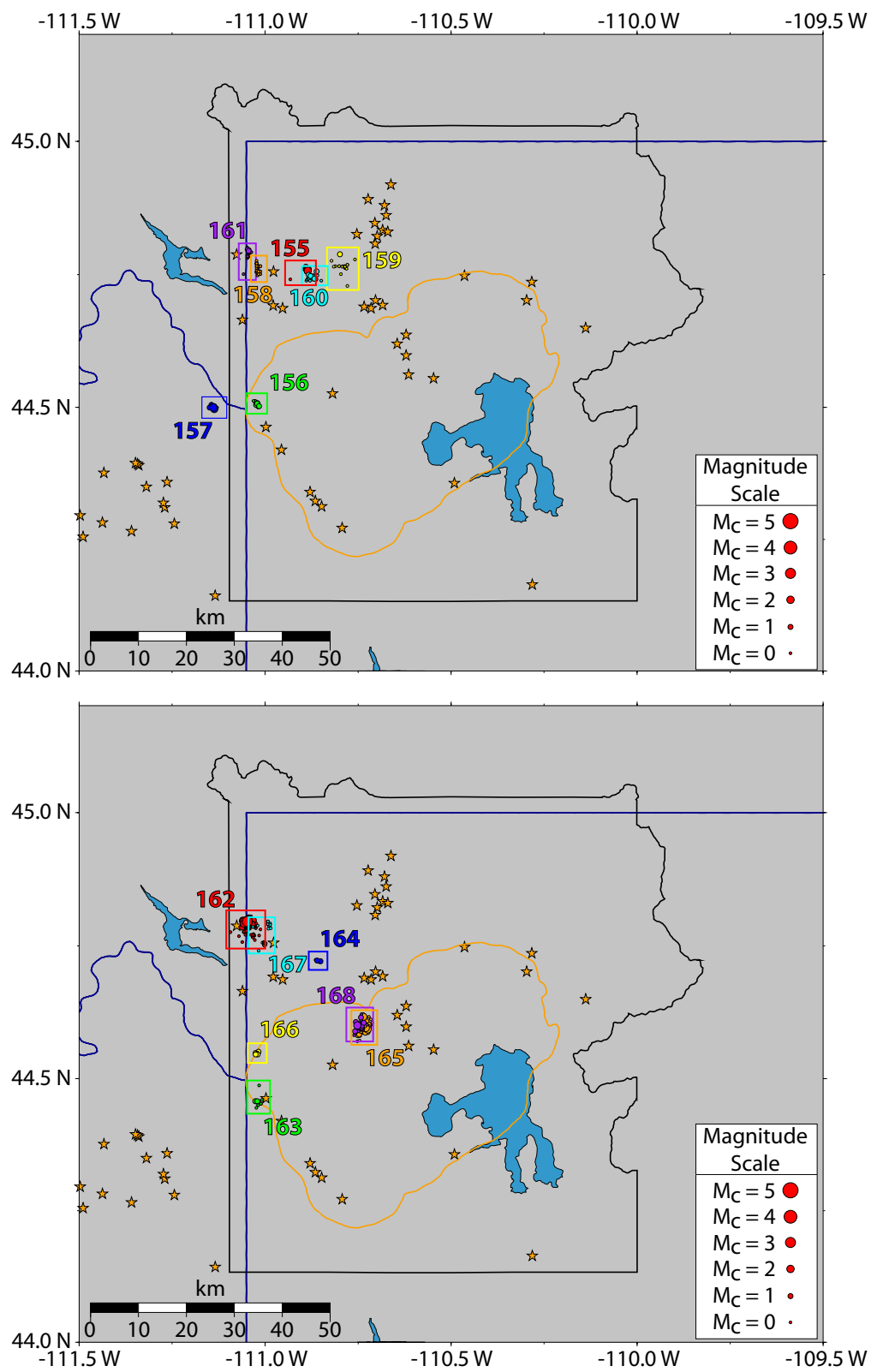


Figure C.12 - Swarm epicenter maps for swarms 155 - 168.

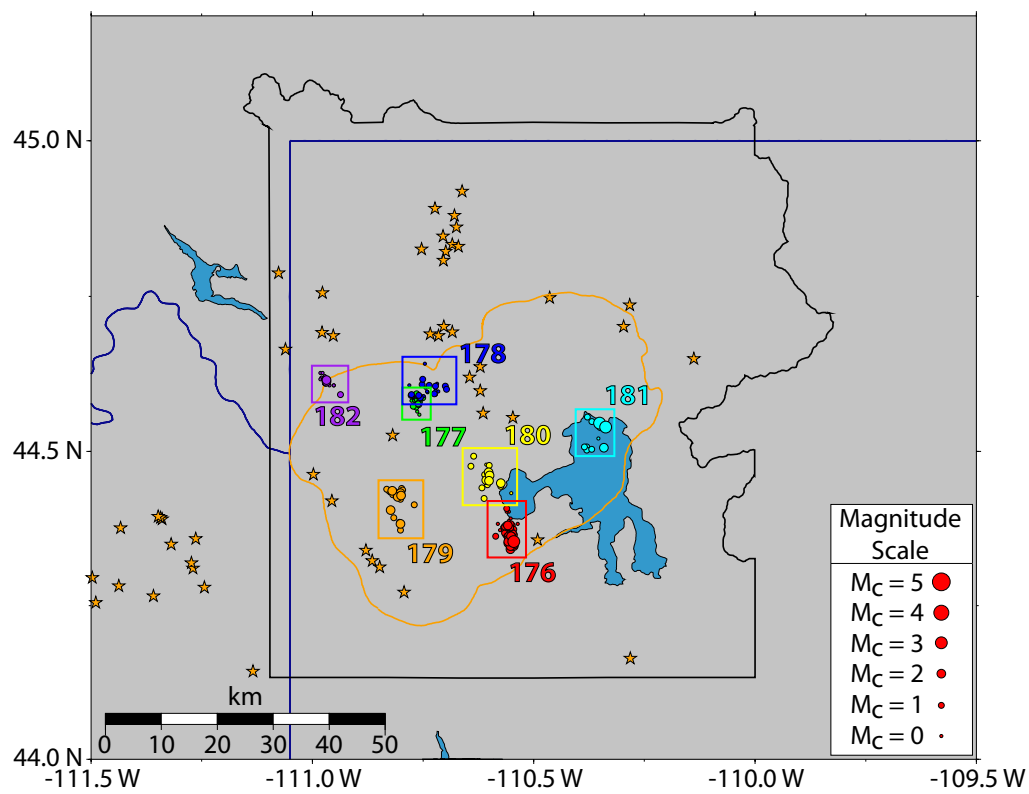
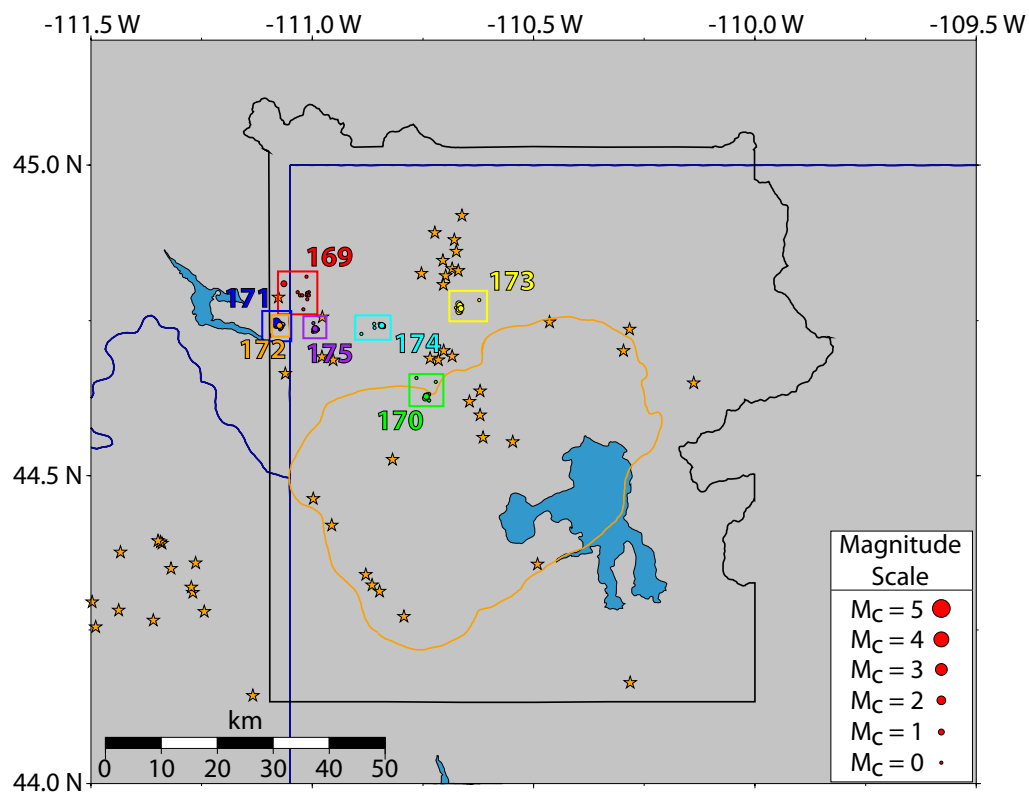


Figure C.13 - Swarm epicenter maps for swarms 169 - 182.

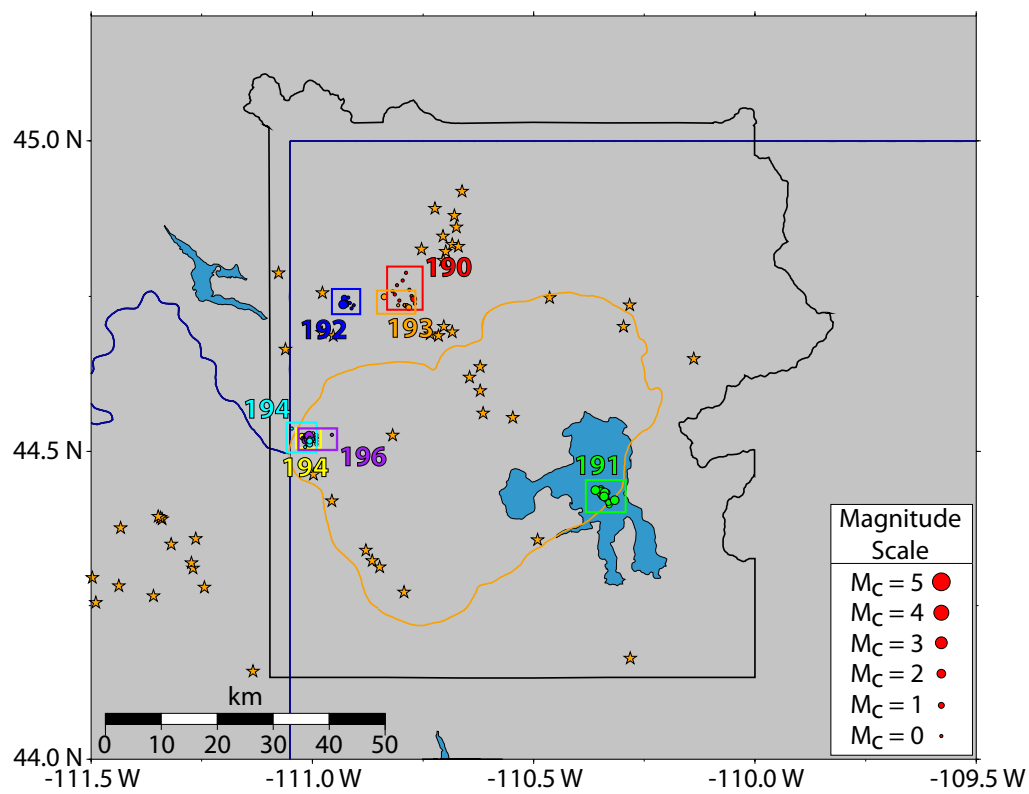
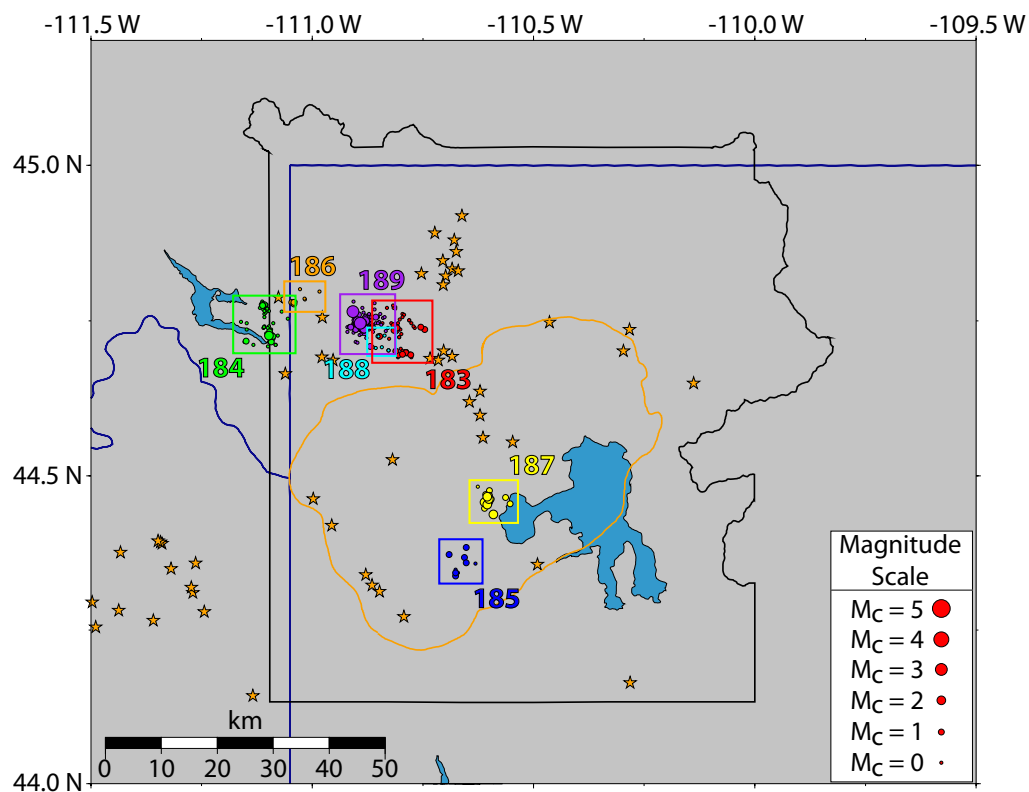


Figure C.14 - Swarm epicenter maps for swarms 183 - 196.

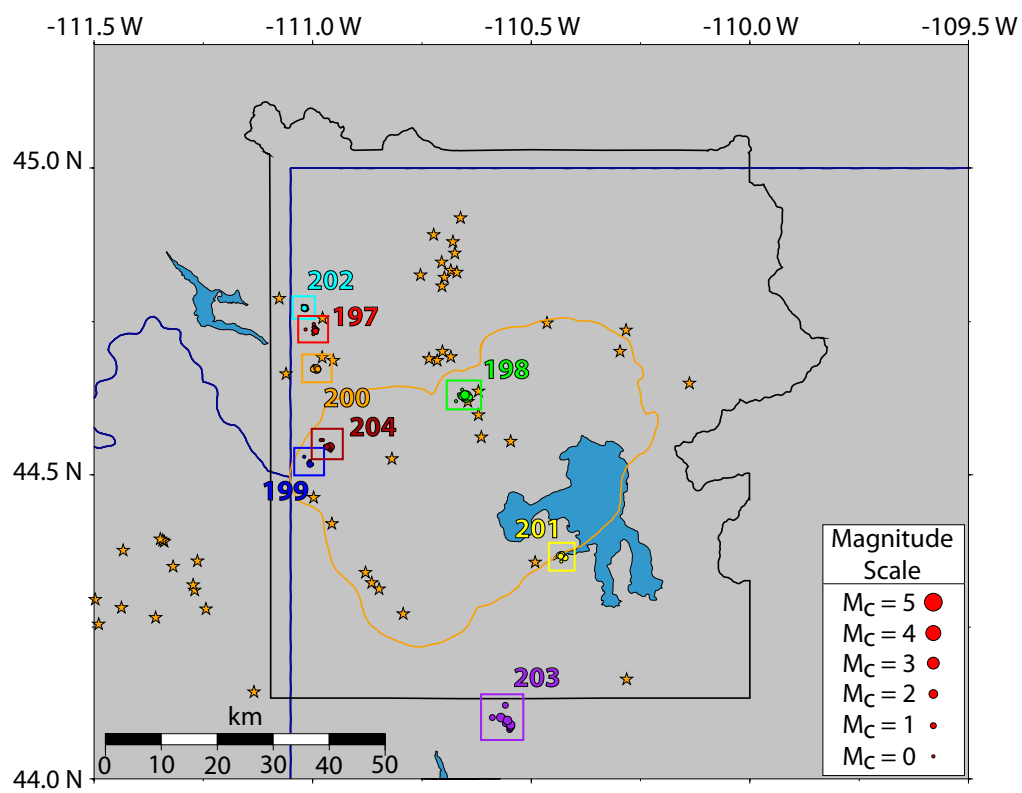


Figure C.15 - Swarm epicenter map for swarms 197 - 204.

## APPENDIX D

### LIST OF CURRENT AND PLANNED DATA IN THE YELLOWSTONE GIS DATABASE

This appendix consists of a list of data that is both currently available and planned to be included in the Yellowstone GIS Database.

Data (raw) Products to served up:

- DEMs (10 m and 30m)
- Boundaries of geographic, planimetric features (roads, towns, rivers, lakes, etc.)
- Geologic formations
- Fault digitized segments, dips, ages
- Volcano boundary data, thicknesses, ages
- Gravity data: free-air, Bouguer, terrain correction
- Magnetic data, values, flight lines and coordinates
- Geoid data
- Continuous GPS data raw in rinex format
- Campaign GPS data raw in rinex format
- GPS processed coordinates and velocities with ITR
- GPS time series
- Earthquake data, waveforms, P files, calibrations, etc.
- Earthquake locations 1D models, magnitudes, errors
- Crustal structure data: x,y,z P and S velocities, errors
- Earthquake locations 3D models, magnitudes, errors
- Focal mechanism solutions and parameters
- Stress data from focal mechanisms, faults, alignment of vents
- Moment tensors
- Receiver function data
- Surface wave data and dispersion curve
- Yellowstone Lake heat flow data
- Yellowstone Lake raw data
- Yellowstone Lake thermal water column data
- UUSS geophysical instrument locations
- Heat flow maps
- Lake bathymetry and Seismic data from Utah and USGS
- New Yellowstone 3D earthquake catalog
- Geologic data
- 3D mantle velocity models
- Vp/Vs ratios and Poisson's ratios
- Anisotropy data
- Shear wave velocities from surface wave velocities and receiver functions
- Effective elastic thickness data
- Mantle data set for western U.S.

## Derived products

Geologic Maps

Fault map

Volcanic feature map

Gravity maps

Magnetic maps

Geoid maps

GPS velocities by campaign

Earthquake maps

3D earthquake animations

Map of focal mechanisms and moment tensors

Stress field map of all parameters

3D seismic velocity models (crust and mantle)

Receiver function profiles and point velocity estimates

Anisotropy directions with errors

S wave velocities from surface waves

Vp/Vs maps in 3D

Receiver functions

Heat flow maps

Lake bathymetry and seismic data from Utah and USGS

Yellowstone thermal gradient map

Yellowstone Lake heat flow map

Depth to boiling map

New Yellowstone 3D earthquake catalog

Snake River Plain maps and data

Interpretive Products (analytic analysis data):

- Seismicity and deformation series
- GPS displacement and strain-rate maps
- Tomograms (crustal)
- Tomograms (mantle)
- Mantle anisotropy map for Yellowstone
- Mantle anisotropy map for YSRP
- Mantle anisotropy map for Basin Range
- Seismic discontinuity map
- Fault and volcano time series
- GPS velocity maps x, y and z
- Strain rate maps
- Displacement gradient maps
- Interpolated strain-rate maps
- Yellowstone deformation maps
- Lidar and InSAR images
- Earthquake time series
- Stress field maps
- Effects of large earthquakes on seismicity
- Effects of large earthquakes on hydrothermal features
- Montelli's tomography data
- Steinberger's YSRP mantle flow model 3D data

Knowledge Products (ultimate scientific interpretation):

- Yellowstone Lake depth to boiling map
- Kinematic: FE and other models of deformation
- Volcano source model of Mogi
- Integrated fault-stress, fault-caldera, fault-magmatic models
- Viscoelastic fault interaction models
- Elastic fault interaction models for Yellowstone-Teton
- Tomographic images
- YSRP mantle flow model 3D images

## REFERENCES

- Akaike, H. (1974), A new look at the statistical model identification, *IEEE Trans. Automatic Control*, *19*, 716-723.
- Anderson, J. G., J. N. Brune, J. N. Louie, Y. Zeng, M. Savage, G. Yu, Q. Chen, and D. dePolo (1994), Seismicity in the western Great Basin apparently triggered by the Landers, California, earthquake, 28 June 1992, *Bull. Seismol. Soc. Am.*, *84*, 863-891.
- Armstrong, R. L., W. P. Leeman, and H. E. Malde (1975), K-Ar dating, Quaternary and Neo-gene volcanic rocks of the Snake River Plain, Idaho, *Am. J. Sci.*, *275*, 225-251.
- Blackwell, D. D. (1969), Heat-flow determinations in the northwestern United States, *J. Geophys. Res.*, *74*, 992-1007.
- Bender, B. (1983), Maximum likelihood estimation of  $b$  values for magnitude grouped data, *Bull. Seismol. Soc. Am.*, *73*, 831-851.
- Benz, H. M., and R. B. Smith (1984), Simultaneous inversion for lateral velocity variations and hypocenters in the Yellowstone region using earthquake and refraction data, *J. Geophys. Res.*, *89*, 1208-1220.
- Byrd, J. O. D. (1991), Paleoseismicity of the southern section of the Teton fault, Wyoming, *Geol. Soc. Amer. Abstr. Programs*, *23*, A481.
- Byrd, J. O. D., R. B. Smith, and J. W. Geissman (1994), The Teton fault, Wyoming: Topographic signature, neotectonics, and mechanisms of deformation, *J. Geophys. Res.*, *99*, 20,095-20,122.
- Byrd, J. O. D. (1995), Neotectonics of the Teton fault, Wyoming: Ph.D. Thesis, University of Utah, Salt Lake City, Utah.
- Chang, W.-L., and R. B. Smith (2002), Integrated seismic-hazard analysis of the Wasatch Front, Utah, *Bull. Seismol. Soc. Am.*, *92*, 1904-1922.
- Christiansen, R. L., and H. R. Blank, Jr. (1972), Volcanic stratigraphy of the Quaternary rhyolite plateau in Yellowstone National Park, *U.S. Geol. Surv. Profess. Pap.* *516-E*, 6.

- Christiansen, R. L. (1984), Yellowstone magmatic evolution: its bearing on understanding large-volume explosive volcanism, in *Explosive Volcanism: Inception, Evolution and Hazards*, pp. 84-95, National Academy Press, Washington D.C.
- Christiansen, R. L. (2001), The Quaternary and Pliocene Yellowstone plateau volcanic field of Wyoming, Idaho, and Montana, *U.S. Geol. Surv. Profess. Pap.* 729-G, 145.
- Dickinson, W. R. (2006), Geotectonic evolution of the Great Basin, *Geosphere*, 2(7), 353-368.
- Doser, D. I. (1985), Source parameters and faulting processes of the 1959 Hebgen Lake, Montana, earthquake sequence, *J. Geophys. Res.*, 90, 4537-4555.
- Fournier, R. O. (1989), Geochemistry and dynamics of the Yellowstone National Park hydro-thermal system, *Ann. Rev. Earth Planet. Sci.*, 17, 13-53.
- Fournier, R. O. (1999), Hydrothermal processes related to movement of fluid from plastic into brittle rock in the magmatic-epithermal environment, *Economic Geology*, 94, no. 8, 1193-1212.
- Frolich, C., and S. Davis (1993), Teleseismic  $b$ -values: or much ado about 1.0, *J. Geophys. Res.*, 98, 631-644.
- Gilbert, J. D., D. Ostenaar, and C. Wood (1983), Seismotectonic study of Jackson Lake Dam and Reservoir, Minidoka Project, Idaho-Wyoming: Bureau of Reclamation Seismotectonic Report, 83-8, 123.
- Gomberg, J., and P. Bodin (1994), Triggering of the  $M_s = 5.4$  Little Skull Mountain, Nevada, earthquake with dynamic strains, *Bull. Seismol. Soc. Am.*, 84, 844-853.
- Wall, B.R. (2005), Surface and subsurface hydrothermal flow pathways at Norris Geyser Basin, Yellowstone National Park, *Eos Trans. AGU*, 86(52), Fall Meet. Suppl., Abstract T23B-0544.
- Guo, Z., and Y. Ogata (1997), Statistical relations between the parameters of aftershocks in time, space, and magnitude, *J. Geophys. Res.*, 102, 2857-2873.
- Gutenberg, B., and C. F. Richter (1944), Frequency of earthquakes in California, *Bull. Seismol. Soc. Am.*, 34, 185-188.
- Hill, D. P. (1977), A model for earthquake swarms, *J. Geophys. Res.*, 82, 1347-1352.
- Hill, D. P. (1992), Temperatures at the base of the seismogenic crust beneath Long Valley Caldera, California, and the Phlegrean Fields Caldera, Italy. In: Gasparini, P.; Scarpa, R.; Aki, K. ed. *Volcanic Seismology*. Berlin, Springer-Verlag. Pp. 432-461.

- Hill, D. P., P. A., Reasenber, A. Michael, W. J. Arabasz, G. Beroza, D. Brumbaugh, J. N. Brune, R. Castro, S. Davis, D. dePolo, W. L. Ellsworth, J. Gomberg, S. Harmsen, L. House, S. M. Jackson, M. J. S. Johnston, L. Jones, R. Keller, S. Malone, L. Munguia, S. Nava, J. C. Pechmann, A. Sanford, R. W. Simpson, R. B. Smith, M. Stark, M. Stickney, A. Vidal, S. walter, V. Wong, And J. Zollweg (1993), Seismicity remotely triggered by the magnitude 7.3 Landers, California, earthquake, *Science*, 260, 1617-1623.
- Hill, D. P., F. Pollitz, and C. Newhall (2002), Earthquake-volcano interactions, *Phys. Today*, 55, 41-47.
- Husen, S., and R. B. Smith (2004), Probabilistic earthquake relocation in three-dimensional velocity models for the Yellowstone National Park region, Wyoming, *Bull. Seismol. Soc. Am.*, 94, 880-896.
- Husen, S., R. B. Smith, and G. P. Waite (2004a), Evidence for gas and magmatic sources beneath the Yellowstone volcanic field from seismic tomographic imaging, *J. Volcanol. Geotherm. Res.*, 131, 397-410.
- Husen, S., S. Wiemer, and R. B. Smith (2004b), Remotely Triggered Seismicity in the Yellowstone National Park region by the 2002  $M_w$  7.9 Denali fault earthquake, Alaska, *Bull. Seismol. Soc. Am.*, 94, no. 6B, S317-S331.
- Husen, S. R. Taylor, R. B. Smith, and H. Heasler (2004c), Changes in geyser eruption behavior and remotely triggered seismicity in Yellowstone National Park produced by the 2002 M 7.9 Denali fault earthquake, Alaska, *Geology*, 32, 537-540.
- Ishimoto, M., and K. Iida (1939), Observations of earthquakes registered with the microseismograph constructed recently, *Bull. Earthquake Res. Inst. Tokyo Univ.*, 17, 443-478.
- Jolly, A. D., and S. R. McNutt (1999), Relationship between  $b$ -values and maximum depths of seismicity at Martin and Mageik volcanoes, Katmai National Park, Alaska; July 1995-December 1997, *J. Volcanol. Geotherm. Res.*, 93, 173-190.
- Jordan, M., R. B. Smith, C. M. Puskas, J. Farrell, and G. P. Waite (2005), The Yellowstone hot spot and related plume: volcano-tectonics, tomography, kinematics, dynamics and mantle flow, *Eos Trans. AGU*, 86(52), Fall Meet. Suppl., Abstract T51D-1388.
- Kanamori, H., and D. L. Anderson (1975), Theoretical basis of some empirical relations in seismology, *Bull. Seism. Soc. Am.*, 65, 1073-1095.

- King, G. C. P., R. S. Stein, and J. Lin (1994), Static stress changes and the triggering of earthquakes, *Bull. Seismol. Soc. Am.*, *84*, no. 3, 935-953.
- Krukoski, J. C. (2002), A geologic database (GEOGIS) and three-dimensional inversion for the density structure of the Yellowstone volcanic system: M. S. thesis, University of Utah, Salt Lake City.
- Lehman, J. A., R. B. Smith, M. M. Schilly, and L. W. Braile (1982), Upper crustal structure of the Yellowstone caldera from delay time analyses and gravity correlations, *J. Geo-phys. Res.*, *87*, 2713-2730.
- Lynch, D. P. (1999), Three-dimensional finite difference tomography of the Basin and Range-Colorado Plateau-Rocky Mountain transition using earthquake and controlled source data: M.S. thesis, University of Utah, Salt Lake City.
- McNutt, S. R. (2005), Volcanic seismology, *Annu. Rev. Earth. Planet. Sci.*, *33*, 461-491.
- Miller, D. S., and R. B. Smith (1999), *P* and *S* velocity structure of the Yellowstone volcanic field from local earthquake and controlled source tomography, *J. Geophys. Res.*, *104*, 15105-15121.
- Mogi, K. (1962), Magnitude-frequency relation for elastic shocks accompanying fractures of various materials and some related problems in earthquakes, *Bull. Earthquake Res. Inst. Univ. Tokyo*, *40*, 831-853.
- Mogi, K. (1963), Some discussions on aftershocks, foreshocks and earthquake swarms – The fracture of a semi-infinite body caused by an inner stress origin and its relation to the earthquake phenomena, *3, Bull. Earthquake Res. Inst. Tokyo Univ.*, *41*, 615-658.
- Murru, M., C. Montuori, M. Wyss, and E. Privitera (1999), The locations of magma chambers at Mt. Etna, Italy, mapped by *b*-values, *Geophys. Res. Lett.*, *26*, 2553-2556.
- Pechmann, J. C., J. C. Bernier, S. J. Nava, F. M. Terra, and W. J. Arabasz (2001), Correction of systematic time-dependent coda magnitude errors in the Utah and Yellowstone National Park region earthquake catalogs, 1981-2001, *EOS Trans. AGU* *82*(47), Fall Meet. Suppl., Abstract S11B-0572.
- Perkins, M. E., and B. P. Nash (2002), Explosive silicic volcanism of the Yellowstone hotspot: The ashfall tuff record, *Geol. Soc. Am. Bull.*, *114*, 367-381.
- Pierce, K. L., and L. A. Morgan (1992), The track of the Yellowstone hot spot: volcanism, faulting, and uplift., in *Regional Geology of Eastern Idaho and Western Wyoming*, edited by P. K. Link, M. A. Kuntz, and L. B. Platt, pp. 1-53, Geological Society of America, Boulder, Colorado.

- Pitt, A. M., C. S. Weaver, and W. Spence (1979), The Yellowstone Park earthquake of June 30, 1975, *Bull. Seismol. Soc. Am.*, *69*, 187-205.
- Power, J. A., M. Wyss, and J. L. Latchman (1998), Spatial variations in the frequency-magnitude distribution of earthquakes at Soufriere Hills volcano, Montserrat, West Indies, *Geophys. Res. Lett.*, *25*, 3653-3656.
- Puskas, C. M., R. B. Smith, C. M. Meertens, and W. L. Chang (2007), Crustal deformation of the Yellowstone-Snake River Plain volcanic system: campaign and continuous GPS observations, 1987-2004, *J. Geophys. Res.*, *112*, B03401, doi:10.1029/2006JB004325.
- Reasenber, P. (1985), Second-order moment of central California seismicity, 1969-1982, *J. Geophys. Res.*, *90*, 5479-5495.
- Sanchez, J. J., S. R. McNutt, J. A. Power, and M. Wyss (2004), Spatial variations in the frequency-magnitude distribution of earthquakes at Mount Pinatubo volcano, *Bull. Seismol. Soc. Am.*, *94*, 430-438.
- Scholz, C. H. (1968), The frequency-magnitude relation of microfracturing in rock and its relation to earthquakes, *Bull. Seismol. Soc. Am.*, *58*, 399-415.
- Schorlemmer, D. and S. Wiemer (2004), Earthquake statistics at Parkfield: 1. stationarity of b values, *J. Geophys. Res.*, *109*, B12307, doi:10.1029/2004JB003234.
- Schorlemmer, D., S. Wiemer, and M. Wyss (2005), Variations in earthquake-size distribution across different stress regimes, *Nature*, *437*, 539-542.
- Schorlemmer, D., and S. Wiemer (2005), Microseismicity data forecast rupture area, *Nature*, *434*, 1086.
- Shi, Y., and B. A. Bolt (1982), The standard error of the magnitude-frequency *b*-value, *Bull. Seismol. Soc. Am.*, *72*, 1677-1687.
- Sibson, R. H. (1982), Fault zone models, heat flow, and the depth distribution of earthquakes in the continental crust of the United States, *Bull. Seismol. Soc. Am.*, *72*, no. 1, 151-163.
- Smith, R. B., and R. L. Bruhn (1984), Intraplate extensional tectonics of the eastern basin-range: Inferences on structural style from seismic reflection data, regional tectonics, and thermal-mechanical models of brittle-ductile deformation, *J. Geophys. Res.*, *89*, 5733-5762.

- Smith, R. B., W. C. Nagy, K. A. Julander, J. Viveiros, C. A. Barker, and D. G. Gants (1989a), Geophysical and tectonic framework of the eastern Basin and Range-Colorado Plateau-Rocky Mountain transition, in *Geophysical Framework of the Continental United States*, L. C. Pakiser and W. D. Mooney (Editors), *Mem. Geol. Soc. Am.* 172, 205-233.
- Smith, R. B., R. E. Reilinger, C. M. Meertens, J. R. Hollis, S. R. Holdahl, D. Dzurisin, W. K. Gross, and E. E. Klingele (1989b), What's moving at Yellowstone! The 1987 crustal deformation survey from GPS, leveling, precision gravity and trilateration, *Eos, Amer. Geophys. Union*, 70, 113-125.
- Smith, R. B., and W. J. Arabasz (1991), Seismicity of the Intermountain Seismic Belt, in *Neo-tectonics of North America*, edited by D. B. Slemmons, E. R. Engdahl, M. D. Zoback, and D. D. Blackwell, Geological Society of America, Boulder, Colorado.
- Smith, R. B., K. L. Pierce, and R. J. Wold (1993), Quaternary history and structure of Jackson Lake, Wyoming, from seismic reflection surveys, in A. W. Snoke, J. Steidtmann, and S. M. Roberts, editors "Geology of Wyoming", *Geological Survey of Wyoming Memoir No. 5*, 668-693.
- Smith, R. B., and L. W. Braile (1994), The Yellowstone Hotspot, *J. Volcanol. Geotherm. Res.*, 61, 121-187.
- Smith, R. B., and L. Siegel (2000), *Windows into the Earth: The Geology of Yellowstone and Grand Teton Parks*, Oxford University Press, London, 247.
- Susong, D. D., R. B. Smith, and R. L. Bruhn (1987), Quaternary faulting and segmentation of the Teton fault zone, Grand Teton National Park, Wyoming, *Eos Transactions, Amer. Geophys. Union*, 68, 1452.
- Sykes, L. R. (1970), Earthquake swarms and sea-floor spreading, *J. Geophys. Res.*, 75, 6598-6611.
- Urbancic, T. I., C. I. Trifu, J. M. Long, and R. P. Tong (1992), Space-time correlations of  $b$  values with stress release, *Pure Appl. Geophys.*, 139, 449-462.
- Utsu, T. (1965), A method for determining the value of  $b$  in a formula  $\log N = a - bM$  showing the magnitude frequency for earthquakes, *Geophys. Bull. Hokkaido Univ.*, 13, 99-103.
- Utsu, T. (1992), On seismicity, in *Report of the Joint Research Institute for Statistical Mathematics*, vol. 34, 139-157, Inst. For Stat. Math., Tokyo.
- Utsu, T. (1999), Representation and analysis of the earthquake size distribution: A historical review and some approaches, *Pure Appl. Geophys.*, 155, 509-535.

- Velasco, A., C. Ammon, J. Farrell, and K. L. Pankow (2004), Rupture directivity of the 3 November 2002 Denali fault earthquake determined from surface waves, *Bull. Seism. Soc. Am.*, *94*, no. 6B, S293-S299.
- Vidale, J. E., K. L. Boyle, and P. M. Shearer (2006), Crustal earthquake bursts in California and Japan: Their patterns and relation to volcanoes, *Geophys. Res. Lett.*, *33*, L20313, doi:10.1029/2006GL027723.
- Waite, G. P. (1999), Seismicity of the Yellowstone Plateau: space-time patterns and stresses from focal mechanism inversion: M. S. thesis, University of Utah, Salt Lake City.
- Waite, G. P., and R. B. Smith (2002), Seismic evidence for fluid migration accompanying subsidence of the Yellowstone caldera, *J. Geophys. Res.*, *107*(B9), 2177, doi:10.1029/2001JB000586.
- Waite, G. P., and R. B. Smith (2004), Seismotectonics and stress field of the Yellowstone volcanic plateau from earthquake first-motions and other indicators, *J. Geophys. Res.*, *109*, B02301, doi:10.1029/2003JB002675.
- Waite, G. P., R. B. Smith, and R. A. Allen (2006),  $V_P$  and  $V_S$  structure of the Yellowstone hot spot from teleseismic tomography: Evidence for an upper mantle plume, *J. Geophys. Res.*, *111*, B04303, doi:10.1029/2005JB003867.
- Warren, N. W., and G. V. Latham (1970), An experimental study of thermally induced microfracturing and its relation to volcanic seismicity, *J. Geophys. Res.*, *75*, 4455-4464.
- Wessel, P., and W. H. F. Smith (1998), New, improved version of the Generic Mapping Tools released, *Eos Trans. AGU*, *79*, 579.
- Wicks, C., W. Thatcher, and D. Dzurisin (1998), Migration of fluids beneath Yellowstone caldera inferred from satellite radar interferometry, *Science*, *282*, 458-462.
- Wicks, C., W. Thatcher, D. Dzurisin, and J. Svarc (2006), Uplift, thermal unrest and magma intrusion at Yellowstone caldera, *Nature*, *440*, 72-75.
- Wiemer, S., and J. P. Benoit (1996), Mapping the  $b$ -value anomaly at 100 km depth in Alaska and New Zealand subduction zones, *Geophys. Res. Lett.*, *24*, 189-192.
- Wiemer, S., and S. R. McNutt (1997), Variations in the frequency-magnitude distribution with depth in two volcanic areas: Mount St. Helens, Washington, and Mt. Spurr, Alaska, *Geophys. Res. Lett.*, *24*, 189-192.

- Wiemer, S. and M. Wyss (1997), Mapping the frequency-magnitude distribution in asperities: An improved technique to calculate recurrence times?, *J. Geophys. Res.*, *102*, 15115-15128.
- Wiemer, S., S. R. McNutt, and M. Wyss (1998), Temporal and three-dimensional spatial analyses of the frequency-magnitude distribution near Long Valley Caldera, California, *Geophys. J. Int.*, *134*, 409-421.
- Wiemer, S. and M. Wyss (2000), Minimum magnitude of completeness in earthquake catalogs: Examples from Alaska, the western United States, and Japan, *Bull. Seismol. Soc. Am.*, *90*, no. 4, 859-869.
- Wiemer, S. (2001), A software package to analyze seismicity: ZMAP, *Seism. Res. Lett.*, *72*, 373-382.
- Wiemer, S., and M. Wyss (2002), Mapping spatial variability of the frequency-magnitude distribution of earthquakes, *Adv. Geophys.*, *45*, 259-302.
- Wong, I., S. Olig, and M. Dober (2000), Preliminary Probabilistic Seismic Hazard Analysis; Island Park, Grassy Lake, Jackson Lake, Palisades, and Ririe Dams, U.R.S. Griener Woodward Clyde, Final report prepared for the Bureau of Reclamation.
- Wyss, M. (1973), Towards a physical understanding of the earthquake frequency distribution, *Geophys. J. R. Astron. Soc.*, *31*, 341-359.
- Wyss, M., S. Shimazaki, and S. Wiemer (1997), Mapping active magma chambers beneath the off-Ito volcano, Japan, *J. Geophys. Res.*, *102*, 413-420.
- Wyss, M., F. Klein, K. Nagamine, and S. Wiemer (2001), Anomalously high *b*-values in the South Flank of Kilauea volcano, Hawaii: evidence for the distribution of magma below Kilauea's East rift zone, *J. Volcanol. Geotherm. Res.*, *106*, 23-37.
- Youngs, R. R., F. H. Swan, M. S. Power, D. P. Schwartz, and R. K. Green (1987), Probabilistic analysis of earthquake ground shaking hazard along the Wasatch Front, Utah, in *Assessment of regional earthquake hazards and risk along the Wasatch Front, Utah*, edited by P. L. Gori, and W. W. Hays, pp. M1-M110, USGS, Reston, VA.